RONY CRISTIANO

Bifurcation Analysis in Discontinuous Piecewise-Smooth Systems: Applications in Power Electronics

FLORIANÓPOLIS
2018

Federal University of Santa Catarina
Postgraduate Program in
Automation Engineering and Systems

Bifurcation Analysis in Discontinuous Piecewise-Smooth Systems: Applications in Power Electronics

Thesis submitted to the Postgraduate Program
in Automation Engineering and Systems
of the Federal University of Santa Catarina,
as part of the requirements for obtaining the degree of
Doctor in Automation Engineering and Systems.

Rony Cristiano

Advisor: Prof. Daniel Juan Pagano, Dr.

Florianópolis, 03/September/2018.

Ficha de identificação da obra elaborada pelo autor,
através do Programa de Geração Automática da Biblioteca Universitária da UFSC.

Cristiano, Rony
Bifurcation Analysis in Discontinuous Piecewise-Smooth Systems: Applications in Power Electronics / Rony Cristiano ; orientador, Daniel Juan Pagano, 2018.
346 p.

Tese (doutorado) - Universidade Federal de Santa Catarina, Centro Tecnológico, Programa de Pós-Graduação em Engenharia de Automação e Sistemas, Florianópolis, 2018.

Inclui referências.

1. Engenharia de Automação e Sistemas. 2. Non-smooth Dynamical Systems. 3. Non-linear Control. 4. Bifurcation Theory and Applications. 5. Power Electronic Systems. I. Pagano, Daniel Juan. II. Universidade Federal de Santa Catarina. Programa de Pós-Graduação em Engenharia de Automação e Sistemas. III. Título.

Rony Cristiano

Bifurcations Analysis in Discontinuous Piecewise-Smooth Systems: Applications in Power Electronics

This Thesis has been evaluated and approved for obtaining the degree of Doctor in Automation Systems Engineering, and was also approved in its final format by the Postgraduate Program of Automation Systems Engineering at the Federal University of Santa Catarina.

Florianópolis, 03/Set/2018

Daniel J. Pagano, Dr.
Advisor

Werner Kraus Junior, Dr.
Coordinator
Postgraduate Program in Automation Systems Engineering, Federal University of Santa Catarina, Florianópolis, Brazil

Examination Committee:

Prof. Daniel J. Pagano, Dr. - DAS/UFSC
Advisor

Prof. Joao Carlos da Rocha Medrado, Dr. - IME/UFG

Prof. Marcelo Lobo Heldwein, Dr. - INEP/UFSC

Prof. Hector Bessa Silveira, Dr. - DAS/UFSC

Dedicated to my mother, Zoê Freitas Pereira Cristiano.

ACKNOWLEDGEMENTS

My thanks to my father João Navalte Cristiano and my mother Zoê F. Pereira Cristiano, my brother Rodrigo Cristiano and my sister Djema Maria Cristiano, for the support and incentive.

Many thanks to my friend Professor Daniel Juan Pagano, for the doctoral supervision, teachings and motivation.

I would like to thank the professors João Carlos da Rocha Medrado, Hector Bessa Silveira and Marcelo Lobo Heldwein, for the participating in the examination committee and contributions to this work.

I want to thank all the collaborators, Enrique Ponce, Emilio Freire, Luis Benadero, Tiago Carvalho, Durval J. Tonon and Mathieu Granzotto, for the contributions to this work.

Many thanks to the Professor Enrique Ponce, for the supervision during the *sandwich* period in the Department of Applied Mathematics II of the Technical School of Engineering (University of Seville - Seville - Spain), for his friendship and teachings.

My thanks to the *Conselho Nacional de Desenvolvimento Científico e Tecnológico* - CNPq, in particular to the Science without Borders program, for the financial support during the *sandwich* period.

I would also like to thank the *Coordenação de Aperfeiçoamento de Pessoal de Nível Superior* - CAPES and Postgraduate Program in Automation Engineering and Systems of the Federal University of Santa Catarina, for the Doctoral Research Fellowship.

Abstract of thesis submitted to the Federal University of Santa Catarina as part of the requirements for obtaining the degree of Doctor in Automation Engineering and Systems.

Bifurcation Analysis in Discontinuous Piecewise-Smooth Systems: Applications in Power Electronics

Rony Cristiano

September/2018

Advisor: Daniel Juan Pagano, Dr.
Specialized field: Non-smooth Dynamical Systems and Non-linear Control
Keywords: DPWS systems, Filippov systems, sliding vector field, first return map, pseudo-equilibrium, boundary equilibrium, Teixeira singularity, crossing limit cycle, sliding mode control, boost converter, buck converter, stability, bifurcations.

ABSTRACT: This thesis considers the discontinuous piecewise-smooth systems in $\mathbb{R}^3$ (3D-DPWS systems) that exhibit a single discontinuity surface, typically flat and denoted by Σ. The concept of Filippov's solution is used to described the sliding dynamics contained in a region of Σ given that it fulfils certain conditions. 3D-DPWS systems exhibit the classical bifurcations (saddle-node, Hopf, *etc.*) of smooth systems and also non-conventional bifurcations, unique to nonsmooth systems, known as discontinuity-induced bifurcations (DIBs). The general objective is to classify and characterize bifurcations in 3D-DPWS systems. In this sense, this thesis focuses on the qualitative and geometric analysis of bifurcations and their unfolding, in particular, of

codimension 1 and 2, involving natural equilibria, boundary equilibria, pseudo-equilibria, T-singularities (Teixeira singularities), limit cycles and invariant surfaces. One way to generalize this study is to determine canonical forms which describe certain required topological configurations, which minimize the number of system parameters and end up simplifying the calculations and the associated geometry. This thesis presents varied original contributions, which are obtained from (i) some case studies considering applications for dc-dc power converters under a sliding mode control strategy; (ii) a pioneering experimental analysis with a dc-dc boost converter, showing the effects caused by the TS-bifurcation (T-singularity bifurcation); (iii) a detailed analysis, with analytical and numerical results, of local bifurcations in sliding vector fields, on the boundary equilibrium bifurcations and on bifurcations at T-singularities; (iv) numerical results on the existence, stability and some bifurcations of crossing limit cycles.

Resumo de tese submetida à Universidade Federal de Santa Catarina como parte dos requisitos para a obtenção do grau de Doutor em Engenharia de Automação e Sistemas.

Análise de Bifurcações em Sistemas Descontínuos Suaves por Partes: Aplicações em Eletrônica de Potência

Rony Cristiano

Setembro/2018

Orientador: Daniel Juan Pagano, Dr.
Área de Concentração: Sistemas Dinâmicos Não-Suaves e Controle Não-Linear
Palavras-chave: Sistemas DPWS, sistemas de Filippov, campo vetorial deslizante, mapa de primeiro retorno, pseudo-equilíbrio, equilíbrio de fronteira, singularidade de Teixeira, ciclo limite de cruzamento, controle por modo deslizante, conversor boost, conversor buck, estabilidade, bifurcação.

RESUMO: Esta tese considera sistemas dinâmicos descontínuos suaves por partes em $\mathbb{R}^3$ (sistemas 3D-DPWS) exibindo uma única superfície de descontinuidade, denotada por Σ e tipicamente plana. O conceito de solução de Filippov é usado para descrever a dinâmica deslizante presente em uma região de Σ cumprindo certas condições. Sistemas DPWS exibem as bifurcações clássicas (sela-nó, Hopf, etc.) dos sistemas suaves e também bifurcações não convencionais, próprias dos sistemas suaves por partes, conhecidas como bifurcações induzidas pela descontinuidade (DIBs). O objetivo geral desta tese é o de classificar e de caracterizar bifurcações em sistemas 3D-DPWS. Nesse sentido, esta tese apresenta uma análise qualitativa e geométrica de bifurcações e de seus desdobramentos, em particular, de codimensão 1 e 2, envol-

vendo equilíbrios naturais, equilíbrios de fronteira, pseudo-equilíbrios, T-singularidades (singularidades de Teixeira), ciclos limite e superfícies invariantes. Para generalizar este estudo, são determinadas formas canônicas que descrevem certas configurações topológicas exigidas, minimizando o número de parâmetros do sistema e simplificando os cálculos e a geometria envolvida. Esta tese apresenta contribuições originais variadas, as quais são obtidas a partir de (i) alguns estudos de caso considerando aplicações para conversores de potência cc-cc sob uma estratégia de controle por modos deslizantes; (ii) uma análise experimental pioneira com um conversor boost cc-cc, mostrando os efeitos causados pela bifurcação da T-singularidade; (iii) uma análise detalhada sobre bifurcações locais em campos vetoriais deslizantes, sobre as bifurcações de equilíbrio de fronteira e sobre bifurcações em T-singularidades; (iv) resultados numéricos sobre a existência, estabilidade e algumas bifurcações de ciclos limite de cruzamento.

Contents

List of Figures

List of Tables

Chapter 1

Introduction

1.1 Motivation and goals

The piecewise-smooth (PWS) systems belong to an important class of non-linear dynamical systems that have no continuity in the vector field or in its derivatives. PWS systems are often used in physical systems and engineering applications to describe phenomena involving friction, impact, saturation, hysteresis or processes with switching components.

This thesis is dedicated to the study of mechanisms through which the system phase portrait loses its structural stability, i.e., bifurcations. In particular, we are interested in non-standard phenomena which are unique to PWS systems. Bifurcations in PWS systems have been the object of study in several works in recent years, but there is not yet a complete understanding of local bifurcations, so that there is a great interest in the development of bifurcation theory for these systems.

We will consider the PWS systems in $\mathbb{R}^3$ which exhibit a two-dimensional discontinuity surface, denoted by Σ and typically a flat surface, where the vector field is discontinuous (we named 3D-DPWS systems); see [51, 117]. This discontinuity surface is called switching

boundary[1]. Several physical systems such as friction mechanical systems, power electronics converters and control systems are modelled by DPWS systems.

An important feature of 3D-DPWS systems is the presence of different types of equilibrium points (natural equilibrium, boundary equilibrium, pseudo-equilibrium). In particular, the so-called pseudo-equilibrium is a point at Σ where the sliding vector field becomes null, being reached in finite time by trajectories initiated outside Σ. In sliding mode control (SMC) processes [122], the desired operating point is a stable pseudo-equilibrium of the system that belongs to an attractive region of Σ where the sliding occurs. The output of the pseudo-equilibrium of this attractive sliding region, induced by the variation of a system parameter, is usually associated with typical bifurcations of 3D-DPWS systems such as the boundary equilibrium bifurcations (BEBs) and the TS-bifurcation, which will be studied in detail in this thesis.

3D-DPWS systems exhibit the classical bifurcations (saddle-node, transcritical, Hopf, homoclinic, *etc.*) of smooth systems and also non-conventional bifurcations, unique to non-smooth systems, known as discontinuity-induced bifurcations (DIBs); see [42]. In this thesis the notion of bifurcation is associated with a qualitative change in the topology of the phase portraits of a dynamical system, due to the variation of one or more parameters. Bifurcations that determine changes in the number and nature of the equilibria and of the limit cycles of the system are of particular importance to this study.

The general objective is to classify and characterize bifurcations in 3D-DPWS systems. Specifically, it aims to: (i) determine a classification of BEBs from its unfoldings and from the sliding dynamics at the boundary equilibrium, considering a family of systems with discontinuous piecewise-linear (DPWL) vector field and that exhibit two parallel tangency lines on the switching boundary; (ii) revise the theory on the

[1] Also called switching manifold or discontinuity manifold.

Teixeira singularity (T-singularity), in order to structure more deeply the bifurcations at this point, describing the complete characterization on its unfolding dynamics, and providing new and more efficient tools for the local analysis of the T-singularity bifurcation (TS-bifurcation) in applications; (iii) describe the dynamics and the bifurcations in a family of systems with two T-singularities, with particular attention to the possibles degenerate cases of the T-singularity bifurcation; (iv) establish mechanisms for the birth (or vanishing) of Crossing Limit Cycles - CLCs, considering some case studies; (v) describe the dynamics and the bifurcations in a dc-dc boost, and buck, converters with sliding mode control.

In this sense, this thesis focuses on the qualitative and geometric analysis of bifurcations and their unfolding, in particular, of codimension 1 and 2. We will deal with bifurcations in the sliding vector field (saddle-node, transcritical, pitchfork, Hopf) [29, 98], boundary equilibrium bifurcations [45, 51, 67, 78], bifurcations at T-singularities [26, 69, 117, 118] and bifurcations of crossing limit cycles [26, 32, 55, 117] (from the first return map analysis).

One way to generalize this study is to determine canonical forms that allow it to minimize the number of system parameters. This thesis determines canonical forms for families of 3D-DPWS systems with specific configurations, such as the existence of two regular T-singularities bifurcating from a type of degenerate T-singularity, [118]. Such canonical forms are used for a detailed study of stability and bifurcations in each family of systems considered, in particular for the investigation of the BEBs and of bifurcations at T-singularities, as well as the associated dynamic phenomena.

For case studies we will consider applications in power electronics, in which dc-dc power converters are used under a SMC strategy with washout filter (SMC-Washout); see [91]. Experimental analysis with a dc-dc boost converter, showing the effects caused by the TS-bifurcation, are also considered in this thesis. These experimental results were also

obtained in [29]. The power converters exhibit discontinuous models, the discontinuity being related to their implementation by means of electronic switches that are designed to be permanently switching between two discrete states, on and off. Due to this switching characteristic, sliding mode controllers are considered for the voltage regulation of power converters since they are naturally suitable for the control of switched systems [108]. Although in general they have a piecewise-linear model, power converters exhibit a complex and varied dynamic behaviour [121], as we will see in this thesis.

The bifurcation theory [37, 77] contains powerful tools for the analysis of nonlinear dynamics. From the analysis of bifurcations we can, for instance, determine the region in the parameter space of a control system where the control objectives are attained and, thus, design more efficient controllers capable of inhibiting the undesired dynamics caused by bifurcations, see [29, 92]. In this sense, the study of bifurcations and the related dynamic phenomena have great relevance in the fields of applied mathematics and control engineering.

1.2 Piecewise-smooth dynamical systems

Qualitative theory and typical bifurcations of PWS systems are introduced by Di Bernardo *et al.* [37], which is an important book in the literature containing a series of applications (mechanical impact and friction oscillators, power electronic and control systems with switches) with numerical results and some experimental ones. Based on it, we draw attention to the pioneering work on non-smooth equilibrium bifurcations of Andronov *et al.* [3], on border-collision bifurcations of Feigin [48], on impact oscillators in [8, 97] of Babitskii and Peterka, respectively, on sliding motion of Filippov [51] and Teixeira [117] on singularities of discontinuous PWS three-dimensional systems. More recent studies in PWS systems with important applications in non-smooth mechanics are found in [17, 34, 56, 57, 76, 82, 87]; also in elec-

trical and electronic devices [12, 20, 36, 41, 99, 121], in discontinuous control systems [9, 29, 84, 123], in mathematical biology and medicine [27, 31, 33, 120].

Regarding bifurcations, there is a variety of interesting works published in the last two decades, for instance, the detailed work of Kuznetsov *et al.* [78] on local and global one-parameter bifurcations in planar Filippov systems (discontinuous PWS systems); Di Bernardo & Hogan [42], presenting an important review on the discontinuity-induced bifurcations in continuous PWS, discontinuous PWS and impacting systems; in addition to other important contributions in the development of the bifurcation theory in PWS systems, continuous [52, 85, 100, 107] and discontinuous [11, 24, 26, 64, 67, 93, 118] and also on bifurcations of limit cycles [32, 53, 54, 55, 68, 106].

PWS systems are described by a finite set of ordinary differential equations

$$\dot{x} = f^{(i)}(x), \quad x \in R^{(i)} \subset \mathbb{R}^n, \tag{1.1}$$

where $R^{(i)}$, $i = 1, 2, 3, ..., m$, are open regions separated by borders Σ_{ij} of $(n-1)$-dimension. The functions $f^{(i)} : R^{(i)} \to \mathbb{R}^n$ and boundaries Σ_{ij} are supposed to be smooth and the union of all boundaries Σ_{ij} and all regions $R^{(i)}$ covers the entire state space of (1.1). The non-smoothness occurs on the switching boundaries Σ_{ij}. Moreover, PWS systems are classified depending on the type of non-smoothness [37]:

(i) Systems with abrupt discontinuities in states, such as the *impact systems* with reverse speed.

(ii) Continuous piecewise-smooth systems (CPWS systems), if the vector field (1.1) is continuous but it is not differentiable at some points, that is, $f^{(i)}(x) = f^{(j)}(x)$ but $f_x^{(i)}(x) \neq f_x^{(j)}(x)$ for some $x \in \Sigma_{ij}$. No sliding motion occurs in CPWS systems. Examples of this class are the elastic mechanical systems with constraints in the states, the control systems with constraints on actuators such as saturation in the amplitude and/or speed of the control

action and nonsmooth oscillators.

(iii) Discontinuous piecewise-smooth systems (DPWS systems), if $f^{(i)}(x) \neq f^{(j)}(x)$ for some $x \in \Sigma_{ij}$. In DPWS systems there can be sliding motion in a region of Σ_{ij} fulfilling certain conditions. Such systems are also known in the literature as Filippov systems [78], which are described by a set of first order ordinary differential equations with a discontinuous right-hand side. As shown by Filippov in [51], it is possible to construct an appropriate vector field to describe this sliding motion, called sliding vector field. Examples of this class are the mechanical systems with dry friction and the sliding mode control systems.

In this thesis we will consider only DPWS systems in $\mathbb{R}^3$ (3D-DPWS systems) and its applications involving power electronics converters and SMC; see [108, 123]. In the qualitative analysis of these systems we dedicate special attention to the constant solutions at Σ_{ij} associated with the equilibria of the sliding vector field, since one of these equilibria is the desired point of operation in the SMC process. A point at Σ_{ij}, which is an equilibrium of the sliding vector field, is called a pseudo-equilibrium, because it is not in general an equilibrium of $f^{(i)}$ neither of $f^{(j)}$. Other invariant sets, such as limit cycles, homoclinic or heteroclinic connections, are also relevant from the point of view of robustness issues and global stability.

1.3 Outline of the thesis

In Chapter 2 we start by introducing some definitions, the notations and the elementary concepts regarding DPWS systems, as well as tools for the analysis of dynamic behaviour of these systems.

In Chapter 3 we will study the Hopf and Homoclinic bifurcations that occur in the sliding vector field of switching systems in $\mathbb{R}^3$. In particular, we will analyse a dc-dc boost converter with SMC-Washout

with the objective of investigating a new mechanism to produce a homoclinic bifurcation, where the closing point of the homoclinic loop is a two-fold singularity. This is a result known in the literature due to recent works [12, 29], but here, in this thesis, the approach is more detailed. This chapter has originated the paper: R. Cristiano, T. Carvalho, D. J. Tonon and D. J. Pagano. Hopf and Homoclinic bifurcations on the Sliding Vector Field of Switching systems in $\mathbb{R}^3$: A case study in power electronics. *Physica D: Nonlinear Phenomena*, 347:12 - 20, 2017.

Chapter 4 is dedicated to the study of 3D-DPWS systems that present the T-singularity (Teixeira singularity). The T-singularity can undergo an interesting bifurcation, namely when a pseudo-equilibrium point crosses the two-fold singularity, passing from the attractive sliding region to the repulsive sliding region (or vice versa) and, simultaneously, a crossing limit cycle arises. This bifurcation is denominated in this thesis as TS-bifurcation. After carefully deriving a local canonical form, we will revise some previous works regarding this bifurcation so as to correct some detected misconceptions. Furthermore, we will provide by means of a more direct approach the critical coefficients characterizing the bifurcation, also giving computational procedures for them. The achieved results on TS-bifurcation will be applied to some illustrative examples and also in a dc-dc boost converter under a sliding mode control strategy and washout filter. The TS-bifurcation and all its unfolding are known in the literature (see [26]), however, this bifurcation had not been correctly described. In this sense, our main goal in this chapter will be is the restructuring of TS-bifurcation, providing detailed tools to investigate such bifurcation in application systems. This chapter has originated the paper: R. Cristiano, E. Freire, E. Ponce and D. J. Pagano. Revisiting the Teixeira singularity bifurcation analysis. Application to the control of power converters. *International Journal of Bifurcation and Chaos*, 28(9)1850106 (31 pages), 2018.

In Chapter 5 we will consider the model of a dc-dc boost converter with sliding mode control and washout filter. This chapter is dedicated

to the study of local and global bifurcations, in particular focused on TS-bifurcation and crossing limit cycles (CLCs). Apart from the TS-bifurcation characterization in this power converter, we will explore numerically other non-local phenomena like a saddle-node bifurcation of CLCs. Experimental results that illustrate the effects of the TS-bifurcation in a real circuit prototype of a boost converter will also be shown. The experimental identification of the Teixeira singularity in a real circuit of power electronic is a pioneering result in the literature. Besides the experimental results we will also present analytical and numerical results on the TS-bifurcation and others bifurcations, helping us to unravel the dynamical richness of this circuit. Moreover, we will study global mechanisms for the vanishing (or birth) of a CLC (saddle-node bifurcation and non-standard homoclinic bifurcation), besides the existence and stability analysis of CLCs from its birth to its annihilation. This chapter has originated the paper: R. Cristiano, E. Ponce, D. J. Pagano and M. Granzotto. On the Teixeira Singularity Bifurcation in a DC-DC Power Electronic Converter. *Submitted to Nonlinear Dynamics*, 2018.

Chapter 6 contains a detailed analysis of bifurcations in a family of 3D-DPWS systems that have two points of T-singularity. In addition, from the variation of a system parameter, these T-singularities collide and then disappear along with the attractive sliding region. In this case, a fold bifurcation occurs and, at the bifurcation point, appears a type of degenerate T-singularity. We provide a local canonical form for systems with 1-degenerate T-singularity (following [69, 118], but providing more detail on derivation of the canonical form) and its unfolding in two regular or none T-singularities, along with the pathways to obtain it. Under certain conditions, there is a pseudo-equilibrium that collides with one of the T-singularities or, the two T-singularities simultaneously collide with the pseudo-equilibrium. In the first case a TS-bifurcation occurs and, in second case, a non regular case of larger co-dimension of this bifurcation occurs, that we have named double TS-bifurcation. Like the TS-bifurcation, the double TS-bifurcation also is associated with

the birth of a crossing limit cycle, but here, it arises from a degenerate T-singularity. We will describe the sliding and crossing dynamics around the T-singularities, regular or degenerate, and also the sliding dynamics at the pseudo-equilibrium. Moreover, we will prove the existence, the stability and the bifurcations of crossing limit cycles from the considered case study. To the best of our knowledge, the present work is the first one in which the appearance of two T-singularities in piecewise-smooth dynamical systems is studied. The fold bifurcation of T-singularities and the double TS-bifurcation are unknown in the literature, as far as we know, the given names for each are just our suggestions.

In Chapter 7 we will study a family of DPWS systems in $\mathbb{R}^3$ in which the vector fields are linear (DPWL systems) on both sides of the switching boundary, and with two parallel tangency lines containing a singularity cusp each. Such an adopted model often appears in engineering problems being used to describe the dynamics of discontinuous control systems such as sliding mode control. We will provide a canonical form for such systems and then we will simplify the calculations and the geometry related to the topological configuration on the switching boundary. We will describe the associated sliding vector field as well as the dynamic characteristics on the switching boundary from a proposed canonical form. Also, we will analyse the existence of natural equilibria, pseudo-equilibria and boundary equilibria. Moreover, this chapter is dedicated to the study of BEBs in $\mathbb{R}^3$ and of the different types of boundary equilibria with respect to the sliding dynamics at this point. The main goal will be the classification of BEBs, explicitly providing the conditions on the system parameters for the occurrence of each of the two scenarios, persistence and nonsmooth fold, and also the characterization of the dynamics of its unfoldings in the sliding vector field. The results obtained on stability and bifurcations will be applied to two examples in power electronics systems involving the sliding mode control of dc-dc buck converters.

Finally, in Chapter 8, we will discuss the main results and con-

tributions of this thesis to the field of non-smooth dynamical systems and we will present some proposals for future works. More details on goals, results achieved and contributions are discussed in each chapter.

Chapter 2

Preliminary Results on DPWS

In this chapter we present the definitions, the notations and the elementary concepts regarding DPWS systems as well as the tools for the analysis of dynamic behaviour of these systems. In particular, we are interested in three-dimensional DPWS systems with two regions in $\mathbb{R}^3$ separated by a planar surface Σ.

2.1 Introduction to 3D-DPWS systems

Let us assume two vector fields $\mathbf{F}^{\pm} : \mathbb{R}^3 \to \mathbb{R}^3$ and a scalar C^∞ function $h : \mathbb{R}^3 \to \mathbb{R}$ with non-vanishing gradient on a C^∞ two-dimensional surface

$$\Sigma = \{\mathbf{x} \in \mathbb{R}^3 : \ h(\mathbf{x}) = 0\} \tag{2.1}$$

and so that we have possibly $\mathbf{F}^+(\mathbf{x}) \neq \mathbf{F}^-(\mathbf{x})$ for some $\mathbf{x} \in \Sigma$. This surface is chosen to be a switching boundary, by dividing the $\mathbb{R}^3$-space into two open regions: $R^- = \{\mathbf{x} \in \mathbb{R}^3 : \ h(\mathbf{x}) < 0\}$ and $R^+ = \{\mathbf{x} \in \mathbb{R}^3 :$

$h(\mathbf{x}) > 0\}$, and such that $\mathbb{R}^3 = R^- \cup \Sigma \cup R^+$. Moreover, we assume $\mathbf{F}^{\pm} = (f_1^{\pm}, f_2^{\pm}, f_3^{\pm}) \in \mathfrak{X}^r$, in which $\mathfrak{X}^r$ denotes the space of C^r-vector fields on $\mathbb{R}^3$ endowed with the C^r-topology[1] with $r = \infty$ or $r \geq 1$ large enough for our purposes.

A 3D-DPWS dynamical system is usually expressed as the set of ordinary differential equations

$$\dot{\mathbf{x}} = \begin{cases} \mathbf{F}^-(\mathbf{x}), & \text{if } \mathbf{x} \in R^-, \\ \mathbf{F}^+(\mathbf{x}), & \text{if } \mathbf{x} \in R^+, \end{cases} \tag{2.2}$$

where $\mathbf{x}$ is the three-dimensional state vector and the " $\dot{}$ " denotes the differentiation in relation to time t.

The switching boundary Σ can be partitioned into regions with different dynamical behaviours (see Figure 2.1): (i) *crossing* regions ($\Sigma_c^{\pm}$), where one vector field is pointing to Σ and the other is pointing out of the boundary; (ii) *attractive sliding* region (Σ_{as}), where the vector fields $\mathbf{F}^+$ and $\mathbf{F}^-$ point towards Σ from both sides; (iii) *repulsive sliding* region (Σ_{rs}), where both $\mathbf{F}^+$ and $\mathbf{F}^-$ are pointing out of Σ from either sides. Points in such regions are qualified accordingly[2].

In order to study the dynamic behaviour of systems (2.2) on the switching boundary Σ we introduce the orbital derivative of h in relation to vector fields $\mathbf{F}^{\pm}$, in terms of the Lie derivative: $L_{\mathbf{F}^{\pm}} h = \langle \nabla h, \mathbf{F}^{\pm} \rangle$, where ∇h is the gradient of smooth function h and $\langle ., . \rangle$ denotes the usual inner product. The higher order Lie derivatives are given by $L^n_{\mathbf{F}^{\pm}} h = \langle \nabla L^{n-1}_{\mathbf{F}^{\pm}} h, \mathbf{F}^{\pm} \rangle$ for $n = 2, 3, ...$ Thus, we can explicitly determine the sliding and crossing regions as follows:

$$\Sigma_{as} = \{\mathbf{x} \in \Sigma : L_{\mathbf{F}^+} h(\mathbf{x}) < 0 < L_{\mathbf{F}^-} h(\mathbf{x})\}, \tag{2.3}$$

$$\Sigma_{rs} = \{\mathbf{x} \in \Sigma : L_{\mathbf{F}^-} h(\mathbf{x}) < 0 < L_{\mathbf{F}^+} h(\mathbf{x})\}, \tag{2.4}$$

[1] This will be considered throughout the thesis, but will no longer be addressed.

[2] We use the appointment attractive/repulsive sliding region following [45, 81]. Some authors, as for example [71, 117], prefer to qualify as sliding only the attractive case, being the repulsive sliding named as escaping.

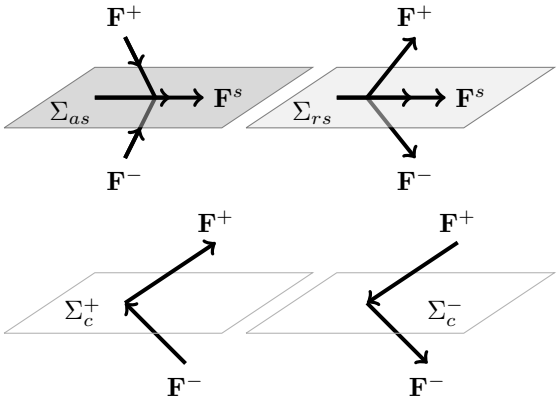

Figure 2.1: Illustrative dynamical behaviours in Σ: (top-left) Attractive sliding; (top-right) repulsive sliding; (bottom) crossing.

$$\Sigma_c^- = \{\mathbf{x} \in \Sigma : L_{\mathbf{F}^-} h(\mathbf{x}) < 0 \text{ and } L_{\mathbf{F}^+} h(\mathbf{x}) < 0\}, \tag{2.5}$$

$$\Sigma_c^+ = \{\mathbf{x} \in \Sigma : L_{\mathbf{F}^-} h(\mathbf{x}) > 0 \text{ and } L_{\mathbf{F}^+} h(\mathbf{x}) > 0\}. \tag{2.6}$$

The orbits of system (2.2) can be constructed by concatenating *standard* solutions in $R^{\pm}$ and *sliding* solutions on Σ following the Filippov convex method, see [37, 51, 78, 117] and its explicit definition later in (2.9). The forward (with positive time evolution) orbit of (2.2) that crosses Σ, goes from R^- to R^+ through some $\mathbf{x}_0 \in \Sigma_c^+$ and goes from R^+ to R^- through $\mathbf{x}_0 \in \Sigma_c^-$. The forward orbit of (2.2) that intersects Σ at a point $\mathbf{x}_0 \in \Sigma_{as}$, continues from this point $\mathbf{x}_0$ on a contained sliding motion in Σ. The forward orbits of (2.2) through $\mathbf{x}_0 \in R^{\pm}$ never reach the repulsive sliding region Σ_{rs}, so that the dynamics in Σ_{rs} will not be observed in numerical integration of (2.2). But if $\mathbf{x}_0 \in \Sigma_{rs}$, we can assume that there is a sliding motion starting at $\mathbf{x}_0$ that follows the orbit defined by Filippov's method.

The Filippov convex method is used to construct solutions in $\Sigma_{as} \cup \Sigma_{rs} \subset \Sigma$ as an extension to solutions of (2.2); see Figure 2.2. For this, we introduce a new vector field, denoted by $\mathbf{F}^s$ and called *sliding*

vector field, calculated from a convex combination of the vector fields $\mathbf{F}^{\pm}$, namely

$$\mathbf{F}^s(\mathbf{x}) = (1-\alpha)\mathbf{F}^-(\mathbf{x}) + \alpha\mathbf{F}^+(\mathbf{x}). \tag{2.7}$$

For each $\mathbf{x} \in \Sigma_{as} \cup \Sigma_{rs} \subset \Sigma$, the value of α is chosen so that the sliding vector field $\mathbf{F}^s$ is tangent to Σ, that is

$$L_{\mathbf{F}^s} h(\mathbf{x}) = (1-\alpha) L_{\mathbf{F}^-} h(\mathbf{x}) + \alpha L_{\mathbf{F}^+} h(\mathbf{x}) = 0,$$

resulting in

$$\alpha = \alpha(\mathbf{x}) = \frac{L_{\mathbf{F}^-} h(\mathbf{x})}{L_{\mathbf{F}^-} h(\mathbf{x}) - L_{\mathbf{F}^+} h(\mathbf{x})}. \tag{2.8}$$

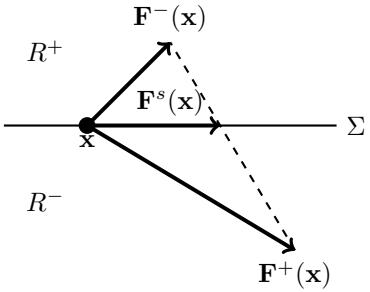

Figure 2.2: Geometric definition of the sliding vector field.

Note that $L_{\mathbf{F}^-} h(\mathbf{x}) - L_{\mathbf{F}^+} h(\mathbf{x}) \neq 0$ and $0 < \alpha(\mathbf{x}) < 1$ for all $\mathbf{x} \in \Sigma_{as} \cup \Sigma_{rs}$. Replacing (2.8) in (2.7) we can explicitly determine the sliding vector field by

$$\mathbf{F}^s(\mathbf{x}) = \frac{L_{\mathbf{F}^-} h(\mathbf{x})\mathbf{F}^+(\mathbf{x}) - L_{\mathbf{F}^+} h(\mathbf{x})\mathbf{F}^-(\mathbf{x})}{L_{\mathbf{F}^-} h(\mathbf{x}) - L_{\mathbf{F}^+} h(\mathbf{x})}. \tag{2.9}$$

The solution of (2.2) with initial condition $\mathbf{x}_0 \in \Sigma_{as} \cup \Sigma_{rs} \subset \Sigma$ is obtained from the sliding system

$$\dot{\mathbf{x}} = \mathbf{F}^s(\mathbf{x}).$$

For an initial condition $\mathbf{x}_0 \in \Sigma_{as}$, the solution is unique in forward time but it is not unique in backward time; in this case, there are three possible solutions: each one follows the flow of $\mathbf{F}^s$ or $\mathbf{F}^-$ or $\mathbf{F}^+$. The opposite occurs for an initial condition $\mathbf{x}_0 \in \Sigma_{rs}$, so that the solution is unique in backward time, but it is not unique in forward time. Studies about the existence and uniqueness of solutions of discontinuous differential equations are found in [7, 50, 51].

Sliding regions are delimited by points where the vector fields $\mathbf{F}^{\pm}$ are tangent to Σ, which are calculated from the tangency condition: $L_{\mathbf{F}^-}h(\mathbf{x}) = 0$ and $h(\mathbf{x}) = 0$, in relation to $\mathbf{F}^-$; and $L_{\mathbf{F}^+}h(\mathbf{x}) = 0$ and $h(\mathbf{x}) = 0$, in relation to $\mathbf{F}^+$. Then, we define two sets of tangential singularities:

$$T_+ = \{\mathbf{x} \in \Sigma \,|\, L_{\mathbf{F}^+}h(\mathbf{x}) = 0\}$$

and

$$T_- = \{\mathbf{x} \in \Sigma \,|\, L_{\mathbf{F}^-}h(\mathbf{x}) = 0\};$$

one for each vector field involved. These sets of tangency points are assumed to be smooth curves contained in Σ, and we refer to T_+ (resp. T_-) as the *tangency line* of $\mathbf{F}^+$ (resp. $\mathbf{F}^-$). Moreover, if $\mathbf{F}^+$ (resp. $\mathbf{F}^-$) vanishes at $\mathbf{x} \in \Sigma$, then $\mathbf{x} \in T_+$ (resp. $\mathbf{x} \in T_-$). Points where one of the vector fields $\mathbf{F}^{\pm}$ vanishes on Σ are known as *boundary equilibrium* points; see Section 2.3 and references [37, 44, 45, 78].

At points $\mathbf{x} \in \Sigma$ such that $L_{\mathbf{F}^-}h(\mathbf{x}) - L_{\mathbf{F}^+}h(\mathbf{x}) = 0$, either both vector fields $\mathbf{F}^{\pm}$ are tangent to Σ, or one of them vanishes while the other is tangent to Σ, or they both vanish, or both are identical; see *singular sliding points* in [78]. Points where both vector fields $\mathbf{F}^{\pm}$ are tangent to Σ, that is, points $\mathbf{x} \in T_+ \cap T_-$, are *double tangency* points which are classified generically as *two-fold* singularities; see Section 2.2 and references [49, 69, 71, 117].

The transverse intersection between the tangency lines T_+ and T_- determine four quadrants on Σ (in a neighbourhood of this intersection point): Σ_{as} in Q1, Σ_c^+ in Q2, Σ_{rs} in Q3 and Σ_c^- in Q4, as shown in

Figure 2.3(a). If T_- and T_+ become parallel curves, then only three of these regions remain on Σ: (i) sliding mode (Σ_{as} or Σ_{rs}) in the central region and crossing mode in the regions outside (Σ_c^- on one side and Σ_c^+ on the other), as shown in Figure 2.3(b); (ii) or the opposite case, with crossing mode in the central region and sliding mode in the outer regions.

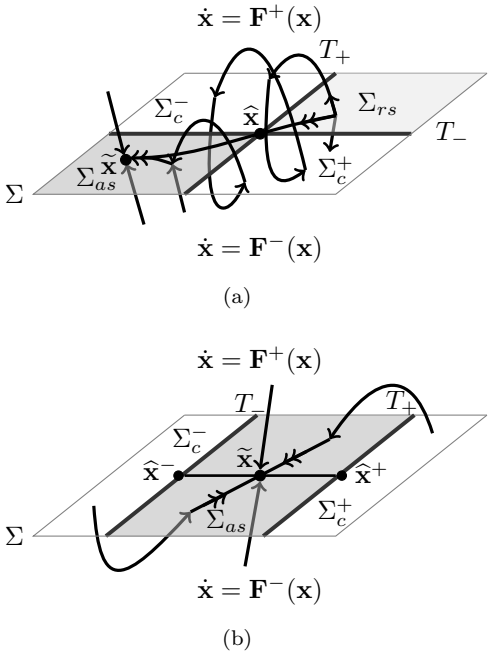

Figure 2.3: Phase portraits (illustrated) of 3D-DPWS systems. In (a) we have transverse tangency lines presenting a Teixeira singularity at the point $\widehat{\mathbf{x}} \in T_- \cap T_+$ and a pseudo-equilibrium at the point $\widetilde{\mathbf{x}} \in \Sigma_{as}$. In (b) we have parallel tangency lines presenting a cusp point at $\widehat{\mathbf{x}}^- \in T_-$ and another at $\widehat{\mathbf{x}}^+ \in T_+$, and also a pseudo-equilibrium at the point $\widetilde{\mathbf{x}} \in \Sigma_{as}$. For further information, see next sections.

Figure 2.3 illustrates the geometry of the dynamic behaviour in typical 3D-DPWS systems near the switching boundary Σ. In addition, the main elements involved are represented in this figure. Chapter 7 of

this thesis is devoted to the study of 3D-DPWS systems with parallel tangency lines, while in the Chapter 4 we study those with transversal tangency lines, in particular, presenting a *Teixeira singularity*. Both types of systems are of great relevance to the literature of the field and they appear as models of many real physical systems; see for instance [14, 25, 39, 43, 72, 111].

Thus, we have completed the switching boundary of (2.2) as $\Sigma = \Sigma_s \cup T \cup \Sigma_c$, where $\Sigma_s = \Sigma_{as} \cup \Sigma_{rs}$ represents the set of points at sliding mode, $\Sigma_c = \Sigma_c^+ \cup \Sigma_c^-$ represents the set of points at crossing mode and $T = T_+ \cup T_-$ represents the set of tangency points. In Section 2.2 the *tangency points* in $T_\pm$ are classified according to the type of contact between the vector fields $\mathbf{F}^\pm$ and the switching boundary Σ; see [78, 109, 117, 118].

2.2 Tangential singularities

We now introduce the definitions of the tangency points of system (2.2). Figure 2.4 shows the dynamic behavior associated with tangency points and planar representation is shown in Figure 2.5.

Definition 2.1. $\widehat{\mathbf{x}} \in \Sigma$ *is a fold point of* $\mathbf{F}^+$ *if* $\widehat{\mathbf{x}} \in T_+$ *and* $L^2_{\mathbf{F}^+} h(\widehat{\mathbf{x}}) \neq 0$*, i.e., the contact of* $\mathbf{F}^+$ *with* Σ *is quadratic. In addition, we say that* $\widehat{\mathbf{x}}$ *is a visible (resp. invisible) fold if the orbit of* $\dot{\mathbf{x}} = \mathbf{F}^+(\mathbf{x})$*, starting at* $\widehat{\mathbf{x}}$*, belongs to* R^+ *(resp.* R^-*) for all sufficiently small* $|t| \neq 0$*, i.e., if* $L^2_{\mathbf{F}^+} h(\widehat{\mathbf{x}}) > 0$ *(resp.* $L^2_{\mathbf{F}^+} h(\widehat{\mathbf{x}}) < 0$*).*

Definition 2.2. $\widehat{\mathbf{x}} \in \Sigma$ *is a fold point of* $\mathbf{F}^-$ *if* $\widehat{\mathbf{x}} \in T_-$ *and* $L^2_{\mathbf{F}^-} h(\widehat{\mathbf{x}}) \neq 0$*, i.e., the contact of* $\mathbf{F}^-$ *with* Σ *is quadratic. In addition, we say that* $\widehat{\mathbf{x}}$ *is a visible (resp. invisible) fold if the orbit of* $\dot{\mathbf{x}} = \mathbf{F}^-(\mathbf{x})$*, starting at* $\widehat{\mathbf{x}}$*, belongs to* R^- *(resp.* R^+*) for all sufficiently small* $|t| \neq 0$*, i.e., if* $L^2_{\mathbf{F}^-} h(\widehat{\mathbf{x}}) < 0$ *(resp.* $L^2_{\mathbf{F}^-} h(\widehat{\mathbf{x}}) > 0$*).*

Definition 2.3. $\widehat{\mathbf{x}} \in \Sigma$ *is a cusp point of* $\mathbf{F}^+$ *if* $\widehat{\mathbf{x}} \in T_+$*,* $L^2_{\mathbf{F}^+} h(\widehat{\mathbf{x}}) = 0$*,* $L^3_{\mathbf{F}^+} h(\widehat{\mathbf{x}}) \neq 0$ *and* $\{\nabla h(\widehat{\mathbf{x}}), \nabla L_{\mathbf{F}^+} h(\widehat{\mathbf{x}}), \nabla L^2_{\mathbf{F}^+} h(\widehat{\mathbf{x}})\}$ *is linearly independent.*

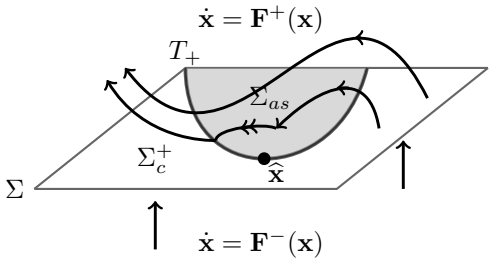

Figure 2.4: Tangency points of $\mathbf{F}^+$ and the dynamics involved. Through the generic cusp point $\widehat{\mathbf{x}} \in T_+$ emanate two branches of fold points. The right branch is composed of invisible fold points and the left branch is composed of visible fold points.

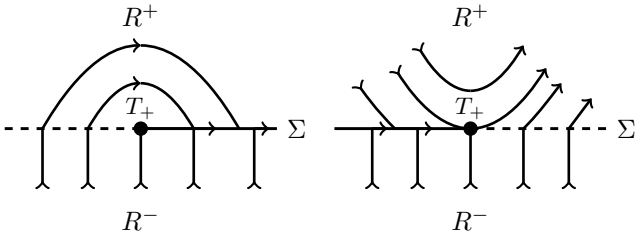

(a) Invisible Fold. (b) Visible Fold.

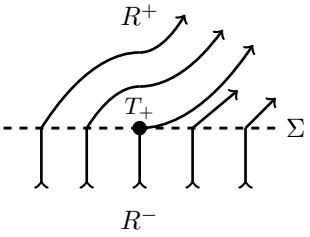

(c) Cusp.

Figure 2.5: Planar representation of the dynamics at the tangency points.

Definition 2.4. $\widehat{\mathbf{x}} \in \Sigma$ *is a cusp point of* $\mathbf{F}^-$ *if* $\widehat{\mathbf{x}} \in T_-$, $L^2_{\mathbf{F}^-}h(\widehat{\mathbf{x}}) = 0$, $L^3_{\mathbf{F}^-}h(\widehat{\mathbf{x}}) \neq 0$ *and* $\{\nabla h(\widehat{\mathbf{x}}), \nabla L_{\mathbf{F}^-}h(\widehat{\mathbf{x}}), \nabla L^2_{\mathbf{F}^-}h(\widehat{\mathbf{x}})\}$ *is linearly independent.*

A double tangency point appears where both vector fields $\mathbf{F}^+$ and $\mathbf{F}^-$ are tangent to Σ. If the contact between orbits of $\mathbf{F}^\pm$ with Σ is quadratic, then this double tangency point is classified as a two-fold singularity (see Figure 2.6). If such contact is quadratic on one side of Σ and cubic on the other, then it is classified as cusp-fold singularity. Furthermore, when the contact is cubic on both sides of Σ, it is classified as two-cusp singularity. The two-fold singularity is a generic point of 3D-DPWS systems (see [51, 71, 117]) and a double tangency point of our interest in this thesis, which is defined with more details below.

Definition 2.5. $\widehat{\mathbf{x}} \in \Sigma$ *is a two-fold point if* $\widehat{\mathbf{x}} \in T_- \cap T_+$, $L^2_{\mathbf{F}^-}h(\widehat{\mathbf{x}}) \neq 0$ *and* $L^2_{\mathbf{F}^+}h(\widehat{\mathbf{x}}) \neq 0$. *Moreover, it is assumed that the tangency lines* T_- *and* T_+ *intersect transversely in* $\widehat{\mathbf{x}}$*, i.e., the set*

$$\{\nabla h(\widehat{\mathbf{x}}), \nabla L_{\mathbf{F}^+}h(\widehat{\mathbf{x}}), \nabla L_{\mathbf{F}^-}h(\widehat{\mathbf{x}})\}$$

is linearly independent (*regular case*)*. The two-fold point can be classified into:*

(i) Invisible, if $L^2_{\mathbf{F}^+}h(\widehat{\mathbf{x}}) < 0 < L^2_{\mathbf{F}^-}h(\widehat{\mathbf{x}})$ (elliptic case)*;*

(ii) Visible, if $L^2_{\mathbf{F}^-}h(\widehat{\mathbf{x}}) < 0 < L^2_{\mathbf{F}^+}h(\widehat{\mathbf{x}})$ (hyperbolic case)*;*

(iii) Visible-Invisible, if $L^2_{\mathbf{F}^+}h(\widehat{\mathbf{x}}) \cdot L^2_{\mathbf{F}^-}h(\widehat{\mathbf{x}}) > 0$ (parabolic case)*.*

Remark 2.1. *An invisible two-fold point is also known as a Teixeira Singularity and in this thesis will be named as such, or abbreviated as T-singularity. See Figure 2.6(a). T-singularity is an important point for the dynamics of 3D-DPWS systems since this typical singularity always has, in its neighborhood on* Σ*, sliding and crossing regions. The existence of a T-singularity enables the construction of first return applications that build up in the crossing regions of* Σ*, such that this*

T-singularity is a fixed point for the associated map. In addition, the T-singularity behaves as an equilibrium for the sliding vector field, see [71, 117].

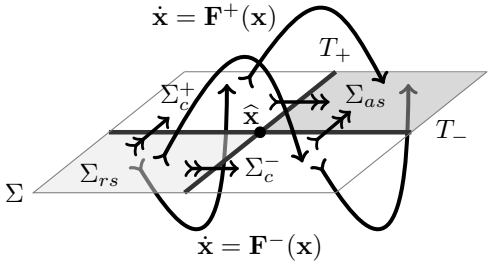

(a)

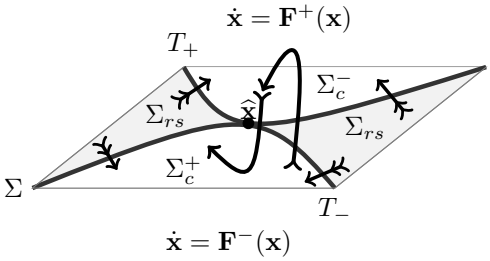

(b)

Figure 2.6: Dynamics on Σ presenting a T-singularity at $\widehat{\mathbf{x}}$. In (a) is the regular case and in (b) is the 1-degenerate case.

A non-generic contact between the tangency lines T_- and T_+, as shown in the Figure 2.6(b), is defined right below (see [69, 118]). Chapter 6 is dedicated to the study of systems that present this type of singularity and its unfolding, from which a pair of regular two-fold points can arise.

Definition 2.6. $\widehat{\mathbf{x}} \in \Sigma$ *is a 1-degenerate two-fold point if it is a two-fold point where the contact between* T_+ *and* T_- *is quadratic at* $\widehat{\mathbf{x}}$.

The following lemmas were proved in [117].

Lemma 2.1. *Assume that* $\widehat{\mathbf{x}} \in T_-$ *(resp.* T_+*) is a fold point of* $\mathbf{F}^-$ *(resp.* $\mathbf{F}^+$*) and* $\widehat{\mathbf{x}} \notin T_+$ *(resp.* T_-*). Then, the sliding vector field* $\mathbf{F}^s$ *is transversal to* T_- *(resp.* T_+*) at* $\widehat{\mathbf{x}}$*.*

Proof. Note that if $L_{\mathbf{F}^-}h(\widehat{\mathbf{x}}) = 0$ and $L_{\mathbf{F}^+}h(\widehat{\mathbf{x}}) \neq 0$ then $\mathbf{F}^s(\widehat{\mathbf{x}}) = \mathbf{F}^-(\widehat{\mathbf{x}})$. We define $g(\mathbf{x}) = L_{\mathbf{F}^-}h(\mathbf{x})$ and so $L_{\mathbf{F}^s}g(\widehat{\mathbf{x}}) = L^2_{\mathbf{F}^-}h(\widehat{\mathbf{x}}) \neq 0$. Therefore, $\mathbf{F}^s$ is transversal to T_- at all the fold points $\widehat{\mathbf{x}} \in T_-$. Similarly, $\mathbf{F}^s$ is transversal to T_+ at all fold points $\widehat{\mathbf{x}} \in T_+$. □

Lemma 2.2. *Assume that* $\widehat{\mathbf{x}} \in T_-$ *(resp.* T_+*) is a cusp point of* $\mathbf{F}^-$ *(resp.* $\mathbf{F}^+$*) and* $\widehat{\mathbf{x}} \notin T_+$ *(resp.* T_-*). Then, the sliding vector field* $\mathbf{F}^s$ *has a quadratic contact with* T_- *(resp.* T_+*) at* $\widehat{\mathbf{x}}$*.*

Proof. In this case, we have $L_{\mathbf{F}^s}g(\widehat{\mathbf{x}}) = L^2_{\mathbf{F}^-}h(\widehat{\mathbf{x}}) = 0$ and $L^2_{\mathbf{F}^s}g(\widehat{\mathbf{x}}) = L^3_{\mathbf{F}^-}h(\widehat{\mathbf{x}}) \neq 0$. Therefore, $\mathbf{F}^s$ has a quadratic contact with T_- at a cusp point $\widehat{\mathbf{x}} \in T_-$. Similarly, $\mathbf{F}^s$ has a quadratic contact with T_+ at a cusp point $\widehat{\mathbf{x}} \in T_+$. □

2.3 Equilibria

In system (2.2) it is possible to identify different types of equilibria. Below, we give the definitions of this equilibria, see [37, 58, 78].

Definition 2.7. *A point* $\overline{\mathbf{x}} \in \mathbb{R}^3$ *is a natural equilibrium of* (2.2) *if it is an equilibrium of the vector field* $\mathbf{F}^+$ *or* $\mathbf{F}^-$*. In addition, we say that* $\overline{\mathbf{x}}$ *is a real* (admissible) *equilibrium if*

$$\mathbf{F}^+(\overline{\mathbf{x}}) = \mathbf{0} \quad \textit{and} \quad h(\overline{\mathbf{x}}) > 0$$

or

$$\mathbf{F}^-(\overline{\mathbf{x}}) = \mathbf{0} \quad \textit{and} \quad h(\overline{\mathbf{x}}) < 0.$$

Alternatively, we say that $\overline{\mathbf{x}}$ *is a virtual* (non admissible) *equilibrium if*

$$\mathbf{F}^+(\overline{\mathbf{x}}) = \mathbf{0} \quad but \quad h(\overline{\mathbf{x}}) < 0$$

or

$$\mathbf{F}^-(\overline{\mathbf{x}}) = \mathbf{0} \quad but \quad h(\overline{\mathbf{x}}) > 0.$$

Definition 2.8. *A point* $\overline{\mathbf{x}}_b \in \mathbb{R}^3$ *is a boundary equilibrium of* (2.2) *if*

$$\mathbf{F}^+(\overline{\mathbf{x}}_b) = \mathbf{0} \quad or \quad \mathbf{F}^-(\overline{\mathbf{x}}_b) = \mathbf{0} \quad with \quad h(\overline{\mathbf{x}}_b) = 0.$$

Remark 2.2. *Note that a boundary equilibrium* $\overline{\mathbf{x}}_b$ *is always located on the boundary* T_+ *(or* T_-*) of the sliding region where the vector field* $\mathbf{F}^+$ *(or* $\mathbf{F}^-$*) vanishes, since* $L_{\mathbf{F}^+}h(\overline{\mathbf{x}}_b) = 0$ *(or* $L_{\mathbf{F}^-}h(\overline{\mathbf{x}}_b) = 0$*). It is easy to see from* (2.9) *that* $\mathbf{F}^s(\overline{\mathbf{x}}_b) = \mathbf{0}$*, and so the boundary equilibrium is an equilibrium for both vector fields* $\mathbf{F}^s$ *and* $\mathbf{F}^+$ *(or* $\mathbf{F}^-$*).*

Definition 2.9. *A point* $\widetilde{\mathbf{x}} \in \mathbb{R}^3$ *is a pseudo-equilibrium of* (2.2) *if* $\widetilde{\mathbf{x}} \in \Sigma_{as} \cup \Sigma_{rs}$ *and it is an equilibrium of the sliding vector field* $\mathbf{F}^s$*, i.e.,*

$$\begin{aligned} \mathbf{F}^s(\widetilde{\mathbf{x}}) &= \mathbf{0}, \\ h(\widetilde{\mathbf{x}}) &= 0. \end{aligned}$$

If the pseudo-equilibrium $\widetilde{\mathbf{x}}$ *behaves as a node, a focus or a saddle for the dynamics on* Σ*, we say that* $\widetilde{\mathbf{x}}$ *is a pseudo-node, pseudo-focus or pseudo-saddle, respectively.*

Remark 2.3. *In the equilibria calculation of the sliding vector field* $\mathbf{F}^s$*, we can find* $\widetilde{\mathbf{x}} \in \Sigma_c^+ \cup \Sigma_c^-$*. In this case, we say that* $\widetilde{\mathbf{x}}$ *is a* virtual (*non admissible*) *pseudo-equilibrium. Moreover, we can also find* $\widetilde{\mathbf{x}} \in T_+$ *or* $\widetilde{\mathbf{x}} \in T_-$*, and so* $\widetilde{\mathbf{x}}$ *becomes a* boundary *equilibrium. Whenever* $\widetilde{\mathbf{x}} \in \Sigma_{as} \cup \Sigma_{rs}$ *we have a* real (*admissible*) *pseudo-equilibrium. In this last one, both vector fields* $\mathbf{F}^+$ *and* $\mathbf{F}^-$ *are transversal and anti-collinear to* Σ *at* $\widetilde{\mathbf{x}}$*, that is, there exists* $\alpha = \alpha(\widetilde{\mathbf{x}})$ (*see equation* (2.8)) *such that*

$0 < \alpha < 1$ *and*

$$\mathbf{F}^{+}(\widetilde{\mathbf{x}}) = -\frac{\alpha}{1-\alpha}\mathbf{F}^{-}(\widetilde{\mathbf{x}}).$$

Thus, the point $\widetilde{\mathbf{x}}$ *can be reached in a finite time from a suitable initial condition outside* Σ*, but in an infinite time from the sliding vector field* $\mathbf{F}^{s}$*.*

Remark 2.4. *To investigate the stability of the equilibria of a smooth vector field* $\mathbf{F}^{i}$ *(where* $i = +, -, s$*) we use the classical theory of smooth dynamical systems; see [77, 86].*

2.4 Sliding vector field dynamics

Consider in system (2.2) the vector fields as $\mathbf{F}^{\pm} = (f_1^{\pm}, f_2^{\pm}, f_3^{\pm})$. Assume with no loss generality that the switching boundary of (2.2) is

$$\Sigma = \{(x, y, z) \in \mathbb{R}^3 : h(x, y, z) = z = 0\}.$$

This is possible from a local coordinate change of the form $(x', y', z') = (x, y, h(x, y, z))$. Then, the sliding vector field of (2.2) is calculated by (2.9) and expressed in coordinates $\mathbf{x} = (x, y, z)$ as

$$\mathbf{F}^{s}(\mathbf{x}) = \frac{1}{(f_3^{-} - f_3^{+})(\mathbf{x})} \begin{bmatrix} (f_1^{+} f_3^{-} - f_1^{-} f_3^{+})(\mathbf{x}) \\ (f_2^{+} f_3^{-} - f_2^{-} f_3^{+})(\mathbf{x}) \\ 0 \end{bmatrix}.$$

Associated with $\mathbf{F}^{s}$ there exists the desingularized sliding vector field:

$$\mathbf{F}^{as}(x, y) = \begin{bmatrix} (f_1^{+} f_3^{-} - f_1^{-} f_3^{+})(x, y) \\ (f_2^{+} f_3^{-} - f_2^{-} f_3^{+})(x, y) \end{bmatrix},$$

for all $\mathbf{x} \in \Sigma_{as}$. Note that $(f_3^{-} - f_3^{+})(\mathbf{x}) > 0$ if $\mathbf{x} \in \Sigma_{as}$, so that $\mathbf{F}^{as}$ has the same vector orientation as $\mathbf{F}^{s}$;

$$\left(\frac{dx}{d\tau}, \frac{dy}{d\tau}\right) = \mathbf{F}^{as}(x, y), \tag{2.10}$$

and

$$\left(\frac{dx}{dt}, \frac{dy}{dt}, \frac{dz}{dt}\right) = \mathbf{F}^s(x, y, 0), \tag{2.11}$$

have the same phase portrait in Σ_{as}; and it can be C^r-extended to the closure $\overline{\Sigma_{as}}$ of Σ_{as}[3] (see [92, 117]).

We can take advantage of the invariance of Σ under the flow determined by $\mathbf{F}^s$ and reduce the dimension of the problem by one, taking $z = 0$. So, all the analysis of the attractive sliding dynamics contained in this thesis is based on the two-dimensional system (2.10) such that the time scale is redefined implicitly on every solution, by writing

$$dt = |(f_3^- - f_3^+)(x, y, 0)|d\tau,$$

whenever $(f_3^- - f_3^+)(x, y, 0) > 0$.

Obviously, systems (2.10) and (2.11) are topologically equivalent for all $(x, y, 0) \in \Sigma_{as}$, since their orbits are identical and it is the velocity of the motion that makes them different, i.e., the systems are distinguished only by the time parametrization along the orbits; see [77], page 42.

Remark 2.5. *If $\widetilde{\mathbf{x}} = (\widetilde{x}, \widetilde{y}, 0) \in \Sigma_{as}$ is a pseudo-equilibrium point of* (2.2)*, then $(\widetilde{x}, \widetilde{y})$ is a standard equilibrium point of* (2.10)*. We study the stability of* (2.2) *at $\widetilde{\mathbf{x}}$ from the two-dimensional system* (2.10) *at $(\widetilde{x}, \widetilde{y})$.*

Remark 2.6. *If T_- and T_+ are transversal at $\widehat{\mathbf{x}} = (\widehat{x}, \widehat{y}, 0)$ (a double tangency point of* (2.2)*), then $f_3^-(\widehat{\mathbf{x}}) = f_3^+(\widehat{\mathbf{x}}) = 0$ and so $(\widehat{x}, \widehat{y})$ is an equilibrium point of* (2.10)*. The interesting point here is that the sliding dynamics described by $\dot{\mathbf{x}} = \mathbf{F}^s(\mathbf{x})$ is not defined at $\widehat{\mathbf{x}} = (\widehat{x}, \widehat{y}, 0)$. However, this point governs the sliding dynamics around it, acting as a true equilibrium point from the analysis of the system* (2.10)*. In this case, we assume that $\mathbf{F}^s$ is C^r-extended to a full neighborhood of $\widehat{\mathbf{x}}$ in Σ and that $\widehat{\mathbf{x}}$ is an equilibrium point of this vector field, see [117].*

[3] Similarly, we define $\mathbf{F}^{rs}(x, y) = -\mathbf{F}^{as}(x, y)$ for all $\mathbf{x} \in \Sigma_{rs}$ and the repulsive sliding dynamics is described by $\left(\frac{dx}{d\tau}, \frac{dy}{d\tau}\right) = \mathbf{F}^{rs}(x, y)$.

2.5 Discontinuous-induced bifurcations

The classical bifurcations of smooth dynamical systems (saddle-node, transcritical, Hopf, etc., see, for instance [65, 77, 89, 119]) also occur in DPWS systems. In addition, DPWS systems exhibt other bifurcations that do not appear on smooth systems, known in the literature as *Discontinuous-Induced Bifurcations* (DIBs), see [37, 82]. The DIBs are unique bifurcations of PWS systems. Such bifurcations occur when an invariant set of the system (equilibrium point, limit cycle, etc) crosses or touches tangentially the switching boundary Σ in state space; see [24, 35, 38, 40, 41, 44] and references therein.

An overview of the current state of the art in the analysis of DIBs of piecewise-smooth systems is found in [42]. This reference presents a classification of the most common types of DIBs involving non-trivial interactions of the equilibria of flows (and fixed points of maps) with the manifolds in state space where the system is non-smooth.

We highlight the DIB so-called *Boundary Equilibrium Bifurcation* (BEB). Boundary equilibrium points represent intermediate situations between real and virtual equilibrium points; see Figure 2.7. The topological changes from real to virtual equilibrium points (or vice versa), due to changes in some system parameter, can lead to a BEB; see [45, 60, 78]. There are others DIBs, such as the *Grazing bifurcation* of limit cycles, that occurs when a limit cycle intersects tangentially a switching boundary, and *Sliding bifurcations* of limit cycles that occur when a limit cycle develops an intersection (tangential or transversal) with a sliding region; see [35, 36, 43].

A new bifurcation, typical of 3D-DPWS systems, has recently drawn attention to its variety of unfolded dynamics and its *compound*[4] bifurcation characteristic; see [26, 29, 30, 49]. This bifurcation occurs at a T-singularity and involves simultaneously a pseudo-equilibrium

[4]We say that the TS-bifurcation is a compound bifurcation since it is associated with a bifurcation of the sliding vector field and a bifurcation of the first return map, occurring simultaneously at the same point. See Chapter 4.

transition from Σ_{as} to Σ_{rs} (or vice versa) and the birth of a non-smooth limit cycle in $\mathbb{R}^3$-space, composed of two segments of orbits, one for each vector field $\mathbf{F}^+$ and $\mathbf{F}^+$, transversely intersecting the switching boundary Σ at two crossing points, one point on Σ_c^+ and the other on Σ_c^-. We name such a phenomenon *TS-bifurcation*; and the limit cycle that arises from this bifurcation, we call it *crossing limit cycle* (CLC); see Figure 2.8. In this thesis we consider the TS-bifurcation as a DIB, as well as other bifurcations that occur due to the presence of the discontinuity manifold.

In the next two subsections, let us give a brief introduction on the *BEB* and the *TS* bifurcations. For this, consider the system (2.2) conditioned to the parameter $\mu \in (-\varepsilon, \varepsilon)$, written as

$$\dot{\mathbf{x}} = \begin{cases} \mathbf{F}^-(\mathbf{x}, \mu), & \text{if } h(\mathbf{x}, \mu) < 0, \\ \mathbf{F}^+(\mathbf{x}, \mu), & \text{if } h(\mathbf{x}, \mu) > 0, \end{cases} \tag{2.12}$$

so that the state space is composed of $\Sigma(\mu) = \{\mathbf{x} \in \mathbb{R}^3 : h(\mathbf{x}, \mu) = 0\}$, $R^-(\mu) = \{\mathbf{x} \in \mathbb{R}^3 : h(\mathbf{x}, \mu) < 0\}$ and $R^+(\mu) = \{\mathbf{x} \in \mathbb{R}^3 : h(\mathbf{x}, \mu) > 0\}$. Finally, we deal with bifurcations of the sliding vector field (sliding bifurcations).

2.5.1 On boundary equilibrium bifurcations

The appearance of a boundary equilibrium in a DPWS system represent a codimension-one DIB known as BEB. A BEB is classified according to two possible scenarios [37, 93], that take into account only the positions of the equilibria involved in relation to the boundaries of their respective vector fields:

(i) The *persistence* scenario is observed when a natural equilibrium turns into a pseudo-equilibrium. In this case, if the natural equilibrium is real (resp. virtual), then the pseudo-equilibrium is virtual (resp. real).

(ii) The *nonsmooth fold* scenario is observed when both a natural

equilibrium and a pseudo-equilibrium collide and disappear. In this case, if the natural equilibrium is real (resp. virtual), then the pseudo-equilibrium is also.

Each of them can present varied dynamic phenomena from the combination of stability and dynamics of the equilibria involved.

In Figure 2.7 we visualize the persistence and nonsmooth scenarios described above, with respect to the system (2.12). For this, we assume that $\overline{\mathbf{x}}(\mu)$ is an equilibrium related to vector field $\mathbf{F}^-$ and $\widetilde{\mathbf{x}}(\mu)$ a pseudo-equilibrium, both continually dependent on μ. In the persistence scenario, for $\mu < 0$, we have that $\overline{\mathbf{x}}$ is real and $\widetilde{\mathbf{x}}$ is virtual, that is, $\overline{\mathbf{x}} \in R^-$ and $\widetilde{\mathbf{x}} \in \Sigma_c^-$; for $\mu = 0$, they collide giving rise to a boundary equilibrium at the point of collision $\overline{\mathbf{x}}(0) = \widetilde{\mathbf{x}}(0) = \mathbf{0} \in T_-$; for $\mu > 0$, the equilibrium $\overline{\mathbf{x}}$ becomes virtual and $\widetilde{\mathbf{x}}$ becomes real, that is, $\overline{\mathbf{x}} \in R^+$ and $\widetilde{\mathbf{x}} \in \Sigma_{as}$. In the nonsmooth fold scenario, for $\mu < 0$, we have that both $\overline{\mathbf{x}}$ and $\widetilde{\mathbf{x}}$ are real; for $\mu = 0$, they collide giving rise to a boundary equilibrium at $\mathbf{0} \in T_-$; for $\mu > 0$, both $\overline{\mathbf{x}}$ and $\widetilde{\mathbf{x}}$ become virtual.

To distinguish between the persistence and nonsmooth fold scenarios, we use the BEB-Theorem[5] found in [45, 93], which is given below.

Theorem 2.1. *Assume that for $\mu = 0$, an equilibrium branch of the vector field $\mathbf{F}^-(\mathbf{x}, \mu)$ crosses the switching boundary $h(\mathbf{x}, \mu) = 0$ at the origin, this point being regular, that is, $A = D_{\mathbf{x}}\mathbf{F}^-(0,0)$ is a nonsingular matrix. Furthermore, suppose that the crossing is transversal, that is, if $M = D_\mu \mathbf{F}^-(0,0)$, $N = D_\mu h(0,0)$ and $C^T = D_{\mathbf{x}} h(0,0)$, then*

$$\frac{d}{d\mu} h(\overline{\mathbf{x}}(\mu), \mu)\Big|_{\mu=0} = N - C^T A^{-1} M \neq 0,$$

and the nondegeneracy condition $C^T A^{-1} B \neq 0$, where $B = \mathbf{F}^+(0,0)$, is satisfied. The following statements hold:

(a) *The persistence scenario occurs if $C^T A^{-1} B > 0$.*

[5]The Proof is given in the cited references.

(b) *The nonsmooth fold scenario occurs if* $C^T A^{-1} B < 0$.

Furthermore, it was also proved that if the vector field of reference is $\mathbf{F}^+$, then, the persistence scenario occurs if $C^T A^{-1} B < 0$ and nonsmooth fold if $C^T A^{-1} B > 0$.

Collisions of equilibria with boundaries have been the subject of investigation of many works in the last years and they have been identified in mathematical models of a wide variety of physical systems; see for instance [13, 75, 90, 102, 114, 126]. For two-dimensional DPWS systems there is a complete classification of the BEBs and their unfolding, see [22, 35, 45, 51, 60, 64, 67, 78]. For three-dimensional DPWS systems, the BEBs present a greater complexity of phenomena, with many possible geometric combinations. We still do not find a classification in the literature that is similar to the two-dimensional systems for the three-dimensional ones, although there are recent studies focused on the study of phenomena linked to BEBs as, for example, [19, 29, 61, 62, 104, 105].

In Chapter 7 of this thesis, we give the starting point for the classification of BEBs in 3D-DPWS systems from a proposed canonical form to a typical family of these systems, where we present a two-parameter analysis of the BEBs and sliding dynamics. In addition, we provide the conditions on the system parameters under study for a BEB to occur, classifying them into BEB persistence or nonsmooth fold. Also, we give a complete description of the sliding dynamics. The results obtained are applied in two practical examples involving the sliding mode control of buck power converters.

2.5.2 On the TS-bifurcation

The TS-bifurcation in 3D-DPWS systems is a codimension-one local DIB. Figure 2.8 shows some of the possible scenarios of the TS-bifurcation. In Figure 2.8(a) we have supercritical cases, where a stable pseudo-node in Σ_{as} for $\mu < 0$ crosses the T-singularity becoming a

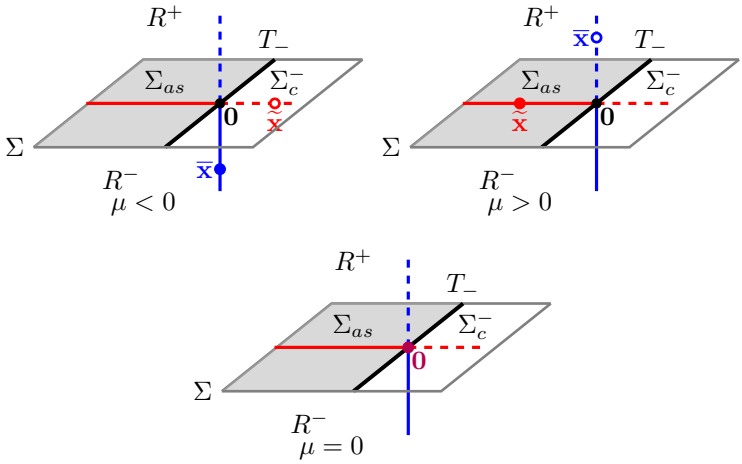

(a) Persistence case.

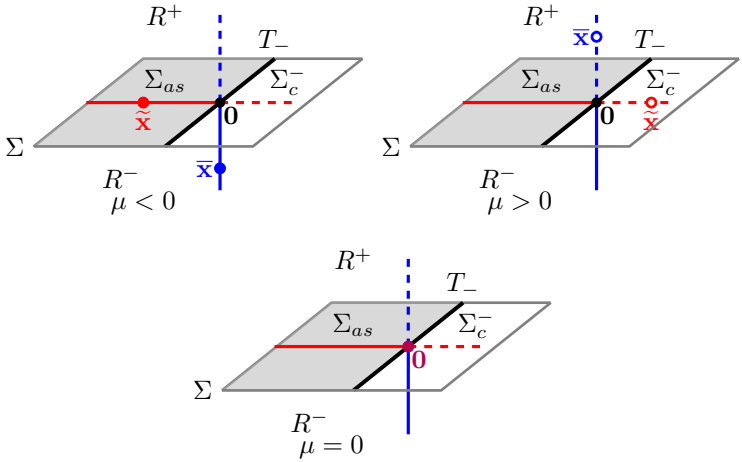

(b) Nonsmooth fold case.

Figure 2.7: Illustrative scenarios of boundary equilibrium bifurcations. The blue line represents the branch of natural equilibria and the red line represents the branch of pseudo-equilibria, being that the real is in the solid part and the virtual is in the dashed part. The point $\mathbf{0}$ is a cusp for $\mu \neq 0$ and a boundary equilibrium for $\mu = 0$.

pseudo-saddle in Σ_{rs} for $\mu > 0$. In Figure 2.8(b) we have subcritical cases, where an unstable pseudo-node in Σ_{rs} for $\mu < 0$ crosses the T-singularity becoming a pseudo-saddle in Σ_{as} for $\mu > 0$. In both supercritical and subcritical cases, the CLC that arises along with a pseudo-node has saddle dynamics, while the CLC that arises along with a pseudo-saddle can have a node or a focus dynamics, stable or unstable. For more details, see Chapter 4.

Below, we give a definition for the TS-bifurcation in 3D-DPWS systems, from simple topological conditions on Σ.

Definition 2.10. *3D-DPWS system* (2.12) *undergoes a TS-bifurcation for* $\mu = 0$*, if there is a two-fold point* $\widehat{\mathbf{x}}(\mu)$ *and a pseudo-equilibrium point* $\widetilde{\mathbf{x}}(\mu)$*, defined for all* $\mu \in (-\varepsilon, \varepsilon)$*, such that* $\widetilde{\mathbf{x}}(0) = \widehat{\mathbf{x}}(0)$ *and*

$$\frac{d}{d\mu} L_{\mathbf{F}^+} h(\widetilde{\mathbf{x}}(\mu), \mu) \frac{d}{d\mu} L_{\mathbf{F}^-} h(\widetilde{\mathbf{x}}(\mu), \mu)\Big|_{\mu=0} < 0, \tag{2.13}$$

along with

$$L^2_{\mathbf{F}^+} h(\widehat{\mathbf{x}}(0), 0) < 0, \quad L^2_{\mathbf{F}^-} h(\widehat{\mathbf{x}}(0), 0) > 0. \tag{2.14}$$

Note that $L_{\mathbf{F}^+} h(\widetilde{\mathbf{x}}(0), 0) = L_{\mathbf{F}^-} h(\widetilde{\mathbf{x}}(0), 0) = 0$, because $\widetilde{\mathbf{x}}(0) = \widehat{\mathbf{x}}(0)$ is a two-fold point. Condition (2.13) indicates that, for $\mu \neq 0$, the functions $L^+(\mu) = L_{\mathbf{F}^+} h(\widetilde{\mathbf{x}}(\mu), \mu)$ and $L^-(\mu) = L_{\mathbf{F}^-} h(\widetilde{\mathbf{x}}(\mu), \mu)$ have opposite signs, and its graphs are transversal at $\mu = 0$. Therefore, $\widetilde{\mathbf{x}}(\mu) \in \Sigma_{rs}(\mu)$ for $\mu < 0$ (or the opposite) and $\widetilde{\mathbf{x}}(\mu) \in \Sigma_{as}(\mu)$ for $\mu > 0$ (or the opposite). Condition (2.14) ensures that the two-fold $\widehat{\mathbf{x}}$ is of the invisible type for $\mu = 0$, i.e., $\widehat{\mathbf{x}}(0) = \widetilde{\mathbf{x}}(0)$ is a T-singularity. For a small perturbation in the parameter μ, from the critical value $\mu = 0$, we can ensure that $\widehat{\mathbf{x}}(\mu)$ remains a T-singularity for $|\mu| \neq 0$.

The TS-bifurcation exhibits different dynamic scenarios with a total of ten possible combinations between the types of dynamics involving the pseudo-equilibrium and the CLC. All these scenarios are completely studied in [26] and revised in Chapter 4, where we given the local conditions for the occurrence of each one. The Chapters 4, 5 and 6 are devoted to the study of TS-bifurcation and the consequences

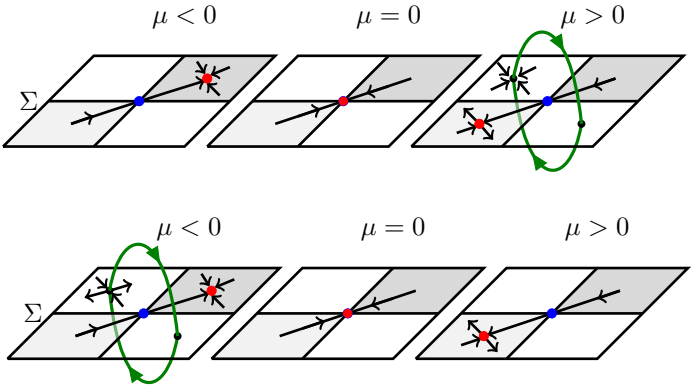

(a) Supercritical cases: (above) for $\mu > 0$ there appears a pseudo-saddle in Σ_{rs} along with a stable CLC of node dynamics; (below) the stable pseudo-node in Σ_{as} along with an unstable CLC of saddle dynamics that exists for $\mu < 0$ disappears for $\mu > 0$.

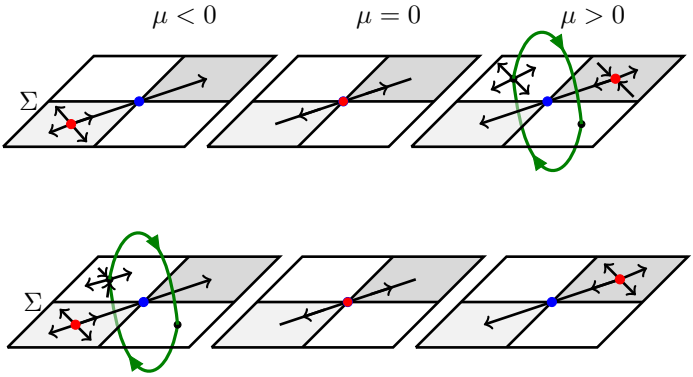

(b) Subcritical cases: (above) for $\mu > 0$ there appears a pseudo-saddle in Σ_{as} along with an unstable CLC of node dynamics; (below) the unstable pseudo-node in Σ_{rs} along with an unstable CLC of saddle dynamics that exists for $\mu < 0$ and disappears for $\mu > 0$.

Figure 2.8: Some possible scenarios for the TS-bifurcation. (a) supercritical cases; (b) subcritical cases. The blue point is the T-singularity, the red point is the pseudo-equilibrium, light gray region is Σ_{rs}, dark grey region is Σ_{as}, white regions are $\Sigma_c^{\pm}$ and the (non-smooth) limit cycle in green-color is the CLC.

on the dynamics of the system produced by it.

In Chapter 5, we present a case study on TS-bifurcation and its implications on the dynamics of a power electronics control system, where we determine the existence, the stability and some global bifurcations of CLCs created in the T-singularity. This study is based on the numerical analysis of the solution of *closing equations* and the characteristic multipliers associated to the first return map; see [3, 20, 77, 117].

In Chapter 6, we study a degenerate case of TS-bifurcation in which the T-singularity is non regular at the critical value $\mu = 0$ of the bifurcation parameter. In this case, the T-singularity is classified as 1-degenerate invisible two-fold (Q2 singularity in [118]), that is, the tangency lines T_+ and T_- of invisible folds touch the T-singularity with quadratic contact. This bifurcation is characterized by the simultaneous collision between a pair of regular T-singularities and a *real* pseudo-equilibrium point, such that the pseudo-equilibrium persists but the pair of T-singularities disappear after the collision, determining a pitchfork bifurcation in the sliding dynamics. We named this bifurcation *double TS-bifurcation*. Moreover, we present a case study on stability and bifurcations of CLCs created from a degenerate T-singularity.

2.5.3 Bifurcations in the sliding vector field

For 3D-DPWS systems as (2.12), the sliding dynamics is investigated from a two-dimensional sliding vector field, which is smooth at all points of attractive/repulsive sliding region. Thus, we can use the known tools of the bifurcation theory for two-dimensional smooth systems. In addition, the sliding vector field can display the classical bifurcations of equilibria and limit cycles. See references [2, 77, 88, 89].

We call the bifurcations that occur in sliding vector field as *sliding bifurcations*. In all chapters of this thesis we will study local sliding bifurcations such as saddle-node, transcritical, pitchfork and Hopf. Detailed applied studies on sliding bifurcations in power electronics, such

as the transcritical, saddle-node, Hopf, Bogdanov-Takens, homoclinic, and their pecularities due to the boundaries of the sliding region, are found in [28, 29, 98]. We also cite the works [70, 118, 124], which contain important results on sliding bifurcations at a double tangency point, being that the most interesting case is when this double tangency is of the T-singularity type.

In Chapter 3 we will carry out a case study, from the dc-dc boost converter model with SMC-washout, on the Hopf bifurcation of sliding vector field. Furthermore, we will show that the limit cycle that is born in the Hopf bifurcation disappears when it touches the two-fold point of the invisible-visible type, creating a homoclinic loop closes at this two-fold point. Such a mechanism of vanishing of this limit cycle is natural, since the a two-fold is a saddle equilibrium of the sliding vector field.

2.6 Power converters and control

One of the emerging topics in electrical engineering is the efficient design of dc-dc power converters, nowadays based in the extensive use of discontinuous models. The discontinuous character of these models comes from their implementation by means of electronic switches that are designed to be permanently changing between its *on* and *off* states. In each configuration, the device has behavior (approximately) linear and, thus, we are naturally dealing with piecewise-linear dynamical systems (DPWL systems).

Examples of dc-dc power converters are: *buck*, *boost*, *buck-boost*, *Cúk*, *Zeta*; where the control action is constituted by a single switch acting as a control input, see [108] and references therein. In the case of boost converters, for example, the goal is to pass from a low voltage to a higher voltage needed to feed some particular load device.

In this Section we present the boost converter model under a sliding mode control strategy using a washout filter, which is described

by a 3D-DPWL system. This system will be studied in Chapters 3, 4 and 5.

2.6.1 Modelling of the dc-dc boost converter

The behavior of a dc-dc boost converter can be studied using the circuit topology depicted in Figure 2.9. We consider some simplifying hypotheses for this circuit: (i) the semiconductor devices are assumed to be ideal, i.e., free of loss and state switching at time zero; (ii) the capacitor is considered ideal, i.e., it has no loss or self-inductance; (iii) the inductor has only one resistor and one series inductance that can be considered constant. Using the Kirchhoff's circuit laws, the dynamic model of the system, operating in Continuous[6] Conduction Mode (CCM), is given by

$$\begin{aligned} L\frac{di_L}{dt} &= V_{\text{in}} - r_L i_L - u v_C, \\ C\frac{dv_C}{dt} &= u i_L - \frac{v_C}{R}, \end{aligned}$$

where $v_C \geq 0$ is the capacitor voltage, $i_L > 0$ is the inductor current and $u = 1-q \in \{0,1\}$ is the control action, representing the two possible positions of the electronic switch S, open when $u = 1$ ($q = 0$), closed when $u = 0$ ($q = 1$). The variable V_{in} represents the input voltage, r_L gives the equivalent series resistance of the inductor, R is the resistive load, C and L are the circuit's capacitor and inductor, respectively.

The analysis of the model becomes easier if the system is normalized as follows: take a new time τ such that $t = \tau\sqrt{LC}$, and introduce the new variables

$$(x, y) = \left(\frac{i_L}{V_{\text{in}}}\sqrt{\frac{L}{C}}, \frac{v_C}{V_{\text{in}}} \right),$$

[6] In power electronics, this *continuous* qualifier makes reference to the fact that the current is not allowed to be zero, nothing to do with the continuity of the vector field. In this case, the converter operates with a non-null inductance current at any time, i.e. $i_L > 0$.

and parameters

$$b = r_L\sqrt{\frac{C}{L}} \quad \text{and} \quad a = \frac{1}{R}\sqrt{\frac{L}{C}};$$

thus, obtaining the boost converter model in dimensionless normal form

$$\dot{x} = 1 - bx - uy \tag{2.15}$$

$$\dot{y} = ux - ay, \tag{2.16}$$

for $x > 0$ and $y \geq 0$, where $u = \{0, 1\}$, $b > 0$ (it can be considered in some cases $b = 0$, i.e., with ideal inductance) and $a > 0$.

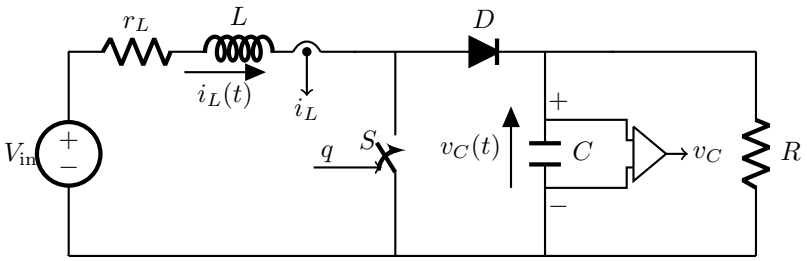

Figure 2.9: Topology of a dc-dc *boost* converter.

Note that for $u = 0$, the system has a stable equilibrium point at $(x, y) = (1/b, 0)$, and since b is usually rather small, this leads to a big current with zero voltage, which is completely undesirable. Otherwise, for $u = 1$, the *standard* stable equilibrium point appears at

$$(x, y) = \left(\frac{a}{1+ab}, \frac{1}{1+ab}\right),$$

where the asymptotic value achieved for y is $1/(1 + ab) < 1$.

Our goal is, by the use of an adequate and repeated interchange between these two possibles values of u, to *boost* the voltage across the load looking for a pseudo-equilibrium point with $y = y_r$, where $y_r > 1$ is the desired normalized reference voltage. Although it is theoretically

possible to keep the problem in this two-dimensional setting, the use of a third state variable turns to be a more efficient approach, as explained below.

2.6.2 Adding the washout filter and the sliding mode controller

We will introduce a *washout* filtering process for the current in the inductor, as illustrated in Figure 2.10(a), see [112] and references therein. Such washout filter works as a high pass filter that blocks steady state inputs while passing transient inputs, and it leads to a new state variable z_F. The filtered value of i_L can be written as $i_L - z_F$ where z_F satisfies the dynamic equation

$$\frac{dz_F}{dt} = \omega_F(i_L - z_F), \tag{2.17}$$

and ω_F is the parameter responsible for cut-off frequency of the filter, being that it is always less than $1/\sqrt{LC}$ rad/s which is the approximate natural frequency of the system.

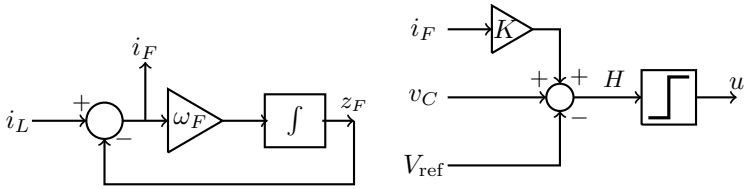

(a) Washout filter. (b) Sliding mode controller.

Figure 2.10: Control diagram. The control law is $u = \frac{1}{2}(1 + \text{sign}[H])$ and the filtered inductor current given by $i_F = i_L - z_F$ represents the difference between the inductor current i_L and the filtered signal z_F.

For the creation of the desired operating (pseudo-equilibrium) point with $v_C = V_{\text{ref}} > V_{\text{in}}$ we use a sliding mode controller. For this, we choose (see [91]) an appropriate scalar function $H : \mathbb{R}^3 \to \mathbb{R}$,

namely

$$H(i_L, v_C, z_F) = v_C - V_{\text{ref}} + K(i_L - z_F),$$

where $K > 0$ and V_{ref} are, respectively, the control parameter (to be adequately tuned) and the reference voltage parameter. Now we have to impose a control law as follows: to keep open the switch ($u = 1$) while $H(i_L, v_C, z_F) > 0$ and to keep it closed ($u = 0$) whenever $H(i_L, v_C, z_F) < 0$, see Figure 2.10(b).

We also apply a normalization to the washout filter equation (2.17), taking the new variable and parameter:

$$\overline{z} = \frac{z_F}{V_{\text{in}}}\sqrt{\frac{L}{C}} \quad \text{and} \quad \omega = \omega_F\sqrt{LC},$$

respectively; and, then we obtain

$$\dot{\overline{z}} = \omega(x - \overline{z}). \tag{2.18}$$

In addition, we defined the switching boundary as

$$\Sigma = \{(x, y, \overline{z}) \in \mathbb{R}^3 : h(x, y, \overline{z}) = y - y_r + k(x - \overline{z}) = 0\}, \tag{2.19}$$

where

$$k = K\sqrt{\frac{C}{L}} \quad \text{and} \quad y_r = \frac{V_{\text{ref}}}{V_{\text{in}}}$$

are, respectively, the normalized parameters of control and reference voltage; and such that $h(x, y, \overline{z}) = H(i_L, v_C, z_F)/V_{\text{in}}$.

To improve the visualization of phase portraits and simplify the calculations a little more, we introduced another variable change to rewrite the switching boundary (2.19) as a horizontal plane. Such a form is obtained by defining

$$z = y - y_r + k(x - \tilde{z}),$$

and so the washout filter normalized equation (2.18) is rewrite as

$$\dot{z} = (u - kb)x + (\omega - a - uk)y - \omega z + k - \omega y_r. \tag{2.20}$$

In this case, the switching boundary is the horizontal plane given by

$$\Sigma = \{(x, y, z) \in \mathbb{R}^3 : h(x, y, z) = z = 0\}$$

and the control variable is

$$u = \frac{1}{2}(1 + \text{sign}[z]). \tag{2.21}$$

Then, we get the control process normalized model described as the 3D-DPWL system given by

$$\dot{\mathbf{x}} = \begin{cases} \mathbf{F}^+(\mathbf{x}), \text{ if } z > 0, \\ \mathbf{F}^-(\mathbf{x}), \text{ if } z < 0, \end{cases} \tag{2.22}$$

$$\mathbf{F}^+(\mathbf{x}) = \begin{bmatrix} 1 - bx - y \\ x - ay \\ f_3^+(\mathbf{x}) \end{bmatrix}, \quad \mathbf{F}^-(\mathbf{x}) = \begin{bmatrix} 1 - bx \\ -ay \\ f_3^-(\mathbf{x}) \end{bmatrix},$$

where $\mathbf{x} = (x, y, z)$ and

$$f_3^+(\mathbf{x}) = (1 - kb)x + (\omega - a - k)y - \omega z + k - \omega y_r,$$
$$f_3^-(\mathbf{x}) = -kbx + (\omega - a)y - \omega z + k - \omega y_r.$$

The sliding vector field on Σ associated to the system (2.22) is calculated according to (2.9), obtaining

$$\mathbf{F}^s(x, y, 0) = \frac{1}{ky - x} \begin{bmatrix} bx^2 - x + ay^2 - \omega y(y - y_r) \\ -k(bx^2 - x + ay^2) + \omega x(y - y_r) \\ 0 \end{bmatrix}, \tag{2.23}$$

provided that $ky - x \neq 0$. The desired operating point for boost converter is one of the pseudo-equilibria $\widetilde{\mathbf{x}}^{\pm} = (\widetilde{x}^{\pm}, y_r, 0)$, where

$$\widetilde{x}^{\pm} = \frac{1 \pm \sqrt{1 - 4aby_r^2}}{2b} > 0,$$

for all $a \leq \frac{1}{4by_r^2}$. In some cases, we can consider ideal inductance with $b = 0$ ($r_L = 0$). Thus, there is a single pseudo-equilibrium, namely $\widetilde{\mathbf{x}} = \big(ay_r^2, y_r, 0\big)$.

More details on the dynamics of the boost converter with SMC-Washout are given in the Chapter 5.

For the implementation of the proposed sliding mode control, we must replace the *signal* function in the control law (2.21) by the *hysteresis* function; see [47]. In this case

$$u = \begin{cases} 1\,, & \text{if} \quad z > -\varepsilon \\ 0\,, & \text{if} \quad z < \varepsilon \end{cases}, \tag{2.24}$$

for some $\varepsilon > 0$ chosen in order to be small. The hysteresis works as follows: a trajectory with $u = 1$ holds this value until it reaches the plane $z = -\varepsilon$, then switch to $u = 0$; in the continuation, a trajectory with $u = 0$ holds this value until it reaches the plane $z = \varepsilon$, then switch to $u = 1$; see Figure 2.11.

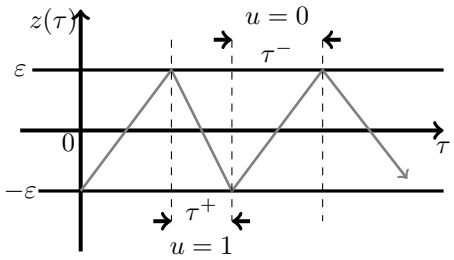

Figure 2.11: Behavior illustrative of the evolution of the variable z over time t, when there is sliding with hysteresis.

Considering Figure 2.11, then for $u = 1$ we have $\dot{z}^+ = -2\varepsilon/\tau^+ < 0$ and for $u = 0$ we have $\dot{z}^- = 2\varepsilon/\tau^- > 0$, where $\tau^{\pm} > 0$ are the respective time for each mode. Note that $\dot{z}^{\pm} = L_{\mathbf{F}^{\pm}} h(\mathbf{x})$, therefore we can write

$L_{\mathbf{F}^+}h(\mathbf{x}) = -2\varepsilon/\tau^+ < 0$ and $L_{\mathbf{F}^-}h(\mathbf{x}) = 2\varepsilon/\tau^- > 0$. In this case, there is an α according to equation (2.8), with $0 < \alpha < 1$ and

$$\alpha = \frac{\tau^+}{\tau^+ + \tau^-},$$

so that the *Filippov* sliding vector field (2.7) can be written as the *average* vector field

$$\mathbf{F}^s(\mathbf{x}) = \frac{\tau^-\mathbf{F}^-(\mathbf{x}) + \tau^+\mathbf{F}^+(\mathbf{x})}{\tau^- + \tau^+}.$$

Figure 2.12 shows simulation results of the sliding vector field (2.23) along with the complete system with hysteresis (2.15), (2.16), (2.20) and (2.24). In 2.12(a) we visualize the time response referring to the normalized variables of voltage ($y(\tau)$) and current ($x(\tau)$). Observe the permanent oscillations centered on the reference value $y = y_r$ (and also at $x = x_r$) indicating the presence of a limit cycle around the operating point (see illustration from (y, z)-plane in 2.12(b)). In 2.12(b) the sliding dynamics is visualized in the (x, y)-plane, where the trajectory in black color is the solution $(x(\tau), y(\tau))$ of $\dot{\mathbf{x}} = \mathbf{F}^s(x, y, 0)$ and in green color is the solution $(x(\tau), y(\tau))$ of the complete system with hysteresis, for the same initial condition $(x(0), y(0), z(0)) = (1, 1, 0)$. Note that the solution of $\dot{\mathbf{x}} = \mathbf{F}^s(x, y, 0)$ is the average solution of the complete system with hysteresis. In fact, since we can define two sliding vector fields, one on the plane $z = \varepsilon$ and another on the plane $z = -\varepsilon$, namely

$$\mathbf{F}^s(x, y, \varepsilon) = \mathbf{F}^s(x, y, 0) + \varepsilon\mathbf{G}(x, y, 0),$$
$$\mathbf{F}^s(x, y, -\varepsilon) = \mathbf{F}^s(x, y, 0) - \varepsilon\mathbf{G}(x, y, 0),$$

where $\mathbf{G}(x, y, 0) = \frac{\omega}{ky - x}\begin{bmatrix} y & -x & 0 \end{bmatrix}^T$, then

$$\mathbf{F}^s(x, y, 0) = \frac{1}{2}\left(\mathbf{F}^s(x, y, \varepsilon) + \mathbf{F}^s(x, y, -\varepsilon)\right).$$

Remark 2.7. *In this thesis, all simulation results of 3D-DPWS sys-*

tems, such as the boost converter with SMC-Washout, are taken with the application of a small hysteresis range. Thus, the sliding dynamics is induced and it arises naturally when a trajectory of the system reaches the attractive sliding region on the switching boundary. Therefore, the operating point is, actually, a (non-smooth) limit cycle with small amplitude around the pseudo-equilibrium point, see Figure 2.12.

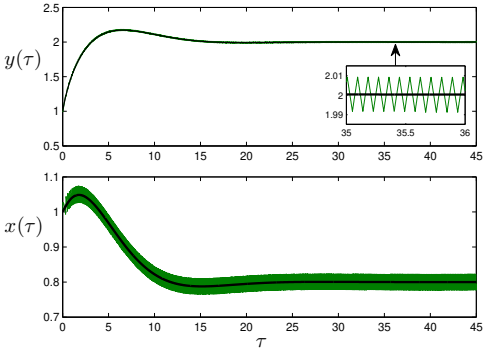

(a) Simulation in time.

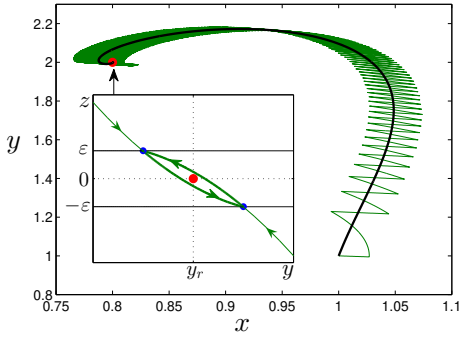

(b) Simulation in state space.

Figure 2.12: Comparison between the ideal (in black color) and hysteresis (in green color) sliding dynamics, referring to the SMC-Washout boost converter system (2.22). Parameters: $b = 0$, $\omega = 1$, $y_r = 2$, $k = 5$ and $a = 1/5$. The red dot indicates the pseudo-equilibrium located at $\widetilde{\mathbf{x}} = (0.8, 2, 0)$. Hysteresis range: $\varepsilon = 1/10$.

2.6.3 A brief description on sliding mode control

Discontinuous feedback control systems as the sliding mode control (SMC) have been exhaustively explored in many works, see [123] and references therein. The sliding mode controllers are naturally suitable for switched systems such as dc-dc power converters, see [108] and references therein. Such systems are efficient for controlling complex non-linear dynamic plants operating under uncertainty conditions, which is a common problem for many technology processes.

We consider the affine control system

$$\dot{\mathbf{x}} = \mathbf{f}(\mathbf{x}) + \mathbf{g}(\mathbf{x})u \tag{2.25}$$

where $\mathbf{x} \in \mathbb{R}^n$ and the functions $\mathbf{f}(\mathbf{x})$ and $\mathbf{g}(\mathbf{x}) \neq 0$ are smooth and the control signal u is supposed to be a scalar discontinuous function. We assume a smooth non-constant scalar function $h : \mathbb{R}^n \to \mathbb{R}$ that defines the switching boundary (*discontinuity manifold*)

$$\Sigma = \{\mathbf{x} \in \mathbb{R}^n : h(\mathbf{x}) = 0\},$$

is supposed to be regular, that is, $\nabla h(\mathbf{x}) \neq 0, \forall \mathbf{x} \in \Sigma$, and splitting the state space into two open regions $R^- = \{\mathbf{x} \in \mathbb{R}^n : h(\mathbf{x}) < 0\}$ and $R^+ = \{\mathbf{x} \in \mathbb{R}^n : h(\mathbf{x}) > 0\}$. Accordingly, the switching control law is u, namely as

$$u = u(\mathbf{x}) = \begin{cases} u^-(\mathbf{x}), \text{ if } h(\mathbf{x}) < 0, \text{ i.e. } \mathbf{x} \in R^-, \\ u^+(\mathbf{x}), \text{ if } h(\mathbf{x}) > 0, \text{ i.e. } \mathbf{x} \in R^+, \end{cases} \tag{2.26}$$

where u^- and u^+ are scalar smooth functions of $\mathbf{x}$ (typically constant ones) to be later specified. System (2.25) endowed with the control law (2.26) constitutes a discontinuous dynamical system that, depending on the state, uses one of the two different smooth vector fields

$$\mathbf{F}^{\pm}(\mathbf{x}) = \mathbf{f}(\mathbf{x}) + \mathbf{g}(\mathbf{x})u^{\pm}(\mathbf{x}). \tag{2.27}$$

Example 2.1. *Regarding the boost converter with SMC-Washout described by equations* (2.15), (2.16), (2.20) *and* (2.21), *we obtain* $\mathbf{f}(\mathbf{x}) = \mathbf{F}^-(\mathbf{x})$, $\mathbf{g}(\mathbf{x}) = \begin{bmatrix} -y & x & 0 \end{bmatrix}^T$, $u^- = 0$ *and* $u^+ = 1$.

We define the rate variations of the value of h along the different orbits when extended continuously to the boundary of the open regions $R^{\pm}$, that is, for all $\mathbf{x} \in \overline{R^-} = R^- \cup \Sigma$ the orbital derivative of h or Lie derivative is

$$L_{\mathbf{F}^-} h(\mathbf{x}) = \frac{d}{dt} h(\mathbf{x}(t)) = \left\langle \nabla h(\mathbf{x}), \mathbf{F}^-(\mathbf{x}) \right\rangle .$$

Similarly, the corresponding case is obtained, for all $\mathbf{x} \in \overline{R^+} = R^+ \cup \Sigma$. Note that $\Sigma = \overline{R^-} \cap \overline{R^+}$. This is the tool used to study the dynamic behavior of the control system in the neighborhood of the switching boundary Σ, which determines the sliding and crossing regions, see definitions in (2.3)-(2.6). It is a fact that we are mainly interested in the attractive sliding region Σ_{as}, where the two vector fields from both sides out of Σ push orbits towards Σ.

From (2.3) we can also write Σ_{as} as

$$\left\{ \mathbf{x} \in \Sigma : -L_{\mathbf{g}} h(\mathbf{x}) u^- < L_{\mathbf{f}} h(\mathbf{x}) < -L_{\mathbf{g}} h(\mathbf{x}) u^+ \right\} .$$

Note that if $L_{\mathbf{g}} h(\mathbf{x}) < 0$ (resp. $L_{\mathbf{g}} h(\mathbf{x}) > 0$) then we must take $u^- < u^+$ (resp. $u^- > u^+$) so that the attractive sliding region defined above can exist.

Example 2.2. *Again regarding our example under study, we obtain* $L_{\mathbf{g}} h(\mathbf{x}) = x - ky < 0$ *for all* $\mathbf{x} \in \Sigma_{as}$ *and therefore the choice* $u^- = 0$ *and* $u^+ = 1$ *is appropriate.*

According to Filippov's method [51], which is the most natural way of obtaining the sliding dynamics induced by the discontinuous vector field (2.25)-(2.26), we must consider the sliding vector field $\mathbf{F}^s$

defined in (2.9), which clearly simplifies to

$$\mathbf{F}^s(\mathbf{x}) = \mathbf{f}(\mathbf{x}) - \mathbf{g}(\mathbf{x})\frac{L_{\mathbf{f}}h(\mathbf{x})}{L_{\mathbf{g}}h(\mathbf{x})}, \tag{2.28}$$

since $L_{\mathbf{g}}h(\mathbf{x}) \neq 0$. It is also usual to introduce the notation

$$\mathbf{F}^s(\mathbf{x}) = \mathbf{f}(\mathbf{x}) + \mathbf{g}(\mathbf{x})u_{eq} \tag{2.29}$$

where

$$u_{eq} = -\frac{L_{\mathbf{f}}h(\mathbf{x})}{L_{\mathbf{g}}h(\mathbf{x})} = -\frac{\langle \nabla h(\mathbf{x}), \mathbf{f}(\mathbf{x})\rangle}{\langle \nabla h(\mathbf{x}), \mathbf{g}(\mathbf{x})\rangle} \tag{2.30}$$

is the so called *equivalent control*, see [122]. Note that the transversality condition $L_{\mathbf{g}}h(\mathbf{x}) \neq 0$ is a necessary condition for the existence of u_{eq}.

Remark 2.8. *The equivalent control for our example under study is*

$$u_{eq}(x, y) = \frac{-bkx + (\omega - a)y + k - \omega y_r}{ky - x}.$$

The *Filippov's method* (convex combination) and *Utkin's method* (equivalent control) are algebraically equivalent. However, there are some special cases where the two methodologies lead to different results, see [15, 122].

As usual, we search for a stable operating point $\widetilde{\mathbf{x}}$ belonging to Σ, which should be a point where the vector fields $\mathbf{F}^{\pm}$ are anti-collinear and transversal to Σ, that is, there is a point $\widetilde{\mathbf{x}} \in \Sigma$ and $\lambda > 0$ such that $\mathbf{F}^+(\widetilde{\mathbf{x}}) = -\lambda\mathbf{F}^-(\widetilde{\mathbf{x}})$. This point is called pseudo-equilibrium and it is a sliding vector field equilibrium, that is, $\mathbf{F}^s(\widetilde{\mathbf{x}}) = \mathbf{0}$. In terms of the equivalent control, we say that $\widetilde{\mathbf{x}} \in \Sigma$ is a sliding vector field equilibrium if there is a $u^- < \widetilde{u}_{eq} < u^+$ (supposing that $u^- < u^+$) such that $\mathbf{f}(\widetilde{\mathbf{x}}) = -\widetilde{u}_{eq}\mathbf{g}(\widetilde{\mathbf{x}})$.

The condition $\widetilde{\mathbf{x}} \in \Sigma_{as}$ is essential for the sliding mode control process. In this sense, it is important to know the boundaries of the region Σ_{as} (which occur on the tangency lines T_+ and T_-), what are the phenomena associated when the operating point exceeds one of

these boundaries, and what is the condition on system parameters that ensures $\widetilde{\mathbf{x}} \in \Sigma_{as}$. The bifurcations that we are going to study in this thesis, as the boundary equilibrium bifurcation and TS-bifurcation, are associated to the breach of this condition.

Chapter 3

Hopf and Homoclinic Bifurcations in a Boost Converter

In this chapter we study the Hopf and Homoclinic bifurcations that occur in the sliding vector field of switching systems in $\mathbb{R}^3$. In particular, a dc-dc boost converter with sliding mode control and washout filter is analyzed. This device is modelled as a three-dimensional DPWS system, characterized by the existence of sliding movement and restricted to the switching manifold. The operating point of the converter is a stable pseudo-equilibrium and it undergoes a subcritical Hopf bifurcation. Such a bifurcation occurs in the sliding vector field and creates, in this field, an unstable limit cycle. The limit cycle is connected to the switching manifold and disappears when it touches the visible-invisible two-fold point, resulting in an homoclinic loop which itself closes in this two-fold point. The study of these dynamic phenomena that can be found in different power electronic circuits controlled by sliding mode control strategies are relevant from the viewpoint of the global stability and robustness of the control design.

3.1 Introduction

Switching power electronic devices are strongly non-linear and can be modelled as piecewise smooth dynamical systems. It has been shown that this class of systems can exhibit various types of complex phenomena, including the classic bifurcations (Hopf, Saddle-Node, Homoclinic, etc.) and bifurcations induced by discontinuity [37].

In case where the dynamical system is discontinuous piecewise smooth, orbits can be confined to the switching manifold. This phenomenon is known as sliding motion and this class of systems is called as DPWS systems (or Filippov systems) [51]. The occurrence of such a phenomenon has been reported in various applications involving sliding mode control. Here we highlight the applications in power electronics converters [23, 91, 92, 98, 113].

In this Chapter, we study the Hopf and Homoclinic bifurcations that appear in the sliding vector field of three-dimensional DPWS systems. For this study we consider the model of a dc-dc boost power electronics converter with sliding mode control and washout filter (SMC-Washout) to reject load changes [92]. These bifurcations on the sliding vector field are analogous to the standard continuous case, and will be called Sliding Hopf and Sliding Homoclinic bifurcations. However, sliding homoclinic bifurcations differ a little from the standard case, since the closing point of the homoclinic loop is not on a saddle equilibrium point, but in a visible-invisible two-fold singularity that has dynamics saddle in the sliding region. Moreover, the homoclinic bifurcation exhibited here is of codimension-one and is obtained when a single parameter is varied.

Dynamical systems that have a two-fold singularity possess a very rich and complex dynamics. In [26, 68, 69, 71] two-fold singularities are studied and in [25, 39] applications of such theory in electrical and control systems, respectively, are exhibited.

The Hopf bifurcation is a local bifurcation in which an equilib-

rium point of a smooth dynamical system loses stability when a pair of complex conjugate eigenvalues crosses the imaginary axis of the complex plane. In this case, an unstable limit cycle (subcritical Hopf) or stable (supercritical Hopf) arises from an equilibrium point.

The Homoclinic bifurcation is a global bifurcation that occurs when a limit cycle collides with a saddle equilibrium point. The existence of an homoclinic orbit implies global changes in system dynamics. On two-dimensional systems studied by Andronov et al. [2], the existence of an homoclinic orbit causes the sudden appearance of a limit cycle with same stability of the homoclinic orbit. In the same way, we can say that Homoclinic bifurcation is the mechanism by which a limit cycle, created for example from a Hopf bifurcation, is destroyed. More details about the Hopf and Homoclinic bifurcation in smooth dynamical systems, can be found in [59, 77, 88, 95].

In the literature there are several works on Homoclinic bifurcation and Hopf bifurcation analysis in nonsmooth dynamical systems [11, 18, 35, 78, 83, 85, 107, 128], where the bifurcations studied are induced by the discontinuity. For example, in Kuznetsov et al. [78], are study "Pseudo-Homoclinic" bifurcations where a standard saddle equilibrium point may have an homoclinic loop containing a sliding segment. In Dercole et al. [35], a bifurcation of codimension 2 where a limit cycle that arises from an equilibrium point associated with a Boundary Equilibrium Bifurcation, is analysed. On the Sliding Hopf and Sliding Homoclinic bifurcations we highlight the pioneering works of Ponce and Pagano [91, 98], identifying the occurrence of such bifurcations in a boost converter model, and recent studies with application in systems compose by interconnected power converters in an islanded direct current (DC) microgrid, in the works of Cristiano et al. [29] and Benadero et al. [12]. In both the analysis is partial, without delving into these subjects. Here, we will analyze them in more detail.

The main contribution of this chapter is the characterization of a new mechanism to produce a homoclinic bifurcation, where the closing

point of the homoclinic loop is a two-fold singularity. A rigorous analysis of the Sliding Hopf and Sliding Homoclinic bifurcations is presented. In order to do that, a case study in power electronics is considered.

This Chapter is organized as follows. The modelling of the boost converter with SMC, the analysis of the tangential singularities and the dynamics of the sliding vector field are shown in Section 3.2. The occurrence of Sliding Hopf and Sliding Homoclinic bifurcations are shown in Section 3.3. From the analysis of stability and bifurcations, in Sections 3.4 and 3.5 we present some results about the attraction basin and the set of values of the parameters for a correct performance of the control system under study.

Previous results on Filippov theory in Chapter 2 are important for the development that follows.

3.2 Dynamics of boost converter with SMC-Washout

In this Chapter we consider the model of a dc-dc Boost converter, operating in Continuous Conduction Mode (CCM), with sliding mode control and washout filter (SMC-Washout). Such a model was introduced in Chapter 2, Section 2.6, see Figures 2.9 and 2.10. We assume the dimensionless model given in (2.15)-(2.16)-(2.20), but with ideal inductance, that is $b = 0$ (equivalent to $r_L = 0$).

Then, we take

$$\begin{aligned} \dot{x} &= 1 - uy \\ \dot{y} &= ux - ay \\ \dot{z} &= u(x - ky) + (\omega - a)y - \omega z + k - \omega y_r, \end{aligned} \tag{3.1}$$

where $(x, y, z) \in \mathbb{R}^3$ are the state variables and the parameters are $\omega \in (0, 1]$ (normalized filter parameter), $y_r > 1$ (normalized reference parameter), $k > 0$ (normalized control parameter) and $a > 0$ (normal-

ized resistive load parameter). We stress that $x > 0$ is the normalized inductor current, $y \geq 0$ is the normalized output voltage and $z \in \mathbb{R}$ depends on the filtered current.

The control variable u is defined as

$$u = \frac{1}{2}(1 + \text{sign}[z]) \tag{3.2}$$

and the switching manifold as

$$\Sigma = \{(x, y, z) \in \mathbb{R}^3 : h(x, y, z) = z = 0\}.$$

System (3.1) with the control law (3.2) can be represented by the dynamical system

$$(\dot{x}, \dot{y}, \dot{z}) = \begin{cases} \mathbf{F}^+ = (1 - y, x - ay, f_3^+) & \text{if } z > 0 \\ \mathbf{F}^- = (1, -ay, f_3^-) & \text{if } z < 0 \end{cases}, \tag{3.3}$$

where

$$f_3^+(x, y, z) = x + (\omega - a - k)y - \omega z + k - \omega y_r,$$
$$f_3^-(x, y, z) = (\omega - a)y - \omega z + k - \omega y_r.$$

3.2.1 Tangential singularities

The tangential sets of $\mathbf{F}^+$ and $\mathbf{F}^-$ are given, respectively, by the *straight lines*:

$$T_+ = \{(x, y, 0) \in \Sigma : x = (a + k - \omega)y - k + \omega y_r\},$$
$$T_- = \left\{(x, y, 0) \in \Sigma : y = \frac{k - \omega y_r}{a - \omega}, \text{ for } a \neq \omega\right\}.$$

The next result summarizes the possibilities of tangential singularities according to the parameters a, y_r, k and ω.

A straightforward calculation shows that the point $\widehat{\mathbf{x}}_c = (x_c, y_c, 0)$

with

$$x_c = \frac{\omega(y_r - 1) + a(1 + (a + k - \omega)(k - \omega y_r))}{(a + k - \omega)(k - \omega) + 1}$$
$$y_c = \frac{(a + k - \omega)(k - \omega y_r) + 1}{(a + k - \omega)(k - \omega) + 1},$$

is a *cusp singularity*, since $L^2_{\mathbf{F}^+} h(\widehat{\mathbf{x}}_c) = 0$ and the third Lie derivative evaluated at the cusp point is given by $L^3_{\mathbf{F}^+} h(\widehat{\mathbf{x}}_c) = \omega(1 - y_r) < 0$, i.e., the trajectory of $\mathbf{F}^+$ passing through the cusp point $\widehat{\mathbf{x}}_c$ departs from Σ. The point $\widehat{\mathbf{x}}_c$ separates T_+ into two branches of fold singularities. The *branch of visible fold singularities* for $y < y_c$ and the *branch of invisible fold singularities* for $y > y_c$.

Since $L^2_{\mathbf{F}^-} h(\widehat{\mathbf{x}}_f) = a(k - \omega y_r)$ for all $\widehat{\mathbf{x}}_f \in T_-$ we get that all points in T_- are *invisible fold singularities* if $k > \omega y_r$, or *visible fold singularities* if $k < \omega y_r$.

The double tangency point, $\widehat{\mathbf{x}}$, is given by $T_+ \cap T_-$, i.e.,

$$\widehat{\mathbf{x}} = \Big(\frac{k(k - y_r\omega)}{a - \omega}, \frac{k - \omega y_r}{a - \omega}, 0\Big). \tag{3.4}$$

The point $\widehat{\mathbf{x}}$ is a two-fold singularity if $a \neq a_c(k)$ or a fold-cusp singularity if $a = a_c(k)$, for all $k \neq \omega y_r$, where

$$a_c(k) = \frac{1}{2(k - \omega y_r)}\Big[-1 + \omega(k - \omega y_r) \tag{3.5}$$
$$+ \sqrt{1 + (k - \omega y_r)(2\omega + (4 + (\omega - 2k)^2)(k - \omega y_r))}\Big]$$

Table 3.1 shows the kinds of double tangency points according to the parameters (a, k). Following, choosing $\omega = 1$ and $y_r = 3/2$, we represent Table 3.1 in the plane of parameters (a, k) shown in Figure 3.1. Taking a point (a, k) in one of the regions V-I, V-V, I-V or I-I, we obtain a double tangency fold of the type visible-invisible, visible-visible, invisible-visible or invisible-invisible, respectively. While, for points (a, k) on the curve $a = a_c(k)$ the double tangency is of the kind

fold (invisible in part I-C or visible in part V-C) on one side and cusp on the other. For each one of the kinds cited, we illustrate (on the side) the geometry involving the "invisible" and "visible" dynamics of the vector fields $\mathbf{F}^+$ and $\mathbf{F}^-$ around the double tangency point[1].

Kind of tangency (legend)	**Region on the plane** (a, k)
Two-Fold Visible-Invisible (V-I)	$a_c(k) < a < \omega$ for $k < \omega y_r$
Two-Fold Visible-Visible (V-V)	$a < a_c(k)$ for $k < \omega y_r$
Two-Fold Invisible-Invisible (I-I)	$\omega < a < a_c(k)$ for $k > \omega y_r$
Two-Fold Invisible-Visible (I-V)	$a > a_c(k)$ for $k > \omega y_r$
Fold Invisible-Cusp (I-C)	$a = a_c(k)$ for $k > \omega y_r$
Fold Visible-Cusp (V-C)	$a = a_c(k)$ for $k < \omega y_r$

Table 3.1: Kinds of tangential points according to the parameters (a, k).

Remark 3.1. *Observe that, for practical reasons,* $x > 0$ *and* $y > 0$. *As a consequence, for* $\widehat{\mathbf{x}}$ *given in* (3.4)*, either* $a > \omega$ *and* $k > \omega y_r$ *or* $a < \omega$ *and* $k < \omega y_r$.

3.2.2 Sliding vector field and pseudo-equilibrium

The sliding vector field is calculated from the equation (2.9) in background Chapter 2, resulting in

$$\mathbf{F}^s(\mathbf{x}) = \frac{1}{x - ky} \begin{bmatrix} x - ay^2 + \omega y(y - y_r - z) \\ -k(x - ay^2) - \omega x(y - yr - z) \\ 0 \end{bmatrix}, \tag{3.6}$$

whose equilibrium point is

$$\widetilde{\mathbf{x}} = (ay_r^2, y_r, 0). \tag{3.7}$$

[1]In the expressions Visible-Invisible, Visible-Visible, Invisible-Visible, Invisible-Invisible, Fold Invisible-Cusp and Fold Visible-Cusp, the first description refers to the vector field $\mathbf{F}^-$ and the second to the vector field $\mathbf{F}^+$. For example, Visible-Invisible indicates a two-fold whose quadratic tangency is visible to $\mathbf{F}^-$ and invisible to $\mathbf{F}^+$, or even, Fold Invisible-Cusp, where the double tangency is quadratic invisible to $\mathbf{F}^-$ and cubic to $\mathbf{F}^+$.

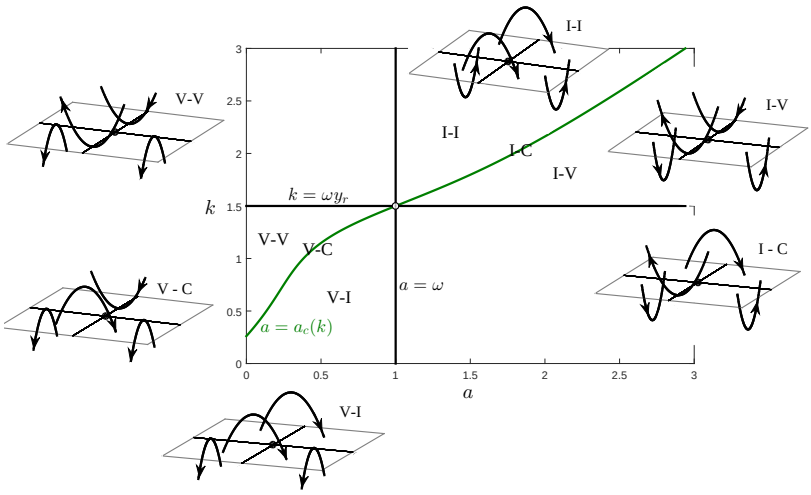

Figure 3.1: Kinds of the double tangency point in the (a, k)-plane, according to Table 3.1. The quadrants $\{k > \omega y_r\} \cap \{a < \omega\}$ and $\{k < \omega y_r\} \cap \{a > \omega\}$ are not considered in our study according to Remark 3.1.

This is the operating point of the boost converter controlled by the proposed SMC-Washout. The washout filter is responsible for the elimination of the output voltage dependence in relation to the changes of the parameter a produced by load changes of R. In this way, after a perturbation on a, the output voltage maintains the desired value y_r.

Now, we proceed to analyze the parameter conditions to obtain a pseudo-equilibrium $\mathbf{q}$ real and located in the sliding region. In order to do that, the following conditions

$$L_{\mathbf{F}^-} h(\widetilde{\mathbf{x}}) = k - a y_r > 0,$$
$$L_{\mathbf{F}^+} h(\widetilde{\mathbf{x}}) = -(y_r - 1)(k - a y_r) < 0,$$

must be verified for $\widetilde{\mathbf{x}} \in \Sigma_{as}$. We remember that the parameter $y_r > 1$. Therefore, if $k - a y_r > 0$ (respectively, $k - a y_r < 0$) then $\widetilde{\mathbf{x}} \in \Sigma_{as}$ (respectively, $\widetilde{\mathbf{x}} \in \Sigma_{rs}$) and if $k - a y_r = 0$ then $\widetilde{\mathbf{x}}$ coincides with the

double tangency point $\widehat{\mathbf{x}}$ given in (3.4).

In sliding mode control it is necessary that the pseudo-equilibrium (i.e., the operating point) remains in the sliding region Σ_{as}. So, the control parameter k must fulfill:

$$k > ay_r. \tag{3.8}$$

Moreover, the pseudo-equilibrium must be stable and whenever possible, without to exhibit an unstable limit cycle around it in order to enlarge the stability region.

In order to analyze the stability of the pseudo-equilibrium $\widetilde{\mathbf{x}}$, we use the planar sliding vector field $\mathbf{F}^{as}$ given by

$$\mathbf{F}^{as}(x,y) = \begin{bmatrix} -x + ay^2 - \omega y(y - y_r) \\ k(x - ay^2) + \omega x(y - yr) \end{bmatrix}. \tag{3.9}$$

The pseudo-equilibrium $\widetilde{\mathbf{x}}$ in reduced coordinates is denoted by $\widetilde{\mathbf{x}}_s = (ay_r^2, y_r)$. This point is an equilibrium of $\mathbf{F}^{as}$ and its stability can be extended to the pseudo-equilibrium $\widetilde{\mathbf{x}}$ since it satisfies the condition (3.8).

The Jacobian matrix of the normalized sliding vector field (3.9) evaluated at the point $\widetilde{\mathbf{x}}_s$ is given by

$$J(\widetilde{\mathbf{x}}_s) = \begin{pmatrix} -1 & (2a - \omega)y_r \\ k & ay_r(\omega y_r - 2k) \end{pmatrix}.$$

The determinant and trace of $J(\widetilde{\mathbf{x}}_s)$, are given by

$$\begin{aligned} \mathrm{Det}[J(\widetilde{\mathbf{x}}_s)] &= \omega y_r(k - ay_r), \\ \mathrm{Tr}[J(\widetilde{\mathbf{x}}_s)] &= -1 + ay_r(\omega y_r - 2k). \end{aligned}$$

Imposing the condition (3.8) on the parameter k, then $\mathrm{Det}[J(\widetilde{\mathbf{x}}_s)] > 0$. Therefore, the pseudo-equilibrium $\widetilde{\mathbf{x}}$, when in Σ_{as}, can be a pseudo-node or pseudo-focus, stable or unstable. In this case it will be stable

if and only if, $\mathrm{Tr}[J(\widetilde{\mathbf{x}}_s)] < 0$, i.e., k must be chosen such that it fulfill, in addition of (3.8), inequality

$$k > \frac{a\omega y_r^2 - 1}{2ay_r}. \tag{3.10}$$

Remark 3.2. *If $k < ay_r$ the pseudo-equilibrium $\widetilde{\mathbf{x}}$ is on the repulsive sliding region Σ_{rs} and it is a pseudo-saddle, because $Det[J^{rs}(\widetilde{\mathbf{x}}_s)] = Det[J(\widetilde{\mathbf{x}}_s)] < 0$, where J^{rs} is the Jacobian matrix of the planar sliding vector field defined on Σ_{rs} as $\mathbf{F}^{rs}(x,y) = -\mathbf{F}^{as}(x,y)$.*

More precisely, in order to distinguish if $\widetilde{\mathbf{x}}$ is a pseudo-focus or a pseudo-node we have to analyze the sign of the discriminant Δ of the characteristic polynomial of $J(\widetilde{\mathbf{x}}_s)$. Explicitly,

$$\begin{aligned}\Delta &= \mathrm{Tr}[J(\widetilde{\mathbf{x}}_s)]^2 - 4\mathrm{Det}[J(\widetilde{\mathbf{x}}_s)] \\ &= 4a^2y_r^2k^2 - 4y_r(\omega + a(a\omega y_r^2 - 1))k + (1 + a\omega y_r^2)^2.\end{aligned}$$

This expression is a polynomial of degree two in the variable k. The solutions of $\Delta = 0$ are given by:

$$k_\pm = k_H + \frac{\omega \pm \sqrt{\omega(1 + 2a^2y_r^2)(\omega - 2a)}}{2a^2y_r}, \tag{3.11}$$

where

$$k_H = \frac{a\omega y_r^2 - 1}{2ay_r}. \tag{3.12}$$

Note that $k > k_H$ satisfies the stability condition (3.10) and $k = k_H$ implies $\mathrm{Tr}[J(\widetilde{\mathbf{x}}_s)] = 0$. Furthermore, the roots $k_\pm$ of polynomial $\Delta = 0$ exist only for $a \leq \dfrac{\omega}{2}$, otherwise we will have $\Delta > 0$ for all k.

In Table 3.2, we summarize these results on the dynamics of the sliding vector field at the pseudo-equilibrium point $\widetilde{\mathbf{x}}$. These stability conditions were obtained considering that $y_r \geq \frac{2\sqrt{2}}{\omega}$, otherwise $\widetilde{\mathbf{x}}$ is always stable for all $k > ay_r$. This condition on the parameter y_r assure us the existence of a *Bogdanov-Takens* bifurcation (BT) at points

$(a_-, y_r a_-)$ and $(a_+, y_r a_+)$ of the (a,k)-plane (see Figure 3.6), such that

$$a_\pm = \frac{1}{4y_r}\left(\omega y_r \pm \sqrt{\omega^2 y_r^2 - 8}\right). \tag{3.13}$$

Kind of dynamics	**Conditions under the parameters** (a,k)
pseudo-saddle	$k < ay_r$
stable pseudo-node	$k > ay_r$ and $a \geq \frac{\omega}{2}$, or $k > k_+$ and $a < \frac{\omega}{2}$, or $ay_r < k < k_-$ and $a_+ < a < \frac{\omega}{2} \cup 0 < a < a_-$
unstable pseudo-node	$ay_r < k < k_-$ and $a_- < a < a_+$
stable pseudo-focus	$k_- < k < k_+$ and $a_+ < a < \frac{\omega}{2} \cup 0 < a < a_-$, or $k_H < k < k_+$ and $a_- < a < a_+$
unstable pseudo-focus	$k_- < k < k_H$ and $a_- < a < a_+$

Table 3.2: Kinds of dynamics of the sliding vector field at pseudo-equilibrium point $\widetilde{\mathbf{x}}$, according to parameters (a,k).

The Hopf and Homoclinic bifurcations corresponding to the sliding vector field of the boost converter system with SMC-Washout are studied in the next Section.

3.3 A Sliding Hopf bifurcation followed by a Homoclinic loop at the two-fold point

In this section we analyze two bifurcations that occur in the sliding vector field (3.6). First a Sliding Hopf bifurcation takes place giving rise to a unstable limit cycle C. Second, C persists when the parameter k varies (from $k = 1.375$ to $k = 1.573$, for the case $\omega = 1$, $y_r = 4$, $a = 0.2$, see simulations in Figures 3.2-3.3 and the bifurcation diagrams in Figure 3.4), and then it collides with the two-fold point, which behaves like a saddle. This collision produces an homoclinic loop destroying the limit cycle.

3.3.1 Sliding Hopf bifurcation

In previous section, we proved that $\widetilde{\mathbf{x}}$ is an unstable focus when $k_- < k < k_H$ and a stable one when $k_H < k < k_+$, since $a_- < a < a_+$. Then we can state the following result:

Proposition 3.1. *If $k = k_H$ and $a \in (a_-, a_+)$, where $a_\pm$ are given in* (3.13) *and k_H is given in* (3.12)*, then a subcritical Hopf bifurcation occurs at $\widetilde{\mathbf{x}} = (ay_r^2, y_r, 0)$ in the sliding vector field* (3.6)*.*

Proof. For this proof, we consider the planar sliding vector field (3.9) that is topologically equivalent to (3.6) in Σ_{as} and the point $\widetilde{\mathbf{x}}_s = (ay_r^2, y_r)$ equivalent to the pseudo-equilibrium $\widetilde{\mathbf{x}}$ in Σ.

The following necessary conditions to get a Hopf bifurcation are satisfied for $k = k_H$:

$$\begin{aligned}
\mathrm{Det}[J(\widetilde{\mathbf{x}}_s)]\Big|_{k=k_H} &= \frac{\omega(-1+\omega y_r^2 a - 2y_r^2 a^2)}{2a} > 0\\
\mathrm{Tr}[J(\widetilde{\mathbf{x}}_s)]\Big|_{k=k_H} &= 0\\
\frac{d\mathrm{Tr}[J(\widetilde{\mathbf{x}}_s)]}{dk}\Big|_{k=k_H} &= -2ay_r \neq 0,
\end{aligned}$$

since $a_- < a < a_+$. Then let us consider the system

$$\begin{aligned}
\dot{u} &= u + v(\omega(v+y_r) - a(v+2y_r))\\
\dot{v} &= -v\omega(u+ay_r^2) + k(-u + av(v+2y_r)),
\end{aligned} \tag{3.14}$$

obtained from a translation of (3.9) in such a way that $\widetilde{\mathbf{x}}_s$ is translated to the origin.

According to [2] (see page 253), if the number

$$\begin{aligned}
\sigma &= -\frac{1}{y_r(2a-\omega)\sqrt{\frac{\omega^3(ay_r^2(\omega-2a)-1)^3}{a^3}}}(3\sqrt{2}\pi\omega(-2a^2k^2y_r\\
&\quad +a(2k^3+k^2\omega y_r + k - 2\omega y_r) + \omega(k+\omega y_r)))
\end{aligned}$$

is not null, then a Hopf bifurcation occurs at the origin in the planar analytic system (3.14). In fact, the number σ, also known as *Lyapunov coefficient*, is the first non null coefficient of the Taylor's polynomial expansion of the displacement map $d(x) = \varphi(x) - x$, where $\varphi(x)$ is the first return map associated to (3.14) (see [59] for details). Moreover, we have $\sigma > 0$ for all $a \in (a_-, a_+)$ and, thus, a subcritical Hopf bifurcation occurs when $k = k_H$. Therefore, a unique unstable limit cycle bifurcates from the point $\widetilde{\mathbf{x}}$ in the sliding vector field (3.6) (see Figures 3.2(a)-3.2(c)). So Proposition 3.1 is proved. □

Figures 3.2(a) and 3.2(c) show the phase portrait of the boost converter with the SMC-Washout given by (3.3), on the switching boundary Σ and in the (x, y, z)-space, respectively. On both we note the existence of an unstable limit cycle $C \subset \Sigma_{as}$ around the stable focus $\widetilde{\mathbf{x}} \in \Sigma_{as}$. The red closed curve, the blue point and the green point represent the limit cycle C, the pseudo-equilibrium point $\widetilde{\mathbf{x}}$ and the two-fold point $\widehat{\mathbf{x}}$, respectively. While the red solid denoted by Γ indicates the basin of attraction of the pseudo-equilibrium $\widetilde{\mathbf{x}}$ (more details in Subsection 3.4). Figure 3.2(b) shows the response time from simulation results, where we observe that for an initial condition outside the region delimited by the limit cycle C the system is unstable (solution represented in blue color), and only for conditions within this region is that the system stabilizes at the desired operation point (solutions represented in green and orange color). The parameter values used in the simulation are: $\omega = 1$, $y_r = 4$, $a = 0.2$ and $k = 1.5$.

3.3.2 Sliding Homoclinic bifurcation

The unique limit cycle C, that emerged from the Sliding Hopf Bifurcation of Subsection 3.3.1, persists until the homoclinic loop occurs at the two-fold point. This is the subject of the next proposition.

Proposition 3.2. *The limit cycle C emerges from the Sliding Hopf Bifurcation in Proposition 3.1, when the parameter k assumes the critical*

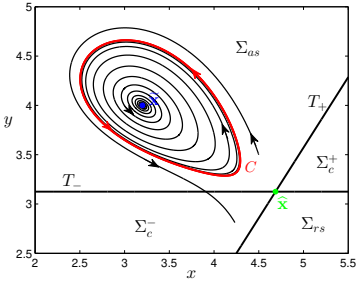

(a) Dynamics on Σ.

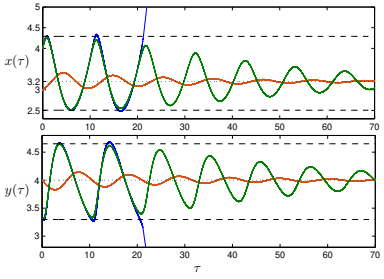

(b) Response time.

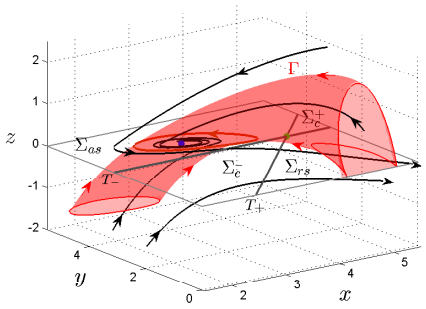

(c) Three-dimensional basin of attraction of the pseudo-equilibrium point displayed in red color.

Figure 3.2: Unstable limit cycle in the nonsmooth vector field (3.3) and the corresponding basin of attraction for $\omega = 1$, $y_r = 4$, $a = 0.2$ and $k = 1.5$.

value $k = k_H$. It persists when the parameter k varies from $k = k_H$ to $k = k_{HC}$, where k_{HC} stands for the critical value of parameter k needed to connect the limit cycle with the two-fold point, until to touch the homoclinic loop at the two-fold point and then disappears.

Proof. According to Table 3.1, the double tangency point $\widehat{\mathbf{x}}$ is a visible-invisible two-fold singularity whenever $a_c(k) < a < \omega$ and $k < \omega y_r$. Note that the sliding Homoclinic bifurcation curve in plane$-(a, k)$ is contained in the quadrant $a_- < a < a_+$ and $y_r a_- < k < y_r a_+$ (see

Figure 3.6). As $a_+ < \frac{\omega}{2}$ and $a_- > a_c$, then the double tangency point is classified as visible-invisible two-fold when the sliding Homoclinic bifurcation occurs.

Moreover, we consider the point $\widehat{\mathbf{x}}$ in reduced coordinates given by $\widehat{\mathbf{x}}_s = (k\widehat{y}, \widehat{y})$, where $\widehat{y} > 0$ is the y-coordinate of the double tangency point $\widehat{\mathbf{x}}$ given in (3.4). The point $\widehat{\mathbf{x}}_s$ is an equilibrium of the planar sliding vector field $\mathbf{F}^{as}$, whose dynamics in its neighborhood on Σ_{as} is saddle type whenever the pseudo-equilibrium is located in Σ_{as}, because

$$\text{Det}[J(\widehat{\mathbf{x}}_s)] = -\omega(k - ay_r)y_t < 0$$

for $k > ay_r$. Thus it is natural that the homoclinic loop passes through this point.

Since the two coordinates of system (3.9) have no roots in common and the cycle emerged from Proposition 3.1 is unique, we are able to use the *Perko's Planar Termination Principle* (see [94, 96]). More precisely, the parameter k represents the Hopf bifurcation parameter and this principle guarantee that this family of periodic orbits is unbounded or terminates at a critical point as shown in Figure 3.3(a). So, we conclude that the family of periodic orbits persists until reach a saddle point defined by the separatrices of $\widehat{\mathbf{x}}_s$, which is a visible-invisible two-fold point, giving rise to a homoclinic loop. See Figures 3.3(a)-3.3(b). □

The previous proposition states the existence of homoclinic bifurcation for the planar sliding vector fields $\mathbf{F}^{as}$. Note that this vector field is smooth and therefore the homoclinic orbit posses the two-fold point $\widehat{\mathbf{x}}_s$ as α- and ω-limits, which is reached when $t \to -\infty$ and $t \to +\infty$, respectively. However, the trajectories of the vector fields $\mathbf{F}^+$ and $\mathbf{F}^-$ reach the two-fold point in a finite time. This is an important issue and a difference between the smooth and piecewise smooth world.

Figures 3.3(a) and 3.3(b) illustrate the phase portrait of (3.9) and the simulations of the boost converter with SMC-Washout given by (3.3), respectively. In Figure 3.3(a) we observe the homoclinic loop

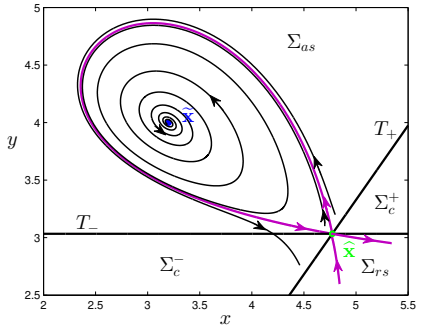

(a) Dynamics on Σ.

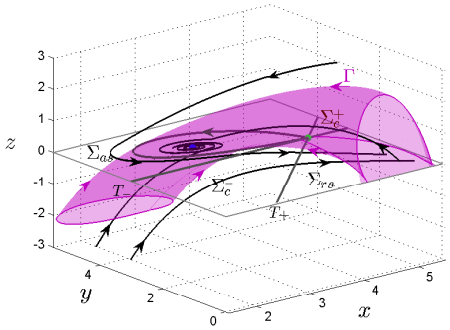

(b) Three-dimensional basin of attraction of the pseudo-equilibrium point displayed in purple color.

Figure 3.3: Homoclinic loop at the two-fold point and the corresponding basin of attraction for $\omega = 1$, $y_r = 4$, $a = 0.2$ and $k = 1.573$.

(purple curve) passing through $\widehat{\mathbf{x}}_s$ that is a saddle equilibrium point of $\mathbf{F}^{as}$ and is the closing point of the homoclinic orbit. In Figure 3.3(b), the purple solid represents the basin of attraction Γ of the pseudo-equilibrium $\widetilde{\mathbf{x}}$; and $\widehat{\mathbf{x}}$ (green dot) is a visible-invisible two-fold singularity of the model. The parameter values used in the simulation are: $\omega = 1$, $y_r = 4$, $a = 0.2$ and $k = 1.573$.

Remark 3.3. *The homoclinic loop L_0 is simple since*

$$\sigma_0 = \nabla \cdot \mathbf{F}^{as} = Tr[J(\widehat{\mathbf{x}}_s)] = \frac{k(2a-\omega)(\omega y_r - k)}{a-\omega} - 1 \neq 0.$$

We say that a separatrix cycle is called stable or unstable if the displacement map $d(s)$ satisfies $d(s) < 0$ or $d(s) > 0$, respectively, for all s in some neighbourhood of $s = 0$ where $d(s)$ is defined.

As shown in [2] (see page 304), if L_0 is simple ($\sigma_0 \neq 0$), the homoclinic loop L_0 is stable (unstable) if and only if $\sigma_0 < 0$ ($\sigma_0 > 0$) and besides that there exists some neighbourhoods V_ε of L_0 and $\mathcal{V}$ of $\mathbf{F}^{as}$ (in a C^1-norm) such that for all vector field $g \in \mathcal{V}$ has at most one limit cycle in V_ε with the same stability of L_0.

Moreover, as expected, from this homoclinic loop can arise from an homoclinic bifurcation only one limit cycle, as proved in [2] (see page 309).

3.4 A brief comment about the basin of attraction

An important part of the local stability analysis is the determination of the *basin of attraction* (see [10]), because it reveals the region in the state space where for any initial condition the system (3.3) reaches its equilibrium point. The basin of attraction, here, is defined as the subset of $\mathbb{R}^3$ formed by all the initial states $\mathbf{x}_0 = \mathbf{x}(\tau_0)$, $\tau_0 \geq 0$, that reach the switching boundary Σ on the sliding region Σ_{as} (in finite time $\tau = \tau_1 \geq \tau_0$), and remain confined to Σ (for all positive time $\tau > \tau_1$) sliding under the dynamics of $\mathbf{F}^s$, tending asymptotically to the pseudo-equilibrium $\widetilde{\mathbf{x}} = \mathbf{x}(\infty)$. Note that the pseudo-equilibrium can be reached in finite time from some initial condition outside Σ_{as}.

The knowledge of the basin of attraction for different values of the control parameter k is of great importance for the control design, because it allow us to find a value for k in which the basin of attraction

of the pseudo-equilibrium is as large as possible. However, the complete analysis of the attraction basin is a difficult task and in general is not analytically solvable. This is a very comprehensive topic and we leave the complete analysis out of this work. What we will do next in this subsection is a previous analysis on the subject from the results obtained with the analysis of the sliding Hopf and sliding Homoclinic bifurcations present in the previous subsections.

We present the case shown in Figure 3.2(c), where the presence of a limit cycle $C \in \Sigma_{as}$ creates a solid Γ with cylindrical shape representing the basin of attraction. In this case, the boundary of the basin of attraction is formed by all initial states that reach Σ_{as} exactly on the unstable limit cycle C. Note that our set of initial states for the boost converter to reach the operating point is reduced to the interior of the solid Γ.

The area in Σ_{as} delimited by the unstable limit cycle around the stable pseudo-focus, represents the basin of attraction confined to Σ_{as}. We have seen in the previous subsections that this area persists with the increase in the value of parameter k (for a fixed value of a). The basin of attraction in Σ_{as} becomes larger when we increase the value of k. This increase can be observed by comparing the Figures 3.2(a) and 3.3(a), and also, numerically verified from the bifurcation diagrams in Figure 3.4, which indicate an amplitude of limit cycle C, in both state variables, increasing as a function of k. These arguments lead us to a basin of attraction in $\mathbb{R}^3$ which increases along with k, as seen of Figure 3.2(c) to Figure 3.3(b), where the solids denoted by Γ represent the basin of attraction in each case.

From this previous analysis, it is clear that the basin of attraction containing the largest possible part of $\mathbb{R}^3$ will be obtained for some value of k after the sliding Homoclinic bifurcation and the disappearance of the unstable limit cycle C. However, further studies are needed to find the optimal value of k that maximizes the attraction domain, so we leave this task for a future work.

3.5 Choice of control parameter from the bifurcation analysis

The bifurcation diagrams of Figure 3.4 show the displacement in the x and y coordinates of the points of pseudo-equilibrium and double tangency and the variation of amplitude of the limit cycle C as a function of the parameter k. These numerical results are expected according to the analysis of bifurcations discussed in the previous subsections, where we prove that, by varying parameter k in an increasing way, the system (3.3) undergoes a subcritical sliding Hopf bifurcation followed by a sliding Homoclinic bifurcation. Moreover, we verified through the analysis of the bifurcation diagrams that the amplitude of C is an increasing function of k, starting (with zero amplitude) in the Hopf and disappearing (with maximum amplitude) in the Homoclinic.

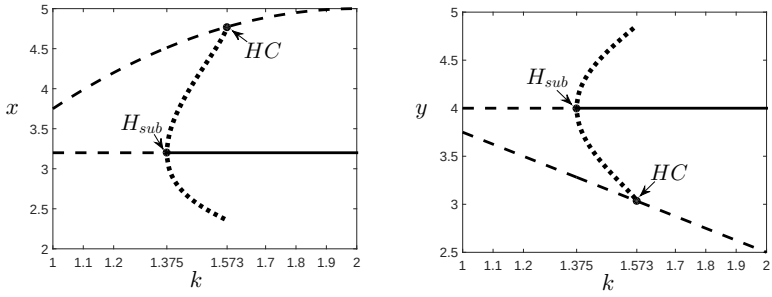

(a) $(x,k)-$plane (b) $(y,k)-$plane

Figure 3.4: Bifurcation diagrams showing the Hopf and Homoclinic sliding bifurcations in $(x,k)-$plane and $(y,k)-$plane, considering k as the bifurcation parameter, for $\omega = 1$, $y_r = 4$, $a = 0.2$. The dashed and solid lines represent unstable and stable equilibria, respectively. While the dotted line represents the unstable limit cycle.

In Figure 3.4 is shown: the dotted curve representing the amplitude of the unstable limit cycle C; the straight line representing the coordinates x and y of the pseudo-equilibrium $\widetilde{\mathbf{x}}$, which is an unstable

focus in the dashed part and a stable one at the solid part; the dashed curve represents the coordinates x and y of the two-fold singularity $\widehat{\mathbf{x}}$, which has characteristics of a saddle (unstable) equilibrium in the vector field sliding; the black points indicate the subcritical sliding Hopf bifurcation (H_{sub}), where the unstable limit cycle born; and the sliding Homoclinic bifurcation (HC), where the unstable limit cycle collides with the two-fold singularity $\widehat{\mathbf{x}}$ and disappears.

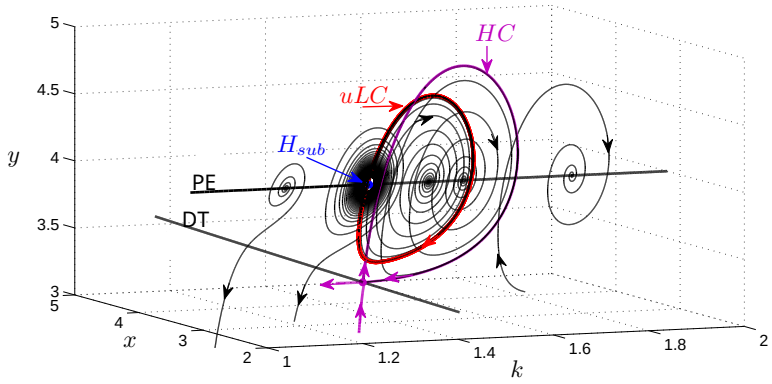

Figure 3.5: Bifurcation diagram in $(x, y, k)-$space considering k as the bifurcation parameter. The "uLC" stands for unstable limit cycle, while PE and DT indicate the branch of pseudo-equilibrium and double tangency, respectively.

Figure 3.5 illustrates the displacement of the pseudo-focus $\widetilde{\mathbf{x}}$, of the two-fold singularity $\widehat{\mathbf{x}}$ and of the unstable limit cycle C, in relation to the parameter k. The pseudo-focus $\widetilde{\mathbf{x}}$ is unstable before the subcritical sliding Hopf bifurcation (H_{sub}) and stable after it. The unstable limit cycle surrounds $\widetilde{\mathbf{x}}$ and there exists for $k \in (1.375, 1.573)$. It disappears, for $k = 1.573$, colliding to $\widehat{\mathbf{x}}$ in an homoclinic loop (HC).

We summarize the dynamics on the diagram of Figure 3.6, where it can be observed that: the two points denoted as BT, given by $(a_-, y_r a_-)$ and $(a_+, y_r a_+)$ with $a_\pm$ given in (3.13), represent Bogdanov-Takens bifurcations of $\widetilde{\mathbf{x}}$; the blue curve, given by $k = k_H(a)$ with k_H

defined in (3.12), stands for the subcritical sliding Hopf bifurcation (H_{sub}) of $\widetilde{\mathbf{x}}$; the red curve, of equation $k = ay_r$, indicates the transcritical bifurcation (T) involving the two-fold singularity $\widehat{\mathbf{x}}$ and the pseudo-equilibrium $\widetilde{\mathbf{x}}$; the purple curve, numerically obtained, represents the sliding Homoclinic bifurcation (HC) of limit cycle C; and the green curve point out the transition of the pseudo-equilibrium $\widetilde{\mathbf{x}}$ from node to focus.

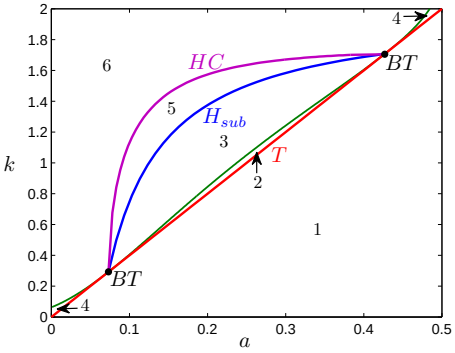

Figure 3.6: Bifurcation set in $(a, k)-$plane.

A given value of the parameter pair (a, k) on region 1 means that $\widetilde{\mathbf{x}}$ is a pseudo-saddle, on region 2 stands for an unstable pseudo-node, on region 3 means that it is an unstable pseudo-focus, on region 4 implies that it is a stable pseudo-node and on regions 5 and 6 denotes that it is a stable pseudo-focus (on region 5 there exists an unstable limit cycle). Moreover, on region 1 we get $\widetilde{\mathbf{x}} \in \Sigma_{rs}$ and on regions 2, 3, 4, 5 and 6 we get $\widetilde{\mathbf{x}} \in \Sigma_{as}$.

The results obtained in this work on Sliding Hopf and Sliding Homoclinic bifurcations can be used in the control design of a boost converter. More specifically, our analysis can be used to find the values (a, k) that make the operating point locally stable, and from this, to choose the "best" value of k from a prior knowledge of the variation range of the load parameter a. Following our analysis, the value

searched for k must be in region 6 of Figure 3.6, namely the *safe operating region* of the system (3.3).

3.6 Conclusion

In this Chapter, by means of a case study in power electronics (boost converter controlled by a sliding mode control), we proved the existence of two different sliding bifurcations: (i) Sliding Hopf and (ii) Sliding Homoclinic. The Sliding Hopf bifurcation occurs in the sliding vector field and is analogous to the standard case. The limit cycle that arises from the Sliding Hopf bifurcation is unstable and it is confined to the switching manifold. The Sliding Homoclinic bifurcation occurs when the limit cycle disappears by touching visible-invisible two-fold point, whose dynamics in the sliding region is of the saddle type. The homoclinic loop has a sliding segment which itself closes at the two-fold singularity.

The result of the bifurcation analysis was summarized in the (a, k)-plane bifurcation set showed in Figure 3.6. This methodology is useful to choose an appropriate value for the control parameter k in order to ensure the system stability at the desired operating point and prevent the birth of a limit cycle around it, even after a change in the load parameter a.

The mechanism described in the case studied in this work, from which a sliding limit cycle collapses when it touches a two-fold point is a dynamic phenomenon that is specific to nonsmooth dynamical systems. Further studies will be conducted in order to prove and to characterize this collapse mechanism for general nonsmooth dynamical systems in $\mathbb{R}^3$.

Chapter 4

Teixeira Singularity Bifurcation Theory and Application Method

In the 1990s Teixeira [117] showed that for a discontinuous piecewise smooth dynamical system in $\mathbb{R}^3$, whose state space is divided in two open regions by a plane acting as the switching boundary, there generically appear two lines of quadratic tangency, one for each involved vector field. When these two tangency lines have a transversal intersection, such a point is called two-fold. If furthermore both tangencies are of invisible type, then the two-fold is known as Teixeira singularity (T-singularity). The T-singularity can undergo an interesting bifurcation, namely when a pseudo-equilibrium point collide with the two-fold point, passing from the attractive sliding region to the repulsive sliding region (or vice versa) and, simultaneously, a crossing limit cycle arises. This bifurcation is named TS-bifurcation. After deriving carefully a local canonical form, we revisit the previous works regarding this bifurcation so correcting some detected misconceptions. Furthermore, we provide by means of a more direct approach the critical coefficients characteriz-

ing the bifurcation, also giving computational procedures for them. The achieved results are applied to some illustrative examples, within the realm of discontinuous piecewise-linear (DPWL) systems. This family acts like a normal form for the TS-bifurcation, since DPWL systems are able to reproduce all the unfolded dynamics. The study of the TS-bifurcation in a dc-dc boost power converter under a sliding mode control strategy is addressed. Apart from being a relevant application, it allows to show the real usefulness of the analysis done.

4.1 Introduction

Several physical systems such as mechanical systems with friction, electronic power converters and control systems are modelled by ordinary differential equations with discontinuous right-hand sides, also called Filippov's systems, see [51]. Other relevant references involving PWS systems are for instance [3, 37, 76, 82]. A generic singularity of these discontinuous systems for dimension greater than two is the so-called Teixeira singularity [117, 118] (or T-singularity).

The T-singularity is a generic point in 3D-DPWS systems defined by the aggregation of two different vector fields, one on each side of a given switching boundary, appearing at the transversal intersection of the corresponding fold lines. More specifically, it is assumed that in both fold lines the tangency is of invisible type, so that it is possible to have orbits that cross the switching boundary with recurrent behavior, see [117].

The possible degeneration of the T-singularity and its associated bifurcation behavior have been the subject of several papers, see [26, 49, 69, 71, 118]. No doubt, the most complete analysis can be found in [26], where a detailed description of the different dynamics associated to the bifurcation unfolding is given. However, it turns out necessary to revisit these previous works correcting some misconceptions; in doing so, we will provide by means of a more direct approach the critical

coefficients characterizing the bifurcation, also giving computational procedures for them, paving the way to practitioners.

In this chapter, we start in Section 4.2 by including the complete derivation of a canonical form for 3D-DPWS systems having the T-singularity, see Theorem 4.1. In the subsequent Remark 4.1, we put in evidence the differences of the canonical form in Theorem 4.1 with respect to the proposed one in [26].

In Section 4.3, we include all the theoretical results needed to characterize the Teixeira singularity bifurcation (TS-bifurcation). First, for the transcritical bifurcation affecting the pseudo-equilibrium point of the sliding dynamics, we obtain the coefficient κ_S in Theorem 4.2, see Subsection 4.3.1. This coefficient is given explicitly in terms of the entries of the derived canonical form in Theorem 4.1, putting in evidence that only the linear parts given in (4.13)-(4.14) are needed. Next, in Subsection 4.3.2 the crossing dynamics bifurcation is analyzed by defining in a natural way two half-return maps. Such maps turn to be involutions [116], so that the composition of these two half-return maps leads to a *reversible* first return map, see Section 3.1 in [101]. The fixed points of such first return map, excluding of course the T-singularity point, represent crossing limit cycles (CLCs), so that the stability analysis of the fixed points can be naturally extended to the CLCs. This *reversible* character is very relevant when studying the bifurcation for the crossing dynamics behavior and had not been recognized; therefore, the bifurcation had not been correctly termed. For instance, regarding the associated return map, authors spoke of "a degenerated (codimension-three) Bogdanov-Takens bifurcation" in p. 433 of [26] when actually one deals with a non-degenerated (codimension-one) *reversible* Bogdanov-Takens bifurcation.

In Subsections 4.3.2 and 4.3.3 we tackle the topological determination of degenerate T-singularity, in relation the crossing dynamics, and the complete characterization on its unfolding dynamics. We achieve these results by a direct use of the two half return maps taking advan-

tage of its involutive character. This approach avoids to build the first return map by composition of the above half-return maps, and leads to a direct study of the degeneration and the existence of fixed points and their stability without needing the derivation of a normal form for the map. On the contrary, in [26] authors adopt the usual approach of making nonlinear changes of variables to obtain a normal form for such first return map, so that they were not able of giving explicit expressions for all the normal form coefficients. Moreover, it is not clear that such changes of variables do preserve the reversibility of the map. Our approach provides two coefficients obtained from the Taylor expansions of the two half-return maps, namely σ and ρ, allowing the topological determination of the degeneration (see Theorem 4.3) and the complete characterization of its unfolding (see Theorem 4.4).

Regarding the problems we are interested in, Section 4.4 is devoted to the explicit computation of coefficients σ and ρ for the specific case of discontinuous piecewise-linear (DPWL) systems, a rather common situation in applications. Thus, thanks to Lemmas 4.1 and 4.2 such computation can be made directly from the entries of the canonical vector field. We remark that even our analysis starts from general cases, not necessarily being DPWL systems, such family of DPWL systems acts like a normal form for the bifurcation under study and so it deserves a specific treatment.

In Section 4.5, thanks to the previous theoretical results, we study some illustrative examples that reproduce the different dynamic scenarios for the TS-bifurcation. In particular, in Subsection 4.5.2 we revisit an example already studied in [26] by numerical simulation, and show how our theoretical results go further. The computations needed to put a generic 3D-DPWL system into the canonical form of the Theorem 4.1 are detailed in Section 4.6, since they are needed in Section 4.7. In Section 4.7 we introduce a real application regarding electronic power converters, which apart from being our main motivation, constitutes by itself an example within the realm of applied dynamical systems.

Previous results on Filippov theory in Chapter 2 are important for the development that follows.

4.2 Derivation of a canonical form

Without loss at generality, we assume in $\mathbb{R}^3$ that the switching boundary is the first coordinate plane[1]

$$\Sigma = \{\mathbf{x} = (x, y, z) \in \mathbb{R}^3 : \ h(\mathbf{x}) = x = 0\},$$

and that the T-singularity is located at the origin; more general situations can be recast to this situation after some elementary transformation. We will use for our piecewise-smooth system the notation

$$\dot{\mathbf{x}} = \begin{cases} \mathcal{F}^-(\mathbf{x}) = (\mathrm{f}^-(\mathbf{x}), \mathrm{g}^-(\mathbf{x}), \mathrm{r}^-(\mathbf{x})), & \text{if } x < 0, \\ \mathcal{F}^+(\mathbf{x}) = (\mathrm{f}^+(\mathbf{x}), \mathrm{g}^+(\mathbf{x}), \mathrm{r}^+(\mathbf{x})), & \text{if } x > 0, \end{cases} \tag{4.1}$$

where the $\dot{\mathbf{x}} = \frac{d\mathbf{x}}{dt}$ and we assume a transversal intersection at the origin of the two quadratic tangency lines. More precisely, we require

(H1) The conditions $L_{\mathcal{F}^\pm} h(\mathbf{0}) = \mathrm{f}^\pm(\mathbf{0}) = 0$ hold (there is tangency at the origin from both sides of Σ).

(H2) The two-fold is of invisible character, namely

$$\begin{cases} L^2_{\mathcal{F}^-} h(\mathbf{0}) = (\mathrm{f}^-_y \cdot \mathrm{g}^- + \mathrm{f}^-_z \cdot \mathrm{r}^-)(\mathbf{0}) > 0, \\ \\ L^2_{\mathcal{F}^+} h(\mathbf{0}) = (\mathrm{f}^+_y \cdot \mathrm{g}^+ + \mathrm{f}^+_z \cdot \mathrm{r}^+)(\mathbf{0}) < 0. \end{cases} \tag{4.2}$$

Note that if we define

$$\widetilde{f}^\pm(y, z) = \mathrm{f}^\pm(0, y, z),$$

[1] We have now chosen as switching boundary the first coordinate plane in order to facilitate the comparison of our results with those found in [26].

then from (H1) we see that $\widetilde{f}^{\pm}(0,0)=0$ and from (4.2) we get

$$(\widetilde{f}_y^{\pm}(0,0),\widetilde{f}_z^{\pm}(0,0))=(\mathrm{f}_y^{\pm}(\mathbf{0}),\mathrm{f}_z^{\pm}(\mathbf{0}))\neq(0,0), \tag{4.3}$$

so that by invoking the implicit function theorem we conclude the local existence of two smooth curves

$$T_{\pm}=\{(x,y,z):x=0,\widetilde{f}^{\pm}(y,z)=0\}$$

of fold tangency points, intersecting at the origin. To ensure the transversality of the two lines $T_{\pm}$ at the origin, we only need the linear independence of the two gradient vectors in (4.3), but following the usual convention in all previous works [26, 71, 74, 117], we suppose in (4.3) the conditions to assure that the curves $T_{\pm}$ are tangent to the coordinate axes at the origin, namely

$$(\mathbf{H2'})\quad \mathrm{f}_y^{-}(\mathbf{0})=0,\mathrm{f}_z^{-}(\mathbf{0})>0,\mathrm{r}^{-}(\mathbf{0})>0,$$

and

$$\mathrm{f}_y^{+}(\mathbf{0})<0,\mathrm{g}^{+}(\mathbf{0})>0,\mathrm{f}_z^{+}(\mathbf{0})=0.$$

Resorting now to the implicit function theorem, we can parameterize the tangency lines in a neighborhood of the origin in the form

$$T_{+}=\{(x,y,z):x=0,y=\varphi_{+}(z)\},$$

so that $\widetilde{f}^{+}(\varphi_{+}(z),z)=0$ and $\varphi_{+}(0)=\varphi'_{+}(0)=0$; similarly,

$$T_{-}=\{(x,y,z):x=0,z=\varphi_{-}(y)\},$$

so that $\widetilde{f}^{-}(y,\varphi_{-}(y))=0$ and $\varphi_{-}(0)=\varphi'_{-}(0)=0$. It turns very convenient to introduce a change of variables in order to get that the tangency lines T_{+} and T_{-} coincide with the second and third coordinate axis, respectively.

We introduce so the near-identity change of variables

$$\begin{aligned} u &= x, \\ v &= y - \varphi_+(z), \\ w &= z - \varphi_-(y), \end{aligned}$$

so that, by the inverse function theorem, we locally obtain

$$\begin{aligned} x &= u, \\ y &= v + \psi_+(v, w), \\ z &= w + \psi_-(v, w). \end{aligned}$$

Obviously, we have $\psi_\pm(0,0) = 0$, and also

$$\frac{\partial \psi_\pm}{\partial v}(0,0) = \frac{\partial \psi_\pm}{\partial w}(0,0) = 0. \tag{4.4}$$

Therefore, we get

$$\begin{aligned} \dot{u} &= \mathrm{f}^\pm(u, v + \psi_+(v,w), w + \psi_-(v,w)), \\ \dot{v} &= \dot{y} - \varphi'_+(z)\dot{z} = \mathrm{g}^\pm(u, v + \psi_+, w + \psi_-) - \\ &- \varphi'_+(w + \psi_-) \cdot \mathrm{r}^\pm(u, v + \psi_+, w + \psi_-), \\ \dot{w} &= \dot{z} - \varphi'_-(y)\dot{y} = \mathrm{r}^\pm(u, v + \psi_+, w + \psi_-) - \\ &- \varphi'_-(v + \psi_+) \cdot \mathrm{g}^\pm(u, v + \psi_+, w + \psi_-), \end{aligned}$$

where in the two last components the arguments of $\psi_\pm$ are omitted for brevity. For convenience, the above system is rewritten as

$$\begin{aligned} \dot{u} &= \hat{f}^\pm(u, v, w), \\ \dot{v} &= \hat{g}^\pm(u, v, w), \\ \dot{w} &= \hat{r}^\pm(u, v, w), \end{aligned}$$

where

$$\hat{g}^+(\mathbf{0}) = \mathrm{g}^+(\mathbf{0}) - \varphi'_+(0)\mathrm{r}^+(\mathbf{0}) = \mathrm{g}^+(\mathbf{0}) > 0,$$

and

$$\hat{r}^-(\mathbf{0}) = \mathrm{r}^-(\mathbf{0}) - \varphi'_-(0)\mathrm{g}^-(\mathbf{0}) = \mathrm{r}^-(\mathbf{0}) > 0.$$

We see that, for w in a neighborhood of 0, we get

$$\hat{f}^+(0,0,w) = \mathrm{f}^+(0,\psi_+(0,w), w + \psi_-(0,w)) = \widetilde{f}^+(\varphi_+(z),z) = 0,$$

and so the new tangency line T_+ coincides with the axis $v = 0$; similarly, for v in a neighborhood of 0, we get

$$\hat{f}^-(0,v,0) = \mathrm{f}^-(0, v + \psi_+(v,0), \psi_-(v,0)) = \widetilde{f}^-(y,\varphi_-(y)) = 0,$$

and so the new tangency line T_- coincides with the axis $w = 0$.

The above change of variables allows us to write

$$\hat{f}^+(0,v,w) = -v\rho^+(v,w), \tag{4.5}$$

so that

$$\begin{aligned}\hat{f}^+(u,v,w) &= \hat{f}^+(u,v,w) - \hat{f}^+(0,v,w) + \hat{f}^+(0,v,w) = \\ &= \hat{\hat{f}}^+(u,v,w) - v\rho^+(v,w),\end{aligned}$$

where $\hat{\hat{f}}^+(0,v,w) = 0$ for all (v,w) in a neighborhood of $(0,0)$.

Anagolously, we have

$$\hat{f}^-(0,v,w) = w\rho^-(v,w), \tag{4.6}$$

and so

$$\begin{aligned}\hat{f}^-(u,v,w) &= \hat{f}^-(u,v,w) - \hat{f}^-(0,v,w) + \hat{f}^-(0,v,w) = \\ &= \hat{\hat{f}}^-(u,v,w) + w\rho^-(v,w),\end{aligned}$$

where $\hat{\hat{f}}^-(0,v,w) = 0$ for all (v,w) in a neighborhood of $(0,0)$. It should be also noticed that the invisible character for the two-fold leads to the

inequalities $\rho^{\pm}(0,0) > 0$. Effectively, by introducing the functions

$$q^{\pm}(v,w) = \hat{f}^{\pm}(0,v,w) = \mathrm{f}^{\pm}(0, v + \psi_+(v,w), w + \psi_-(v,w)),$$

we obtain from (4.4) and (H2')

$$\frac{\partial q^+}{\partial v}(0,0) = \mathrm{f}_y^+(\mathbf{0}) \cdot \left(1 + \frac{\partial \psi^+}{\partial v}(0,0)\right) + \mathrm{f}_z^+(\mathbf{0}) \cdot \frac{\partial \psi^-}{\partial v}(0,0) = \mathrm{f}_y^+(\mathbf{0}) < 0,$$

and

$$\frac{\partial q^-}{\partial w}(0,0) = \mathrm{f}_y^-(\mathbf{0}) \cdot \frac{\partial \psi^+}{\partial w}(0,0) + \mathrm{f}_z^-(\mathbf{0}) \cdot \left(1 + \frac{\partial \psi^-}{\partial w}(0,0)\right) = \mathrm{f}_z^-(\mathbf{0}) > 0,$$

and then, using (4.5) and (4.6), both $\rho^{\pm}(0,0) > 0$ follow.

Summarizing, after the above computations, we arrive at the system

$$\begin{cases} \dot{u} &= \hat{\hat{f}}^+(u,v,w) - v\rho^+(v,w), \\ \dot{v} &= \hat{g}^+(u,v,w), \\ \dot{w} &= \hat{r}^+(u,v,w), \end{cases} \qquad (u > 0)$$

and

$$\begin{cases} \dot{u} &= \hat{\hat{f}}^-(u,v,w) + w\rho^-(v,w), \\ \dot{v} &= \hat{g}^-(u,v,w), \\ \dot{w} &= \hat{r}^-(u,v,w), \end{cases} \qquad (u < 0)$$

where $\hat{\hat{f}}^{\pm}(0,v,w) = 0$ for all (v,w) near $(0,0)$, $\rho^{\pm}(0,0) > 0$, $\hat{g}^+(\mathbf{0}) > 0$ and $\hat{r}^-(\mathbf{0}) > 0$.

We are now ready to apply a reparameterization of the time t, different on each side of Σ, along with a rescaling of variables to achieve the aimed canonical form. Thus, for $u > 0$ we define a new time τ_+ such that

$$\frac{d\tau_+}{dt} = \rho^+(u,v)\sqrt{\frac{\hat{g}^+(\mathbf{0})}{\rho^+(0,0)}}, \qquad (4.7)$$

while for $u < 0$ the new time τ_- is chosen to satisfy

$$\frac{d\tau_-}{dt} = \rho^-(u,v)\sqrt{\frac{\hat{r}^-(\mathbf{0})}{\rho^-(0,0)}}, \tag{4.8}$$

and restoring the original symbols for the state variables, we write

$$x = u, \quad y = v\sqrt{\frac{\rho^+(0,0)}{\hat{g}^+(\mathbf{0})}}, \quad z = w\sqrt{\frac{\rho^-(0,0)}{\hat{r}^-(\mathbf{0})}}.$$

After applying such time reparametrization along with the above change of variables, we have achieved the following local canonical form.

Theorem 4.1. *Under hypotheses (H1) and (H2'), it is possible to rewrite system* (4.1) *in the canonical form*

$$\dot{\mathbf{x}} = \begin{cases} \mathbf{F}^-(\mathbf{x}), & \text{if } x < 0, \\ \mathbf{F}^+(\mathbf{x}), & \text{if } x > 0, \end{cases} \tag{4.9}$$

where the vector fields $\mathbf{F}^\pm : \mathbb{R}^3 \longrightarrow \mathbb{R}^3$ *are*

$$\mathbf{F}^+(\mathbf{x}) = \begin{bmatrix} f^+(x,y,z) - y \\ g^+(x,y,z) \\ r^+(x,y,z) \end{bmatrix}, \quad \mathbf{F}^-(\mathbf{x}) = \begin{bmatrix} f^-(x,y,z) + z \\ g^-(x,y,z) \\ r^-(x,y,z) \end{bmatrix}, \tag{4.10}$$

with $f^\pm(0,y,z) = 0$ *for all* (y,z) *in a neighborhood of* $(0,0)$*, and* $g^+(\mathbf{0}) = r^-(\mathbf{0}) = 1$.

The detailed derivation of this canonical form is included here in order to be able to cope with real applications and not only with academic examples. It will be useful later, when we tackle the analysis of sliding and crossing dynamics regarding the degeneration of the T-singularity. The required changes in the original vector field, introduced to get the canonical form, become simpler in the specific case of piecewise-linear systems, and are summarized in Section 4.6.

We remark that by introducing in (4.9)-(4.10) the parameters

$$v_+ = r^+(\mathbf{0}), \quad v_- = g^-(\mathbf{0}),$$

we see that at the origin the two vector fields turns out to be

$$\mathbf{F}^+(\mathbf{0}) = \begin{bmatrix} 0 \\ 1 \\ v_+ \end{bmatrix}, \quad \mathbf{F}^-(\mathbf{0}) = \begin{bmatrix} 0 \\ v_- \\ 1 \end{bmatrix},$$

so that they become anti-collinear when $v_+ < 0$, $v_- < 0$ and

$$v_+ v_- - 1 = 0.$$

This suggests to introduce the parameter

$$\varepsilon := v_+ v_- - 1,$$

so that, as it will be shown later, the vanishing of this parameter is associated to a degeneracy of the T-singularity.

Remark 4.1. *Comparing Theorem 4.1 with the local form near the T-singularity given in p. 427 of [26], we observe that the quoted authors proposed the approximation*

$$\begin{aligned} \mathbf{F}^+(\mathbf{x}) &= \begin{bmatrix} -y + O(x, \|y, z\|^2) \\ 1 + O(\|\mathbf{x}\|) \\ v_+ + O(\|\mathbf{x}\|) \end{bmatrix}, \\ \mathbf{F}^-(\mathbf{x}) &= \begin{bmatrix} z + O(x, \|y, z\|^2) \\ v_- + O(\|\mathbf{x}\|) \\ 1 + O(\|\mathbf{x}\|) \end{bmatrix}. \end{aligned} \tag{4.11}$$

They did not give explicitly the changes needed to arrive at (4.11) *but in any case the non-specified terms in the first components are not in agreement with their own statement that the fold lines $T_\pm$ are located on the coordinate axes y and z. In other words, the key property assuring*

that $f^{\pm}(0, y, z) = 0$ for all (y, z) in a neighborhood of $(0, 0)$ was not ensured, as is in Theorem 4.1, being crucial for the remaining analysis. For instance, the structure of the half-return maps deduced in Appendix B of [26] comes from the involution condition and assume that such return maps preserve the y and z axis, respectively, in contradiction with the proposed approximation. Furthermore, the quadratic terms y^2, yz and z^2 appearing in the first $\mathbf{F}^{\pm}$-components of (4.11) would invalidate the formula (A.1) given for their coefficient a_2 controlling the sliding bifurcation, corresponding to our coefficient κ_S in (4.22).

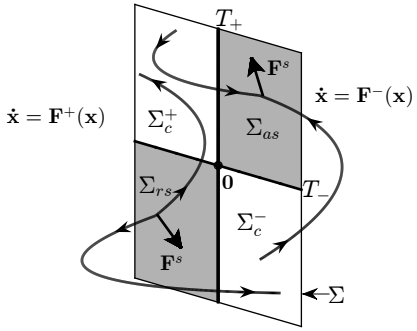

Figure 4.1: Dynamical behavior of a DPWS system in $\mathbb{R}^3$ near an invisible two-fold point (T-singularity).

For system (4.9)-(4.10), and focusing our attention to a neighborhood of the origin, it is now easy to distinguish on Σ different regions regarding the crossing and sliding dynamics (see Figure 4.1), namely[2]

$$\begin{aligned}
\Sigma_{as} &= \{(x, y, z) \in \mathbb{R}^3 : \ x = 0, \ y > 0 \text{ and } z > 0\}, \\
\Sigma_{rs} &= \{(x, y, z) \in \mathbb{R}^3 : \ x = 0, \ y < 0 \text{ and } z < 0\}, \\
\Sigma_c^- &= \{(x, y, z) \in \mathbb{R}^3 : \ x = 0, \ y > 0 \text{ and } z < 0\}, \\
\Sigma_c^+ &= \{(x, y, z) \in \mathbb{R}^3 : \ x = 0, \ y < 0 \text{ and } z > 0\}.
\end{aligned}$$

First, we define the *attractive sliding* set Σ_{as}, as the subset of Σ where

[2]Such sets are calculated as (2.3), (2.4), (2.5) and (2.6), respectively.

the vector fields $\mathbf{F}^{\pm}$ point towards Σ from both sides, that is,

$$L_{\mathbf{F}^+}h(0,y,z) = -y < 0,$$
$$L_{\mathbf{F}^-}h(0,y,z) = z > 0.$$

In this positive quadrant, to determine the solution of (4.1) starting at points of Σ_{as} it is usual to introduce the sliding vector field[3]

$$\mathbf{F}^s(0,y,z) = \frac{y\mathbf{F}^-(0,y,z) + z\mathbf{F}^+(0,y,z)}{y+z}, \tag{4.12}$$

where $\mathbf{F}^s$ is to be evaluated for $x = 0$ and is obtained from the convex combination of $\mathbf{F}^+$ and $\mathbf{F}^-$ that is tangent to Σ, see [78]. We remark that the time reparameterizations (4.7)-(4.8) lead to a new time in the Filippov vector field that preserves their orbits. If for some point $\mathbf{x} \in \Sigma_{as}$ the vector fields $\mathbf{F}^{\pm}$ are not only transversal to Σ but also anti-collinear, then the point is an equilibrium for $\mathbf{F}^s$ and is called a pseudo-equilibrium of system (4.1), see [58].

The repulsive sliding set Σ_{rs} corresponds to the region where $\mathbf{F}^{\pm}$ are pointing out of Σ from both sides. The solution of (4.1) starting at point $\mathbf{x} \in \Sigma_{rs}$ also follows the solution of $\mathbf{F}^s$ given in (4.12).

The crossing set Σ_c determines the region where one of vector field is pointing to Σ and the other is pointing out of the boundary. If an orbit of (4.1) starting at a point $\mathbf{x} \in R^- = \{(x,y,z) \in \mathbb{R}^3 : x < 0\}$ falls on Σ_c, then it crosses Σ to enter the other part of the space ($R^+ = \{(x,y,z) \in \mathbb{R}^3 : x > 0\}$). In this case, the crossing set is denoted by Σ_c^+. The opposite situation can also happens (see Figure 4.1), and then the crossing set is denoted by Σ_c^-.

As it will be shown, the degeneracy of T-singularity is the organizing center for the unfolding of the bifurcation behaviour, which we call TS-bifurcation. This bifurcation implies that a pseudo-equilibrium point crosses from the attractive sliding region to the repulsive sliding region (or vice versa). Simultaneously with such a passage of the

[3]The sliding vector field is calculated as (2.9).

pseudo-equilibrium point, a closed orbit composed by two arcs, each one defined by one of the vector fields $\mathbf{F}^{\pm}$, is born crossing the manifold Σ in two points and without any sliding segments. This limit cycle that arises from the TS-bifurcation is called crossing limit cycle (CLC).

In Figure 4.2, one of the possible dynamic scenarios for the bifurcation is sketched, taking ε as the bifurcation parameter. In the case of the picture, a stable pseudo-node in Σ_{as} for $\varepsilon < 0$ crosses the T-singularity becoming a pseudo-saddle in Σ_{rs} for $\varepsilon > 0$, and a CLC with stable dynamics emerges for $\varepsilon > 0$.

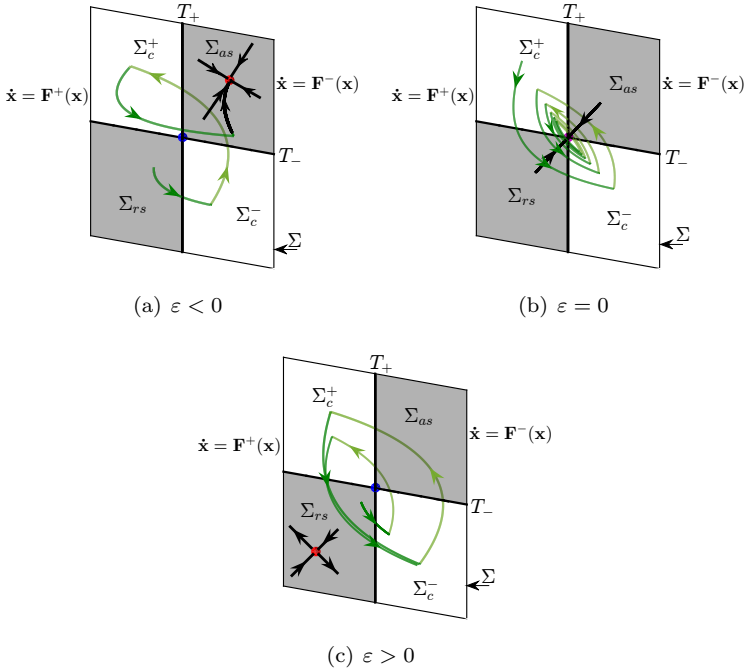

Figure 4.2: An illustrative scenario of the bifurcation at the T-singularity.

Next, in Section 4.3, we review the dynamics around the Teixeira singularity for DPWS dynamical systems, regarding first the sliding dynamics and next the crossing dynamics.

4.3 Compound bifurcation analysis

In this section, starting from the canonical form given in (4.9)-(4.10) we analyze the TS-bifurcation regarding both the sliding and crossing dynamics, computing the coefficients that generically characterize the different possibilities for the bifurcation. This bifurcation is compound in the sense that involves two different bifurcations, each one depending on different entries of the canonical form. We start by considering the pseudo-equilibrium bifurcation undergone by the sliding vector field that can be thought as a *transcritical bifurcation*; next we study the reversible *Bogdanov-Takens bifurcation* for maps associated to the generation of limit cycles, which use points belonging to the crossing regions.

To facilitate the effective application of our analysis, we write the canonical form obtained in Theorem 4.1 by emphasizing the linear terms, namely

$$\mathbf{F}^{+}(\mathbf{x}) = \begin{bmatrix} f_1^{+}x - y + x \cdot O(1) \\ 1 + g_1^{+}x + g_2^{+}y + g_3^{+}z + O(2) \\ v_{+} + r_1^{+}x + r_2^{+}y + r_3^{+}z + O(2) \end{bmatrix} \tag{4.13}$$

and

$$\mathbf{F}^{-}(\mathbf{x}) = \begin{bmatrix} f_1^{-}x + z + x \cdot O(1) \\ v_{-} + g_1^{-}x + g_2^{-}y + g_3^{-}z + O(2) \\ 1 + r_1^{-}x + r_2^{-}y + r_3^{-}z + O(2) \end{bmatrix}, \tag{4.14}$$

where $f_1^{\pm}$, $g_1^{\pm}$, $g_2^{\pm}$, $g_3^{\pm}$, $r_1^{\pm}$, $r_2^{\pm}$, $r_3^{\pm}$ are given constants, being $v_{\pm}$ the bifurcation parameters.

4.3.1 Sliding dynamics

From (4.12) with vector fields (4.13)-(4.14), we obtain the sliding vector field

$$\mathbf{F}^s(0,y,z)=\frac{1}{y+z}\begin{bmatrix}0\\ v_-y+z+g_2^-y^2+(g_2^++g_3^-)yz+g_3^+z^2+O(3)\\ y+v_+z+r_2^-y^2+(r_2^++r_3^-)yz+r_3^+z^2+O(3)\end{bmatrix}. \tag{4.15}$$

We observe that this vector field is not defined for points in Σ located in the straight line $y+z=0$. These points are at crossing regions, where the sliding vector field is not to be used, but note that the T-singularity at the origin is a singular point for it.

We recall that equilibrium points $\widetilde{\mathbf{x}}=(0,\widetilde{y},\widetilde{z})\in\Sigma$ of the sliding vector field (4.15) are called pseudo-equilibrium points for system (4.9)-(4.10). As the relevant pseudo-equilibrium points must be not located at the crossing regions, if $\widetilde{y}\widetilde{z}<0$ then $\widetilde{\mathbf{x}}\in\Sigma_c^+\cup\Sigma_c^-$ is called virtual and only if $\widetilde{y}\widetilde{z}>0$ then $\widetilde{\mathbf{x}}\in\Sigma_{as}\cup\Sigma_{rs}$ is a real pseudo-equilibrium point.

To facilitate the analysis of the sliding vector field, it is convenient to make a desingularization by redefining implicitly the time scale on every solution, namely by writing $d\tau=|y+z|d\widehat{\tau}$, where it is assumed $y+z\neq 0$. With this change, we arrive at the desingularized dynamical systems

$$\begin{cases}\dfrac{dy}{d\widehat{\tau}}=v_-y+z+g_2^-y^2+(g_2^++g_3^-)yz+g_3^+z^2+O(3),\\[2ex] \dfrac{dz}{d\widehat{\tau}}=y+v_+z+r_2^-y^2+(r_2^++r_3^-)yz+r_3^+z^2+O(3),\end{cases} \tag{4.16}$$

for $y+z>0$, and

$$\begin{cases}\dfrac{dy}{d\widehat{\tau}}=-\left[v_-y+z+g_2^-y^2+(g_2^++g_3^-)yz+g_3^+z^2+O(3)\right],\\[2ex] \dfrac{dz}{d\widehat{\tau}}=-\left[y+v_+z+r_2^-y^2+(r_2^++r_3^-)yz+r_3^+z^2+O(3)\right],\end{cases} \tag{4.17}$$

for $y+z<0$.

If $\widetilde{\mathbf{x}}=(0,\widetilde{y},\widetilde{z})$ is a pseudo-equilibrium point of (4.9)-(4.10), then,

depending on the sign of $\widetilde{y}+\widetilde{z}$, the point $(\widetilde{y},\widetilde{z})$ is an equilibrium of system (4.16) or (4.17), but in any case we must have that it fulfills the equations

$$v_-y+z+\begin{bmatrix}y & z\end{bmatrix}G\begin{bmatrix}y\\z\end{bmatrix}+O(3)=0, \tag{4.18}$$

$$y+v_+z+\begin{bmatrix}y & z\end{bmatrix}R\begin{bmatrix}y\\z\end{bmatrix}+O(3)=0, \tag{4.19}$$

where

$$G=\begin{bmatrix}g_2^- & g_3^-\\ g_2^+ & g_3^+\end{bmatrix} \quad \text{and} \quad R=\begin{bmatrix}r_2^- & r_3^-\\ r_2^+ & r_3^+\end{bmatrix}. \tag{4.20}$$

If $(\widetilde{y},\widetilde{z})$ is an equilibrium of type node, focus or saddle, then the pseudo-equilibrium $\widetilde{\mathbf{x}}$ is said to be a pseudo-node, pseudo-focus or pseudo-saddle, respectively. Note that thanks to the desingularization, the point $(0,0)$ is always an equilibrium for systems (4.16) and (4.17), even $(0,0,0)$ is not a proper equilibrium of $\mathbf{F}^s$.

Remark 4.2. *For the analysis of sliding dynamics, we can just consider the vector field* (4.16) *as defined in the whole* $\mathbb{R}^2$ *looking for the possible equilibrium bifurcation near the origin and taking into account that we must reverse the time when passing to the zone* $y+z<0$.

From (4.18)-(4.19), we note that for all values of parameters v_- and v_+ the origin is a solution. Since the Jacobian matrix at the origin is

$$J(0,0)=\begin{bmatrix}v_- & 1\\ 1 & v_+\end{bmatrix},$$

we can surmise for $v_-v_+-1=0$ the existence of another bifurcating branch of solutions. Using the parameter $\varepsilon=v_-v_+-1$, and assuming $v_+\neq 0$ and fixed, then

$$v_-=\frac{1+\varepsilon}{v_+}, \tag{4.21}$$

and we can state the following result about the bifurcation undergone by system (4.16) when $\varepsilon=0$.

Proposition 4.1. *Assuming in system* (4.16) *that the parameter* v_- *is given as* (4.21)*, where* v_+ *is fixed, and that the coefficient*

$$\kappa_S = \begin{bmatrix} -v_+ & 1 \end{bmatrix} (v_+ G - R) \begin{bmatrix} -v_+ \\ 1 \end{bmatrix} \neq 0, \tag{4.22}$$

where the matrices G *and* R *are given in* (4.20)*, the following statements hold.*

(a) *System* (4.16) *undergoes a transcritical bifurcation for* $\varepsilon = 0$*, so that, apart from the trivial solution, there exists another branch of equilibria* $(\widetilde{y}(\varepsilon), \widetilde{z}(\varepsilon))$ *with* $(\widetilde{y}(0), \widetilde{z}(0)) = (0, 0)$ *and*

$$(\widetilde{y}'(0), \widetilde{z}'(0)) = \left(-\frac{v_+^2}{\kappa_S}, \frac{v_+}{\kappa_S} \right).$$

(b) *For the particular case where* $v_+ < 0$*, the emanating branch* $(\widetilde{y}(\varepsilon), \widetilde{z}(\varepsilon))$ *is located at the quadrants with* $yz > 0$*. If* $\kappa_S > 0$ $(\kappa_S < 0)$ *then in passing from* $\varepsilon < 0$ *to* $\varepsilon > 0$ *the origin passes from being a saddle to a stable node, while the nontrivial equilibrium* $(\widetilde{y}, \widetilde{z})$ *passes from being a stable node in the first (third) quadrant to be a saddle in the third (first) quadrant.*

Proof. Since the parameter v_+ is fixed, by applying the implicit function theorem at $(\widetilde{y}, \widetilde{z}) = (0, 0)$ to the equation (4.19), which does not depend on v_-, we can assure for any solution with $|\widetilde{z}|$ small the expansion

$$\widetilde{y} = -v_+ \widetilde{z} + O(\widetilde{z}^2). \tag{4.23}$$

Using (4.21), multiplying (4.18) by v_+ and subtracting (4.19), we get the scalar equation

$$\varepsilon \widetilde{y} + \begin{bmatrix} \widetilde{y} & \widetilde{z} \end{bmatrix} (v_+ G - R) \begin{bmatrix} \widetilde{y} \\ \widetilde{z} \end{bmatrix} + O(3) = 0. \tag{4.24}$$

Substituting (4.23) in (4.24) we obtain the equation

$$-v_+\varepsilon\widetilde{z} + \kappa_S\widetilde{z}^2 + \widetilde{z}^2\phi(\widetilde{z},\varepsilon) = 0,$$

with κ_S given in (4.22), being ϕ a smooth function defined at a neighborhood of $(\widetilde{z},\varepsilon) = (0,0)$ satisfying $\phi(0,0) = 0$. After removing the trivial solution $\widetilde{z} = 0$, we desingularize the equation, and from the hypothesis $\kappa_S \neq 0$ we can apply to it the implicit function theorem at $(\widetilde{z},\varepsilon) = (0,0)$ to solve for $\widetilde{z}$. We get

$$\widetilde{z}(\varepsilon) = \frac{v_+}{\kappa_S}\varepsilon + O(\varepsilon^2).$$

Statement (a) comes now directly after using the expansion (4.23) to get the local parametrization of the bifurcating branch.

The nontrivial branch of equilibria $(\widetilde{y}(\varepsilon),\widetilde{z}(\varepsilon))$ uses for $|\varepsilon|$ small the quadrants with $yz > 0$ when $\widetilde{y}'(0)\widetilde{z}'(0) > 0$, that is, when $v_+ < 0$. In such a case, according to statement (b), if $\kappa_S > 0$ ($\kappa_S < 0$), then the nontrivial equilibrium is in the first (third) quadrant for $\varepsilon < 0$, being in the third (first) quadrant for $\varepsilon > 0$.

To show all the assertions of statement (b), it remains to analyze the stability of the equilibria $(0,0)$ and $(\widetilde{y}(\varepsilon),\widetilde{z}(\varepsilon))$ of system (4.16). Denoting by $J_{ij}(y,z)$ the entries of its Jacobian matrix $J(y,z)$ in a generic point (y,z), we have

$$J_{11}(y,z) = v_- + \begin{bmatrix}1 & 0\end{bmatrix} G \begin{bmatrix}y\\ z\end{bmatrix} + \begin{bmatrix}y & z\end{bmatrix} G \begin{bmatrix}1\\ 0\end{bmatrix} + O(2) =$$
$$= v_- + \begin{bmatrix}y & z\end{bmatrix} (G + G^T) \begin{bmatrix}1\\ 0\end{bmatrix} + O(2),$$

and similarly,

$$J_{12}(y,z) = 1 + \begin{bmatrix}y & z\end{bmatrix} (G + G^T) \begin{bmatrix}0\\ 1\end{bmatrix} + O(2),$$

$$J_{21}(y,z) = 1 + \begin{bmatrix} y & z \end{bmatrix} (R + R^T) \begin{bmatrix} 1 \\ 0 \end{bmatrix} + O(2),$$

$$J_{22}(y,z) = v_+ + \begin{bmatrix} y & z \end{bmatrix} (R + R^T) \begin{bmatrix} 0 \\ 1 \end{bmatrix} + O(2).$$

Using (4.21), the Jacobian matrix of system (4.16) at the origin is

$$J(0,0) = \begin{pmatrix} \frac{1+\varepsilon}{v_+} & 1 \\ 1 & v_+ \end{pmatrix},$$

so that $\det J(0,0) = \varepsilon$, and

$$\operatorname{trace} J(0,0) = \frac{1+v_+^2}{v_+} + \frac{\varepsilon}{v_+}.$$

For the nontrivial branch $(\widetilde{y}(\varepsilon), \widetilde{z}(\varepsilon))$ we also have

$$\operatorname{trace} J\left(\widetilde{y}(\varepsilon), \widetilde{z}(\varepsilon)\right) = \frac{1+v_+^2}{v_+} + O(\varepsilon),$$

while, after substituting the first terms of its expansion in ε, we get

$$\begin{aligned} \det J\left(\widetilde{y}(\varepsilon), \widetilde{z}(\varepsilon)\right) = \varepsilon + v_+ \frac{v_+}{\kappa_S} \begin{bmatrix} -v_+ & 1 \end{bmatrix} (G + G^T) \begin{bmatrix} 1 \\ 0 \end{bmatrix} \varepsilon + \\ + \frac{1}{v_+} \frac{v_+}{\kappa_S} \begin{bmatrix} -v_+ & 1 \end{bmatrix} (R + R^T) \begin{bmatrix} 0 \\ 1 \end{bmatrix} \varepsilon - \\ - \frac{v_+}{\kappa_S} \begin{bmatrix} -v_+ & 1 \end{bmatrix} (G + G^T) \begin{bmatrix} 0 \\ 1 \end{bmatrix} \varepsilon - \\ - \frac{v_+}{\kappa_S} \begin{bmatrix} -v_+ & 1 \end{bmatrix} (R + R^T) \begin{bmatrix} 1 \\ 0 \end{bmatrix} \varepsilon + O(\varepsilon^2). \end{aligned}$$

We claim that $\det J\left(\widetilde{y}(\varepsilon), \widetilde{z}(\varepsilon)\right) = -\varepsilon + O(\varepsilon^2)$. In fact, we see that the

above expression is equivalent to

$$\varepsilon - \frac{v_+}{\kappa_S}\begin{bmatrix}-v_+ & 1\end{bmatrix}(G+G^T)\begin{bmatrix}-v_+\\ 1\end{bmatrix}\varepsilon +$$
$$+\frac{1}{\kappa_S}\begin{bmatrix}-v_+ & 1\end{bmatrix}(R+R^T)\begin{bmatrix}-v_+\\ 1\end{bmatrix}\varepsilon + O(\varepsilon^2) =$$
$$= \varepsilon - \frac{2v_+}{\kappa_S}\begin{bmatrix}-v_+ & 1\end{bmatrix}G\begin{bmatrix}-v_+\\ 1\end{bmatrix}\varepsilon + \frac{2}{\kappa_S}\begin{bmatrix}-v_+ & 1\end{bmatrix}R\begin{bmatrix}-v_+\\ 1\end{bmatrix}\varepsilon + O(\varepsilon^2) =$$
$$= \varepsilon - \frac{2}{\kappa_S}\begin{bmatrix}-v_+ & 1\end{bmatrix}(v_+G-R)\begin{bmatrix}-v_+\\ 1\end{bmatrix}\varepsilon + O(\varepsilon^2) = -\varepsilon + O(\varepsilon^2),$$

where we have substituted the definition (4.22) of the criticality coefficient κ_S.

Under the assumption $v_+ < 0$, we conclude that for $\varepsilon < 0$ the point $(0,0)$ is a saddle while $(\widetilde{y},\widetilde{z})$ is a stable node. On the other hand, for $\varepsilon > 0$ the point $(0,0)$ is a stable node and $(\widetilde{y},\widetilde{z})$ is a saddle. Statement (b) is shown and the proof is complete. □

From Proposition 4.1, we see that when $\varepsilon = 0$ we have $\widetilde{\mathbf{x}}(0) = (0,0,0)$, i.e., $\widetilde{\mathbf{x}}$ collides with the T-singularity. Assuming $v_+ < 0$ and $v_- < 0$, in changing the sign of ε, one pseudo-equilibrium passes from the region Σ_{as} to Σ_{rs} or *vice versa*. Note that in the case $\kappa_S < 0$, when $\varepsilon < 0$ the pseudo-node $\widetilde{\mathbf{x}}$ in Σ_{rs} is unstable, because in this case the point $(\widetilde{y}(\varepsilon),\widetilde{z}(\varepsilon))$ is actually an equilibrium for system (4.17) and not for system (4.16). Taking this observation into account, we can state our first main result, whose proof is now immediate.

Theorem 4.2. *Consider $v_+ < 0$ constant and $\varepsilon = v_-v_+ - 1$. Assume that the criticality coefficient defined in* (4.22) *satisfies $\kappa_S \neq 0$. System* (4.9)-(4.13)-(4.14) *undergoes for $\varepsilon = 0$ a pseudo-equilibrium transition from Σ_{as} to Σ_{rs} (or vice versa) in its sliding dynamics. More precisely, there exists for $|\varepsilon| > 0$ small, one pseudo-equilibrium point*

$$\widetilde{\mathbf{x}}(\varepsilon) = (0, \widetilde{y}(\varepsilon), \widetilde{z}(\varepsilon))$$

such that

$$(\widetilde{y}(\varepsilon), \widetilde{z}(\varepsilon)) = \left(-\frac{v_+^2}{\kappa_S}, \frac{v_+}{\kappa_S}\right)\varepsilon + O(\varepsilon^2),$$

and the following statements hold.

(a) (Supercritical case) *If* $\kappa_S > 0$*, then for* $\varepsilon < 0$ *the point* $\widetilde{\mathbf{x}}(\varepsilon) \in \Sigma_{as}$ *is a stable pseudo-node, being* $\widetilde{\mathbf{x}}(\varepsilon) \in \Sigma_{rs}$ *a pseudo-saddle for* $\varepsilon > 0$.

(b) (Subcritical case) *If* $\kappa_S < 0$*, then for* $\varepsilon < 0$ *the point* $\widetilde{\mathbf{x}}(\varepsilon) \in \Sigma_{rs}$ *is an unstable pseudo-node, being* $\widetilde{\mathbf{x}}(\varepsilon) \in \Sigma_{as}$ *a pseudo-saddle for* $\varepsilon > 0$.

We emphasize that the expression (4.22) characterizing the sliding dynamics bifurcation depends only on the coefficients of linear terms in system (4.9) with vector fields given in (4.13)-(4.14).

4.3.2 Crossing dynamics

As it will be shown at once, the sliding dynamics bifurcation studied in Theorem 4.2 is generically accompanied by the generation of a CLC having two points at Σ_c.

In order to analyze the possible existence of CLCs, we consider a trajectory $\phi^+(\tau)$ of system (4.9)-(4.10) with initial condition $\mathbf{x}_0 = (0, y_0, z_0) \in \Sigma_c^+$, such that for $\tau = \tau_1$ the trajectory transversally returns for the first time to Σ at the point $\mathbf{x}_1 = (0, y_1, z_1) \in \Sigma_c^-$, i.e., $\phi^+(\tau_1) = \mathbf{x}_1$. Accordingly, we define a half-return map P_+ such that $P_+(y_0, z_0) = (y_1, z_1)$. Next, for system (4.9)-(4.10), we consider the trajectory $\phi^-(\tau)$ with initial condition $\mathbf{x}_1 = (0, y_1, z_1) \in \Sigma_c^-$, such that for $\tau = \tau_2$ it returns transversally to the plane $x = 0$ at the point $\mathbf{x}_2 = (0, y_2, z_2) \in \Sigma_c^+$, that is, $\phi^-(\tau_2) = \mathbf{x}_2$. We also define a half-return map P_- such that $P_-(y_1, z_1) = (y_2, z_2)$, see Figure 4.3(a). Clearly, when $\mathbf{x}_0 = \mathbf{x}_2$ system (4.9)-(4.10) exhibits a closed orbit that crosses the plane $x = 0$ at the points $\mathbf{x}_0$ and $\mathbf{x}_1$, which belong to the crossing regions, as shown in Figure 4.3(b).

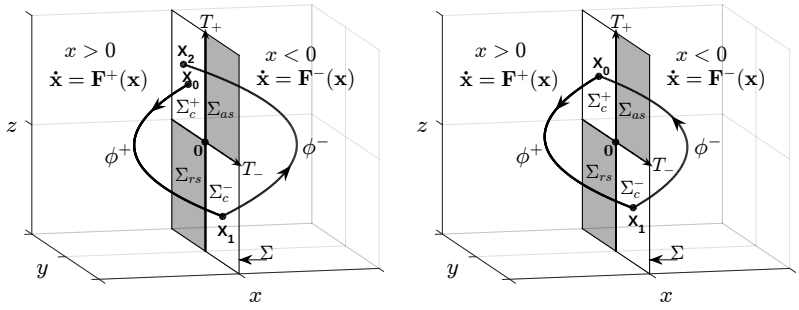

Figure 4.3: Determining the existence of CLCs via the half-return maps.

We will analyze the existence and stability of CLCs by studying the fixed points of the first return map, which can be obtained after the composition of the above two half-return maps. We know from [116] that both half-return maps are involutions; furthermore, each one must leave invariant the corresponding tangency line. Thus, these half-return maps possess a certain structure in their coefficients; in particular, the fact that in a neighborhood of $(y, z) = (0, 0)$ we have $P_+(0, z) = (0, z)$ and $P_-(y, 0) = (y, 0)$ imposes expansions of the form

$$P_+(y,z) = \begin{bmatrix} l_1^+ & 0 \\ l_2^+ & 1 \end{bmatrix} \begin{bmatrix} y \\ z \end{bmatrix} + y \begin{bmatrix} q_{11}^+ y + q_{12}^+ z \\ q_{21}^+ y + q_{22}^+ z \end{bmatrix} + \\ + y \begin{bmatrix} c_{11}^+ y^2 + c_{12}^+ yz + c_{13}^+ z^2 \\ c_{21}^+ y^2 + c_{22}^+ yz + c_{23}^+ z^2 \end{bmatrix} + O(4),$$

$$P_-(y,z) = \begin{bmatrix} 1 & l_1^- \\ 0 & l_2^- \end{bmatrix} \begin{bmatrix} y \\ z \end{bmatrix} + z \begin{bmatrix} q_{11}^- y + q_{12}^- z \\ q_{21}^- y + q_{22}^- z \end{bmatrix} + \\ + z \begin{bmatrix} c_{11}^- y^2 + c_{12}^- yz + c_{13}^- z^2 \\ c_{21}^- y^2 + c_{22}^- yz + c_{23}^- z^2 \end{bmatrix} + O(4),$$

where the letters l, q and c are used for coefficients of linear, quadratic and cubic terms, respectively. If we impose now that both maps are involutions and we exclude the trivial case in which both maps are equal to the identity, we get that $l_1^+ = l_2^- = -1$, along with the conditions

$$q_{12}^+ = c_{13}^+ = 0, \qquad q_{21}^+ = \frac{l_2^+}{2}(q_{22}^+ - q_{11}^+),$$

$$c_{11}^+ = \frac{l_2^+ c_{12}^+}{2} - (q_{11}^+)^2, \quad c_{22}^- = \frac{l_2^+}{2}(2c_{23}^+ - c_{12}^+) + \frac{q_{22}^+}{2}(q_{22}^+ - q_{11}^+),$$

and

$$q_{21}^- = c_{21}^- = 0, \qquad q_{12}^- = \frac{l_1^-}{2}(q_{11}^- - q_{22}^-),$$

$$c_{23}^- = \frac{l_1^- c_{22}^-}{2} - (q_{22}^-)^2, \quad c_{12}^- = \frac{l_1^-}{2}(2c_{11}^- - c_{22}^-) + \frac{q_{11}^-}{2}(q_{11}^- - q_{22}^+).$$

The effective computation of all these coefficients for system (4.9)-(4.13)-(4.14) is still a pending task. The specific case of DPWL system is done in Section 4.4, and the used ideas there can be extended to the general case with some additional work. We advance however that in any case we have $l_2^+ = -2v_+$, and $l_1^- = -2v_-$.

When $v_- = 1/v_+$, we see that the linear part of the first return map turns out to be

$$\begin{pmatrix} 1 & -2/v_+ \\ 0 & -1 \end{pmatrix} \cdot \begin{pmatrix} -1 & 0 \\ -2v_+ & 1 \end{pmatrix} = \begin{pmatrix} 3 & -2/v_+ \\ 2v_+ & -1 \end{pmatrix},$$

with 1 as double eigenvalue and $[1, v_+]^T$ as the only eigenvector. To analyze the topological type of this degeneration, we study the possible existence of local invariant manifolds and the dynamics on them. Such local manifolds must be tangent to the above eigendirection. Thus, we can assume for the local invariant manifolds to be the graph of a

function

$$z = a(y) = v_+ y + a_2 y^2 + a_3 y^3 + O(y^4)$$

with $v_+ < 0$, so that after building the composition $(P_- \circ P_+)(y, z)$, we must have

$$(\tilde{y}, a(\tilde{y})) = (P_- \circ P_+)(y, a(y)),$$

and this condition allows to define the iteration function governing the dynamics on the local invariant manifold, namely

$$\tilde{y} = \alpha(y) = y + \alpha_2 y^2 + \alpha_3 y^3 + O(y^4).$$

We can assure that the above composition of half-return maps is well-defined in a wedge-shaped neighborhood around the eigenvector $[1, v_+]^T$, within Σ_c^+.

Taking advantage of the involution property for P_-, we can write instead

$$P_-^{-1}(\tilde{y}, a(\tilde{y})) = P_-(\tilde{y}, a(\tilde{y})) = P_+(y, a(y)),$$

arriving to the equivalent condition

$$P_-(\alpha(y), a(\alpha(y))) = P_+(y, a(y)), \tag{4.25}$$

where all the coefficients of P_- are evaluated for $v_- = 1/v_+$. By construction, equation (4.25) is satisfied up to first order term in y. Computing the second order terms in y, and imposing their cancellation in both coordinates, we get the two equalities

$$\begin{aligned} \frac{1}{v_+}\left(2a_2 + q_{11}^+ v_+ - q_{22}^- v_+^2 + v_+\alpha_2\right) &= 0, \\ 2a_2 + q_{11}^+ v_+ - q_{22}^- v_+^2 + v_+\alpha_2 &= 0, \end{aligned} \tag{4.26}$$

which are clearly redundant, and do not allow to solve for a_2 and α_2. We can state so the following remark.

Remark 4.3. *The second order terms of half-return maps do not suffice to determine the degeneracy of the T-singularity, according to what is*

stated later, in Remark 4.4.

If we compute for (4.25) the third order terms in y, and impose their cancellation in both coordinates, we get two new equalities, namely

$$\frac{1}{2v_+}\left(4a_3+8a_2\alpha_2+2(a_2q_{11}^- - 2a_2q_{22}^- - (q_{11}^+)^2+\alpha_3)v_+ + \right.$$
$$\left. +2(c_{11}^- - c_{22}^- - 2q_{22}^-\alpha_2)v_+^2 + q_{11}^-(q_{22}^- - q_{11}^-)v_+^3 - 2c_{13}^-v_+^4\right)=0$$

and

$$\frac{1}{2}\left(4a_3+4a_2\alpha_2+2c_{21}^+ + 2a_2q_{22}^+ + (q_{22}^+(q_{22}^+ - q_{11}^+) - 4q_{22}^-a_2 + 2\alpha_3)v_+ + \right.$$
$$\left. +2(c_{12}^+ - c_{23}^+ - 2q_{22}^-\alpha_2)v_+^2 + 2(q_{22}^-)^2v_+^3\right)=0,$$

where we see that there appear the new unknowns a_3 and α_3. Fortunately, they can be removed after a simple combination of both equalities to get

$$\begin{aligned} &4a_2\alpha_2 - 2(q_{22}^+ - q_{11}^-v_+)a_2 - 2c_{21}^+ - \\ &-(2(q_{11}^+)^2 - q_{11}^+q_{22}^+ + (q_{22}^+)^2)v_+ + 2(c_{11}^- - c_{22}^- - c_{12}^+ + c_{23}^+)v_+^2 - \\ &-((q_{11}^-)^2 - q_{11}^-q_{22}^- + 2(q_{22}^-)^2)v_+^3 - 2c_{13}^-v_+^4 = 0. \end{aligned} \tag{4.27}$$

Solving any of the equations (4.26) for α_2, we have

$$\alpha_2 = -\frac{1}{v_+}\left(2a_2 + q_{11}^+v_+ - q_{22}^-v_+^2\right)$$

and substituting in the previous expression, we get a quadratic in a_2, namely

$$\begin{aligned} &8a_2^2 + 2\left((2q_{11}^+ + q_{22}^+)v_+ - (q_{11}^- + 2q_{22}^-)v_+^2\right)a_2 + 2c_{21}^+v_+ + \\ &+(2(q_{11}^+)^2 - q_{11}^+q_{22}^+ + (q_{22}^+)^2)v_+^2 - 2(c_{11}^- - c_{22}^- - c_{12}^+ + c_{23}^+)v_+^3 + \\ &+((q_{11}^-)^2 - q_{11}^-q_{22}^- + 2(q_{22}^-)^2)v_+^4 + 2c_{13}^-v_+^5 = 0. \end{aligned} \tag{4.28}$$

On the other hand, if we solve any of the equations (4.26) for a_2, we have

$$a_2 = -\frac{v_+}{2}\left(\alpha_2 + q_{11}^+ - q_{22}^- v_+\right),$$

leading by using (4.27) to a quadratic in α_2, namely

$$\begin{aligned}
&2v_+\alpha_2^2 + \left((2q_{11}^+ - q_{22}^+)v_+ + (q_{11}^- - 2q_{22}^-)v_+^2\right)\alpha_2 + 2c_{21}^+ + \\
&+ (2(q_{11}^+)^2 - 2q_{11}^+q_{22}^+ + (q_{22}^+)^2)v_+ - \\
&- (2(c_{11}^- - c_{22}^- - c_{12}^+ + c_{23}^+) - q_{11}^-q_{11}^+ - q_{22}^-q_{22}^+)v_+^2 + \\
&+ ((q_{11}^-)^2 - 2q_{11}^-q_{22}^- + 2(q_{22}^-)^2)v_+^3 + 2c_{13}^-v_+^4 = 0.
\end{aligned}$$

This second quadratic is the more relevant one to characterize the local dynamics of the degenerated T-singularity, by using the sign of its roots.

We rewrite it in the form

$$2\alpha_2^2 - \sigma\alpha_2 + \rho = 0, \tag{4.29}$$

where

$$\sigma = -2q_{11}^+ + q_{22}^+ + (2q_{22}^- - q_{11}^-)v_+ \tag{4.30}$$

and

$$\begin{aligned}
\rho = \frac{1}{v_+}\big(&2c_{21}^+ + (2(q_{11}^+)^2 - 2q_{11}^+q_{22}^+ + (q_{22}^+)^2)v_+ - \\
&- (2c_{11}^- - 2c_{22}^- - 2c_{12}^+ + 2c_{23}^+ - q_{11}^-q_{11}^+ - q_{22}^-q_{22}^+)v_+^2 + \\
&+ ((q_{11}^-)^2 - 2q_{11}^-q_{22}^- + 2(q_{22}^-)^2)v_+^3 + 2c_{13}^-v_+^4\big)
\end{aligned} \tag{4.31}$$

Both quadratics (4.28) and (4.29) have equal discriminant up to a constant positive factor, namely

$$\begin{aligned}
\Theta = \sigma^2 - 8\rho = -\frac{1}{v_+}\big[&16c_{21}^+ + \left(12(q_{11}^+)^2 - 12q_{11}^+q_{22}^- + 7(q_{22}^-)^2\right)v_+ - \\
&-16(c_{11}^- - c_{22}^- - c_{12}^+ + c_{23}^+)v_+^2 + \\
&+ (4q_{11}^-q_{11}^+ + 8q_{11}^+q_{22}^- + 2q_{11}^-q_{22}^+ + 4q_{22}^-q_{22}^+)v_+^2 + \\
&+ \left(7(q_{11}^-)^2 - 12q_{11}^-q_{22}^- + 12(q_{22}^-)^2\right)v_+^3 + 16c_{13}^-v_+^4\big].
\end{aligned} \tag{4.32}$$

Therefore, depending on the sign of Θ, we have none ($\Theta < 0$), one ($\Theta = 0$) or two ($\Theta > 0$) local invariant manifolds. We can state the following result, which is valid for any 3D-DPWS system having a T-singularity, once expressed in its local canonical form, as stated in Theorem 4.1. See Figure 4.4.

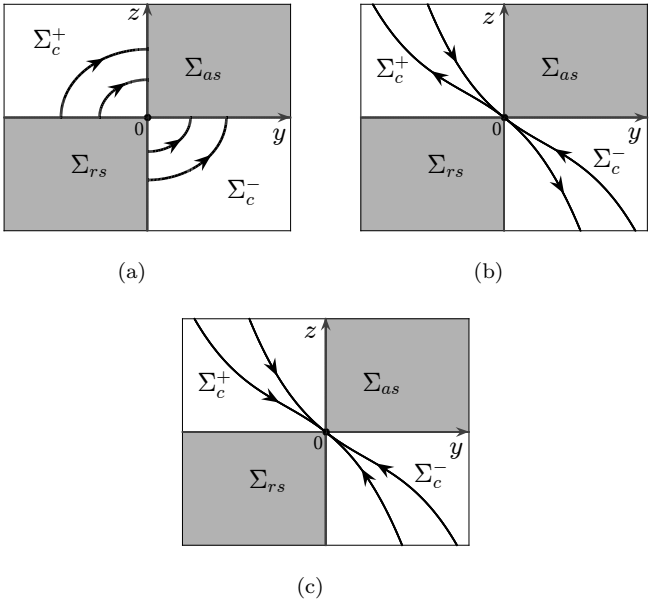

Figure 4.4: The three main topological types for the T-singularity at its degeneracy regarding the crossing dynamics: (a) center; (b) saddle; (c) node.

Theorem 4.3. *Consider system* (4.9)-(4.13)-(4.14)*, where the parameter* $v_- = 1/v_+$*, being* $v_+ < 0$ *and fixed, and assume that the half-return maps* P_- *and* P_+ *are given, so that the values* σ *and* ρ *as defined in* (4.30) *and* (4.31) *are known. The following statements hold.*

(a) *The origin is a fixed point for the composition* $P_- \circ P_+$ *whose linearization is non-hyperbolic having non-semisimple double one eigenvalue.*

(b) *If* $\sigma^2 < 8\rho$ *then the origin is of elliptic (center) type.*

(c) *If* $\rho < 0$ *then the origin is of hyperbolic (saddle) type. If* $0 < 8\rho < \sigma^2$ *then the origin is of parabolic (node) type.*

Remark 4.4. *In the above theorem, we have used for the topological type (see Figure 4.4) of the fixed point the terms elliptic (center), hyperbolic (saddle) and parabolic (node) because it is usual to study maps near fixed points by resorting to unit-time shifts along orbits of autonomous differential equations, see [77]. In fact, in our case, a planar model differential equation would be*

$$\begin{aligned} \dot{u} &= v, \\ \dot{v} &= \eta u + auv - bu^3, \end{aligned} \tag{4.33}$$

where the condition $ab \neq 0$ *is needed in order to get a determined topological type, and* η *is the unfolding parameter. Note the reversibility* $(u, v, t) \to (-u, v, -t)$*. This model corresponds with a normal form for the reversible co-dimension one Bogdanov-Takens bifurcation of the origin, see Section 4.1.2 in [66]. It is easy to study the non-hyperbolic origin for* $\eta = 0$*, concluding that for* $b < 0$ *we have a nonlinear saddle (hyperbolic type), while for* $b > 0$ *two cases arise. If* $a^2 - 8b > 0$ *then we have a nonlinear node (parabolic type), being the case* $a^2 - 8b < 0$ *corresponding to a nonlinear center (elliptic type). Thus, the reversibility property clarifies the bifurcation problem, compare with Section 3.2 and Appendix D in [26].*

We remark that in our approach we have avoided the temptation of computing the normal form for the map $P = P_- \circ P_+$ *near the organizing center, so following an alternative way to the usual analysis, as appearing in [26, 77]. We have taken advantage of the structure of the map* P*, being the composition of two involutions that allow us to deal with the reversibility property in a more direct way. Furthermore, we can so give in Theorem 4.3 the explicit expressions for the coefficients* σ *and* ρ *in terms of the data.*

4.3.3 Existence and stability of bifurcating CLCs

In looking for bifurcating crossing limit cycles, we must compose the two half-return maps P_+ and P_- by forcing the equality

$$(P_- \circ P_+)(y_0, z_0) = (y_0, z_0),$$

that is $(y_2, z_2) = (y_0, z_0)$. However, it is more direct to write the condition

$$P_+(y_0, z_0) = P_-^{-1}(y_0, z_0) = P_-(y_0, z_0),$$

where the second equality comes from the involution property of P_-. Thus, suppressing the subscript 0 for coordinates, and rearranging terms, we will work with the equations

$$\begin{aligned} 0 &= -2y + 2v_- z + q_{11}^+ y^2 - q_{11}^- yz - q_{12}^- z^2 + c_{11}^+ y^3 + \\ &\quad + (c_{12}^+ - c_{11}^-) y^2 z - c_{12}^- yz^2 - c_{13}^- z^3 + \cdots , \end{aligned} \tag{4.34}$$

$$\begin{aligned} 0 &= -2v_+ y + 2z + q_{21}^+ y^2 + q_{22}^+ yz - q_{22}^- z^2 + c_{21}^+ y^3 + \\ &\quad + c_{22}^+ y^2 z + (c_{23}^+ - c_{22}^-) yz^2 - c_{23}^- z^3 + \cdots . \end{aligned} \tag{4.35}$$

Apart from the origin, which corresponds with the T-singularity, we see that a fixed point, leading to a CLC, can bifurcate when $v_- v_+ - 1 = 0$. This fact suggests to introduce again the parameter $\varepsilon = v_- v_+ - 1$ and do a new bifurcation analysis assuming all parameters fixed excepting v_-, to be defined as in (4.21).

We start by considering (4.35). A standard application of the implicit function theorem allows to assure the existence of a smooth function $p(y, \varepsilon)$ such that $z = y \cdot p(y, \varepsilon)$, with $p(0, 0) = v_+$. Computations give

$$\begin{aligned} p(y, \varepsilon) = v_+ &- \left(q_{11}^+ - q_{22}^-(\varepsilon) v_+\right) \frac{y}{2} + \big[-2c_{21}^+ + q_{22}^+ (2q_{11}^+ - q_{22}^+) v_+ + \\ &+ \left(2c_{22}^-(\varepsilon) - 2c_{12}^+ + 2c_{23}^+ - 2q_{22}^-(\varepsilon) q_{11}^+ - q_{22}^-(\varepsilon) q_{22}^+\right) v_+^2 - \\ &- 2c_{22}^-(\varepsilon) v_-(\varepsilon) v_+^3 \big] \frac{y^2}{4} + \cdots . \end{aligned}$$

After substituting this expression for z in (4.34), we can desingularize it to get

$$0 = 2\varepsilon - \left(q_{11}^{+} - q_{11}^{-}(\varepsilon)v_{+}\right)\varepsilon y + Q(\varepsilon)y^2 + \cdots \tag{4.36}$$

where

$$\begin{aligned} Q(\varepsilon) = -\frac{1}{2v_+}\big[&2c_{21}^{+} + \left(2(q_{11}^{+})^2 - 2q_{11}^{+}q_{22}^{+} + (q_{22}^{+})^2\right)v_{+} + \\ &+ \left(-2c_{11}^{-}(\varepsilon) + 2c_{22}^{-}(\varepsilon) + 2c_{12}^{+} - 2c_{23}^{+} + q_{11}^{-}(\varepsilon)q_{11}^{+} + q_{22}^{-}(\varepsilon)q_{22}^{+}\right)v_{+}^2 + \\ &+ \left(q_{11}^{-}(\varepsilon)^2 - 2q_{11}^{-}(\varepsilon)q_{22}^{-}(\varepsilon) + 2q_{22}^{-}(\varepsilon)^2\right)v_{+}^3 + 2c_{13}^{-}(\varepsilon)v_{+}^4 + O(\varepsilon)\big]. \end{aligned}$$

Clearly, from (4.36) we can apply the implicit function theorem at $(y, \varepsilon) = (0, 0)$ to solve for ε getting that for the emanating branch we have the expansion

$$\varepsilon = \kappa_C \cdot y^2 + O(y^3),$$

where the criticality coefficient is

$$\begin{aligned} \kappa_C = -\frac{Q(0)}{2} = \frac{1}{4v_+}\big[&2c_{21}^{+} + \left(2(q_{11}^{+})^2 - 2q_{11}^{+}q_{22}^{+} + (q_{22}^{+})^2\right)v_{+} + \\ &+ \left(-2c_{11}^{-}(0) + 2c_{22}^{-}(0) + 2c_{12}^{+} - 2c_{23}^{+} + q_{11}^{-}(0)q_{11}^{+} + q_{22}^{-}(0)q_{22}^{+}\right)v_{+}^2 + \\ &+ \left(q_{11}^{-}(0)^2 - 2q_{11}^{-}(0)q_{22}^{-}(0) + 2q_{22}^{-}(0)^2\right)v_{+}^3 + 2c_{13}^{-}(0)v_{+}^4\big] \end{aligned}$$

Note that $4\kappa_C = \rho$, as given in (4.31). In short, if we assume $v_+ < 0$ then depending on the sign of κ_C we have a subcritical or supercritical bifurcation of non-trivial fixed points (we are focussing our attention in the one with $y < 0$, but clearly there is another one with $y > 0$) and

$$\begin{aligned} z(y) &= v_{+} \cdot y + O(y^2), \\ \varepsilon(y) &= \kappa_C \cdot y^2 + O(y^3). \end{aligned}$$

To characterize the topological type of the new fixed point and its stability, we must compute the derivatives of the Poincaré half-return maps, and evaluate them at this branch of non-trivial fixed points. Computing $DP(y) = D\left(P_{-} \circ P_{+}\right)(y, z(y))$, we get that the expansions

for its determinant and trace share the coefficient of the first degree term, namely

$$\begin{aligned} \det DP(y) &= 1 + \sigma y + d_2 y^2 + O(y^3), \\ \operatorname{trace} DP(y) &= 2 + \sigma y + t_2 y^2 + O(y^3). \end{aligned} \tag{4.37}$$

where

$$\sigma = -2q_{11}^+ + q_{22}^+ + \left(2q_{22}^-(0) - q_{11}^-(0)\right) v_+,$$

as in (4.30), and the second degree terms are

$$\begin{aligned} d_2 = \frac{1}{2} \Big[& 6(q_{11}^+)^2 - 5q_{11}^+ \left(q_{22}^+ - q_{11}^-(0)v_+ + 2q_{22}^-(0)v_+\right) + \\ & + \left(q_{22}^+ - q_{11}^-(0)v_+ + 2q_{22}^-(0)v_+\right)^2 \Big], \\ t_2 = -\frac{1}{2v_+} \Big[& 8c_{21}^+ + \left(2(q_{11}^+)^2 - 3q_{11}^+ q_{22}^+ + 3(q_{22}^+)^2\right) v_+ + \\ & + \left(-8c_{11}^-(0) + 8c_{22}^-(0) + 8c_{12}^+ - 8c_{23}^+ - q_{11}^-(0)q_{11}^+ + \right. \\ & \left. + 10q_{22}^-(0)q_{11}^+ + 2q_{11}^-(0)q_{22}^+\right) v_+^2 + \\ & + \left(3q_{11}^-(0)^2 - 4q_{11}^-(0)q_{22}^-(0) + 4q_{22}^-(0)^2\right) v_+^3 + 8c_{13}^-(0)v_+^4 \Big]. \end{aligned}$$

Furthermore, it turns out that $d_2 - t_2 = 8\kappa_C = 2\rho$. Recall that the standard stability conditions for fixed points of maps in $\mathbb{R}^2$ are

(i) $|\det DP| < 1$, and

(ii) $|\operatorname{trace} DP| < \det DP + 1$

at the fixed point, see Figure 4.5. Therefore, if we assume $\sigma \neq 0$, then we conclude from (4.37) that to satisfy (i), the stability of the bifurcating fixed point requires $\sigma > 0$, since $y < 0$ at the bifurcating point. Checking (ii), we get

$$1 + (t_2 - d_2)y^2 + O(y^3) = 1 - 2\rho y^2 + O(y^3) < 1,$$

what also requires $\kappa_C > 0$.

The topological type of the fixed point can be determined by

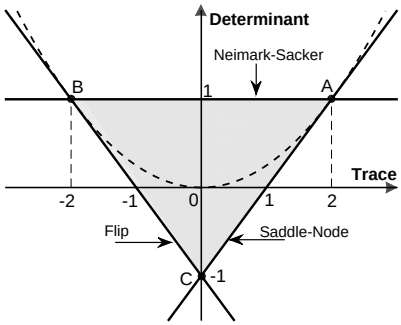

Figure 4.5: The stability region for the fixed point of the return map determines a triangle in the (trace, det)-plane. The degeneracy of the T-singularity corresponds with the labeled vertex A. Each side of the triangle corresponds with the indicated bifurcation.

computing the value of the discriminant

$$\begin{aligned}(\operatorname{trace} DP(y))^2 - 4\det DP(y) &= \left[\sigma^2 + 4(t_2 - d_2)\right] y^2 + O(y^3) = \\ &= \left(\sigma^2 - 8\rho\right) y^2 + O(y^3).\end{aligned}$$

Clearly, when $\rho < 0$ the bifurcating fixed points has two real eigenvalues λ_1 and λ_2 with $0 < \lambda_1 < 1 < \lambda_2$, so that its topological type is a saddle. When $\rho > 0$ we have a node or a focus depending on the sign of $\sigma^2 - 8\rho$. Lastly, when σ vanishes, we have a degeneracy whose characterization should require much longer computations.

Remark 4.5. *It should be noticed that* $\sigma^2 - 8\rho = \Theta$*, as given in* (4.32)*. Thus, we see that the topological type of the new fixed points is inherited from the topological type of the degenerate T-singularity.*

We can summarize all the above analysis in the following result, which amounts a complete characterization of the bifurcating CLC from the T-singularity.

Theorem 4.4. *Consider $v_+ < 0$ constant and $\varepsilon = v_- v_+ - 1$. Assume that the non-degeneracy conditions $\sigma \neq 0$ and $\rho \neq 0$ hold, where σ and ρ have been defined in* (4.30) *and* (4.31)*, respectively. The following statements hold.*

(a) *By varying v_-, the system* (4.9)-(4.13)-(4.14) *undergoes for $\varepsilon = 0$ a bifurcation leading to the appearance or disappearance of a CLC. Such a CLC bifurcates from the origin for $\rho \cdot \varepsilon > 0$ small.*

(b) *The bifurcating CLC is stable whenever $\sigma > 0$ and $\rho > 0$.*

(c) *The topological type of the corresponding fixed point for the first return map is saddle, node or focus depending on whether $\rho < 0$, $0 < 8\rho < \sigma^2$ or $8\rho > \sigma^2$, respectively.*

We remark that Theorem 4.4 provides a characterization of a specific *Takens-Bogdanov bifurcation* for maps, since we are dealing with a reversible map resulting from the composition of the two involutive half-return maps. The above assertions about bifurcating fixed points have a one-to-one correspondence with the existence and stability of bifurcating equilibria of the normal form (4.33) in Remark 4.4 (see Section 4.1.2 in [66]).

To apply later the above results in a convenient way for DPWL systems, we need before a procedure for computing the coefficients of the half-return maps P_+ and P_-, which is obtained in the next section.

4.4 Computing the half-return map coefficients for 3D-DPWL systems

As indicated before, we give in this section the expressions for the coefficients of the return maps in terms of the entries of system (4.9)-(4.10) when we are dealing with a piecewise-linear system, an important case in real applications, see Section 4.7.

We start so from the strictly linear version of the vector fields (4.13)-(4.14), namely

$$\mathbf{F}^{+}(\mathbf{x}) = \begin{bmatrix} f_1^{+}x - y \\ 1 + g_1^{+}x + g_2^{+}y + g_3^{+}z \\ v_{+} + r_1^{+}x + r_2^{+}y + r_3^{+}z \end{bmatrix} \tag{4.38}$$

and

$$\mathbf{F}^{-}(\mathbf{x}) = \begin{bmatrix} f_1^{-}x + z \\ v_{-} + g_1^{-}x + g_2^{-}y + g_3^{-}z \\ 1 + r_1^{-}x + r_2^{-}y + r_3^{-}z \end{bmatrix}, \tag{4.39}$$

and to analyze this issue, it is convenient first to obtain a reduced canonical form that alleviates a little bit the required computations.

Lemma 4.1. *The study of crossing dynamics and in particular the existence of CLCs for system* (4.9)*, with vector fields given in* (4.38)-(4.39)*, can be done by considering the reduced canonical form*

$$\dot{\mathbf{x}} = \begin{cases} \widetilde{\mathbf{F}}^{-}(\mathbf{x}), & \text{if } x < 0, \\ \widetilde{\mathbf{F}}^{+}(\mathbf{x}), & \text{if } x > 0, \end{cases} \tag{4.40}$$

with $\mathbf{x} = (x, y, z) \in \mathbb{R}^3$ *and the linear vector fields* $\widetilde{\mathbf{F}}^{\pm} : \mathbb{R}^3 \longrightarrow \mathbb{R}^3$ *are*

$$\widetilde{\mathbf{F}}^{+}(\mathbf{x}) = \begin{bmatrix} \tilde{f}_1^{+}x - y \\ 1 + \tilde{g}_1^{+}x + g_3^{+}z \\ v_{+} + \tilde{r}_1^{+}x + r_3^{+}z \end{bmatrix}, \quad \widetilde{\mathbf{F}}^{-}(\mathbf{x}) = \begin{bmatrix} \tilde{f}_1^{-}x + z \\ v_{-} + \tilde{g}_1^{-}x + g_2^{-}y \\ 1 + \tilde{r}_1^{-}x + r_2^{-}y \end{bmatrix}, \tag{4.41}$$

where the new entries $\tilde{f}_1^{\pm}$*,* $\tilde{g}_1^{\pm}$*, and* $\tilde{r}_1^{\pm}$ *are related with the old ones by the relations*

$$\begin{aligned} \tilde{f}_1^{+} &= f_1^{+} + g_2^{+}, \\ \tilde{g}_1^{+} &= g_1^{+} + f_1^{+}g_2^{+} - r_2^{+}g_3^{+}, \\ \tilde{r}_1^{+} &= r_1^{+} + f_1^{+}r_2^{+} - r_2^{+}r_3^{+}, \end{aligned} \tag{4.42}$$

and

$$\begin{aligned}\tilde{f}_1^- &= f_1^- + r_3^-,\\ \tilde{g}_1^- &= g_1^- - f_1^- g_3^- + g_2^- g_3^-,\\ \tilde{r}_1^- &= r_1^- - f_1^- r_3^- + r_2^- g_3^-.\end{aligned} \tag{4.43}$$

Proof. It suffices to do the non-smooth continuous change of variables

$$(\bar{x}, \bar{y}, \bar{z}) = (x, y + g_2^+ x, z + r_2^+ x)$$

when $x \geq 0$, along with

$$(\bar{x}, \bar{y}, \bar{z}) = (x, y - g_3^- x, z - r_3^- x)$$

when $x < 0$. This change reduces to the identity for $x = 0$ and so it does not alter coordinates in Σ.

Therefore, any crossing orbit and its transformed by the above change hit the manifold at the same points. This means in particular that crossing limit cycles are mapped into crossing periodic points with the same crossing points. □

Note that from Lemma 4.1 we achieve a reduced canonical form with 4 parameters less, namely g_2^+, r_2^+, g_3^- and r_3^-. Also note that the change of variables needed in its proof does not preserve the sliding dynamics and therefore is only useful for the study of CLCs.

In order to find the explicit expressions for the coefficients of each half-return map, we must determine the solution of system (4.40)-(4.41) for $x > 0$ and for $x < 0$. Such solution for $x > 0$ can be obtained from the variation of constants formula

$$\begin{aligned}\mathbf{x}(\tau) &= e^{A^+\tau}\mathbf{x}_0 + \int_0^\tau e^{A^+(\tau-s)}\mathbf{v}^+ ds =\\ &= e^{A^+\tau}\mathbf{x}_0 + \left(\int_0^\tau e^{A^+ s} ds\right)\mathbf{v}^+,\end{aligned} \tag{4.44}$$

where

$$A^+ = \begin{bmatrix} \tilde{f}_1^+ & -1 & 0 \\ \tilde{g}_1^+ & 0 & g_3^+ \\ \tilde{r}_1^+ & 0 & r_3^+ \end{bmatrix}, \quad \mathbf{x}_0 = \begin{bmatrix} 0 \\ y_0 \\ z_0 \end{bmatrix}, \quad \mathbf{v}^+ = \begin{bmatrix} 0 \\ 1 \\ v_+ \end{bmatrix}, \quad \mathbf{x}(\tau) = \begin{bmatrix} x(\tau) \\ y(\tau) \\ z(\tau) \end{bmatrix},$$

being $y_0 < 0$. It will suffice to have the Taylor's series approximation until the fourth order terms for (4.44), namely

$$\mathbf{x}(\tau) = \mathbf{x}_0 + \left(\tau I + \frac{\tau^2}{2} A^+ + \frac{\tau^3}{6} (A^+)^2 + \frac{\tau^4}{24} (A^+)^3 \right) M + O(\tau^5), \quad (4.45)$$

where $M = A^+ \mathbf{x}_0 + \mathbf{v}^+$ and I is the identity matrix of order 3.

From the first component of (4.45) we can determine an expression for the flight time $\tau_+ = \tau_+(y_0, z_0)$, which depends on y_0 and z_0, such that $x(\tau_+) = 0$. The third order polynomial approximation for the time τ_+ is given by

$$\tau_+(y_0, z_0) = a_{10} y_0 + a_{20} y_0^2 + a_{11} y_0 z_0 + a_{30} y_0^3 + a_{21} y_0^2 z_0 + a_{12} y_0 z_0^2 + \cdots \quad (4.46)$$

where

$$\begin{aligned} a_{10} &= -2, \\ a_{20} &= \frac{2}{3} (\tilde{f}_1^+ - 2 g_3^+ v_+), \\ a_{11} &= 2 g_3^+, \\ a_{30} &= -\frac{2}{9} \left(2 (\tilde{f}_1^+)^2 - 3 \tilde{g}_1^+ - (5 \tilde{f}_1^+ + 3 h_3^+) g_3^+ v_+ + 8 (g_3^+ v_+)^2 \right), \\ a_{21} &= \frac{4}{3} g_3^+ (3 g_3^+ v_+ - \tilde{f}_1^+ - r_3^+), \\ a_{12} &= -2 (g_3^+)^2. \end{aligned}$$

Now, substituting (4.46) in the second and the third component of system (4.45), the half-return map $(y_1, z_1) = P_+(y_0, z_0)$ satisfies

$$y_1 = -y_0 + q_{11}^+ y_0^2 + y_0(c_{11}^+ y_0^2 + c_{12}^+ y_0 z_0) + O(4),$$
$$z_1 = -2v_+ y_0 + z_0 + y_0(q_{21}^+ y_0 + q_{22}^+ z_0) + y_0(c_{21}^+ y_0^2 + c_{22}^+ y_0 z_0 + c_{23}^+ z_0^2) + O(4),$$

where we see that $l_2^+ = -2v_+$, and we get for the quadratic terms

$$\begin{aligned} q_{11}^+ &= \frac{2}{3}\left(\tilde{f}_1^+ + g_3^+ v_+\right), \\ q_{22}^+ &= -2(r_3^+ - g_3^+ v_+), \\ q_{21}^+ &= v_+(q_{11}^+ - q_{22}^+) = \frac{2}{3}\left(\tilde{f}_1^+ - 2g_3^+ v_+ + 3h_3^+\right) v_+, \end{aligned}$$

along with the equalities

$$\begin{aligned} c_{11}^+ &= -v_+ c_{12}^+ + (q_{11}^+)^2 = -\frac{2}{9}\left[2(\tilde{f}_1^+)^2 + (\tilde{f}_1^+ + 3h_3^+)g_3^+ v_+ - 4(g_3^+ v_+)^2\right], \\ c_{12}^+ &= -\frac{2}{3}\left(\tilde{f}_1^+ + 2g_3^+ v_+ - r_3^+\right) g_3^+, \\ c_{21}^+ &= -\frac{2}{9}\left\{3\tilde{r}_1^+ + \left[2(\tilde{f}_1^+)^2 - 3\tilde{g}_1^+ + 6h_3^+(\tilde{f}_1^+ + r_3^+)\right] v_+ \right. \\ &\quad \left. +5g_3^+(\tilde{f}_1^+ + 3h_3^+)v_+^2 + 8(g_3^+)^2 v_+^3\right\}, \end{aligned}$$

$$\begin{aligned} c_{22}^+ &= v_+(c_{12}^+ - 2c_{23}^+) + q_{22}^+(q_{22}^+ - q_{11}^+)/2 \\ &= \frac{2}{3}\left[r_3^+(\tilde{f}_1^+ + 3h_3^+) - 2g_3^+(\tilde{f}_1^+ + 5h_3^+)v_+\right] + 4(g_3^+ v_+)^2, \\ c_{23}^+ &= 2g_3^+(r_3^+ - g_3^+ v_+) = -g_3^+ q_{22}^+, \end{aligned}$$

for the cubic ones.

The computations for the map P_- are totally similar. We use again the formula given in (4.44), this time with

$$A^- = \begin{bmatrix} \tilde{f}_1^- & 0 & 1 \\ \tilde{g}_1^- & g_2^- & 0 \\ \tilde{r}_1^- & r_2^- & 0 \end{bmatrix}, \quad \mathbf{x}_1 = \begin{bmatrix} 0 \\ y_1 \\ z_1 \end{bmatrix}, \quad \mathbf{v}^- = \begin{bmatrix} 0 \\ v_- \\ 1 \end{bmatrix},$$

and compute the approximation up to third order of the return time τ_- spent by the trajectory $\phi^-(\tau)$ that starts in $\mathbf{x}_1 = (0, y_1, z_1)$ to arrive at the point $\mathbf{x}_2 = (0, y_2, z_2)$. This is done by solving the equation $x(\tau_-) = 0$ so that, after the evaluation at such a time for the other two coordinates of the solution, we determine the image of the half-return map $(y_2, z_2) = P_-(y_1, z_1)$, namely

$$y_2 = y_1 - 2v_-z_1 + z_1(q_{11}^- y_1 + q_{12}^- z_1) + z_1(c_{11}^- y_1^2 + c_{12}^- y_1 z_1 + c_{13}^- z_1^2) + O(4)$$
$$z_2 = -z_1 + q_{22}^- z_1^2 + z_1(c_{22}^- y_1 z_1 + c_{23}^- z_1^2) + O(4).$$

Here $l_1^- = -2v_-$, along with the coefficients for the quadratic terms

$$\begin{aligned} q_{11}^- &= -2(g_2^- - r_2^- v_-), \\ q_{12}^- &= v_-(q_{22}^- - q_{11}^-) = \frac{2}{3}\left(\tilde{f}_1^- - 2h_2^- v_- + 3g_2^-\right) v_-, \\ q_{22}^- &= \frac{2}{3}\left(\tilde{f}_1^- + r_2^- v_-\right), \end{aligned}$$

and the following ones for the cubic terms,

$$c_{11}^- = 2h_2^-(g_2^- - r_2^- v_-) = -r_2^- q_{11}^-,$$

$$\begin{aligned} c_{12}^- &= v_-(c_{22}^- - 2c_{11}^-) + q_{11}^-(q_{11}^- - q_{22}^-)/2 \\ &= \frac{2}{3}\left[g_2^-(\tilde{f}_1^- + 3g_2^-) - 2h_2^-(\tilde{f}_1^- + 5g_2^-)v_-\right] + 4(r_2^- v_-)^2, \\ c_{13}^- &= \frac{2}{9}\left\{3\tilde{g}_1^- - \left[2(\tilde{f}_1^-)^2 + 3\tilde{r}_1^- + 6g_2^-(\tilde{f}_1^- + g_2^-)\right] + \right. \\ &\quad \left. + 5h_2^-(\tilde{f}_1^- + 3g_2^-)v_-^2 - 8(r_2^-)^2 v_-^3\right\}, \\ c_{22}^- &= -\frac{2}{3}\left(\tilde{f}_1^- - g_2^- + 2h_2^- v_-\right) r_2^-, \\ c_{23}^- &= v_- c_{22}^- - (q_{22}^-)^2 = -\frac{2}{9}\left[2(\tilde{f}_1^-)^2 + r_2^-(\tilde{f}_1^- + 3g_2^-)v_- - 4(r_2^- v_-)^2\right]. \end{aligned}$$

Just by using the above expresions in (4.30) and (4.31), we can state the following result.

Lemma 4.2. *Assume in* (4.38)-(4.39) *that* $v_+ < 0$ *and all the parameters are fixed, excepting* v_-. *At the critical value* $v_- = 1/v_+$ *the bifurcation of a crossing limit cycle predicted by Theorem 4.4 is ruled by the values*

$$\sigma(v_+) = \frac{2}{3}\left(v_+(g_3^+ + 3g_2^- + 2\tilde{f}_1^-) - 3h_3^+ - r_2^- - 2\tilde{f}_1^+\right)$$

and

$$\begin{aligned}\rho(v_+) =& \frac{4}{3v_+}\left[\tilde{g}_1^-(v_+)^4 + \left((g_2^-)^2 + \tilde{f}_1^- g_3^+ - g_2^- g_3^+ - \tilde{r}_1^-\right)(v_+)^3 - \right.\\ &- \left(\tilde{f}_1^+ g_2^- + g_2^- r_2^- - 2g_3^+ r_2^- + \tilde{f}_1^- r_3^+ + g_3^+ r_3^+\right)(v_+)^2 + \\ &\left. + \left(\tilde{g}_1^+ + \tilde{f}_1^+ r_2^- - r_2^- r_3^+ + (r_3^+)^2\right)v_+ - \tilde{r}_1^+\right],\end{aligned}$$

where the entries $\tilde{f}_1^{\pm}$, $\tilde{g}_1^{\pm}$, *and* $\tilde{r}_1^{\pm}$ *are given in* (4.42)-(4.43).

Thanks to the above results, the application of Theorem 4.4 is straightforward, as shown next.

4.5 Examples

In this section, we study a couple of examples to illustrate the easy application of the achieved theoretical results. Both examples do not have a physical meaning but are useful to better understand the developed methodology. Later, in Section 4.7, we tackle the analysis of a boost power converter, which is our final goal.

4.5.1 Example 1

Consider the DPWL system

$$\dot{\mathbf{x}} = \begin{cases} (z, v_-, 1), & \text{if } x < 0 \\ (-y, 1, ay + bz + v_+), & \text{if } x > 0 \end{cases} \tag{4.47}$$

with $\mathbf{x} = (x, y, z)$, where $v_-, v_+ < 0$ and we take $\text{sign}(a) = \text{sign}(b)$. This system is already in the canonical form (4.38)-(4.39) with coefficients $f_1^{\pm} = r_1^+ = 0$, $r_2^+ = a$ and $r_3^+ = b$, and $g_i^{\pm} = r_i^- = 0$ for $i \in \{1, 2, 3\}$.

Regarding (4.20), here the matrix G vanishes and we have

$$R = \begin{bmatrix} 0 & 0 \\ a & b \end{bmatrix},$$

so that from (4.22) we get

$$\kappa_S = av_+ - b.$$

According to Theorem 4.2 we have that for $\varepsilon = v_-v_+ - 1$ small,

(i) if $a,\ b > 0$ then $\kappa_S < 0$ (*subcritical case*) so that $\widetilde{\mathbf{x}}(\varepsilon) \in \Sigma_{rs}$ is an unstable pseudo-node when $v_-v_+ < 1$, being a pseudo-saddle in Σ_{as} when $v_-v_+ > 1$,

(ii) if $a,\ b < 0$ then $\kappa_S > 0$ (*supercritical case*) so that $\widetilde{\mathbf{x}}(\varepsilon) \in \Sigma_{as}$ is a stable pseudo-node when $v_-v_+ < 1$, being a pseudo-saddle in Σ_{rs} when $v_-v_+ > 1$.

In fact, from (4.15) we see that

$$\mathbf{F}^s(\mathbf{x}) = \frac{1}{y+z} \begin{bmatrix} 0 \\ v_-y + z \\ y + v_+z + ayz + bz^2 \end{bmatrix},$$

so that the pseudo-equilibrium point is located exactly at

$$\widetilde{\mathbf{x}}(\varepsilon) = \left(0, -\frac{\varepsilon}{(a - bv_-)v_-}, \frac{\varepsilon}{a - bv_-}\right),$$

which, after the substitution $v_- = (1 + \varepsilon)/v_+$, coincides with the expression given in Theorem 4.2.

Regarding the crossing dynamics bifurcation, we apply first Lemma 4.1 obtaining that all the new entries are null excepting $\tilde{r}_1^+ = -ab$. Hav-

ing in mind that $r_3^+ = b$ is also non-vanishing, we obtain from Lemma 4.2 that $\sigma = -2b$, while

$$\rho = \frac{4b(a + bv_+)}{3v_+}.$$

We see that for $v_+ < 0$ we have

$$\text{sign}(\rho) = \text{sign}\left(-v_+ - \frac{a}{b}\right),$$

so that $\rho < 0$ for $-a/b < v_+ < 0$, being ρ positive for $v_+ < -a/b$. The condition $8\rho < \sigma^2$ translates to

$$\frac{b(a + bv_+)}{3v_+} < \frac{b^2}{8} \iff v_+ > -\frac{8a}{5b}.$$

Therefore, according to Theorem 4.4, we conclude that for $\varepsilon = v_-v_+ - 1$ small,

(i) the bifurcating CLC has dynamics of saddle type when

$$-\frac{a}{b} < v_+ < 0$$

and arises for $v_-v_+ < 1$;

(ii) the bifurcating CLC has dynamics of node type when

$$-\frac{8a}{5b} < v_+ < -\frac{a}{b}$$

and arises for $v_-v_+ > 1$, being stable (unstable) when $b < 0$ ($b > 0$);

(iii) the bifurcating CLC has dynamics of focus type when

$$v_+ < -\frac{8a}{5b}$$

and arises for $v_-v_+ > 1$, being stable (unstable) when $b < 0$ ($b > 0$).

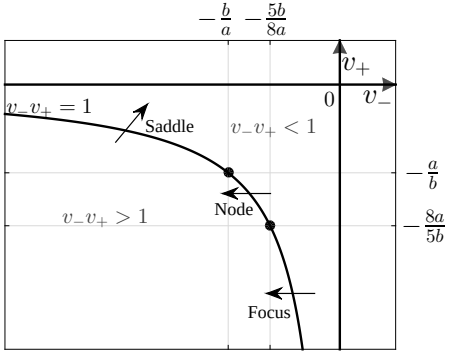

Figure 4.6: Bifurcation set in (v_-, v_+)-plane for system (4.47).

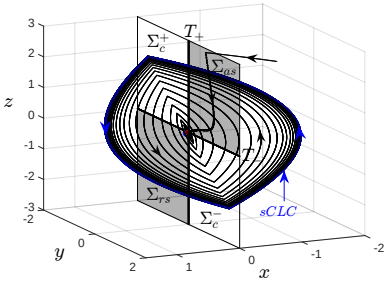

(a) CLC stable node

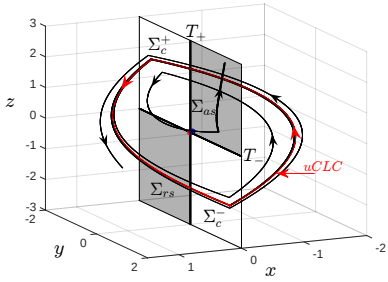

(b) CLC unstable node

Figure 4.7: Simulation results of system (4.47) for parameter values $v_- = -0.85$ and $v_+ = -1.3$. (a) when $a = b = -1$ the bifurcation leads to a stable CLC ($sCLC$); (b) when $a = b = 1$ we have an unstable CLC ($uCLC$). In both cases the CLC has dynamics of node type, the blue point is a pseudo-saddle and the red point at the origin is the T-singularity.

In Figure 4.6, we summarize the crossing dynamics bifurcation, by indicating the dynamical type of the bifurcating CLC; the arrows mark the direction in which one must cross the curve $v_-v_+ = 1$ to get the new limit cycle. Such a curve is divided in three parts, depending on the type of dynamics of the CLC when it is born. Two cases where

the CLC is of node type are shown in Figure 4.7.

Clearly, the bifurcation set in Figure 4.6 is to be completed. In particular, the point $(v_-, v_+) = (-a/b, -b/a)$ should be a co-dimension two bifurcation point, since there is a transition between parabolic (node) character and hyperbolic (saddle) character. This kind of reversible co-dimension two Bogdanov-Takens points is analyzed in [1] for two-dimensional smooth differential systems. The translation of such analysis would lead to the existence of a bifurcation curve emanating from such a point, where saddle-node bifurcations of CLCs take place.

4.5.2 Example 2

As our second example, we study a DPWL system introduced in [26], defined by the vector fields

$$\mathbf{F}^+(\mathbf{x}) = \begin{bmatrix} a_{11}x - y \\ -x - 3y + 1 \\ a_{32}y - 2z + v_+ \end{bmatrix} \text{ and } \mathbf{F}^-(\mathbf{x}) = \begin{bmatrix} 3x + z \\ -2y + v_- \\ x + 3z + 1 \end{bmatrix},$$

where $v_-, v_+ < 0$ and $a_{11}, a_{32} \in \mathbb{R}$. Again, this system is already in the canonical form (4.38)-(4.39) with coefficients $f_1^+ = a_{11}$, $g_1^+ = -1$, $g_2^+ = -3$, $g_3^+ = r_1^+ = 0$, $r_2^+ = a_{32}$, $r_3^+ = -2$, $f_1^- = 3$, $g_1^- = g_3^- = 0$, $g_2^- = -2$, $r_1^- = 1$, $r_2^- = 0$ and $r_3^- = 3$.

Here, from (4.20) we have

$$G = \begin{bmatrix} -2 & 0 \\ -3 & 0 \end{bmatrix}, \quad R = \begin{bmatrix} 0 & 3 \\ a_{32} & -2 \end{bmatrix},$$

so that from (4.22) we get

$$\kappa_S(v_+) = \begin{bmatrix} -v_+ & 1 \end{bmatrix} \begin{bmatrix} -2v_+ & -3 \\ -3v_+ - a_{32} & 2 \end{bmatrix} \begin{bmatrix} -v_+ \\ 1 \end{bmatrix} =$$
$$= 2 + (3 + a_{32})v_+ + 3v_+^2 - 2v_+^3.$$

After applying Lemma 4.1, we obtain the new entries $\tilde{f}_1^+ = a_{11}-3$, $\tilde{g}_1^+ = -1-3a_{11}$, $\tilde{r}_1^+ = (a_{11}+2)a_{32}$, $\tilde{f}_1^- = 6$, $\tilde{g}_1^- = 0$ and $\tilde{r}_1^- = -8$. Therefore, we get from Lemma 4.2

$$\sigma(v_+) = \frac{4}{3}\left(3v_+ - a_{11} + 6\right)$$
$$\rho(v_+) = \frac{4}{3v_+}\left[12(v_+)^3 + 2(3+a_{11})(v_+)^2 + 3(1-a_{11})v_+ - a_{32}(a_{11}+2)\right].$$

To apply Theorems 4.2 and 4.4 without requiring a long discussion, let us consider just the bifurcation point corresponding to $v_- = v_+ = -1$. Then, we have

$$\kappa_S(-1) = 4 - a_{32},$$
$$\sigma(-1) = \frac{4}{3}\left(3 - a_{11}\right)$$
$$\rho(-1) = \frac{4}{3}\left[a_{32}(a_{11}+2) - 5a_{11} + 9\right].$$

Therefore, we see that the sliding bifurcation changes its character when $a_{32} = 4$. Regarding the crossing bifurcation, we detect the existence of the hyperbola $a_{32} = (5a_{11}-9)/(a_{11}+2)$ in the plane (a_{11}, a_{32}) where $\rho = 0$, separating the saddle and node cases for the bifurcating CLC. Furthermore, after computing the expression $\sigma^2 - 8\rho$, we detect another hyperbola, namely $6a_{32} = (24a_{11} + a_{11}^2 - 45)/(a_{11}+2)$, which separates the node and focus cases for the bifurcating CLC.

Regions	**CLC type**
1 and 6	saddle (unstable)
2 and 7	unstable node
3 and 8	unstable focus
4 and 9	stable focus
5 and 10	stable node

Table 4.1: The topological type of the CLC that bifurcates from the T-singularity, with reference to Figure 4.8.

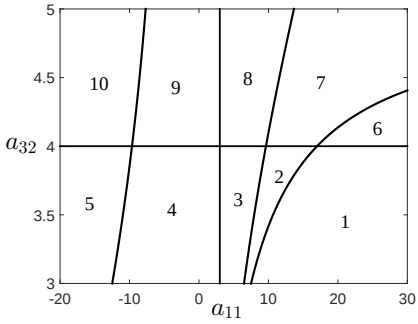

Figure 4.8: By selecting the two parameters a_{11} and a_{32}, one can obtain the ten possible scenarios for the TS-bifurcation for the specific degeneracy that appears for $(v_-, v_+) = (-1, -1)$. Regarding the sliding bifurcation, supercritical cases occurs in the regions from 1 to 5 and subcritical ones from 6 to 10. For the involved crossing dynamics, see Table 4.1.

In Figure 4.8 we show a partial view of the bifurcation set in the parameter plane (a_{11}, a_{32}), where all the ten possible scenarios for the TS-bifurcation appear, according to Table 4.1. Comparing these results with the numerical simulations summarized in Table 1 of [26], we see that we obtain algebraic expressions delimiting the ten possible scenarios, also detecting possible co-dimension two points.

For instance, when $a_{11} = 3$ the point $(v_-, v_+) = (-1, -1)$ should be a codimension-two bifurcation point, since there is a transition from stable to unstable focus (elliptic) character. The analysis in [1] for two-dimensional smooth differential systems, adequately translated for maps, should confirm the existence of two new bifurcation curves emanating from such a point; one for Neimark-Sacker bifurcation points (leading to an invariant closed curve associated to dynamics on a torus) and the other for homoclinic bifurcation points, see [16].

These two examples show the ability of our theoretical results in predicting the local dynamical behaviour around the T-singularities. In Section 4.6, below, we present the transformations in the states and in the time scale, in order to obtain the canonical form (4.38)-(4.39), from

a general discontinuous piecewise-linear (DPWL) system. The results of this section will be useful for the unfolding of Section 4.7, where we analyze a real application problem in power electronics.

4.6 TS-bifurcation in 3D-DPWL systems: a computational procedure

In the applications regarding 3D-DPWL systems, the general situation is to have three vectors $\mathbf{w}^-,\ \mathbf{w}^+,\ \mathbf{v} \in \mathbb{R}^3$, with $\mathbf{v} \neq \mathbf{0}$, two 3×3 square matrices A^- and A^+ and a scalar $\delta \in \mathbb{R}$, such that

$$\dot{\mathbf{x}} = \begin{cases} \mathbf{F}^-(\mathbf{x}) = A^-\mathbf{x} + \mathbf{w}^-, & \text{if } \mathbf{v}^T\mathbf{x} + \delta < 0, \\ \mathbf{F}^+(\mathbf{x}) = A^+\mathbf{x} + \mathbf{w}^+, & \text{if } \mathbf{v}^T\mathbf{x} + \delta > 0, \end{cases} \tag{4.48}$$

and $A^-\mathbf{x} + \mathbf{w}^- \neq A^+\mathbf{x} + \mathbf{w}^+$ generically, when $\mathbf{v}^T\mathbf{x} + \delta = 0$.

The switching boundary is then the plane

$$\Sigma = \{\mathbf{x} \in \mathbb{R}^3 :\ h(\mathbf{x}) = \mathbf{v}^T\mathbf{x} + \delta = 0\}, \tag{4.49}$$

and therefore, the tangency lines are[4]

$$T_- = \{\mathbf{x} \in \Sigma : \mathbf{v}^T\mathbf{F}^-(\mathbf{x}) = 0\}, \tag{4.50}$$

$$T_+ = \{\mathbf{x} \in \Sigma : \mathbf{v}^T\mathbf{F}^+(\mathbf{x}) = 0\}. \tag{4.51}$$

For $\mathbf{x} \in T_-$ the tangency is of the visible (invisible) fold type if[5]

$$\mathbf{v}^T A^-\mathbf{F}^-(\mathbf{x}) < 0\ (> 0). \tag{4.52}$$

Analogously, for $\mathbf{x} \in T_+$ the tangency is of the visible (invisible) fold type if

$$\mathbf{v}^T A^+\mathbf{F}^+(\mathbf{x}) > 0\ (< 0). \tag{4.53}$$

[4]Note that $L_{\mathbf{F}^\pm}h(\mathbf{x}) = \mathbf{v}^T\mathbf{F}^\pm(\mathbf{x})$.
[5]Note that $L^2_{\mathbf{F}^\pm}h(\mathbf{x}) = \mathbf{v}^T A^\pm\mathbf{F}^\pm(\mathbf{x})$.

If the fold tangency lines T_- and T_+ intersect transversally at one point $\widehat{\mathbf{x}} \in \Sigma$, then this intersection point represents a two-fold singularity. When both tangencies are of invisible type, this point is a T-singularity; see [69]. Note that from (4.49), (4.50) and (4.51), a T-singularity is a solution of the equation

$$\begin{bmatrix} \mathbf{v}^T \\ \mathbf{v}^T A^- \\ \mathbf{v}^T A^+ \end{bmatrix} \mathbf{x} + \begin{bmatrix} \delta \\ \mathbf{v}^T w^- \\ \mathbf{v}^T w^+ \end{bmatrix} = \mathbf{0}. \tag{4.54}$$

Thus, a natural first hypothesis is the following.

(A1) *The set* $\{\mathbf{v}^T, \mathbf{v}^T A^-, \mathbf{v}^T A^+\}$ *is linearly independent.*

Note that hypothesis (A1) guarantees the transversality of T_- and T_+ along with the uniqueness of the two-fold point $\widehat{\mathbf{x}}$, solution of (4.54). As a second hypothesis, we assume the needed condition to have invisible tangencies from both sides.

(A2) *At the two-fold point* $\widehat{\mathbf{x}}$*, the conditions* $\mathbf{v}^T A^- \mathbf{F}^-(\widehat{\mathbf{x}}) > 0$ *and* $\mathbf{v}^T A^+ \mathbf{F}^+(\widehat{\mathbf{x}}) < 0$ *hold.*

If we assume $\delta = 0$ and $\mathbf{v}^T = (1, 0, 0)$ then $\mathbf{v}^T \mathbf{x} + \delta = x_1$. So, we would start from the system

$$\dot{\mathbf{x}} = \begin{cases} A^- \mathbf{x} + \mathbf{w}^-, & \text{if } x_1 < 0 \\ A^+ \mathbf{x} + \mathbf{w}^+, & \text{if } x_1 > 0 \end{cases} \tag{4.55}$$

where $\mathbf{x} = [x_1 \ x_2 \ x_3]^T$, $\mathbf{w}^\pm = [w_1^\pm \ w_2^\pm \ w_3^\pm]^T$, the dot "$\cdot$" denotes the derivative in relation to the time variable t and

$$A^\pm = \begin{bmatrix} a_{11}^\pm & a_{12}^\pm & a_{13}^\pm \\ a_{21}^\pm & a_{22}^\pm & a_{23}^\pm \\ a_{31}^\pm & a_{32}^\pm & a_{33}^\pm \end{bmatrix}.$$

Hypothesis (A1) translates to

$$\Delta := \det \begin{bmatrix} \mathbf{v}^T \\ \mathbf{v}^T A^- \\ \mathbf{v}^T A^+ \end{bmatrix} = \det \begin{bmatrix} 1 & 0 & 0 \\ a_{11}^- & a_{12}^- & a_{13}^- \\ a_{11}^+ & a_{12}^+ & a_{13}^+ \end{bmatrix} = a_{12}^- a_{13}^+ - a_{13}^- a_{12}^+ \neq 0. \tag{4.56}$$

Thus, system (4.55) has a double tangency point in the transverse intersection of the tangency lines contained in the plane $x_1 = 0$, defined by the sets

$$T_\pm = \{(0, x_2, x_3) : a_{12}^\pm x_2 + a_{13}^\pm x_3 + w_1^\pm = 0\},$$

if and only if $\Delta \neq 0$, as defined in (4.56). These tangency lines are obtained using the equations (4.50)-(4.51), assuming $\mathbf{v}^T = (1, 0, 0)$. We have so the two-fold point located at $(0, \widehat{x}_2, \widehat{x}_3) \in T_+ \cap T_-$.

We summarize in the next two lemmas the explicit changes needed in this DPWL case to arrive at the canonical form of Theorem 4.1. In the Lemma below, we propose first an invertible change of coordinates to place the double tangency point at the origin of $\mathbb{R}^3$ so that the tangency lines T_- and T_+ become the second and third coordinate axis, respectively. We also impose that the new region with attractive sliding be the quadrant corresponding to positive values of the last two coordinates.

Lemma 4.3. *Assuming Hypothesis (A1), the affine change of coordinates*

$$\begin{bmatrix} x_1 \\ x_2 \\ x_3 \end{bmatrix} = \begin{bmatrix} 1 & 0 & 0 \\ 0 & \alpha_2 & \alpha_3 \\ 0 & \beta_2 & \beta_3 \end{bmatrix} \begin{bmatrix} \overline{x} \\ \overline{y} \\ \overline{z} \end{bmatrix} + \begin{bmatrix} 0 \\ \alpha_1 \\ \beta_1 \end{bmatrix}, \tag{4.57}$$

with

$$\alpha_1 = \frac{a_{13}^- w_1^+ - a_{13}^+ w_1^-}{\Delta},\ \alpha_2 = \frac{a_{13}^-}{\Delta},\ \alpha_3 = \frac{a_{13}^+}{\Delta},$$

and

$$\beta_1 = \frac{a_{12}^+ w_1^- - a_{12}^- w_1^+}{\Delta},\ \beta_2 = \frac{-a_{12}^-}{\Delta} \text{ and } \beta_3 = \frac{-a_{12}^+}{\Delta},$$

transforms system (4.55) *into the system*

$$(\dot{\overline{x}}, \dot{\overline{y}}, \dot{\overline{z}}) = \begin{cases} \mathbf{G}^-(\overline{x}, \overline{y}, \overline{z}), & \text{if } \overline{x} < 0 \\ \mathbf{G}^+(\overline{x}, \overline{y}, \overline{z}), & \text{if } \overline{x} > 0 \end{cases}, \tag{4.58}$$

where

$$\mathbf{G}^-(\overline{x}, \overline{y}, \overline{z}) = \begin{bmatrix} s_1^- \overline{x} + z \\ p_1^- \overline{x} + p_2^- \overline{y} + p_3^- \overline{z} + b_2^- \\ q_1^- \overline{x} + q_2^- \overline{y} + p_3^- \overline{z} + b_3^- \end{bmatrix}$$

and

$$\mathbf{G}^+(\overline{x}, \overline{y}, \overline{z}) = \begin{bmatrix} s_1^+ \overline{x} - \overline{y} \\ p_1^+ \overline{x} + p_2^+ \overline{y} + p_3^+ \overline{z} + b_2^+ \\ q_1^+ \overline{x} + q_2^+ \overline{y} + q_3^+ \overline{z} + b_3^+ \end{bmatrix}$$

with the coefficients

$$\begin{aligned}
s_1^\pm &= a_{11}^\pm, \\
p_1^\pm &= -a_{21}^\pm a_{12}^+ - a_{31}^\pm a_{13}^+, \\
p_2^\pm &= \Delta \left(a_{22}^\pm \alpha_2 \beta_3 + a_{23}^\pm \beta_2 \beta_3 - a_{32}^\pm \alpha_2 \alpha_3 - a_{33}^\pm \alpha_3 \beta_2 \right), \\
p_3^\pm &= \Delta \left(a_{23}^\pm \beta_3^2 - a_{32}^\pm \alpha_3^2 + (a_{22}^\pm - a_{33}^\pm) \alpha_3 \beta_3 \right), \\
q_1^\pm &= -a_{21}^\pm a_{12}^- - a_{31}^\pm a_{13}^-, \\
q_2^\pm &= \Delta \left(a_{32}^\pm \alpha_2^2 - a_{23}^\pm \beta_2^2 + (a_{33}^\pm - a_{22}^\pm) \alpha_2 \beta_2 \right), \\
q_3^\pm &= \Delta \left(a_{33}^\pm \alpha_2 \beta_3 + a_{32}^\pm \alpha_2 \alpha_3 - a_{22}^\pm \alpha_3 \beta_2 - a_{23}^\pm \beta_2 \beta_3 \right), \\
b_2^\pm &= \Delta \left(w_2^\pm \beta_3 + a_{22}^\pm \alpha_1 \beta_3 + a_{23}^\pm \beta_1 \beta_3 - w_3^\pm \alpha_3 - a_{32}^\pm \alpha_1 \alpha_3 - a_{33}^\pm \alpha_3 \beta_1 \right), \\
b_3^\pm &= \Delta \left(w_3^\pm \alpha_2 + a_{32}^\pm \alpha_1 \alpha_2 + a_{33}^\pm \alpha_2 \beta_1 - w_2^\pm \beta_2 - a_{22}^\pm \alpha_1 \beta_2 - a_{23}^\pm \beta_1 \beta_2 \right).
\end{aligned}$$

Proof. As indicated before, we want to transform the tangency lines $T_\pm$ so that in the new variables (x, y, z) we have

$$a_{12}^- x_2 + a_{13}^- x_3 + w_1^- = \overline{z} \tag{4.59}$$

$$a_{12}^+ x_2 + a_{13}^+ x_3 + w_1^+ = -\overline{y}. \tag{4.60}$$

Solving for (x_2, x_3) we get the change of variables (4.57), where the

expressions for α_i and β_i are as shown in the statement of the Lemma.

Note that from (4.57) and (4.59)-(4.60) we can deduce that

$$\begin{bmatrix} a_{12}^{+} & a_{13}^{+} \end{bmatrix} \begin{bmatrix} \alpha_2 & \alpha_3 \\ \beta_2 & \beta_3 \end{bmatrix} = \begin{bmatrix} -1 & 0 \end{bmatrix}, \quad \begin{bmatrix} a_{12}^{-} & a_{13}^{-} \end{bmatrix} \begin{bmatrix} \alpha_2 & \alpha_3 \\ \beta_2 & \beta_3 \end{bmatrix} = \begin{bmatrix} 0 & 1 \end{bmatrix},$$

and

$$\begin{bmatrix} a_{12}^{\pm} & a_{13}^{\pm} \end{bmatrix} \begin{bmatrix} \alpha_1 \\ \beta_1 \end{bmatrix} + w^{\pm} = 0.$$

Taking into account these equalities, the new entries for the vector field come easily after making the change given in (4.57). □

After the application of Lemma 4.3, we have got a new system that have the tangency lines T_- and T_+ at the y- and z-axis, respectively, so that the double tangency is now at the origin. Note that in (4.58) the Hypothesis (A2), regarding the conditions to have an invisible two-fold gives now

$$\begin{aligned} L^2_{\mathbf{G}^-} h(\mathbf{0}) &= b_3^- > 0 \\ L^2_{\mathbf{G}^+} h(\mathbf{0}) &= -b_2^+ < 0. \end{aligned}$$

In the Lemma below, we indicate the additional invertible change of coordinates along with the time scaling needed to rewrite the system (4.58) in the canonical form of Theorem 4.1.

Lemma 4.4. *Assuming Hypothesis (A2), that is $b_3^- > 0$ and $b_2^+ > 0$, the invertible change of coordinates*

$$(\overline{x}, \overline{y}, \overline{z}) = (x, \omega_+ y, \omega_- z)$$

along with the non-uniform time scaling $\tau = \omega_+ t$ for $x > 0$, and $\tau = \omega_- t$ for $x < 0$, with $\omega_+ = \sqrt{b_2^+}$ and $\omega_- = \sqrt{b_3^-}$, transforms system (4.58) *into the system*

$$\dot{\mathbf{x}} = \begin{cases} \mathbf{F}^-(\mathbf{x}), & \text{if } x < 0, \\ \mathbf{F}^+(\mathbf{x}), & \text{if } x > 0, \end{cases} \tag{4.61}$$

with the vector fields

$$\mathbf{F}^{+}(\mathbf{x}) = \begin{bmatrix} f_1^{+}x - y \\ 1 + g_1^{+}x + g_2^{+}y + g_3^{+}z \\ v_{+} + r_1^{+}x + r_2^{+}y + r_3^{+}z \end{bmatrix}, \tag{4.62}$$

$$\mathbf{F}^{-}(\mathbf{x}) = \begin{bmatrix} f_1^{-}x + z \\ v_{-} + g_1^{-}x + g_2^{-}y + g_3^{-}z \\ 1 + r_1^{-}x + r_2^{-}y + r_3^{-}z \end{bmatrix}. \tag{4.63}$$

In system (4.61), $\mathbf{x} = (x, y, z)$ *is the state vector, the dot "·" denotes derivatives in relation to the new time* τ *and the new coefficients are*

$$v_{+} = \frac{b_3^{+}}{\omega_{-}\omega_{+}}, \quad v_{-} = \frac{b_2^{-}}{\omega_{-}\omega_{+}}, \quad f_1^{\pm} = \frac{s_1^{\pm}}{\omega_{\pm}}, \quad g_2^{\pm} = \frac{p_2^{\pm}}{\omega_{\pm}}, \quad r_3^{\pm} = \frac{q_3^{\pm}}{\omega_{\pm}},$$
$$g_1^{-} = \frac{p_1^{-}}{\omega_{-}\omega_{+}}, \quad g_3^{-} = \frac{p_3^{-}}{\omega_{+}}, \quad r_1^{-} = \frac{q_1^{-}}{\omega_{-}^2}, \quad r_2^{-} = \frac{q_2^{-}\omega_{+}}{\omega_{-}^2}, \quad g_1^{+} = \frac{p_1^{+}}{\omega_{+}^2},$$
$$g_3^{+} = \frac{p_3^{+}\omega_{-}}{\omega_{+}^2}, \quad r_1^{+} = \frac{q_1^{+}}{\omega_{-}\omega_{+}}, \quad r_2^{+} = \frac{q_2^{+}}{\omega_{-}}.$$

Proof. Note that $(\dot{\bar{x}}, \dot{\bar{y}}, \dot{\bar{z}}) = \omega_{\pm}\dfrac{d}{d\tau}(x, \omega_{+}y, \omega_{-}z)$ and $\omega_{\pm} > 0$. Thus, we rewrite (4.58) as

$$\omega_{-}\frac{d}{d\tau}(x, \omega_{+}y, \omega_{-}z) = \mathbf{G}^{-}(x, \omega_{+}y, \omega_{-}z) \quad \text{for} \quad x < 0,$$
$$\omega_{+}\frac{d}{d\tau}(x, \omega_{+}y, \omega_{-}z) = \mathbf{G}^{+}(x, \omega_{+}y, \omega_{-}z) \quad \text{for} \quad x > 0.$$

Then, the vector fields $\mathbf{F}^{\pm}$ are easily obtained by writing

$$\mathbf{F}^{-}(\mathbf{x}) = \operatorname{diag}\left[\frac{1}{\omega_{-}}, \frac{1}{\omega_{-}\omega_{+}}, \frac{1}{\omega_{-}^2}\right] \cdot \mathbf{G}^{-}(x, \omega_{+}y, \omega_{-}z)$$

and

$$\mathbf{F}^{+}(\mathbf{x}) = \operatorname{diag}\left[\frac{1}{\omega_{+}}, \frac{1}{\omega_{+}^2}, \frac{1}{\omega_{-}\omega_{+}}\right] \cdot \mathbf{G}^{+}(x, \omega_{+}y, \omega_{-}z);$$

and the new coefficients come directly. □

Remark 4.6. *From the transformations proposed here, we can investigate the occurrence of the TS-bifurcation in 3D-DPWL systems such as* (4.48)*, using the canonical form* (4.61)-(4.63)*. Note that the vector fields* (4.63) *are the linear version of the vector fields* (4.13)-(4.14)*. Therefore, the general system* (4.48) *undergoes a TS-bifurcation if it is possible to rewrite it in canonical form* (4.61)-(4.63) *and if there exists a solution of the equation* $\varepsilon = v_- v_+ - 1 = 0$ *for some parameter of* (4.48) *such that* $v_-(0) < 0$*,* $v_+(0) < 0$ *and* $\kappa_S(0) \neq 0$*, where* κ_S *is given in* (4.22)*. Such a statement is in agreement with the definition of TS-bifurcation given in 2.10. Then, we use the Theorem 4.2 to classify the TS-bifurcation in subcritical or supercritical case and the Theorem 4.4 to determine the stability of the CLC bifurcating from the T-singularity. For this, we resort to the coefficients* σ *and* ρ *given in Lemma 4.2.*

Next section is dedicated to a case study in order to apply the results previously obtained.

4.7 Application in a boost converter with SMC-Washout

For this case study, we consider the model of a dc-dc boost converter, operating in Continuous Conduction Mode (CCM), with sliding mode control and washout filter (SMC-Washout). Such a model was introduced in Chapter 2, Section 2.6, see Figures 2.9 and 2.10.

We assume the dimensionless model given in (2.15)-(2.16)-(2.18)[6], with the scalar function $h(\mathbf{x}) : \mathbb{R}^3 \to \mathbb{R}$ such that the switching boundary is

$$\Sigma = \{\mathbf{x} = (x, y, z) \in \mathbb{R}^3 : h(\mathbf{x}) = y - y_r + k(x - z) = 0\}, \qquad (4.64)$$

where $y_r > 1$ is the normalized reference parameter and $k > 0$ is the

[6]For simplicity, we use z instead of $\overline{z}$ as in (2.18).

normalized control parameter (to be adequately tuned).

Then we get the control process model described as the three-dimensional DPWL system

$$\dot{\mathbf{x}} = \begin{cases} \mathbf{F}^+(\mathbf{x}), \text{ if } h(\mathbf{x}) > 0, \\ \mathbf{F}^-(\mathbf{x}), \text{ if } h(\mathbf{x}) < 0, \end{cases} \tag{4.65}$$

with

$$\mathbf{F}^+(\mathbf{x}) = \begin{bmatrix} 1 - bx - y \\ x - ay \\ \omega(x - z) \end{bmatrix}, \quad \mathbf{F}^-(\mathbf{x}) = \begin{bmatrix} 1 - bx \\ -ay \\ \omega(x - z) \end{bmatrix},$$

where $\mathbf{x} = (x, y, z) \in \mathbb{R}^3$ are the state variables and the parameters are $\omega \in (0, 1]$ (normalized filter parameter), $a > 0$ (normalized resistive load parameter) and $b \geq 0$ (normalized inductor resistance parameter). We stress that $x > 0$ is the normalized inductor current, $y \geq 0$ is the normalized output voltage and $z \in \mathbb{R}$ depends on the filtered current.

The goal is to have a pseudo-equilibrium point fulfilling the control objective $y = y_r > 1$ and adequately located in the region Σ_{as}, in order to get a robust operating point. Although the model seems elementary, the computations in general are cumbersome, so that we will adopt a simplified version.

Remark 4.7. *From now on, we take $y_r = 2$, $a > 1$, and $k > 2$ for definiteness. To facilitate the remaining computations, we also assume $b = 0$, that is, an ideal inductance, and $\omega = 1$.*

According to Remark 4.7 and Section 4.6, since $\mathbf{v}^T = \nabla h = [k, 1, -k]$ the subset of Σ corresponding to Σ_{as} is defined by the inequalities

$$k(1 - y) + x - ay - k(x - z) < 0 < k - ay - k(x - z),$$

or equivalently,

$$k - 2 + x - (a + k - 1)y < 0 < k - 2 - (a - 1)y,$$

where the elimination of z is possible from (4.64), which implies

$$-k(x-z) = y - 2$$

on Σ. We note that all the points in Σ_{as} satisfy $x - ky < 0$. According to (4.12) the corresponding sliding vector field is

$$\mathbf{F}^s(\mathbf{x}) = \frac{1}{k(x-ky)} \begin{bmatrix} k[x - ay^2 - y(2-y)] \\ k[x(2-y) + k(ay^2 - x)] \\ (2-y)(x-ky) \end{bmatrix},$$

where $x - ky < 0$. By construction, the plane Σ is invariant for this vector field. The only pseudo-equilibrium point is obtained on the parabola $x = ay^2$ for $y = 2$, that is at $\widetilde{\mathbf{x}} = (4a, 2, 4a)$, which belongs to Σ_{as} whenever $k > 2a$ (the restriction $k > 2a$ is a key condition for the efficiency of our boost converter). In the following we will show that TS-bifurcation is associated with violation of this restriction.

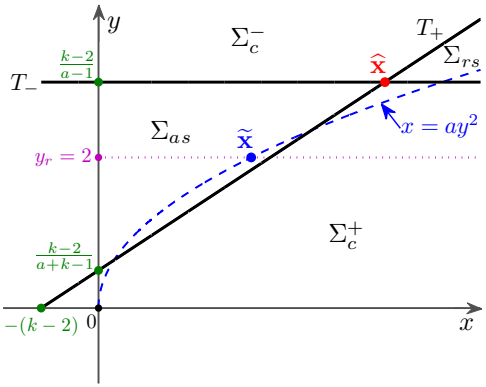

Figure 4.9: Projection on the (x, y)-plane of the notable elements used for the boost converter control design. The point $\widetilde{\mathbf{x}}$ (the operating point) is within the attractive sliding region Σ_{as}. In the degeneracy, such a point collides with the T-singularity $\widehat{\mathbf{x}}$ to enter the repulsive sliding region Σ_{rs}.

If we calculate the tangency lines of each vector field $\mathbf{F}^{\pm}$ according to (4.50)-(4.51), then we see that such tangency lines can be written as

$$T_- = \{\mathbf{x} \in \Sigma : \ (1-a)y + k - 2 = 0\},$$
$$T_+ = \{\mathbf{x} \in \Sigma : \ x + (1-a-k)y + k - 2 = 0\},$$

and they correspond with the boundaries of Σ_{as}. See Figure 4.9 for a geometric view of the projection on the (x, y)-plane of such notable elements.

Hypothesis (A1) of Section 4.6 is clearly true, since the matrix

$$\begin{bmatrix} \mathbf{v}^T \\ \mathbf{v}^T A^- \\ \mathbf{v}^T A^+ \end{bmatrix} = \begin{bmatrix} k & 1 & -k \\ -k & -a & k \\ 1-k & -a-k & k \end{bmatrix}$$

is non-singular whenever $k \neq 0$ and $a \neq 1$. In this case, a two-fold singularity occurs at the point $\hat{\mathbf{x}} = (k\hat{y}, \hat{y}, \hat{z})$, with

$$\hat{y} = \frac{k-2}{a-1} > 0, \quad \hat{z} = \frac{(1+k^2)\hat{y} - 2}{k}.$$

To check Hypothesis (A2), we use inequalities (4.52)-(4.53), and so we need

$$\mathbf{v}^T A^- \mathbf{F}^-(\hat{\mathbf{x}}) = [-k, -a, k] \begin{bmatrix} 1 \\ -a\hat{y} \\ \hat{x} - \hat{z} \end{bmatrix} > 0$$

and

$$\mathbf{v}^T A^+ \mathbf{F}^+(\hat{\mathbf{x}}) = [1-k, -a-k, k] \begin{bmatrix} 1-\hat{y} \\ \hat{x} - a\hat{y} \\ \hat{x} - \hat{z} \end{bmatrix} < 0,$$

so that, after some standard computations, it can be proved that the point $\hat{\mathbf{x}}$ is an invisible two-fold singularity (T-singularity) if and only if

$$a(k-2) > 0, \quad (k-2)a^2 - (k-3)a - (k-1)^3 < 0.$$

Therefore, we have a T-singularity for all (k, a) such that

$$k > 2 \tag{4.66}$$

and

$$1 < a < \frac{k - 3 + \sqrt{(k-3)^2 + 4(k-2)(k-1)^3}}{2(k-2)}. \tag{4.67}$$

Under conditions (4.66) and (4.67) the system (4.65) can be rewritten in the canonical form (4.61)-(4.63). For this, we follow the scheme of Section 4.6 and the transformations indicated in Lemma 4.3 and Lemma 4.4. Previously, we transform the switching boundary Σ into the plane $x_1 = 0$ for a new state space $(x_1, x_2, x_3) \in \mathbb{R}^3$, using the invertible coordinates change

$$(x, y, z) = \left(\frac{x_1 - x_2 + kx_3 + 2}{k}, x_2, x_3 \right).$$

We obtain for the new parameters

$$v_- = \frac{1 - a^2(k-2) - a(3 - 3k + k^2)}{(a-1)\omega_+\omega_-}, \quad v_+ = \frac{(a-k)(k-2)}{\omega_+\omega_-},$$

along with

$$f_1^- = -\frac{1}{\omega_-}, \qquad f_1^+ = -\frac{k-1}{k\omega_+},$$
$$r_1^+ = -\frac{a-1}{k\omega_-\omega_+}, \quad r_3^+ = \frac{k-1}{\omega_+},$$

$$g_2^- = r_1^- = r_2^- = 0, \qquad g_1^- = -\frac{1}{k\omega_-\omega_+},$$
$$g_3^- = \frac{a^2k + a(1-k+k^2) - 1}{(a-1)k\omega_+}, \qquad r_3^- = -\frac{a}{\omega_-},$$
$$g_1^+ = \frac{k^2 + (a-2)k + 1}{k^2\omega_+^2}, \qquad g_2^+ = -\frac{k^2 + (a-1)k + 1}{k\omega_+},$$
$$g_3^+ = -\frac{(k^2 + (a-2)k + 2 - a)\omega_-}{(a-1)\omega_+^2}, \quad r_2^+ = \frac{a-1}{\omega_-},$$

where the two conditions

$$\omega_-^2 = a(k-2) > 0, \quad \omega_+^2 = \frac{(k-1)^3 + (k-3)a - (k-2)a^2}{a-1} > 0,$$

are guaranteed from Hypothesis (A2).

Before applying the Theorems 4.2 and 4.4, we investigate first what is the bifurcation curve in the (k, a)-plane of parameters. We obtain from a direct computation that

$$v_- v_+ - 1 = (2a - k)\hat{y} = 0,$$

i.e., the bifurcation condition in original parameters is $k = 2a$, as suspected. Moreover, we check that, for all $a > 1$

$$v_+\big|_{k=2a} = \frac{2a(1-a)}{\omega_+\omega_-} < 0, \quad v_-\big|_{k=2a} = \frac{-1+2a-6a^2}{\omega_+\omega_-} < 0.$$

Therefore, the TS-bifurcation occurs for $k = 2a$ with $a > 1$ and the sliding bifurcation is supercritical, since

$$\kappa_S|_{k=2a} = \frac{2}{(1-2a+6a^2)^{\frac{3}{2}}} > 0.$$

Therefore, close enough to the T-singularity ($k \approx 2a \Rightarrow v_- v_+ \approx 1$), we have a stable pseudo-node in Σ_{as} for $k > 2a$ ($v_- v_+ < 1$) and a pseudo-saddle in Σ_{rs} for $k < 2a$ ($v_- v_+ > 1$).

Regarding the crossing bifurcation, we obtain

$$\sigma\big|_{k=2a} = \frac{2(4(1+a) + (4a-1)^2 + 24a^3)}{3((1-a)^2 + 5a^2)^{\frac{3}{2}}} > 0$$

and

$$\rho\big|_{k=2a} = \frac{8}{3((1-a)^2 + 5a^2)^2} > 0,$$

so that the bifurcating CLC for $k < 2a$ is stable. By checking that for

all $a > 1$ we have

$$\sigma^2 - 8\rho\big|_{k=2a} = \frac{4(576a^6 + 768a^5 + 64a^4 + 112a^3 - 112a^2 + 56a - 23)}{9((a-1)^2 + 5a^2)^3} =$$
$$= \frac{4(576a^6 + 768a^5 + 64a^4 + 112a^2(a-1) + 33a + 23(a-1))}{9((a-1)^2 + 5a^2)^3} > 0,$$

we conclude that it is of node type.

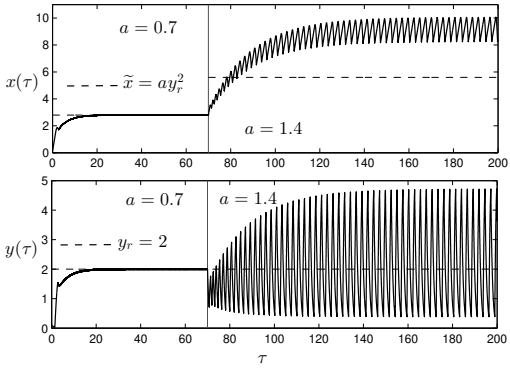

Figure 4.10: Normalized time-domain responses of a boost converter with SMC, modeled by (4.64)-(4.65) and simulated with $b = 0$, $\omega = 1$, $y_r = 2$, $k = 2.5$ and initial (normalized) resistive load $a = 0.7$, changing to $a = 1.4$ after $\tau = 70$ s. The dashed line indicates the operating point required for the converter, but not reached when the normalized resistive load (a) exceeds the value 1.25.

We finish our study by emphasizing the importance of the achieved results: once the control parameter $k > 2$ is fixed, our theorems allow us to predict not only the parameter region where the control strategy is adequate ($2 < 2a < k$) but also the undesirable dynamic consequences of possible changes in the load (whenever $2a > k$) that lead to destabilizing the operating point, by getting an oscillating voltage around it (see Figure 4.10).

In Figure 4.11, some simulation results are presented where we visualize the passage of the stable pseudo-node from the attractive sliding

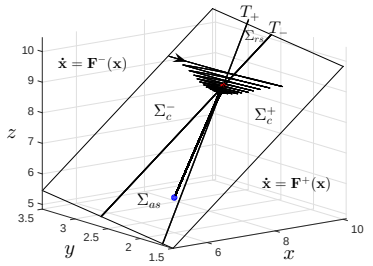

(a) $k > 2a$

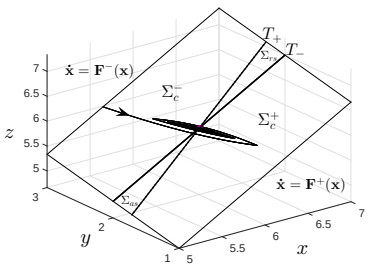

(b) $k = 2a$, birth of the CLC

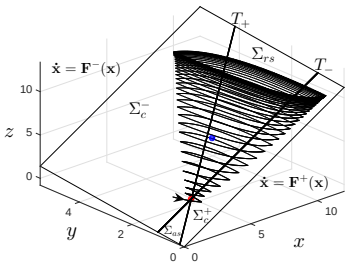

(c) $k < 2a$, stable node CLC

Figure 4.11: Phase portraits of a supercritical TS-bifurcation occurring in the boost converter with SMC, modeled by (4.64)-(4.65) and simulated with $b = 0$, $\omega = 1$, $y_r = 2$, $a = 1.5$ and for three different values of k: (a) $k = 3.3$, (b) $k = 3$, (c) $k = 2.5$.

region to the repulsive sliding region, becoming a pseudo-saddle, and the emergence of the CLC with dynamics of stable node type. Figure 4.10 shows the solution in time of the state variables (normalized voltage and current) of boost converter. After $\tau = 70$ s, the (normalized) resistive load changes from $a = 0.7$ to $a = 1.4$, and so the converter leaves the desired operating point (pseudo-equilibrium) and tends to operate at a periodic orbit (CLC). In this case, for $a = 1.25$ the boost converter, of equations (4.64)-(4.65), undergoes a supercritical TS-bifurcation.

4.8 Conclusion

A computational procedure that allows to characterize the degeneracy of Teixeira singularity for generic DPWS systems has been developed and illustrated with some examples. An application to a simplified, non-trivial model of power electronics, showing the relevance of having such algorithm at our disposal is also included.

Although the dynamic consequences associated to the Teixeira singularity were known after Filippov's impressive work [51] and had been reported with much more detail in [26], the computational procedure obtained in this Chapter fills a gap not only from the practical point of view but also in some theoretical aspects. A canonical form for DPWS systems has been proposed and derived in detail. The topological type of the degeneration has been characterized and the need for third order terms in return maps has been clarified.

It has been emphasized the need of putting the analysis in the context of Takens-Bogdanov bifurcations for reversible maps, whose nonlinear degeneracies and the corresponding higher co-dimension bifurcations ask for future work, see [1] for planar smooth flows. In particular, the possible existence of invariant tori (quasi-periodic behavior) and homoclinic tangles (chaotic regimes) for the crossing dynamics around the T-singularity deserve new research efforts.

Chapter 5

TS-Bifurcation and Crossing Limit Cycles in a Boost Converter

The electronic circuit of a dc-dc boost power converter under a specific sliding mode control strategy is analysed. This circuit is modelled as a discontinuous piecewise-linear three-dimensional system, whose state space is divided in two open regions by a plane acting as the switching boundary. This system displays sliding motion confined to the switching boundary and limited by two straight lines where lie the points of tangency, one for each involved linear vector field. Such tangency lines can intersect transversally on a invisible two-fold point known as Teixeira singularity (T-singularity). Our goal is to investigate an interesting bifurcation that occurs on the T-singularity, involving both a pseudo-equilibrium point and a crossing limit cycle. This bifurcation, named TS-bifurcation, occurs when a pseudo-equilibrium point, capable of moving between the attractive and repulsive sliding regions as a result of the change in a parameter, collides with the T-singularity. Simultaneously, a limit cycle arises from the T-singularity

and crossing the switching boundary in two points. Apart from the TS-bifurcation characterization in the dc-dc converter, we have numerically detected other non-local phenomena like a saddle-node bifurcation of crossing limit cycles. Experimental results to illustrate the effects of the TS-bifurcation on the circuit of a power electronic converter are also shown.

5.1 Introduction

Power converters are electronic circuits associated with conversion, control and conditioning of electric power. Basically, the operation of these power electronic circuits involves cyclic switching between different linear topologies under a feedback control strategy, see [46, 73, 121]. Accordingly, electronic circuits such as switched power converters are naturally discontinuous systems and they can be considered as switched systems or discontinuous piecewise-smooth (DPWS) dynamical systems. Recently, stability analysis methods for switching mode power converters has received significant attention in the literature, see for instance [4, 5, 6] and the references therein.

The DPWS systems have as main characteristic the sliding motion confined to the switching boundary and occurring under certain conditions; see [51, 78]. The occurrence of sliding motions has been reported in the literature involving sliding mode control (SMC) with applications in power electronics converters; see the references [12, 23, 91]. The sliding mode dynamics is governed by a sliding vector field, obtained according to the Filippov convention, for more details see [78] and previous Chapter 2. The sliding vector field is restricted to the switching boundary and its equilibrium points are called pseudo-equilibrium. Typically, in applications such as SMC, a pseudo-equilibrium is the desired operating point. The operating point is naturally reached when the pseudo-equilibrium is in the attractive sliding region. This constraint on the pseudo-equilibrium gives relevance to the analysis of the

sliding region boundaries and what would happen when the pseudo-equilibrium goes through these boundaries, which are constituted by points where one of the involved vector fields is tangent to the switching boundary; see [117].

In this context, a generic singularity of these discontinuous systems for dimension greater than two is the so called Teixeira singularity [25, 26, 116, 117], or simply T-singularity. The T-singularity is a generic singularity in 3D-DPWS systems defined by the aggregation of two different vector fields, one on each side of a given switching boundary, appearing at the transversal intersection of the corresponding fold lines. More specifically, it is assumed that in both fold lines the tangency is of invisible type (see Section 2.2 in Chapter 2), so that it is possible to have orbits that cross the switching boundary with recurrent behaviour, see [117]. In short, we speak of T-singularity as meaning an invisible two-fold point.

Other relevant references involving the possible degeneration of Teixeira singularity and its associated dynamical behavior in control systems and power electronic circuits, are for instance [25, 29]. In these works, the sliding region boundaries on the switching boundary are tangency lines that cross transversally at a point of double tangency classified as invisible two-fold singularity, creating two sliding sectors, one attractive and another repulsive, and both connected only by the two-fold singularity. The transition of a pseudo-equilibrium between the attractive and repulsive sliding regions, passing mandatorily through the invisible two-fold singularity, is one of the main features for a bifurcation at this point, from which there arises a limit cycle that intersects transversally the switching boundary at two points on the crossing regions, see [26, 49].

The bifurcation described in the previous paragraph is named as TS-bifurcation, and the isolated limit cycle originated from this bifurcation is called crossing limit cycle (CLC). The TS-bifurcation is the main subject of this chapter. It will be proven, for the first time, the occur-

rence of this bifurcation in a dc-dc boost converter controlled by a SMC with a high-pass *washout* filter (SMC-washout), modelled by a discontinuous piecewise-linear three-dimensional system (3D-DPWL system). We will show that the TS-bifurcation occurs under two different forms, named in this thesis as *supercritical* and *subcritical*. In supercritical cases the pseudo-equilibrium is stable only when it is within the attractive sliding region, while in subcritical cases the pseudo-equilibrium is unstable in both attractive and repulsive sliding regions. These topics are addressed in detail in next sections.

The identification of the Teixeira singularity in a real circuit of power electronic is one of the main contributions of this chapter, as well as the analytical, numerical and experimental results on bifurcations, helping us to unravel the dynamical richness of this circuit. Among other contributions that can be highlighted in this chapter we can stress (i) a proof of the coexistence of two CLCs, one stable originated in the supercritical case and another unstable arising from the subcritical case; (ii) the numerical identification of global mechanisms for the vanishing (or birth) of CLC (saddle-node bifurcation and non-standard homoclinic bifurcation); (iii) the existence and stability analysis of the CLC from its birth to its annihilation; and (iv) the proposal of a method to investigate the TS-bifurcation, which can easily be applied to other physical systems modelled as 3D-DPWL systems and that exhibit the Teixeira singularity.

This chapter is organized as follows. In Section 5.2, the TS-bifurcation is investigated starting from a case study in power electronics: a boost converter closed-loop controlled by means of a SMC-Washout. In that section, the occurrence of a TS-bifurcation is shown on a 3D-DPWL system that models the boost power converter. Explicit conditions on system parameters for the occurrence of both supercritical and subcritical TS-bifurcations are given. In Section 5.3, a numerical analysis based on the theory of closing equations and the first return maps (see [3, 20, 77, 117]) is introduced to get the location and stability of the possible CLCs, where we also detect other global

bifurcations. Experimental results proving that the TS-bifurcation phenomenon appears in a real circuit prototype of a boost converter are shown in Section 5.4. In Section 5.5, we conclude with a short summary of the obtained results and some final remarks.

Previous results on Filippov theory in Chapter 2 are important for the development that follows.

5.2 Applied analysis to the TS-bifurcation

In this section we prove the occurrence of a TS-bifurcation in a 3D-DPWL system that models a boost power converter controlled by a sliding mode control strategy. Such a model was introduced in Chapter 2, Section 2.6, and in this current Chapter, we begin by reviewing this modelling and, then, we proceeded with study of its equilibria, dynamics and bifurcations.

5.2.1 Modelling and control of a dc-dc boost converter

The basic topology of a boost converter is shown in Figure 5.1, where R, L, C, r_L and V_{in}, are the resistive load, the inductance, the capacitance, the inductor resistance and the voltage source, respectively. The voltage $v_{\text{out}} = v_C$ is equal to the one across the resistive load R and is the system output, which must be regulated at a desired value $v_{\text{out}} > V_{\text{in}}$. To obtain the specified voltage value at the output, a control strategy by sliding modes based on the use of a high-pass washout filter is implemented, as illustrated in Figure 5.1. It is chosen in order to reject load perturbations (see [79] and [127]).

The model of the closed-loop boost converter, operating in Con-

tinuous Conduction Mode (CCM), is given by

$$L\frac{di_L}{dt} = V_{\text{in}} - r_L i_L - u v_C \tag{5.1}$$

$$C\frac{dv_C}{dt} = u i_L - \frac{v_C}{R} \tag{5.2}$$

$$\frac{dz_F}{dt} = \omega_F (i_L - z_F), \tag{5.3}$$

where $v_C \geq 0$ and $i_L > 0$ are the instantaneous capacitor voltage and the inductor current, respectively.

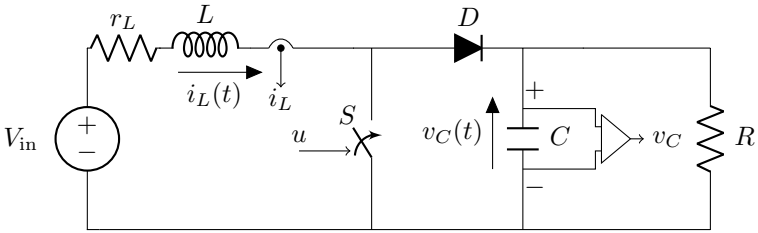

(a) DC-DC *boost* converter.

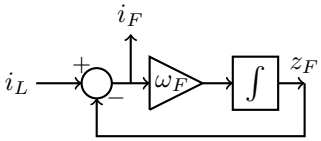

(b) Washout filter.

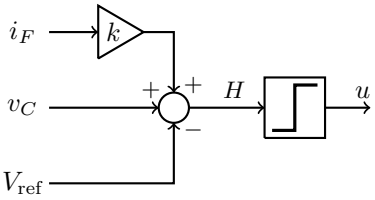

(c) Sliding mode controller.

Figure 5.1: Topology of the boost converter with Sliding Mode Control (SMC) and a washout filter. The control function is $u = \frac{1}{2}(1 + \text{sign}[H])$. In the schemes, the filtered inductor current given by $i_F = i_L - z_F$ represents the difference between the inductor current i_L and the filtered signal z_F.

The filtered inductor current, denoted by the new variable z_F, is the output of the washout filter modeled by equation (5.3), where ω_F is the cut-off frequency of the filter (see [91]). Also, the control law

$u \in \{0, 1\}$ is defined as

$$u = \frac{1}{2}(1 + \text{sign}[H]),$$

such that $u = 1$ implies that the switch S is off, and $u = 0$ when it is on (see Figure 5.1). The control surface is chosen as

$$H(i_L, v_C, z_F) = v_C - V_{\text{ref}} + K(i_L - z_F) = 0, \tag{5.4}$$

where $K > 0$ is a control parameter, to be suitably adjusted, and $V_{\text{ref}} > V_{\text{in}}$ is the reference voltage (desired voltage value at the output). The control objective is to regulate the output voltage v_C such that $v_C \approx V_{\text{ref}} > V_{\text{in}}$, ensuring robustness of the system under parameter variations, mainly produced by load changes in R.

State and Time Variables	**Parameters**
$x = \dfrac{i_L}{V_{\text{in}}}\sqrt{\dfrac{L}{C}}$	$y_r = \dfrac{V_{\text{ref}}}{V_{\text{in}}}$
$y = \dfrac{v_C}{V_{\text{in}}}$	$a = \dfrac{1}{R}\sqrt{\dfrac{L}{C}}$
$z = \dfrac{v_C - V_{\text{ref}} + K(i_L - z_F)}{V_{\text{in}}}$	$k = K\sqrt{\dfrac{C}{L}}$
$\tau = \dfrac{t}{\sqrt{LC}}$	$b = r_L\sqrt{\dfrac{C}{L}}$
	$\omega = \omega_F\sqrt{LC}$

Table 5.1: Normalized new variables, parameters and time.

The equations (5.1)-(5.3) are normalized by applying the change of variables, time and parameters, given in Table 5.1. Thus, we obtain the following dimensionless dynamical system

$$\begin{aligned} \dot{x} &= 1 - bx - uy \\ \dot{y} &= ux - ay \\ \dot{z} &= (u - kb)x + (\omega - a - uk)y - \omega z + k - \omega y_r, \end{aligned} \tag{5.5}$$

where $(x, y, z) \in \mathbb{R}^3$ are the new state variables and the new parameters are $\omega \in (0, 1]$, $y_r > 1$, $a > 0$, $b > 0$ and $k > 0$ (the dot " $\cdot$ " indicates derivatives with respect to the normalized time τ). We highlight that $x > 0$ is the normalized inductor current, $y \geq 0$ is the normalized capacitor voltage and $a > 0$ is the normalized load parameter.

Now, for the normalized system (5.5), the control law is defined by $u = \frac{1}{2}(1 + \text{sign}[z])$ and the switching boundary is $\Sigma = \{h(x, y, z) = z = 0\}$. So, system (5.5) can be represented by the following DPWL system

$$(\dot{x}, \dot{y}, \dot{z}) = \begin{cases} \mathbf{F}^+(x, y, z), \text{ if } z > 0 \\ \mathbf{F}^-(x, y, z), \text{ if } z < 0 \end{cases}, \tag{5.6}$$

composed by the two linear vector fields

$$\mathbf{F}^+(\mathbf{x}) = \begin{bmatrix} 1 - bx - y \\ x - ay \\ f_3^+(\mathbf{x}) \end{bmatrix} \text{ and } \mathbf{F}^-(\mathbf{x}) = \begin{bmatrix} 1 - bx \\ -ay \\ f_3^-(\mathbf{x}) \end{bmatrix},$$

where $\mathbf{x} = (x, y, z)$ and

$$f_3^+ = (1 - kb)x + (\omega - a - k)y - \omega z + k - \omega y_r, \tag{5.7}$$

$$f_3^- = -kbx + (\omega - a)y - \omega z + k - \omega y_r. \tag{5.8}$$

5.2.2 Natural equilibria

The vector field $\mathbf{F}^-$ has an equilibrium at the point

$$\overline{\mathbf{x}}^- = \left(\frac{1}{b}, 0, -y_r\right).$$

It is a stable node since the eigenvalues are real and negative, namely $\{-a, -b, -\omega\}$. Moreover, this is a real equilibrium since

$$h(\overline{\mathbf{x}}^-) = -y_r < 0.$$

The vector field $\mathbf{F}^+$ has an equilibrium point at

$$\overline{\mathbf{x}}^+ = \left(a\bar{y}^+, \bar{y}^+, \bar{y}^+ - y_r\right),$$

where

$$\bar{y}^+ = \frac{1}{1+ab}.$$

It is a stable node (for $a \geq 2+b$) or a focus (for $a < 2+b$) since the eigenvalues have negative real part, namely $\left\{-\frac{a+b}{2} \pm \sqrt{\left(\frac{a-b}{2}\right)^2 - 1}, -\omega\right\}$. Moreover, this is a virtual equilibrium point because

$$h(\bar{\mathbf{x}}^+) = \bar{y}^+ - y_r < 0$$

(remember that $y_r > 1$).

As $\overline{\mathbf{x}}^-$ is always a real equilibrium and $\bar{\mathbf{x}}^+$ is always a virtual equilibrium, no boundary equilibrium bifurcations can occur in (5.6).

5.2.3 Dynamics on the switching boundary

In order to analyse the dynamic behaviour of system (5.6) on the switching boundary Σ, we calculate first and second order Lie derivatives of the scalar function $h(x, y, z) = z$ with respect to the vector fields $\mathbf{F}^\pm$, through the formulas

$$L_{\mathbf{F}^\pm} h = f_3^\pm,$$
$$L^2_{\mathbf{F}^\pm} h = \langle \nabla f_3^\pm, \mathbf{F}^\pm \rangle.$$

The switching boundary Σ is partitioned into four different regions

$$\Sigma_{as} = \{\mathbf{x} \in \Sigma : f_3^+(x, y, 0) < 0 < f_3^-(x, y, 0)\},$$
$$\Sigma_{rs} = \{\mathbf{x} \in \Sigma : f_3^-(x, y, 0) < 0 < f_3^+(x, y, 0)\},$$
$$\Sigma_c^- = \{\mathbf{x} \in \Sigma : f_3^-(x, y, 0) < 0 \text{ and } f_3^+(x, y, 0) < 0\},$$
$$\Sigma_c^+ = \{\mathbf{x} \in \Sigma : f_3^-(x, y, 0) > 0 \text{ and } f_3^+(x, y, 0) > 0\},$$

separated by tangency lines

$$T_- = \{\mathbf{x} \in \Sigma : f_3^-(x, y, 0) = 0\},$$
$$T_+ = \{\mathbf{x} \in \Sigma : f_3^+(x, y, 0) = 0\},$$

which contain all the tangency points of the vector fields $\mathbf{F}^-$ and $\mathbf{F}^+$ with Σ, respectively.

The double tangency point is at the transversal intersection of the lines $T_\pm$. Then, system (5.6) has only one point of double tangency, given by

$$\widehat{\mathbf{x}} = (k\widehat{y}, \widehat{y}, 0)\,, \tag{5.9}$$

where

$$\widehat{y} = \frac{k - \omega y_r}{a + bk^2 - \omega}, \tag{5.10}$$

provided that

$$a \neq \omega - bk^2.$$

There is no double tangency points if $a = \omega - bk^2$ and $k \neq \omega y_r$, since then the tangency lines T^- and T^+ become parallel. In the case $a = \omega - bk^2$ and $k = \omega y_r$, the lines T^- and T^+ are coincident. Both cases are not of our interest, since in the first case there is no point of double tangency and the second is not a regular case. Moreover, the double tangency point must be in the first quadrant with respect to the (x, y)-axes in the plane $z = 0$, since it is required $i_L > 0$ ($x > 0$) and $v_C \geq 0$ ($y \geq 0$) due to operating constraints of the circuit. The double tangency point $\widehat{\mathbf{x}}$ will be a two-fold whenever $L^2_{\mathbf{F}^-} h(\widehat{\mathbf{x}}) \neq 0$ and $L^2_{\mathbf{F}^+} h(\widehat{\mathbf{x}}) \neq 0$ (see Definition 2.5).

The sliding vector field on Σ associated to the dynamical system (5.6) is calculated according to (2.9), getting

$$\mathbf{F}^s(x, y, 0) = \frac{1}{ky - x} \begin{bmatrix} bx^2 - x + ay^2 - \omega y(y - y_r) \\ -k(bx^2 - x + ay^2) + \omega x(y - y_r) \\ 0 \end{bmatrix}$$

provided that $ky - x \neq 0$. Pseudo-equilibrium points of (5.6) are easily obtained by solving the vector equation

$$\mathbf{F}^s(x, y, 0) = (0, 0, 0)^T,$$

which reduces to the quadratic $bx^2 - x + ay^2 = 0$ plus the condition $y = y_r$. So, we have two pseudo-equilibrium points, namely

$$\widetilde{\mathbf{x}}^{\pm} = \left(\widetilde{x}^{\pm}, y_r, 0\right), \tag{5.11}$$

where

$$\widetilde{x}^{\pm} = \frac{1 \pm \sqrt{1 - 4aby_r^2}}{2b} > 0, \tag{5.12}$$

for all $a \leq a_{SN}$ with

$$a_{SN} = \frac{1}{4by_r^2}. \tag{5.13}$$

For $a = a_{SN}$ a collision occurs between them, i.e., $\widetilde{\mathbf{x}}^+ = \widetilde{\mathbf{x}}^-$, and for $a > a_{SN}$ both pseudo-equilibria disappear in a fold or saddle-node bifurcation. Figure 5.2 illustrates this collision through the variation of the parameter a.

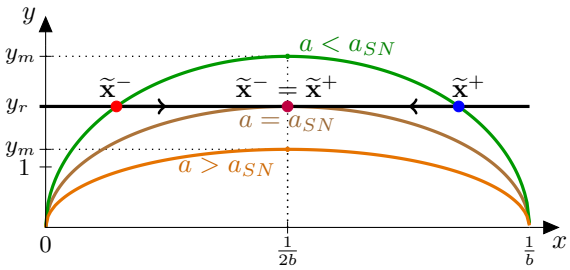

Figure 5.2: Fold bifurcation of pseudo-equilibria. Pseudo-equilibria are the points of intersection between the straight line $y = y_r$ and the ellipse $bx^2 - x + ay^2 = 0$. Take $y_m = \sqrt{\frac{1}{4ab}}$.

Figure 5.3 shows a portrait of Σ in (x, y)-plane, where we assume $\omega < a < a_{SN}$ and $k > \omega y_r$. The slope of the straight line $ky - x = 0$

varies with the parameter k, and so the double tangency point $\widehat{\mathbf{x}}(k)$ moves on the ellipse

$$x - \omega y_r y - bx^2 + (\omega - a)y^2 = 0 \tag{5.14}$$

for $y > 0$, where the maximum value for its y-coordinate is given by

$$Y_{max} = \left[2b\omega y_r \left(1 + \sqrt{1 + \frac{a-\omega}{b\omega^2 y_r^2}}\right)\right]^{-1}.$$

The double tangency point $\widehat{\mathbf{x}}(k)$ is able to collide with the pseudo-equilibrium point $\widetilde{\mathbf{x}}^-$ or $\widetilde{\mathbf{x}}^+$, located at the intersection of $y = y_r$ with this ellipse, since under such condition equation (5.14) coincides with the quadratic equation that defines pseudo-equilibria. From this, the pseudo-equilibria transition between sliding regions can occur, leading to a TS-bifurcation.

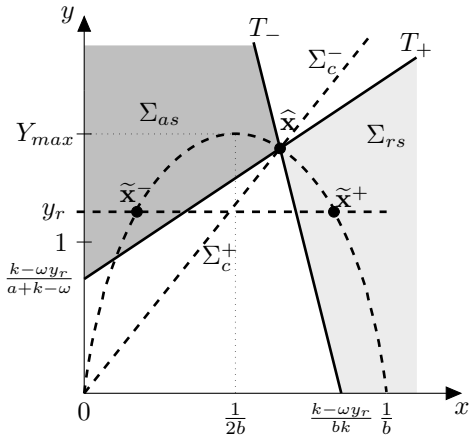

Figure 5.3: Topological configuration on Σ. We assume $\omega < a < a_{SN}$ and $k > \omega y_r$. Both pseudo-equilibria $\widetilde{\mathbf{x}}^{\pm}$ are located at the intersection of the (dashed-line) $y = y_r$ with the (dashed-line) ellipse. The double tangency point $\widehat{\mathbf{x}}$ moves on the dashed-line ellipse by varying the parameter k, since it must also belong to the straight line $x - ky = 0$.

Note that, from expressions (5.7) and (5.8), all the points $\mathbf{x}$ belonging to Σ_{as} fulfill the condition

$$f_3^-(\mathbf{x}) - f_3^+(\mathbf{x}) = ky - x > 0.$$

On the other hand, if $\mathbf{x} \in \Sigma_{rs}$ then $f_3^-(\mathbf{x}) - f_3^+(\mathbf{x}) = ky - x < 0$. On the straight line $ky - x = 0$ we have $f_3^-(\mathbf{x}) = f_3^+(\mathbf{x})$, and then $\mathbf{x}$ is a crossing point if $f_3^-(\mathbf{x}) = f_3^+(\mathbf{x}) \neq 0$, while the point $\mathbf{x} = \widehat{\mathbf{x}}$ is a double tangency point (assuming $a \neq \omega - bk^2$) when $f_3^-(\mathbf{x}) = f_3^+(\mathbf{x}) = 0$. Although the sign of $ky - x$ is not enough to locate points in the different regions of Σ, it is sufficient in the case of pseudo-equilibria, which are always in one of the sliding regions or on the point of transition between the sliding regions, as proved in proposition below.

Lemma 5.1. (*On the position of pseudo-equilibria*) *Assuming*

$$\omega - bk^2 \neq a \leq a_{SN},$$

the points $\widetilde{\mathbf{x}}^{\pm} = (\widetilde{x}^{\pm}, y_r, 0)$ *and* $\widehat{\mathbf{x}} = (k\widehat{y}, \widehat{y}, 0)$ *are well defined, being* $\widehat{y}$ *given in* (5.10) *and* $\widetilde{x}^{\pm}$ *given in* (5.12). *The following statements hold.*

(i) *If* $\widetilde{x}^{\pm} < ky_r$ *then* $\widetilde{\mathbf{x}}^{\pm} \in \Sigma_{as}$.

(ii) *If* $\widetilde{x}^{\pm} > ky_r$ *then* $\widetilde{\mathbf{x}}^{\pm} \in \Sigma_{rs}$.

(iii) *If* $\widetilde{x}^{\pm} = ky_r$ *then* $\widetilde{\mathbf{x}}^{\pm} = \widehat{\mathbf{x}} = (ky_r, y_r, 0)$.

Proof. To simplify the analysis, we think of the parameter a as a function of the coordinate $\widetilde{x}^{\pm}$, by writing $a = \widetilde{x}^{\pm}(1 - b\widetilde{x}^{\pm})/y_r^2$. Then, by eliminating this parameter in the expressions of $L_{\mathbf{F}^-}h(\widetilde{\mathbf{x}}^{\pm})$ and $L_{\mathbf{F}^+}h(\widetilde{\mathbf{x}}^{\pm})$, we obtain

$$L_{\mathbf{F}^-}h(\widetilde{\mathbf{x}}^{\pm}) = \frac{(1 - b\widetilde{x}^{\pm})(ky_r - \widetilde{x}^{\pm})}{y_r},$$
$$L_{\mathbf{F}^+}h(\widetilde{\mathbf{x}}^{\pm}) = -\frac{(b\widetilde{x}^{\pm} + y_r - 1)(ky_r - \widetilde{x}^{\pm})}{y_r}.$$

Note from (5.12) that $0 < \widetilde{x}^{\pm} < 1/b$ and remember that $y_r > 1$, $b > 0$ and $k > 0$. Then $L_{\mathbf{F}^-}h(\widetilde{\mathbf{x}}^{\pm})L_{\mathbf{F}^+}h(\widetilde{\mathbf{x}}^{\pm}) < 0$ if $\widetilde{x}^{\pm} \neq ky_r$, and for $\widetilde{x}^{\pm} < ky_r$ (resp. $\widetilde{x}^{\pm} > ky_r$) we have $L_{\mathbf{F}^-}h(\widetilde{\mathbf{x}}^{\pm}) > 0$ and $L_{\mathbf{F}^+}h(\widetilde{\mathbf{x}}^{\pm}) < 0$ (resp. $L_{\mathbf{F}^-}h(\widetilde{\mathbf{x}}^{\pm}) < 0$ and $L_{\mathbf{F}^+}h(\widetilde{\mathbf{x}}^{\pm}) > 0$). If $\widetilde{x}^{\pm} = ky_r$ then $L_{\mathbf{F}^-}h(\widetilde{\mathbf{x}}^{\pm}) = L_{\mathbf{F}^+}h(\widetilde{\mathbf{x}}^{\pm}) = 0$, that is, $\widetilde{\mathbf{x}}^{\pm} = \widehat{\mathbf{x}}$. The proof is complete. □

The sliding dynamics defined on the plane $z = 0$ and restricted to the sliding regions can be extended to the boundaries T_+ and T_-, as follows. Starting from the sliding vector field $\mathbf{F}^s$, we construct a two-dimensional system whose dynamics is equivalent to $\mathbf{F}^s$ in the attractive sliding region Σ_{as}. For this, we define the desingularized sliding vector field $\mathbf{F}^{ds} = (ky - x)\mathbf{F}^s$, provided that $ky - x > 0$. Then we discard the third component, which is null, to get the planar sliding system

$$\dot{x} = bx^2 - x + ay^2 - \omega y(y - y_r), \tag{5.15}$$

$$\dot{y} = -k(bx^2 - x + ay^2) + \omega x(y - y_r). \tag{5.16}$$

We can also determine a planar sliding system with dynamics equivalent to that of $\mathbf{F}^s$ in the repulsive sliding region Σ_{rs}. For this, just take the opposite sign in equations (5.15)-(5.16), since for $(x, y, 0) \in \Sigma_{rs}$ we have $-(ky - x) > 0$. Then, for $ky - x < 0$, we must consider the system

$$\dot{x} = -bx^2 + x - ay^2 + \omega y(y - y_r), \tag{5.17}$$

$$\dot{y} = k(bx^2 - x + ay^2) - \omega x(y - y_r). \tag{5.18}$$

Clearly, equilibria of (5.15)-(5.16) are also equilibria of (5.17)-(5.18), obtained by solving the system of equations

$$bx^2 - x + ay^2 - \omega y(y - y_r) = 0, \tag{5.19}$$

$$-k(bx^2 - x + ay^2) + \omega x(y - y_r) = 0. \tag{5.20}$$

Note that the pseudo-equilibria $\widetilde{\mathbf{x}}^{\pm} = (\widetilde{x}^{\pm}, y_r, 0)$, once expressed in

reduced coordinates are the points $\mathbf{p}^{\pm} = (\widetilde{x}^{\pm}, y_r)$, with $\widetilde{x}^{\pm}$ given in (5.12), so that they are of course equilibria of (5.15)-(5.16). In order to determine the stability of the pseudo-equilibria $\widetilde{\mathbf{x}}^{\pm}$, it is much easier to work with the equivalent planar sliding systems, and we proceed as follows.

(i) If $\widetilde{\mathbf{x}}^{\pm} = (\widetilde{x}^{\pm}, y_r, 0) \in \Sigma_{as}$ then we must consider the planar sliding system (5.15)-(5.16) and its respective Jacobian matrix

$$J_{as}(\widetilde{x}^{\pm}, y_r) = \begin{pmatrix} 2b\widetilde{x}^{\pm} - 1 & (2a-\omega)y_r \\ k(1-2b\widetilde{x}^{\pm}) & \omega\widetilde{x}^{\pm} - 2aky_r \end{pmatrix}.$$

In this case, the determinant and trace of J_{as} are given by

$$\mathrm{Det}[J_{as}(\widetilde{x}^{\pm}, y_r)] = \omega(1-2b\widetilde{x}^{\pm})(ky_r - \widetilde{x}^{\pm}), \tag{5.21}$$

$$\mathrm{Tr}[J_{as}(\widetilde{x}^{\pm}, y_r)] = (\omega+2b)\widetilde{x}^{\pm} - 2aky_r - 1. \tag{5.22}$$

(ii) If $\widetilde{\mathbf{x}}^{\pm} = (\widetilde{x}^{\pm}, y_r, 0) \in \Sigma_{rs}$ then we must consider the planar sliding system (5.17)-(5.18) and its respective Jacobian matrix $J_{rs}(\widetilde{x}^{\pm}, y_r) = -J_{as}(\widetilde{x}^{\pm}, y_r)$. In this case, $\mathrm{Det}[J_{rs}(\widetilde{x}^{\pm}, y_r)] = \mathrm{Det}[J_{as}(\widetilde{x}^{\pm}, y_r)]$ and $\mathrm{Tr}[J_{rs}(\widetilde{x}^{\pm}, y_r)] = -\mathrm{Tr}[J_{as}(\widetilde{x}^{\pm}, y_r)]$.

For all $a < a_{SN}$ the x-coordinate of the pseudo-equilibrium $\widetilde{\mathbf{x}}^{-}$ fulfils $\widetilde{x}^{-} < \frac{1}{2b}$. In this case, if $\widetilde{x}^{-} < ky_r$ then $\widetilde{\mathbf{x}}^{-} \in \Sigma_{as}$ and $\mathrm{Det}(J_{as}) > 0$. Thus $\widetilde{\mathbf{x}}^{-}$ is a pseudo-node or a pseudo-focus when in Σ_{as}, being stable whenever $\mathrm{Tr}(J_{as}) < 0$, that is, for $k > k_H^-$ with

$$k_H^- = \frac{(w+2b)\widetilde{x}^{-} - 1}{2ay_r}.$$

On the other hand, if $\widetilde{x}^{-} > ky_r$ then $\widetilde{\mathbf{x}}^{-} \in \Sigma_{rs}$ and $\mathrm{Det}(J_{rs}) < 0$, that is, $\widetilde{\mathbf{x}}^{-}$ is a pseudo-saddle in Σ_{rs}.

Regarding $\widetilde{\mathbf{x}}^{+}$, we have $\widetilde{x}^{+} > \frac{1}{2b}$. In this case, if $\widetilde{x}^{+} < ky_r$ then $\widetilde{\mathbf{x}}^{+} \in \Sigma_{as}$ and $\mathrm{Det}(J_{as}) < 0$. Thus, it is a pseudo-saddle when in Σ_{as}. If $\widetilde{\mathbf{x}}^{+} \in \Sigma_{rs}$ then it can be a pseudo-node or a pseudo-focus, since

$\mathrm{Det}(J_{rs}) > 0$. Clearly, $\widetilde{\mathbf{x}}^+$ is always an unstable pseudo-equilibrium of 3D system (5.6). But for the planar sliding system (5.17)-(5.18), it can be a stable equilibrium if $\mathrm{Tr}(J_{rs}) < 0$, that is, for $k < k_H^+$ with

$$k_H^+ = \frac{(w+2b)\widetilde{x}^+ - 1}{2ay_r}.$$

From the previous analysis, we can give the following statements regarding the stability of the pseudo-equilibria $\widetilde{\mathbf{x}}^{\pm}$. Note the conditions that make stable the pseudo-equilibrium point $\widetilde{\mathbf{x}}^-$, the one to be selected as the desired operating point.

Proposition 5.1. *We assume $a < a_{SN}$ and $k \neq k_H^{\pm}$. The point $\widetilde{\mathbf{x}}^-$ is a pseudo-saddle when in Σ_{rs} and a pseudo-node (or pseudo-focus) when in Σ_{as}. The point $\widetilde{\mathbf{x}}^+$ is a pseudo-saddle when in Σ_{as} and a pseudo-node (or pseudo-focus) when in Σ_{rs}. Therefore, $\widetilde{\mathbf{x}}^+$ is always an unstable pseudo-equilibrium while $\widetilde{\mathbf{x}}^-$ is a stable pseudo-equilibrium whenever the control parameter k is selected such that $k > \widetilde{x}^-/y_r$ and $k > k_H^-$.*

We study next several bifurcations that can lead to situations where the above proposition cannot be applied. Sliding bifurcations in a boost converter with SMC-Washout were also analyzed in [28, 29], but for different models of the boost converter.

5.2.4 Partial analysis of sliding bifurcations

Regarding the sliding dynamics, three different one-parameter bifurcations can appear: the saddle-node of equilibria, the Hopf bifurcation, and the transcritical bifurcation.

Recall that the pseudo-equilibria $\widetilde{\mathbf{x}}^{\pm}$ exist for $a \leq a_{SN}$, as given by (5.11)-(5.12) and (5.13), and that they are inside of sliding regions if $ky_r \neq \widetilde{x}^{\pm}$. For $a = a_{SN}$ they collide, i.e., there exists only one pseudo-equilibrium point and the determinant in (5.21) goes to zero, because then $\widetilde{x}^{\pm}(a_{SN}) = 1/(2b)$. Moreover, at $a = a_{SN}$ we have a

non-vanishing $\mathrm{Tr}(J_{as}) = (\omega y_r - k)/(2by_r)$, provided that $k \neq \omega y_r$. Therefore, if $k \neq \omega y_r$ and $k \neq 1/(2by_r)$ then at $a = a_{SN}$ a saddle-node bifurcation occurs for the sliding dynamics. The sign of the expression $ky_r - \widetilde{x}^{\pm}(a_{SN})$ implies that for $k < 1/(2by_r)$ such bifurcation occurs in Σ_{rs} while for $k > 1/(2by_r)$ it occurs in Σ_{as} (see Lemma 5.1). In the first case, for $a < a_{SN}$ and near the critical value a_{SN}, the point $\widetilde{\mathbf{x}}^{-}$ is a pseudo-saddle while the point $\widetilde{\mathbf{x}}^{+}$ is a pseudo-node, both in Σ_{rs}. In the second case, for $a < a_{SN}$ and near the critical value a_{SN}, the point $\widetilde{\mathbf{x}}^{-}$ is a pseudo-node and the point $\widetilde{\mathbf{x}}^{+}$ is a pseudo-saddle, both in Σ_{as}.

A Hopf bifurcation occurs in Σ_{as} for $k = k_H^- > \widetilde{x}^-/y_r$, since $\mathrm{Tr}(J_{as}) = 0$ and $\mathrm{Det}(J_{as}) > 0$. This bifurcation is related to the pseudo-equilibrium $\widetilde{\mathbf{x}}^{-}$, so that (i) for $k > k_H^-$ and near the critical value k_H^-, we have $\widetilde{\mathbf{x}}^{-}$ an unstable pseudo-focus; (ii) for $k < k_H^-$ becomes a stable pseudo-focus and an unstable limit cycle arises around it, entirely contained in Σ_{as}. Another Hopf bifurcation occurs, but now in Σ_{rs} and for $k = k_H^+ < \widetilde{x}^+/y_r$, since $\mathrm{Tr}(J_{rs}) = 0$ and $\mathrm{Det}(J_{rs}) > 0$. This bifurcation is related to the pseudo-equilibrium $\widetilde{\mathbf{x}}^{+}$, so that (i) for $k > k_H^+$ and near the critical value k_H^+, we have that $\widetilde{\mathbf{x}}^{+}$ is an unstable pseudo-focus; (ii) for $k < k_H^+$ it becomes a stable pseudo-focus and an unstable limit cycle arises around it, entirely contained in Σ_{rs}. Both bifurcations are subcritical ones but the full analysis of these Hopf bifurcations is out of the scope of this work and will be done elsewhere.

Regarding the transcritical bifurcation, and assuming $\omega - bk^2 \neq a < a_{SN}$, there are two cases. One of the cases involves the pseudo-equilibrium $\widetilde{\mathbf{x}}^{-}$, and it occurs at $\widetilde{x}^- = ky_r$, while the other involves $\widetilde{\mathbf{x}}^{+}$ and occurs at $\widetilde{x}^+ = ky_r$, provided that the trace (5.22) is not null. Both cases are related to a pseudo-equilibrium transition from Σ_{rs} ($\widetilde{x}^{\pm} > ky_r$) to Σ_{as} ($\widetilde{x}^{\pm} < ky_r$), being the transition point the double tangency point $\widehat{\mathbf{x}}$, as given in (5.9)-(5.10). See Lemma 5.1.

Note, from equations (5.11)-(5.12) and (5.9)-(5.10), that the points $\widetilde{\mathbf{x}}^{\pm} = (\widetilde{x}^{\pm}, y_r, 0)$ depend only on the parameter a, while the point $\widehat{\mathbf{x}} = (k\widehat{y}, \widehat{y}, 0)$ depends on the parameters a and k. Thus, we rewrite

Lemma 5.1 with respect to these two parameters, as follows.

Lemma 5.2. *System* (5.6) *undergoes a pseudo-equilibrium transition from* Σ_{as} *to* Σ_{rs} *(or vice versa) for* $a = a_{TS}(k)$*, where*

$$a_{TS}(k) = \frac{k(1 - bky_r)}{y_r}. \tag{5.23}$$

In addition, regarding the critical value

$$k_c = \frac{1}{2by_r}, \tag{5.24}$$

we have $a_{TS}(k) \leq a_{TS}(k_c) = a_{SN} = 1/(4by_r^2)$ *for all* k*, and the following statements hold.*

(i.1) $\widetilde{\mathbf{x}}^- = \widehat{\mathbf{x}}$ *for all* (k, a) *such that* $\omega y_r \neq k < k_c$ *and* $a = a_{TS}(k)$*;*

(i.2) $\widetilde{\mathbf{x}}^- \in \Sigma_{rs}$ *for all* (k, a) *such that* $k < k_c$ *and* $a_{TS}(k) < a \leq a_{SN}$*;*

(i.3) $\widetilde{\mathbf{x}}^- \in \Sigma_{as}$ *for all* (k, a) *such that* $a < a_{TS}(k)$ *or* $k > k_c$ *and* $a \leq a_{SN}$*;*

(ii.1) $\widetilde{\mathbf{x}}^+ = \widehat{\mathbf{x}}$ *for all* (k, a) *such that* $\omega y_r \neq k > k_c$ *and* $a = a_{TS}(k)$*;*

(ii.2) $\widetilde{\mathbf{x}}^+ \in \Sigma_{as}$ *for all* (k, a) *such that* $k > k_c$ *and* $a_{TS}(k) < a \leq a_{SN}$*.*

(ii.3) $\widetilde{\mathbf{x}}^+ \in \Sigma_{rs}$ *for all* (k, a) *such that* $a < a_{TS}(k)$ *or* $k < k_c$ *and* $a \leq a_{SN}$*.*

(iii) $\widetilde{\mathbf{x}}^- = \widetilde{\mathbf{x}}^+ = \widehat{\mathbf{x}}$ *for* $k = k_c \neq k\omega y_r$ *and* $a = a_{TS}(k_c)$*.*

Proof. From Lemma 5.1, if $\widetilde{x}^{\pm} = ky_r$ then $\widetilde{\mathbf{x}}^{\pm} = \widehat{\mathbf{x}}$. Thus, solving the equation $b^2k^2y_r^2 - ky_r + ay_r^2 = 0$ with respect to a, we get expression (5.23). We note that

$$4by_r^2(a_{TS}(k) - a_{SN}) = (1 - 2bky_r)^2 \geq 0,$$

so that the inequality $a_{TS}(k) \leq a_{TS}(k_c) = a_{SN}$ holds. At the critical value $a = a_{TS}$ we have that

$$\widetilde{x}^{\pm}(a_{TS}) = \frac{1}{2b}\left(1 \pm \left|\frac{k}{k_c} - 1\right|\right),$$
$$\widehat{y}(a_{TS}) = y_r,$$

implying the following situations: (i.1) if $k < k_c$, then $\widetilde{x}^{-}(a_{TS}) = ky_r$ and so $\widetilde{\mathbf{x}}^{-} = \widehat{\mathbf{x}}$; (ii.1) if $k > k_c$, then $\widetilde{x}^{+}(a_{TS}) = ky_r$ and so $\widetilde{\mathbf{x}}^{+} = \widehat{\mathbf{x}}$; (iii) if $k = k_c$, then $\widetilde{x}^{-}(a_{TS}) = \widetilde{x}^{+}(a_{TS}) = ky_r$ and so $\widetilde{\mathbf{x}}^{-} = \widetilde{\mathbf{x}}^{+} = \widehat{\mathbf{x}}$, since $a_{TS}(k_c) = a_{SN}$. Note that the constraint $k \neq \omega y_r$ ensures that $\widehat{\mathbf{x}}(k, a)$ is defined for $a = a_{TS}(k)$, since $a_{TS}(\omega y_r) = \omega - bk^2$. See equation (5.10).

If we define the functions $g^{\pm}(a) = \widetilde{x}^{\pm}(a) - ky_r$ for all $a \leq a_{SN}$, then we get $g^{\pm}(a_{TS}) = 0$,

$$g^{\pm}(a) = \frac{1 - \frac{k}{k_c} \pm \sqrt{1 - \frac{a}{a_{SN}}}}{2b},$$
$$\frac{dg^{-}}{da}(a) = \frac{y_r^2}{\sqrt{1 - \frac{a}{a_{SN}}}} > 0,$$
$$\frac{dg^{+}}{da}(a) = -\frac{y_r^2}{\sqrt{1 - \frac{a}{a_{SN}}}} < 0.$$

Then, we can conclude that: (i.2) if $k < k_c$ and $a_{TS}(k) < a \leq a_{SN}$, then $\widetilde{x}^{-}(a) > ky_r$ and so $\widetilde{\mathbf{x}}^{-} \in \Sigma_{rs}$; (i.3) if $a < a_{TS}$ or $k > k_c$ and $a \leq a_{SN}$, then $\widetilde{x}^{-}(a) < ky_r$ and so $\widetilde{\mathbf{x}}^{-} \in \Sigma_{as}$; (ii.2) if $k > k_c$ and $a_{TS}(k) < a \leq a_{SN}$, then $\widetilde{x}^{+}(a) > ky_r$ and so $\widetilde{\mathbf{x}}^{+} \in \Sigma_{as}$; (ii.3) if $a < a_{TS}$ or $k < k_c$ and $a \leq a_{SN}$, then $\widetilde{x}^{+}(a) < ky_r$ and so $\widetilde{\mathbf{x}}^{+} \in \Sigma_{rs}$. See Lemma 5.1. The proof is complete. □

We already know the stability of the pseudo equilibria $\widetilde{\mathbf{x}}^{\pm}$ (see Proposition 5.1). Note that a change from saddle to node occurs when $\widetilde{\mathbf{x}}^{-}$ (resp. $\widetilde{\mathbf{x}}^{+}$) pass from Σ_{rs} to Σ_{as} (resp. Σ_{as} to Σ_{rs}). Furthermore, at the critical point $\widetilde{x}^{-} = ky_r$ (resp. $\widetilde{x}^{+} = ky_r$) the determinant in (5.21)

is null and $\widetilde{\mathbf{x}}^- = \widehat{\mathbf{x}}$ (resp. $\widetilde{\mathbf{x}}^+ = \widehat{\mathbf{x}}$). In fact, the double tangency point $\widehat{\mathbf{x}}$ is an equilibrium of the de-singularized sliding vector field (5.15)-(5.16), and it is possible to show that its character changes from node to saddle after colliding with $\widetilde{\mathbf{x}}^-$ or $\widetilde{\mathbf{x}}^+$.

Effectively, the double tangency point $\widehat{\mathbf{x}} = (k\widehat{y}, \widehat{y}, 0)$, in reduced coordinates, is represented by the point $\mathbf{q} = (k\widehat{y}, \widehat{y})$, which is also an equilibrium point of (5.15)-(5.16)[1]. In fact, multiplying equation (5.19) by k and adding (5.20) we obtain $\omega(x - ky)(y - y_r) = 0$. Choosing $x = ky$, and substituting in (5.19) we have that

$$y\left[(bk^2 + a - \omega)y + \omega y_r - k\right] = 0. \tag{5.25}$$

Thus, the non-trivial solution of equation (5.25) gives by the y-coordinate in (5.10) and the x-coordinate is obtained directly from $x = ky$. We can study the stability of this equilibrium from the determinant given by

$$\mathrm{Det}[J(\mathbf{q})] = \omega y_r(a - a_{TS})\widehat{y},$$

where J denotes the Jacobian matrix of planar sliding system (5.15)-(5.16), evaluated at $\mathbf{q} = (k\widehat{y}, \widehat{y})$.

Consider the equilibria $\mathbf{p}^{\pm} = (\widetilde{x}^{\pm}, y_r)$ (mirroring pseudo-equilibria) and $\mathbf{q} = (k\widehat{y}, \widehat{y})$ (mirroring the double tangency point) of planar sliding system (5.15)-(5.16), and assume that the trace in (5.22) is not null at $a = a_{TS}$. A collision between the equilibria $\mathbf{p}^-$ and $\mathbf{q}$ (resp. $\mathbf{p}^+$ and $\mathbf{q}$) occurs for $\omega y_r \neq k < k_c$ (resp. $\omega y_r \neq k > k_c$) and $a = a_{TS}(k)$, so that $\mathbf{p}^-(a_{TS}) = \mathbf{q}(a_{TS}) = (ky_r, y_r)$ is a non-hyperbolic equilibrium. Moreover, for $a \neq a_{TS}$ and near the critical value a_{TS}, both equilibria $\mathbf{p}^-$ and $\mathbf{q}$ coexist, being one of them of node type and the other of saddle type, and interchanging such types at the value $a = a_{TS}$. Then, under such conditions, for $a = a_{TS}$ a transcritical bifurcation in the sliding dynamics occurs.

[1]The trivial equilibrium point of (5.15)-(5.16) is always in a crossing region or collides with the double tangency if $k = \omega y_r$ (then, $\widehat{\mathbf{x}} = \mathbf{0}$). We do not worry about this trivial equilibrium.

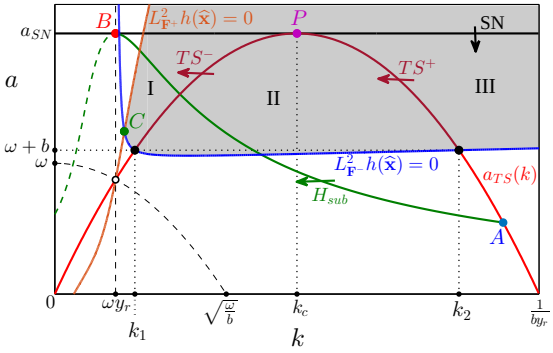

Figure 5.4: Bifurcation set in plane (k, a). For values (a, k) in the shaded region the point $\widehat{\mathbf{x}}$ is a T-singularity, while the double tangency goes to infinity at the dashed semi-parabola, where the denominator in (5.10) goes to zero. At the point C, the point $\widehat{\mathbf{x}}$ becomes a two-cusp. The black horizontal line $a = a_{SN}$ indicates a saddle-node bifurcation (SN) for the pseudo-equilibria $\widetilde{\mathbf{x}}^{\pm}$, which arise for $a < a_{SN}$. The parabola in red color (light and dark parts) marks the transition of the pseudo-equilibria between the sliding regions. The dark part of this parabola, within the shaded region, indicates the TS-bifurcation, which is related with $\widetilde{\mathbf{x}}^-$ in its left-branch (TS^-) and with $\widetilde{\mathbf{x}}^+$ in its right-branch (TS^+). At the point P there occurs a sliding pitchfork bifurcation. The green line stands for a sliding Hopf bifurcation of $\widetilde{\mathbf{x}}^-$, to be studied elsewhere.

We summarize our analysis in the bifurcation set of Figure 5.4. In the black horizontal line $a = a_{SN}$ there occurs the saddle-node bifurcation (SN) of the pseudo-equilibria $\widetilde{\mathbf{x}}^{\pm}$, which are defined for $a \leq a_{SN}$ and such that $\widetilde{\mathbf{x}}^-(a_{SN}) = \widetilde{\mathbf{x}}^+(a_{SN})$. To the left of P-point this bifurcation occurs in Σ_{as} and to the right of P-point occurs in Σ_{rs}. At P we have a degenerate case where $\widetilde{\mathbf{x}}^{\pm} = \widehat{\mathbf{x}}$. If we take $k = k_c$ then for $a < a_{SN} = a_{TS}$, and near to the value a_{SN}, three hyperbolic equilibria appear in the sliding dynamics, equivalent to the pseudo-equilibria $\widetilde{\mathbf{x}}^- \in \Sigma_{as}$, $\widetilde{\mathbf{x}}^+ \in \Sigma_{rs}$ (both node equilibria) and to the double tangency point $\widehat{\mathbf{x}}$ (saddle equilibrium), so that for $a > a_{SN}$ only $\widehat{\mathbf{x}}$ persists, as in a Pitchfork bifurcation.

The parabola of equation $a = a_{TS}(k)$, represented in red color (light and dark parts) in Figure 5.4, depicts the transition of the pseudo-

equilibria between the sliding regions. From Lemma 5.2, we conclude the following.

(i) For $k < k_c$ and $a_{TS}(k) < a \leq a_{SN}$ (to the left of the red parabola left-branch) we get $\widetilde{\mathbf{x}}^- \in \Sigma_{rs}$. For $a < a_{TS}(k)$ or $k > k_c$ and $a \leq a_{SN}$ (to the right of the red parabola left-branch) we get $\widetilde{\mathbf{x}}^- \in \Sigma_{as}$.

(ii) For $k > k_c$ and $a_{TS}(k) < a \leq a_{SN}$ (to the right of the red parabola right-branch) we get $\widetilde{\mathbf{x}}^+ \in \Sigma_{as}$. For $a < a_{TS}(k)$ or $k < k_c$ and $a \leq a_{SN}$ (to the left of the red parabola right-branch) we get $\widetilde{\mathbf{x}}^+ \in \Sigma_{rs}$.

(iii) At $a = a_{TS}(k)$ we get $\widetilde{\mathbf{x}}^- = \widehat{\mathbf{x}}$ for $k < k_c$ (red parabola left-branch), $\widetilde{\mathbf{x}}^+ = \widehat{\mathbf{x}}$ for $k > k_c$ (red para-bola right-branch), and $\widetilde{\mathbf{x}}^- = \widetilde{\mathbf{x}}^+ = \widehat{\mathbf{x}}$ for $k = k_c$, provided that $k \neq \omega y_r$.

Still in relation to Figure 5.4, for all values (a, k) in the shaded region the double tangency $\widehat{\mathbf{x}}$ is a T-singularity, since $L^2_{\mathbf{F}^-} h(\widehat{\mathbf{x}}) > 0$ and $L^2_{\mathbf{F}^+} h(\widehat{\mathbf{x}}) < 0$. From this, we can note that the boost converter system (5.6) presents all the types of two-folds defined in Definition 2.5, besides other cases such as the two-cusp that occurs at the point C and the cusp-folds that appear for (k, a) on the blue line ($L^2_{\mathbf{F}^-} h(\widehat{\mathbf{x}}) = 0$) and also on the orange line ($L^2_{\mathbf{F}^+} h(\widehat{\mathbf{x}}) = 0$).

We have seen already that the transition of a pseudo-equilibrium between the sliding regions induces in the sliding dynamics a transcritical bifurcation. This bifurcation involves a pseudo-equilibrium ($\widetilde{\mathbf{x}}^-$ or $\widetilde{\mathbf{x}}^+$) and the double tangency point ($\widehat{\mathbf{x}}$), with associated equilibria in the sliding dynamics. When the double tangency is indeed a T-singularity (invisible two-fold), this sliding bifurcation is also associated to the birth of a limit cycle that crosses the Σ-plane in two points, one in each crossing region $\Sigma_c^{\pm}$, as shown below. Such a crossing limit cycle, which does not contain sliding points, makes this bifurcation more aggressive.

Among all the bifurcations studied, the transcritical bifurcation is the most interesting for the scope of this work. If we focus our

attention to the case where $\widehat{\mathbf{x}}$ is a T-singularity, then our (k, a)-plane in Figure 5.4 could be reduced to the shaded part, where the parabola in red color (dark part) indicates the occurrence of a TS-bifurcation. We have two distinct scenarios: a supercritical case (TS^-) involving the pseudo-equilibrium $\widetilde{\mathbf{x}}^-$ and another subcritical (TS^+) involving the point $\widetilde{\mathbf{x}}^+$.

In the sequel, we study the TS-bifurcation, proceeding in two steps. First, in next subsection, we finalize our analysis of the sliding dynamics with the TS-bifurcation theorem and its proof. Later, in Section 5.3, we analyze the crossing dynamics and the birth of CLCs, as well as global bifurcations related to the vanishing of CLCs.

5.2.5 The TS-bifurcation

The value of the parameter a can change during the operation of the boost converter since the load represented by the impedance R can vary. For this reason, in what follows, we consider this parameter as the main bifurcation parameter. Note that both pseudo-equilibria $\widetilde{\mathbf{x}}^{\pm}$ and the double tangency $\widehat{\mathbf{x}}$, given in (5.9) and (5.11), respectively, have their coordinates parameterized by a.

We assume $b < b_{max}$, where

$$\begin{aligned} b_{max} &= \frac{\sqrt{1+\omega^2 y_r^2} - \omega y_r}{2y_r} = \\ &= \frac{1}{2y_r(\sqrt{1+\omega^2 y_r^2} + \omega y_r)} < \frac{1}{2\omega y_r^2}, \end{aligned} \tag{5.26}$$

so that we can assure that $1 - 4b(b+\omega)y_r^2 > 0$. Accordingly, we also introduce the values

$$\begin{aligned} k_1 &= \frac{1 - \sqrt{1-4b(b+\omega)y_r^2}}{2by_r} = \\ &= \frac{2(b+\omega)y_r}{1+\sqrt{1-4b(b+\omega)y_r^2}} > (b+\omega)y_r, \end{aligned} \tag{5.27}$$

and

$$k_2 = \frac{1 + \sqrt{1 - 4b(b+\omega)y_r^2}}{2by_r} < \frac{1}{by_r}. \tag{5.28}$$

Apart from k_c given in (5.24), which separates the supercritical and subcritical cases, the values k_1 and k_2 are important for the analysis of TS-bifurcation, since they indicate the lower and upper limits for k, respectively, of the domain of the function $a = a_{TS}(k)$ for which a TS-bifurcation is possible (see Figure 5.4). Thus, a TS-bifurcation occurs at $a = a_{TS}(k)$ for all $k \neq k_c$ such that $k_1 < k < k_2$. We remark that if the condition $b < b_{max}$ is not met, then the TS-bifurcation will not occur, since then for $a = a_{TS}$ the double tangency cannot be of invisible two-fold type (a T-singularity). Theorem 5.1 summarizes the TS-bifurcation in system (5.6) for the boost converter.

Theorem 5.1. *Consider system* (5.6) *with* $b < b_{max}$ *and* $k \neq k_c$ *such that* $k_1 < k < k_2$, *where* k_c, b_{max}, k_1 *and* k_2 *are defined in* (5.24), (5.26), (5.27), *and* (5.28) *respectively. The following statements hold for a near the value* a_{TS} *defined in* (5.23).

(a) (Supercritical TS-bifurcation). *If* $k_1 < k < k_c$ *then for* $a = a_{TS}$ *the system undergoes a TS-bifurcation, so that there exists* $\varepsilon > 0$ *such that for* $a_{TS} - \varepsilon < a < a_{TS}$ *the pseudo-equilibrium* $\widetilde{\mathbf{x}}^- \in \Sigma_{as}$ *and is a stable pseudo-node, while for* $a_{TS} < a < a_{TS} + \varepsilon$ *the pseudo-equilibrium* $\widetilde{\mathbf{x}}^- \in \Sigma_{rs}$ *and is a pseudo-saddle.*

(b) (Subcritical TS-bifurcation). *If* $k_c < k < k_2$ *then for* $a = a_{TS}$ *the system undergoes a TS-bifurcation, so that there exists* $\varepsilon > 0$ *such that for* $a_{TS} - \varepsilon < a < a_{TS}$ *the pseudo-equilibrium* $\widetilde{\mathbf{x}}^+ \in \Sigma_{rs}$ *and is an unstable pseudo-node, while for* $a_{TS} < a < a_{TS} + \varepsilon$ *the pseudo-equilibrium* $\widetilde{\mathbf{x}}^+ \in \Sigma_{as}$ *and is a pseudo-saddle.*

Proof. Remember that $y_r > 1$. To prove the occurrence of a TS-bifurcation we follow Definition 2.10. The critical value a_{TS} of the bifurcation parameter a comes from Lemma 5.2. Recall also from such

lemma that $a_{TS}(k) < a_{SN}$ if $k \neq k_c$. Thus, we can assure that the pseudo-equilibria $\widetilde{\mathbf{x}}^{\pm}$ are defined for all a in a neighborhood of a_{TS}. Moreover, the inequality $a_{TS}(k) > \omega - bk^2$ holds for all $k > k_1$, since it is equivalent to the inequality $k > \omega y_r$, which is true from (5.27). Thus, we can assure that the double tangency $\widehat{\mathbf{x}}$ is defined for all a in a neighborhood of a_{TS}, and that its coordinates are positive, because $k_1 > \omega y_r$. Note also that, from the last inequality in (5.28), the value $a_{TS}(k) > 0$ for all $k < k_2$.

Checking condition (2.13), we get

$$\begin{aligned}
&\frac{d}{da} L_{\mathbf{F}^-} h(\widetilde{\mathbf{x}}^{\pm}(a), a) \frac{d}{da} L_{\mathbf{F}^+} h(\widetilde{\mathbf{x}}^{\pm}(a), a)\Big|_{a=a_{TS}} = \\
&= \frac{y_r^2 \left(bky_r - 1\right) \left(bky_r - 1 + y_r\right)}{\left(1 - \frac{k}{k_c}\right)^2} < 0,
\end{aligned}$$

since $k_c \neq k < k_2 < 1/(by_r)$. Therefore, the pseudo-equilibria $\widetilde{\mathbf{x}}^{\pm}(a)$ pass from the attractive to repulsive sliding regions (or vice versa) as the parameter a varies around its critical value a_{TS}. This transition was already known from Lemma 5.2. We must also check the condition (2.14), namely the inequalities

$$\begin{aligned}
&L^2_{\mathbf{F}^-} h\left(\widehat{\mathbf{x}}(a_{TS}), a_{TS}\right) = \\
&= kb\left(bky_r - 1\right)\left(k - k_1\right)\left(k - k_2\right) > 0, \\
&L^2_{\mathbf{F}^+} h\left(\widehat{\mathbf{x}}(a_{TS}), a_{TS}\right) = \\
&= \left(bky_r - 1 + y_r\right)\left(kb(k - k_1)(k - k_2) - k^2 - 1\right) < 0,
\end{aligned}$$

which have been calculated at $a = a_{TS}$. The first inequality is true under the hypothesis $b < b_{max}$ and $k_1 < k < k_2$, and for the same reasons the second inequality is also true. Therefore, $\widehat{\mathbf{x}}$ is a T-singularity for $a = a_{TS}$.

By using Lemma 5.2, the TS-bifurcation involves the pseudo-equilibrium $\widetilde{\mathbf{x}}^-$ in the supercritical case, since $\widetilde{\mathbf{x}}^-(a_{TS}) = \widehat{\mathbf{x}}(a_{TS})$ for all $k_1 < k < k_c$. In addition, for $a > a_{TS}$ we have $\widetilde{\mathbf{x}}^- \in \Sigma_{rs}$ and

for $a < a_{TS}$ we have $\widetilde{\mathbf{x}}^- \in \Sigma_{as}$. On the other hand, it involves the pseudo-equilibrium $\widetilde{\mathbf{x}}^+$ in the subcritical case, since $\widetilde{\mathbf{x}}^+(a_{TS}) = \widehat{\mathbf{x}}(a_{TS})$ for all $k_c < k < k_2$. In this case, for $a > a_{TS}$ we have $\widetilde{\mathbf{x}}^+ \in \Sigma_{as}$ and for $a < a_{TS}$ we have $\widetilde{\mathbf{x}}^+ \in \Sigma_{rs}$.

Finally, we analyze the stability of pseudo-equilibria when they are close enough to the bifurcation condition. From the determinant and trace of the Jacobian matrix, given in (5.21)-(5.22), we obtain the following result of stability, assuming that $|a-a_{TS}|$ is sufficiently small.

(a) Under the hypotheses of supercritical case, we get

$$\begin{aligned}
&\mathrm{Det}[J_{as}(\widetilde{x}^-, y_r)]\Big|_{a=a_{TS}} = 0,\\
&\frac{d}{da}\mathrm{Det}[J_{as}(\widetilde{x}^-, y_r)]\Big|_{a=a_{TS}} = -\omega y_r^2 < 0,\\
&\mathrm{Tr}[J_{as}(\widetilde{x}^-, y_r)]\Big|_{a=a_{TS}} =\\
&= -2k\left(-by_r(k-k_1)(k-k_2) + \frac{\omega y_r}{2}\right) - 1 < 0.
\end{aligned}$$

Therefore, for $a < a_{TS}$ the point $\widetilde{\mathbf{x}}^-$ is a stable pseudo-node, becoming a pseudo-saddle for $a > a_{TS}$.

(b) Under the hypotheses of subcritical case, we get

$$\begin{aligned}
&\mathrm{Det}[J_{rs}(\widetilde{x}^+, y_r)]\Big|_{a=a_{TS}} = 0,\\
&\frac{d}{da}\mathrm{Det}[J_{rs}(\widetilde{x}^+, y_r)]\Big|_{a=a_{TS}} = -\omega y_r^2 < 0,\\
&\mathrm{Tr}[J_{rs}(\widetilde{x}^+, y_r)]\Big|_{a=a_{TS}} =\\
&= 2k\left(-by_r(k-k_1)(k-k_2) + \frac{\omega y_r}{2}\right) + 1 > 0.
\end{aligned}$$

Therefore, for $a > a_{TS}$ the point $\widetilde{\mathbf{x}}^+$ is a pseudo-saddle, becoming an unstable pseudo-node for $a < a_{TS}$.

The proof is completed. □

In next section, it will be shown that the TS-bifurcation predicted

by Theorem 5.1 is accompanied by the birth of a crossing limit cycle (CLC).

5.3 Numerical analysis of bifurcating CLCs

In this section, simulation results of the boost converter with SMC-Washout modeled by the dynamical system (5.6) are shown in Figures 5.5 and 5.6. From Figure 5.5, it is possible to visualize the TS-bifurcation for the supercritical case and the emergence of a CLC (Γ_s) with stable node dynamics. Figure 5.6 illustrates the subcritical case, where it is possible to detect the emergence of a CLC (Γ_u) with saddle dynamics.

In order to investigate the existence and stability of the CLC we will analyze numerically the dynamics in the crossing region, using the closing equations and the theory of first return maps (see [20]).

5.3.1 Closing equations and solutions

System (5.6) can be rewritten as

$$\dot{\mathbf{x}} = \begin{cases} A^{-}\mathbf{x} + \mathbf{b}, & \text{if } z < 0 \\ A^{+}\mathbf{x} + \mathbf{b}, & \text{if } z > 0 \end{cases}, \tag{5.29}$$

where

$$A^{-} = \begin{bmatrix} -b & 0 & 0 \\ 0 & -a & 0 \\ -kb & \omega - a & -\omega \end{bmatrix}, \; A^{+} = \begin{bmatrix} -b & -1 & 0 \\ 1 & -a & 0 \\ 1 - kb & \omega - a - k & -\omega \end{bmatrix},$$

$$\mathbf{x} = \begin{bmatrix} x \\ y \\ z \end{bmatrix} \text{ and } \mathbf{b} = \begin{bmatrix} 1 \\ 0 \\ k - \omega y_r \end{bmatrix}.$$

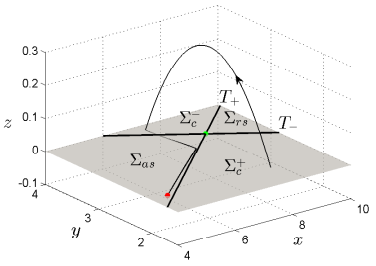

(a) $a = 1.1 < a_{TS}$

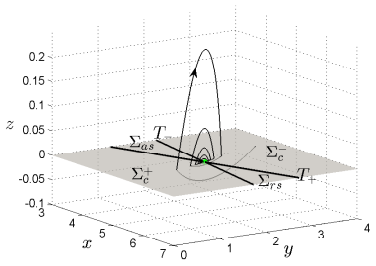

(b) $a = 1.2 = a_{TS}$

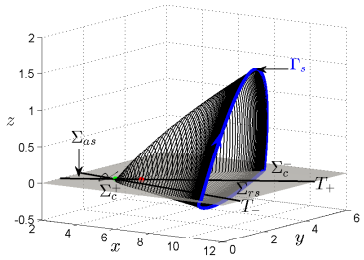

(c) $a = 1.25 > a_{TS}$

Figure 5.5: Simulation results of system (5.6) for the supercritical case. The green and red points indicate the T-singularity and pseudo-equilibrium $\widetilde{\mathbf{x}}^-$, respectively. Simulation parameters are $\omega = 1$, $y_r = 2$, $b = 0.01$ and $k = 2.5$.

Note that $\mathbf{F}^{\pm}(x, y, z) = A^{\pm}\mathbf{x} + \mathbf{b}$. As system (5.29) is piecewise-linear, we can write explicitly the flow in each zone, namely

$$\mathbf{\Phi}^{\pm}(\tau, \mathbf{x}) = \overline{\mathbf{x}}^{\pm} + e^{A^{\pm}\tau}(\mathbf{x} - \overline{\mathbf{x}}^{\pm}),$$

where

$$\overline{\mathbf{x}}^{-} = \begin{bmatrix} \frac{1}{b} \\ 0 \\ -y_r \end{bmatrix} \quad \text{and} \quad \overline{\mathbf{x}}^{+} = \begin{bmatrix} \frac{a}{1+ab} \\ \frac{1}{1+ab} \\ \frac{1}{1+ab} - y_r \end{bmatrix}$$

are the equilibria of (5.29) for $z < 0$ and $z > 0$, respectively.

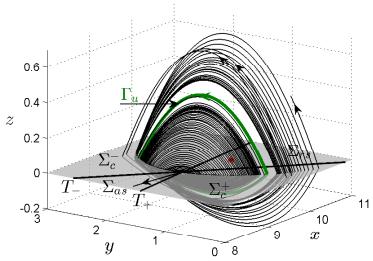

(a) $a = 1.13 < a_{TS}$

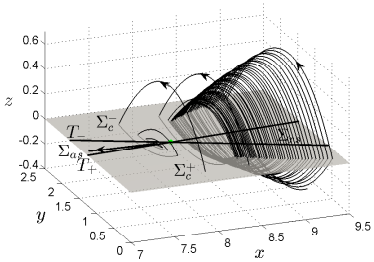

(b) $a = 1.63 = a_{TS}$

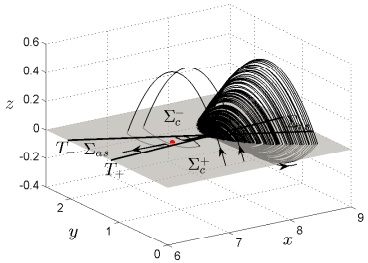

(c) $a = 1.73 > a_{TS}$

Figure 5.6: Simulation results of system (5.6) for the subcritical case. The green and red points indicate the T-singularity and pseudo-equilibrium $\widetilde{\mathbf{x}}^+$, respectively. Simulation parameters are $\omega = 0.6$, $y_r = 1.33$, $b = 0.08$ and $k = 6$.

In what follows, we assume the existence of a CLC that crosses $\Sigma = \{z = 0\}$ at the two points

$$\mathbf{x}_0 = \begin{bmatrix} x_0 \\ y_0 \\ 0 \end{bmatrix} \quad \text{and} \quad \mathbf{x}_1 = \begin{bmatrix} x_1 \\ y_1 \\ 0 \end{bmatrix},$$

so that $\mathbf{x}_0 \in \Sigma_c^+$ and $\mathbf{x}_1 \in \Sigma_c^-$. We denote the flight times [2] spent by

[2] The flight time is the time required for a trajectory, started in Σ, to return to Σ.

the closed orbit using each vector field $\mathbf{F}^-$ (zone $z < 0$) and $\mathbf{F}^+$ (zone $z > 0$) by τ_- and τ_+, respectively. A trajectory of (5.29) starting in $\mathbf{x}_0$ is determined by the vector field $\mathbf{F}^+$ until the time instant τ_+, when it comes back to touch the plane $z = 0$ at the point $\mathbf{x}_1$. Similarly, a trajectory of (5.29) starting in $\mathbf{x}_1$ is determined by the vector field $\mathbf{F}^-$ until the time instant τ_-, touching again the plane $z = 0$ at the point $\mathbf{x}_0$. Therefore, the point $\mathbf{x}_0$ is mapped into $\mathbf{x}_1$ by the flow of (5.29) in zone $z > 0$ and the point $\mathbf{x}_1$ is mapped into $\mathbf{x}_0$ by the flow of (5.29) in zone $z < 0$.

Accordingly, we write the closing equations as follows

$$\mathbf{x}_1 = \overline{\mathbf{x}}^+ + e^{A^+\tau_+}(\mathbf{x}_0 - \overline{\mathbf{x}}^+), \tag{5.30}$$

$$\mathbf{x}_0 = \overline{\mathbf{x}}^- + e^{A^-\tau_-}(\mathbf{x}_1 - \overline{\mathbf{x}}^-). \tag{5.31}$$

These equations form a system with 6 nonlinear equations with 6 unknowns. The vector of unknowns is $(x_0, y_0, x_1, y_1, \tau_-, \tau_+)$, and it is required that $f_3^{\pm}(x_0, y_0, 0) > 0$ ($\mathbf{x}_0 \in \Sigma_c^+$), $f_3^{\pm}(x_1, y_1, 0) < 0$ ($\mathbf{x}_1 \in \Sigma_c^-$) and $\tau_{\pm} > 0$, where f_3^+ and f_3^- are the functions given in (5.7) and (5.8), respectively. The following result is straightforward and is given without proof.

Proposition 5.2. *Assume that the dynamical system* (5.29) *has a CLC that transversely intersects the plane* $z = 0$ *at the points* $\widehat{\mathbf{x}}_1 \in \Sigma_c^-$ *and* $\widehat{\mathbf{x}}_0 \in \Sigma_c^+$, *with flight times* $\widehat{\tau}_+ > 0$ *and* $\widehat{\tau}_- > 0$ *in the zones* $z > 0$ *and* $z < 0$, *respectively. Then, the values* $\widehat{\mathbf{x}}_0$, $\widehat{\mathbf{x}}_1$, $\widehat{\tau}_+$ *and* $\widehat{\tau}_-$ *satisfy the closing equations* (5.30) *and* (5.31).

5.3.2 First return maps and stability of limit cycles

In this section the stability of CLCs is analyzed. Assuming that we have a transversal orbit in $z > 0$ joining the points $\mathbf{x}_0 = (x_0, y_0, 0) \in \Sigma_c^+$, $\mathbf{x}_1 = (x_1, y_1, 0) \in \Sigma_c^-$, we can ensure that there is an open set $U_0 \subset \mathbb{P}_{12}(\Sigma_c^+)$ in the neighbourhood of (x_0, y_0), and an open set $U_1 \subset \mathbb{P}_{12}(\Sigma_c^-)$ in the neighbourhood of (x_1, y_1), where $\mathbb{P}_{12}$ is the canonical

projection on the plane $z = 0$, and an application $\tau_+ : U_0 \to \mathbb{R}$ such that $\mathbf{\Phi}^+(\tau_+(x_0, y_0), \mathbf{x}_0) = \mathbf{x}_1 = (x_1, y_1, 0)$ with $(x_1, y_1) \in U_1$ for all $(x_0, y_0) \in U_0$. So, the half-return map in reduced coordinates, in zone $z > 0$ to be denoted by P_+, is defined by

$$\begin{array}{rccl} P_+ \ : & U_0 & \longrightarrow & U_1 \\ & (x_0, y_0) & \longmapsto & (x_1, y_1) = G_+(x_0, y_0, \tau_+(x_0, y_0)), \end{array}$$

where $G_+(x, y, \tau) = \mathbb{P}_{12}(\mathbf{\Phi}^+(\mathbb{P}_{12}\mathbf{x}, \tau))$ corresponds to first two coordinates of the flow. We will need also the function

$$g_+(x, y, \tau) = \mathbb{P}_3(\mathbf{\Phi}^+(\mathbb{P}_{12}\mathbf{x}, \tau)),$$

where $\mathbb{P}_3$ is the standard projection on the z-axis. This last function implicitly defines the required flight time τ_+ by imposing that, for $(x_0, y_0) \in U_0$, we have

$$g_+(x_0, y_0, \tau_+(x_0, y_0)) = 0. \tag{5.32}$$

Analogously, we can ensure that there is an open set $V_0 \subset \mathbb{P}_{12}\,(\Sigma_c^-)$ in the neighbourhood of (x_1, y_1), $V_1 \subset \mathbb{P}_{12}\,(\Sigma_c^+)$ in the neighbourhood of (x_2, y_2), and an application $\tau_- : V_0 \to \mathbb{R}$ such that $\mathbf{\Phi}-(\tau_-(x_1, y_1), \mathbf{x}_1) = \mathbf{x}_2 = (x_2, y_2, 0)$ with $(x_2, y_2) \in V_1$ for all $(x_1, y_1) \in V_0$. So, the half-return map in reduced coordinates, in zone $z < 0$ and denoted by P_-, is defined by

$$\begin{array}{rccl} P_- \ : & V_0 & \longrightarrow & V_1 \\ & (x_1, y_1) & \longmapsto & (x_2, y_2) = G_-(x_1, y_1, \tau_-(x_1, y_1)), \end{array}$$

where $G_-(x, y, \tau) = \mathbb{P}_{12}(\mathbf{\Phi}^-(\mathbb{P}_{12}\mathbf{x}, \tau))$ corresponds to first two coordinates of the flow. We will need also the function

$$g_-(x, y, \tau) = \mathbb{P}_3(\mathbf{\Phi}^-(\mathbb{P}_{12}\mathbf{x}, \tau)),$$

where $\mathbb{P}_3$ is the standard projection on the z-axis. This last func-

tion implicitly defines the required flight time τ_- by imposing that, for $(x_1, y_1) \in V_0$, we have

$$g_-(x_1, y_1, \tau_-(x_1, y_1)) = 0. \tag{5.33}$$

Thus, based on the conditions stated above and assuming $U_1 \subset V_0$, we define the function that describes in reduced coordinates the complete first return map P as

$$\begin{array}{rccl} P: & U_0 & \longrightarrow & V_1 \\ & (x_0, y_0) & \longmapsto & P = P_- \circ P_+ = (x_2, y_2). \end{array}$$

The fixed points of the first return map, excluding of course the T-singularity, represent CLCs, so that the stability analysis of the fixed points can be naturally extended to the CLCs. A CLC is born when a fixed point bifurcates from a T-singularity, in a reversible *Bogdanov-Takens bifurcation* with two eigenvalues equal to 1; see Chapter 5. Note that, if $(\widehat{x}_0, \widehat{y}_0)$ is a fixed point of the map $P = P_- \circ P_+$, then $(\widehat{x}_0, \widehat{y}_0, 0) \in \Sigma_c^+$ and it is a crossing point of the CLC with the plane $z = 0$. Consequently, $(\widehat{x}_1, \widehat{y}_1)$ is a fixed point of the map $P_+ \circ P_-$ such that $(\widehat{x}_1, \widehat{y}_1, 0) \in \Sigma_c^-$ and it is the other crossing point of the CLC with the plane $z = 0$. The Jacobian matrices are obtained directly from

$$DP_\pm(\mathbf{p}) = \frac{\partial G_\pm}{\partial (x, y)}(\mathbf{p}) + \frac{\partial G_\pm}{\partial \tau}(\mathbf{p}) \frac{\partial \tau_\pm}{\partial (x, y)}, \tag{5.34}$$

where by differentiating (5.32) and (5.33), we obtain

$$\frac{\partial g_\pm}{\partial (x, y)}(\mathbf{p}) + \frac{\partial g_\pm}{\partial \tau}(\mathbf{p}) \frac{\partial \tau_\pm}{\partial (x, y)} = 0,$$

so that

$$\frac{\partial \tau_\pm}{\partial (x, y)} = -\left(\frac{\partial g_\pm}{\partial \tau}(\mathbf{p}) \right)^{-1} \frac{\partial g_\pm}{\partial (x, y)}(\mathbf{p}). \tag{5.35}$$

By substituting (5.35) in (5.34) we obtain

$$DP_{\pm}(\mathbf{p}) = \frac{\partial G_{\pm}}{\partial(x,y)}(\mathbf{p}) - \\ - \left(\frac{\partial g_{\pm}}{\partial \tau}(\mathbf{p})\right)^{-1} \frac{\partial G_{\pm}}{\partial \tau}(\mathbf{p}) \frac{\partial g_{\pm}}{\partial(x,y)}(\mathbf{p}), \tag{5.36}$$

where $\mathbf{p} = \mathbf{p}_0 = (x_0, y_0, \tau_+(x_0, y_0))$ or $\mathbf{p} = \mathbf{p}_1 = (x_1, y_1, \tau_-(x_1, y_1))$, respectively.

Now from (5.36), we can calculate the matrix

$$DP = DP_-(\mathbf{p}_1) \cdot DP_+(\mathbf{p}_0),$$

where the eigenvalues of matrix DP are the characteristic multipliers of the limit cycle Γ.

Remark 5.1. *In order to compute the above expressions in the model of the circuit, we consider the case $b \neq \omega$ and $a < 2 + b$. This is a consistent physical hypothesis and it is sufficient to reproduce all the possible different behaviors.*

Coming back to the computation of the solutions for equations (5.30) and (5.31), we note that the eigenvalues of matrices A^- and A^+ are $\{-a, -b, -\omega\}$ and $\{\alpha \pm i\beta, -\omega\}$, respectively, where $2\alpha = -(a + b)$ and $2\beta = \sqrt{4 - (a - b)^2}$. By defining $p(\tau_+) = e^{\alpha\tau_+} \cos[\beta\tau_+]$ and $q(\tau_+) = e^{\alpha\tau_+} \sin[\beta\tau_+]/\beta$, equations (5.30) and (5.31) are rewritten as

$$\begin{bmatrix} x_1 \\ y_1 \end{bmatrix} = G_+(x_0, y_0, \tau_+) = \\ = M(\tau_+) \left(\begin{bmatrix} x_0 \\ y_0 \end{bmatrix} - \begin{bmatrix} \frac{a}{1+ab}, \\ \frac{1}{1+ab} \end{bmatrix} \right) + \begin{bmatrix} \frac{a}{1+ab} \\ \frac{1}{1+ab} \end{bmatrix}, \tag{5.37}$$

$$\begin{bmatrix} x_0 \\ y_0 \end{bmatrix} = G_-(x_1, y_1, \tau_-) = \\ = N(\tau_-) \left(\begin{bmatrix} x_1 \\ y_1 \end{bmatrix} - \begin{bmatrix} \frac{1}{b} \\ 0 \end{bmatrix} \right) + \begin{bmatrix} \frac{1}{b} \\ 0 \end{bmatrix}, \tag{5.38}$$

$$0 = g_+(x_0, y_0, \tau_+) = \\ = \mathbf{v}(\tau_+)(\mathbf{x}_0 - \overline{\mathbf{x}}^+) + \frac{1}{1+ab} - y_r, \tag{5.39}$$

$$0 = g_-(x_1, y_1, \tau_-) = \mathbf{u}(\tau_-)(\mathbf{x}_1 - \overline{\mathbf{x}}^-) - y_r, \tag{5.40}$$

where

$$M(\tau_+) = \begin{bmatrix} p(\tau_+) + (a+\alpha)q(\tau_+) & -q(\tau_+) \\ q(\tau_+) & p(\tau_+) - (a+\alpha)q(\tau_+) \end{bmatrix},$$

$$N(\tau_-) = \begin{bmatrix} e^{-b\tau_-} & 0 \\ 0 & e^{-a\tau_-} \end{bmatrix},$$

$$\mathbf{u}(\tau_-)^T = \begin{bmatrix} \frac{kb}{b-\omega} & 0 & -\frac{kb}{b-\omega} \\ 0 & 1 & -1 \\ 0 & 0 & 1 \end{bmatrix} \begin{bmatrix} e^{-b\tau_-} \\ e^{-a\tau_-} \\ e^{-\omega\tau_-} \end{bmatrix},$$

$$\mathbf{v}(\tau_+)^T = \begin{bmatrix} c_{11} & c_{12} & c_{13} \\ c_{21} & c_{22} & c_{23} \\ 0 & 0 & 1 \end{bmatrix} \begin{bmatrix} p(\tau_+) \\ q(\tau_+) \\ e^{-\omega\tau_+} \end{bmatrix},$$

$$c_{11} = \frac{k(b(a-\omega)+1)}{(\omega+\alpha)^2+\beta^2},$$

$$c_{12} = \frac{k((a-b)(b(a-\omega)+1)-2\omega)}{2((\omega+\alpha)^2+\beta^2)} + 1,$$

$$c_{13} = -\frac{k(b(a-\omega)+1)}{(\omega+\alpha)^2+\beta^2},$$

$$c_{21} = 1 - \frac{k\omega}{(\omega+\alpha)^2+\beta^2},$$

$$c_{22} = a + \alpha + \frac{k(2(1+ab) - (a+b)\omega)}{2((\omega+\alpha)^2 + \beta^2)},$$
$$c_{23} = \frac{k\omega}{(\omega+\alpha)^2 + \beta^2} - 1.$$

From equations (5.37) and (5.38), we write

$$(x_0, y_0) = (\widehat{x}_0(\tau_+, \tau_-), \widehat{y}_0(\tau_+, \tau_-))$$

and

$$(x_1, y_1) = (\widehat{x}_1(\tau_+, \tau_-), \widehat{y}_1(\tau_+, \tau_-))$$

as functions of the flight times $\tau_+ > 0$ and $\tau_- > 0$, so that

$$\begin{bmatrix} \widehat{x}_0(\tau_+, \tau_-) \\ \widehat{y}_0(\tau_+, \tau_-) \end{bmatrix} = X^{-1} \left(N\widetilde{M} \begin{bmatrix} \frac{a}{1+ab} \\ \frac{1}{1+ab} \end{bmatrix} + \widetilde{N} \begin{bmatrix} \frac{1}{b} \\ 0 \end{bmatrix} \right), \tag{5.41}$$
$$\begin{bmatrix} \widehat{x}_1(\tau_+, \tau_-) \\ \widehat{y}_1(\tau_+, \tau_-) \end{bmatrix} = Y^{-1} \left(M\widetilde{N} \begin{bmatrix} \frac{1}{b} \\ 0 \end{bmatrix} + \widetilde{M} \begin{bmatrix} \frac{a}{1+ab} \\ \frac{1}{1+ab} \end{bmatrix} \right), \tag{5.42}$$

where $X = I - NM$, $Y = I - MN$, $\widetilde{M} = I - M$, $\widetilde{N} = I - N$ and I is the identity matrix of order 2.

We define

$$\widehat{\mathbf{x}}_0 = (\widehat{x}_0(\widehat{\tau}_+, \widehat{\tau}_-), \widehat{y}_0(\widehat{\tau}_+, \widehat{\tau}_-), 0) \in \Sigma_c^+$$

and

$$\widehat{\mathbf{x}}_1 = (\widehat{x}_1(\widehat{\tau}_+, \widehat{\tau}_-), \widehat{y}_1(\widehat{\tau}_+, \widehat{\tau}_-), 0) \in \Sigma_c^-$$

as the natural coordinates in $\mathbb{R}^3$ of the crossing points.

Substituting (5.41) and (5.42) in (5.39) and (5.40), we obtain the non-linear equations

$$\sigma(\tau_+, \tau_-) = \mathbf{v}(\tau_+)\widehat{\mathbf{x}}_0^d(\tau_+, \tau_-) - \widetilde{\mathbf{v}}(\tau_+, \tau_-)\overline{\mathbf{x}}^+ = 0, \tag{5.43}$$
$$\rho(\tau_+, \tau_-) = \mathbf{u}(\tau_-)\widehat{\mathbf{x}}_1^d(\tau_+, \tau_-) - \widetilde{\mathbf{u}}(\tau_+, \tau_-)\overline{\mathbf{x}}^- = 0, \tag{5.44}$$

where we use $\widetilde{\mathbf{v}} = \text{Det}\,[X]\cdot\Big(\mathbf{v} - \begin{bmatrix}0 & 0 & 1\end{bmatrix}\Big)$, $\widetilde{\mathbf{u}} = \text{Det}\,[Y]\cdot\Big(\mathbf{u} - \begin{bmatrix}0 & 0 & 1\end{bmatrix}\Big)$, and the points $\widehat{\mathbf{x}}_0^d = \widehat{\mathbf{x}}_0 \cdot \text{Det}\,[X]$ and $\widehat{\mathbf{x}}_1^d = \widehat{\mathbf{x}}_1 \cdot \text{Det}\,[Y]$ to avoid a cumbersome denominator.

Thus, if $(\widehat{\tau}_+, \widehat{\tau}_-)$ is a solution of the system equations (5.43)-(5.44), such that $\widehat{\tau}_+ > 0$, $\widehat{\tau}_- > 0$, then the dynamical system (5.29) has a CLC that transversely crosses the plane $z = 0$ at the points $\widehat{\mathbf{x}}_0$ and $\widehat{\mathbf{x}}_1$ with the flight times $\widehat{\tau}_+$ and $\widehat{\tau}_-$ in the zones $z > 0$ and $z < 0$, respectively.

By using (5.36) it is not difficult to arrive at the following proposition that allows us to analyze the CLC stability of the system (5.29).

Proposition 5.3. *Let Γ be a CLC of system (5.29), transversely intersecting the plane $z = 0$ at the points $\widehat{\mathbf{x}}_0 = (\widehat{x}_0, \widehat{y}_0, 0) \in \Sigma_c^+$ and $\widehat{\mathbf{x}}_1 = (\widehat{x}_1, \widehat{y}_1, 0) \in \Sigma_c^-$. We denote by $\widehat{\tau}_+ > 0$ and $\widehat{\tau}_- > 0$ the flight times of Γ in the zone $z > 0$ and $z < 0$, respectively. We define the Jacobian matrices*

$$DP_+(\mathbf{p}_0) = \frac{1}{\mathbf{v}'(\widehat{\tau}_+)(\widehat{\mathbf{x}}_0 - \overline{\mathbf{x}}^+)} M(\widehat{\tau}_+)\times$$
$$\times \left(I - \begin{bmatrix} 1 - (b\widehat{x}_0 + \widehat{y}_0) \\ \widehat{x}_0 - a\widehat{y}_0 \end{bmatrix} \mathbf{v}(\widehat{\tau}_+) \begin{bmatrix} 1 & 0 \\ 0 & 1 \\ 0 & 0 \end{bmatrix} \right),$$
$$DP_-(\mathbf{p}_1) = \frac{1}{\mathbf{u}'(\widehat{\tau}_-)(\widehat{\mathbf{x}}_1 - \overline{\mathbf{x}}^-)} N(\widehat{\tau}_-)\times$$
$$\times \left(I - \begin{bmatrix} 1 - b\widehat{x}_1 \\ -a\widehat{y}_1 \end{bmatrix} \mathbf{u}(\widehat{\tau}_-) \begin{bmatrix} 1 & 0 \\ 0 & 1 \\ 0 & 0 \end{bmatrix} \right),$$

where $\mathbf{p}_0 = (\widehat{x}_0, \widehat{y}_0, \widehat{\tau}_+)$, $\mathbf{p}_1 = (\widehat{x}_1, \widehat{y}_1, \widehat{\tau}_-)$, I is the identity matrix of order 2. The eigenvalues of matrix

$$DP = DP_-(\mathbf{p}_1) \cdot DP_+(\mathbf{p}_0),$$

are the characteristic multipliers of the limit cycle Γ.

Example 5.1. *By selecting* $b = 0.01$, $\omega = 1$, $y_r = 2$, $k = 2.5$ *and* $a = 1.238$, *system* (5.43)-(5.44) *has two solutions in the positive quadrant,* $(\widehat{\tau}'_+, \widehat{\tau}'_-) = (0.84, 2.24)$ *and* $(\widehat{\tau}''_+, \widehat{\tau}''_-) = (0.87, 5.18)$. *This case is shown in Figure 5.7 where for each of the two solutions listed in Table 5.2, the respective fixed points and the restriction on the position of these fixed points are given. In this example, two CLCs of system* (5.29) *were detected as shown in Figure 5.10(a). For the first* (Γ_s), *we have* $\mathbf{p}_0 = (10.53, 0.32, 0.84)$ *and* $\mathbf{p}_1 = (8.5, 5.17, 2.24)$, *then, the characteristic multipliers are* $\{0.923, 0.011\}$. *In this case, the limit cycle* Γ_s *has a stable node dynamics. For the second* (Γ_u), *we have* $\mathbf{p}_0 = (19.31, 0.02, 0.87)$ *and* $\mathbf{p}_1 = (15.02, 9.26, 5.18)$, *consequently, the characteristic multipliers are* $\{1.88, 0.0002\}$. *In this case,* Γ_u *has a saddle dynamics.*

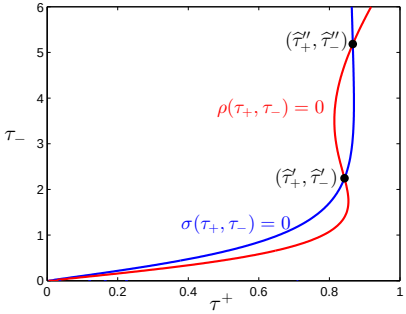

Figure 5.7: Numerical analysis of the existence of CLCs in the example 5.1. The intersecting points between the two curves (in red and blue-color) given by (5.43) and (5.44) denote the presence of two CLCs.

5.3.3 Stability and bifurcations of CLCs

For a more comprehensive view of the evolution of a CLC with respect to variations in the parameter a, we represent the points $(\widehat{x}_0, \widehat{y}_0)$ and $(\widehat{x}_1, \widehat{y}_1)$ in the plane $z = 0$ but with the T-singularity placed at the origin by choosing new variables (u_1, u_2) in such a way that the

Solutions	Fixed points	Constraints satisfied: $f_3^{\pm}(\widehat{x}_0, \widehat{y}_0, 0) > 0, f_3^{\pm}(\widehat{x}_1, \widehat{y}_1, 0) < 0$
$(\widehat{\tau}'_+, \widehat{\tau}'_-) = (0.84, 2.24)$	$(\widehat{x}_0, \widehat{y}_0) = (10.53, 0.32)$ $(\widehat{x}_1, \widehat{y}_1) = (8.5, 5.17)$	$f_3^+ = 9.88 > 0, \quad f_3^- = 0.16 > 0$ $f_3^+ = -5.36 < 0, \quad f_3^- = -0.94 < 0$
$(\widehat{\tau}''_+, \widehat{\tau}''_-) = (0.87, 5.18)$	$(\widehat{x}_0, \widehat{y}_0) = (19.31, 0.02)$ $(\widehat{x}_1, \widehat{y}_1) = (15.02, 9.26)$	$f_3^+ = 19.3 > 0, \quad f_3^- = 0.01 > 0$ $f_3^+ = -10.2 < 0, \quad f_3^- = -2.1 < 0$

Table 5.2: Case study in the example 5.1.

tangency lines T_- and T_+ become the new coordinate axes. See Figures 5.8(b) and 5.9(b). Such normalization is obtained by defining

$$(u_1, u_2) = (-f_3^+(x, y, 0), f_3^-(x, y, 0)).$$

For the subcritical case, the simulation of system (5.29) shown the existence of a CLC (Γ_u) with saddle type dynamics (see Figure 5.6(a)). The numerical analysis of the existence and the stability for the CLC Γ_u is shown in Figure 5.8. In Figure 5.8(a), we visualize the bifurcation diagram for the parameter a in the (a, u_2)-plane, showing the saddle-node bifurcation of pseudo-equilibria (SN) and the TS-bifurcation (TS). The saddle-node bifurcation occurs at $a = a_{SN} = 1.76$ and involves the stable pseudo-node $\widetilde{\mathbf{x}}^- \in \Sigma_{as}$ (sPN-Σ_{as}) and the pseudo-saddle $\widetilde{\mathbf{x}}^+ \in \Sigma_{as}$ (PS-Σ_{as}), indicated by the branch of pseudo-equilibria in purple-color and red-color parts, respectively. The TS-bifurcation occurs at $a = a_{TS} = 1.63$ and is classified as subcritical, involving the pseudo-equilibrium $\widetilde{\mathbf{x}}^+$. It is caused by the transition, through the T-singularity, of the pseudo-saddle in Σ_{as} (PS-Σ_{as}) when $a > a_{TS}$, to become a unstable pseudo-node in Σ_{rs} (uPN-Σ_{rs}) when $a < a_{TS}$. The curve in green-color, relative to the crossing points $(\widehat{x}_0, \widehat{y}_0)$ and $(\widehat{x}_1, \widehat{y}_1)$, indicates the range of existence of the CLC, regarding the parameter a. The CLC Γ_u bifurcates from the T-singularity at $a = 1.63$ and persists until $a = 0.72$, i.e., Γ_u exists for $0.72 < a < 1.63$. At $a = 1.63$ a non-standard homoclinic bifurcation occurs.

In Figure 5.8(b), there appear the locus of the CLC crossing points

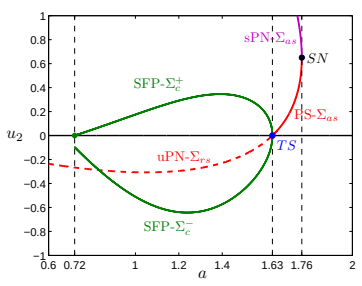

(a) Bifurcation diagram in the (a, u_2)-plane considering a the bifurcation parameter.

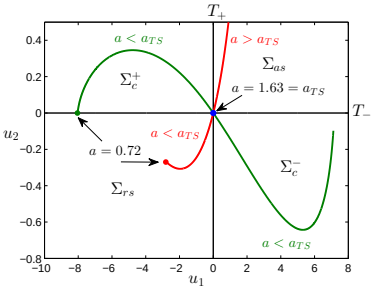

(b) The locus of CLC crossing points (green color) and of pseudo-equilibria (red color) in the (u_1, u_2)-plane.

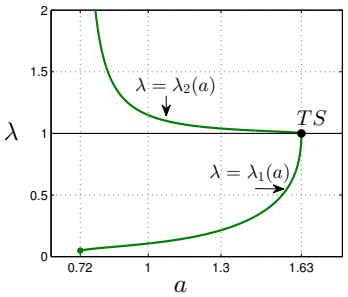

(c) The characteristic multipliers $\lambda_{1,2}$ of Γ_u in the (a, λ)-plane.

Figure 5.8: Numerical analysis of the existence and stability of the limit cycle Γ_u for parameters $\omega = 0.6$, $y_r = 1.33$, $b = 0.08$, $k = 6$ and $0.72 \leq a \leq 1.63$.

and the pseudo-equilibria, both in the normalized plane (u_1, u_2), as the parameter a varies. Such curve (in green-color) is drawn by the intersection points of Γ_u with the plane $z = 0$, in Σ_c^+ and Σ_c^- (SFP-Σ_c^+ and SFP-Σ_c^- in Figure 5.8(a), respectively). The CLC Γ_u disappears when it touches the tangency line T_- at a visible tangency point of $\mathbf{F}^-$. The locus of the pseudo-equilibria (in red-color) is drawn by the pseudo-equilibrium position near the bifurcation. Recall from Theorem 5.1 that $\widetilde{\mathbf{x}}^+ \in \Sigma_{as}$ is a pseudo-saddle for $a > a_{TS}$, while $\widetilde{\mathbf{x}}^+ \in \Sigma_{rs}$ is

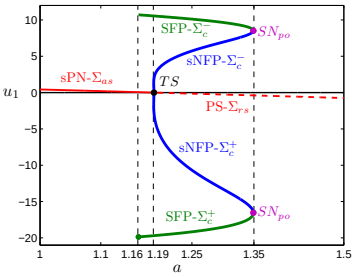

(a) Bifurcation diagram in the (a, u_1)-plane considering a the bifurcation parameter.

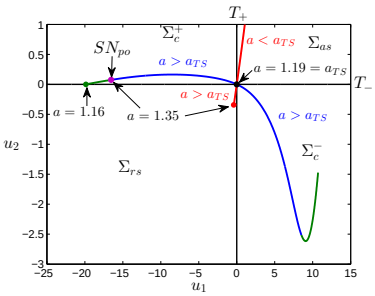

(b) The locus of CLC crossing points (green and blue color) and of pseudo-equilibria (red color) in the (u_1, u_2)-plane.

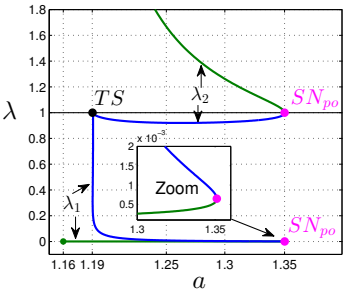

(c) The characteristic multipliers $\lambda_{1,2}$ of Γ_s (blue) and Γ_u (green) in the (a, λ)-plane.

Figure 5.9: Numerical analysis of the existence and stability of the limit cycles Γ_s and Γ_u for parameters $\omega = 1$, $y_r = 2$, $b = 0.01$, $k = 2.5$ and $1.16 \leq a \leq 1.35$.

an unstable pseudo-node for $a < a_{TS}$.

In Figure 5.8(c) we can visualize the characteristic multipliers of Γ_u, from his birth to his disappearance. The CLC Γ_u has always saddle dynamics, since for all $0.72 < a < 1.63$ the characteristic multipliers $\lambda_{1,2}$ are real, with $0 < \lambda_1 < 1 < \lambda_2$, so that when $a = a_{TS} = 1.63$ we have $\lambda_1 = \lambda_2 = 1$, and when $a = 0.72$ we have $\lambda_1 = 0.049$ and $\lambda_2 = 129.4$.

For the supercritical case, the simulation results of system (5.29) show the existence of a CLC (Γ_s) with stable node dynamics (see Figure 5.5(c)).The results of numerical continuation in the parameter a for the CLC Γ_s are shown in Figure 5.9.

In Figure 5.9(a) we give the bifurcation diagram in the (a, u_1)-plane, showing a saddle-node bifurcation of CLCs (SN_{po}) and the TS-bifurcation (TS). The SN_{po} bifurcation occurs at $a = a_{SN_{po}} = 1.35$ and involves the stable CLC Γ_s with node dynamics (sNFP-Σ_c^+ and sNFP-Σ_c^-) and the unstable CLC Γ_u with saddle dynamics (SFP-Σ_c^+ and SFP-Σ_c^-), indicated by the branch of the fixed points with blue and green parts, respectively. The TS-bifurcation occurs at $a = a_{TS} = 1.19$ and is classified as supercritical, involving the pseudo-equilibrium $\widetilde{\mathbf{x}}^-$; as we already know, it is due to the transition through the T-singularity of a stable pseudo-node in Σ_{as} (sPN-Σ_{as}) when $a < a_{TS}$, to become a pseudo-saddle in Σ_{rs} (PS-Σ_{rs}) when $a > a_{TS}$. The branch in blue and green colors, related to the crossing points $(\widehat{x}_0, \widehat{y}_0)$ and $(\widehat{x}_1, \widehat{y}_1)$, indicates the range of existence of the CLCs, regarding the parameter a. The stable CLC Γ_s bifurcates from the T-singularity for $a = 1.19$ and persists until $a = 1.35$, i.e., Γ_s exists for $1.19 < a < 1.35$. The unstable CLC Γ_u exists in the interval $1.16 < a < 1.35$, and such a periodic orbit can be shown to appear after a TS-bifurcation for another value of the control parameter k, in the subcritical case, but still persists for the value of k used in this example.

Figure 5.9(b) shows the locus of crossing points and the pseudo-equilibria, both in the normalized (u_1, u_2)-plane, as the parameter a varies. Regarding the crossing points, the intersection points of Γ_s appear in blue, while the ones of Γ_u appear in green. The locus of the pseudo-equilibria (in red) gives the pseudo-equilibrium position near the bifurcation. From Theorem 5.1, the point $\widetilde{\mathbf{x}}^- \in \Sigma_{as}$ is a stable pseudo-node for $a < a_{TS}$ while $\widetilde{\mathbf{x}}^- \in \Sigma_{rs}$ is a pseudo-saddle for $a > a_{TS}$.

Figure 5.9(c) shows the characteristic multipliers of Γ_s, from his

birth to his disappearance. The CLC Γ_s has always stable node dynamics, since for $1.19 < a < 1.35$ the characteristic multipliers $\lambda_{1,2}$ are real with $|\lambda_1| < 1$ and $|\lambda_2| < 1$. When $a = a_{TS} = 1.19$ we have $\lambda_1 = \lambda_2 = 1$ and when $a = a_{SN_{po}} = 1.35$ we have $\lambda_1 = 6.4 \times 10^{-4}$ and $\lambda_2 = 1$. In Figure 5.9(d) we visualize the characteristic multipliers of Γ_u, always of saddle dynamics, since the characteristic multipliers $\lambda_{1,2}$ are real with $0 < \lambda_1 < 1 < \lambda_2$. For instance, when $a = 1.35$ we have $\lambda_1 = 6.4 \times 10^{-4}$ and $\lambda_2 = 1$, and $\lambda_1 = 1.5 \times 10^{-4}$ and $\lambda_2 = 121.6$ when $a = 1.16$.

Example 5.2. *Simulation results of system* (5.6)*, with parameters* $b = 0.01$*,* $y_r = 2$*,* $\omega = 1$*,* $k = 2.5$*, for* $a = 1.238$ *are shown in Figure 5.10(a) and, for* $a = 1.35$*, in Figure 5.10(b). Here, we visualize one non-hyperbolic CLC (*Γ_{sn}*), created by the collision between the stable node CLC (*Γ_s*) and the saddle CLC (*Γ_u*), in a saddle-node bifurcation of CLCs.*

5.4 Experimental results

This section is dedicated to validate the analytical and numerical results on the TS-bifurcation obtained in previous Sections 5.2 and 5.3, by means of experimental results obtained with a boost power converter controlled by the SMC-Washout controller proposed in Subsection 5.2.1. The experimental setup is shown in Figure 5.11(a) and the boost converter circuit in Figure 5.11(b).

The experimental parameters values are: $L = 1.5mH$, $r_L = 0.4\Omega$, $C = 10\mu F$, $V_{\text{in}} = 11\text{V}$, $V_{\text{ref}} = 13\text{V}$, $\omega_F = 5000\text{rad/s}$ and $K = 27.5\Omega$. The applied hysteresis band is $\pm 1\text{V}$. The resistive load R has an initial value of 21Ω.

Figures 5.11(c) and 5.11(d) show the oscilloscope signals obtained from the experimental circuit corresponding to voltage v_C (in orange-color), current i_L (blue-color), filtered current $i_F = 2.75(i_L - z_F)$ (purple-color) and reference voltage V_{ref} (green color) signals, for re-

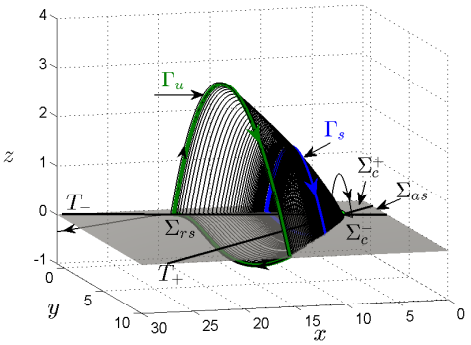

(a) Saddle (green) and stable node (blue) CLCs for $a = 1.238$.

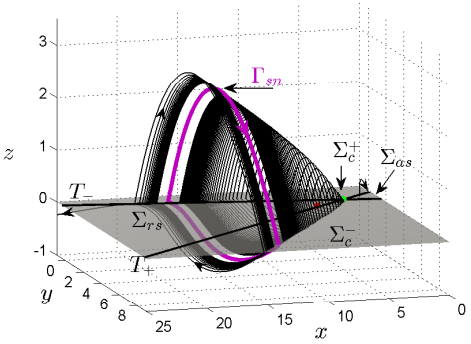

(b) Non hyperbolic CLC for $a = 1.35$.

Figure 5.10: Saddle-Node bifurcation of CLCs. Simulation results for $b = 0.01$, $y_r = 2$, $\omega = 1$, $k = 2.5$.

sistive loads of $R = 21\,\Omega$ and $R = 7\,\Omega$, respectively.

Notice that in Figure 5.11(c), the current and voltage signals are periodic, i.e. the converter operating point is not an equilibrium point as expected for SMC. Instead, there appears a limit cycle with rather small amplitude around the stable pseudo-equilibrium within the attractive sliding region. This is due to the presence of a hysteresis band,

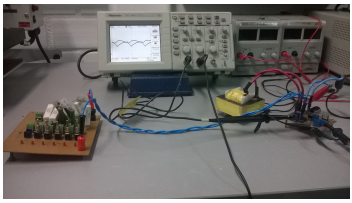

(a) Experimental setup.

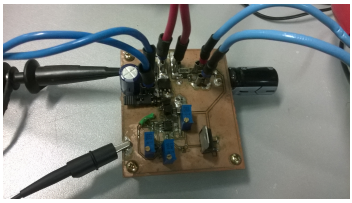

(b) Boost Converter

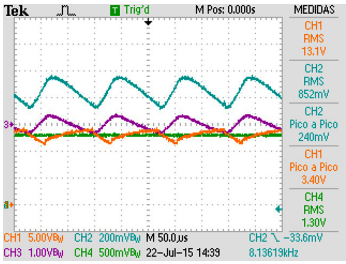

(c) Oscilloscope signals: $R = 21\ \Omega$

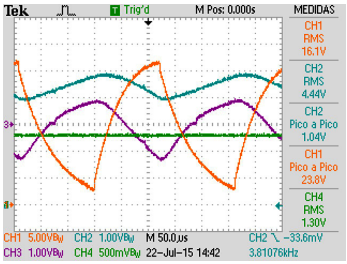

(d) Oscilloscope signals: $R = 7\ \Omega$

Figure 5.11: Experimental results: a) Laboratory setup; b) boost converter circuit; c) and d) oscilloscope signals corresponding to voltage v_C (in orange-color), current i_L (blue-color), filtered current $i_F = 2.75(i_L - z_F)$ (purple-color) and reference voltage V_{ref} (green color), for $R = 21\ \Omega$ and $R = 7\ \Omega$, respectively.

used in practice to implement the sliding control law with a limited switching frequency [108].

In Figure 5.11(d), the resistive load is changed from $R = 21\ \Omega$ to $R = 7\Omega$, so that the converter undergoes the TS-bifurcation, appearing a large CLC.

Experimental and simulation results obtained from the circuit and from the controlled model are compared in Figure 5.12. In Figure 5.12(a), the blue dot stands for the position of the stable pseudo-equilibrium, in (i_L, v_C)-plane for $R = 21\ \Omega$, and calculated by the analytical model. In the same figure, the small limit cycle in purple-color represent the dynamical behavior of the converter, when operating with the hysteresis band SMC.

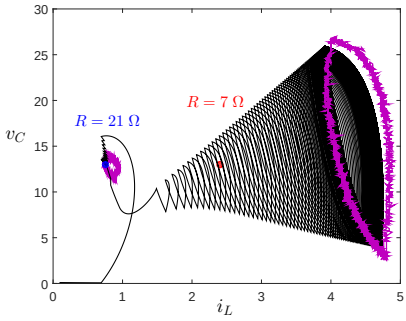

(a)

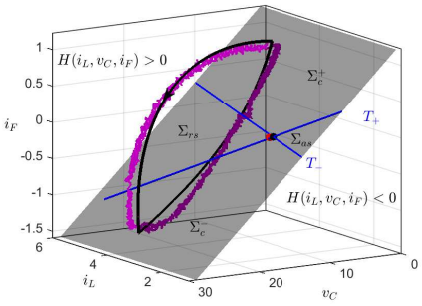

(b)

Figure 5.12: Experimental (in purple color) and simulation (black color) results for $R = 21\Omega$ and $R = 7\Omega$, in (a) the (i_L, v_C)-plane; (b) the (i_L, v_C, i_F)-plane. The different geometric elements used in the analysis are represented. The red dot stands for the pseudo-equilibrium point and the black dot for the T-singularity.

The change in the load value from $R = 21\ \Omega$ to $R = 7\ \Omega$ moves the pseudo-equilibrium (blue dot) from the stable sliding region to the repulsive sliding region (red dot), becoming unstable. Consequently, a CLC arises from a TS-bifurcation, leading to the big limit cycle shown in Figure 5.12 (in purple-color for the experiment and in black-color for the numerical simulation).

From the values of the original control system parameters given

by (5.1)-(5.4), according to Table 5.1, we obtain the dimensionless system parameters given by (5.5): $b = 0.033$, $y_r = 1.182$, $\omega = 0.61$ and $k = 2.25$. The initial normalized load is $a = 0.58$ ($R = 21\ \Omega$), and it changes to $a = 1.75$ ($R = 7\ \Omega$). Thereby, the hypotheses of the Theorem 5.1: $b = 0.033 < b_{max} = 0.217$ and $k_1 = 0.78 < k = 2.25 < 12.82 = k_c$, with b_{max}, k_1 and k_c calculated by (5.26), (5.27) and (5.24), respectively, are satisfied. Then, the bifurcation critical value is found at $a = a_{TS} = 1.735$ ($R_{TS} = 7.06\ \Omega$). The TS-bifurcation occurs as in the supercritical case, since $k_1 < k = 2.25 < k_c$. Now, by applying the CLC stability analysis of the previous section, we obtain the points $\mathbf{p}_0 = (4.79, 0.48, 0.96)$ and $\mathbf{p}_1 = (4.06, 2.16, 0.85)$. Thus, the characteristic multipliers are given by $\{0.965, 0.057\}$, implying a CLC with stable node dynamics.

Obviously, the presence of such limit cycle is not desired and, therefore, it is not acceptable from the practical point of view of control engineers that design the SMC. Thus, it is very important to determine the occurrence of this dynamical phenomenon, as well as, others that can be occur in the operation of the power converter when load changes are carry out. In this way, avoiding undesirable dynamical phenomena such as the TS-bifurcation, it is possible ensure the robustness of the designed control system.

5.5 Conclusion

In this Chapter, a dc-dc boost converter controlled using a sliding mode control strategy was modeled as a DPWL system with two zones in a three-dimensional space split by a flat surface. The main contribution of this Chapter was to prove that, under certain conditions on the circuit parameters, the analyzed model can display a TS-bifurcation. This bifurcation can occur in two different forms, named as supercritical and subcritical. The supercritical case is considered the most important, since it involves the desired operating point for

the boost converter. As a consequence of the TS-bifurcation, a CLC arises from the T-singularity, which in the supercritical case was detected with stable dynamics of node type, while in the subcritical case is of saddle type. The supercritical and subcritical cases do not occur simultaneously. However, the two CLCs that arise from each of these cases can coexist. The two CLCs are born for different critical values of the bifurcation parameter, but they may disappear simultaneously in a saddle-node bifurcation of periodic orbits.

Experimental results obtained on a boost converter specially built in our laboratory allow us to prove the occurrence of a supercritical TS-bifurcation on the circuit. Such bifurcation can be induced varying the value of the resistive load, in such a way that it changes the position of the operating point and its stability from stable to unstable. This change is critical and creates a stable CLC, which can have a large amplitude with catastrophic effects for the converter.

Thus, the analysis of the existence of TS-bifurcations becomes essential in the design and control of converters, since this is a dynamic phenomenon that is not desired and not easy to detect. Therefore, it is of great relevance to know the parametric conditions for the occurrence of this bifurcation and so to establish safeguards in order to avoid it.

Chapter 6

Dynamics and Bifurcations in Systems with Double Teixeira Singularity

This Chapter contain a detailed analysis of bifurcations in a family of 3D-DPWS systems that have two points of T-singularity (Teixeira singularity). In addition, from the variation of a system parameter, these T-singularities collide and then disappear along with the attractive sliding region. In this case a Fold bifurcation occurs and at the bifurcation point appears a type of degenerate T-singularity. Under certain conditions there is a pseudo-equilibrium that collide with one of the T-singularities or the two T-singularities simultaneously collide with the pseudo-equilibrium. In first case a TS-bifurcation occurs and, in second case, a double TS-bifurcation occurs. Both bifurcations are associated with the birth of a crossing limit cycle. We describe the sliding and crossing dynamics around the T-singularities, regular or

degenerate, and also the sliding dynamics at the pseudo-equilibrium. Moreover, we present a case study where we prove the existence, stability and bifurcations of crossing limit cycles.

6.1 Introduction

Discontinuous piecewise-smooth (DPWS) systems are often used to model mechanical systems with friction, switched electronic systems, discontinuous control systems and others. In many of these models the vector fields involved are non-linear and can thus have more complex and varied phenomena; see for instance [29, 110]. In particular, in this Chapter, we will deal with a specific class of DPWS defined in $\mathbb{R}^3$ by two polynomial vector fields of degree two, separated by a flat switching boundary.

One of the most intriguing phenomena concerning 3D-DPWS systems occur in the presence of a T-singularity. In fact, this typical singularity always presents in its neighborhood sliding (attractive and repulsive) and crossing regions. The existence of such regions permits some recurrence around the T-singularity (at the crossing regions) and non-uniqueness of trajectories passing through the T-singularity (at the sliding regions). In particular, the occurrence of non-uniqueness of trajectories produce some phenomena non observed in smooth vector fields. The literature contemplates many exotic behaviors around a single T-singularity, see [21, 26, 68, 69, 71, 117]. Despite of this, we do not know any work in the literature that deals with 3D-DPWS systems presenting two or more T-singularities.

In previous chapters, we have studied 3D-DPWS systems that present one T-singularity and a bifurcation interesting occurring at this point, called *TS-bifurcation*. Such a bifurcation is of codimension-one and involves the collision of a real pseudo-equilibrium with a T-singularity, caused by the pseudo-equilibrium transition from attractive sliding region to repulsive sliding region (or vice versa). Associated with

this bifurcation, there is the birth of a crossing limit cycle arising from the T-singularity.

Now, in this Chapter, we consider 3D-DPWS systems that have two T-singularities and which exhibit the *fold bifurcation* of these T-singularities, a codimension-one bifurcation responsible for annihilation (or generation) of a sliding region or, in the less interesting case, a crossing region. In this bifurcation occurs the collapse of both T-singularities in a single point, giving rise to the *1-degenerate T-singularity*. Moreover, such systems exhibit the TS-bifurcation and also a non regular case of this bifurcation, involving the simultaneous collision between the two T-singularities and a real pseudo-equilibrium point, such that the pseudo-equilibrium persist but the pair of T-singularities disappears after the collision. Named *double TS-bifurcation*, this is a codimension-two bifurcation and also is associated with the birth of a CLC, but here it arises from the 1-degenerate T-singularity. In the double TS-bifurcation, the bifurcation point is the 1-degenerate T-singularity with vector fields anticolinear at this point.

As consequence of our study, some classical bifurcations (saddle-node, transcritical and pitchfork) are observed in the sliding vector field. Some of these bifurcations of the sliding vector field are associated with the birth of a CLC. We describe the stability and some global bifurcations (saddle-node of limit cycles and a non-standard homoclinic) of CLCs, from the analysis of the first return map. Moreover, under certain conditions, we are able to establish an upper bound of the number of CLCs that can coexist. We have also identified the presence of invariant (non-smooth) cones with vertex in one of the regular T-singularities, which bifurcate from an invariant (non-smooth) ellipsoid with vertices at the two regular T-singularities.

TS-bifurcation is little known in the literature, see [26, 29] and Chapter 4. While that the fold bifurcation of T-singularities and the double TS-bifurcation are unknown in the literature, as far as we know, the given names for each are just our suggestions. In this Chapter, we

have described the unfolding dynamics of the double TS-bifurcation and also of the fold bifurcation de T-singularities, characterizing and classifying the different scenarios involving each one. These are the main results of this Chapter.

This chapter is organized in the following way. In Section 6.2 we establish the problem and present a local canonical form, which describes the desired dynamic behaviour. The dynamics of sliding and crossing around the T-singularities, regular or degenerate, is investigated in the Section 6.3, as well as bifurcations involving such singularities. In Section 6.4 is performed a two-parameter analysis of bifurcations in the sliding vector field associated with the canonical form. The results of sliding bifurcations obtained in this section are applied to an example in Section 6.5. Also in Section 6.5, it is described the birth of limit cycles around the T-singularities, upper bound, local dynamics and bifurcations. Finally in Section 6.6 we present a brief conclusion and some remarks.

Previous results on Filippov theory in Chapter 2 are important for the development that follows.

6.2 Derivation of a canonical form

Let us consider a generic 3D-DPWS systems expressed by

$$\dot{\mathbf{x}} = \begin{cases} \mathbf{F}^-(\mathbf{x}), & \text{if } \mathbf{x} \in R^- \\ \mathbf{F}^+(\mathbf{x}), & \text{if } \mathbf{x} \in R^+, \end{cases} \tag{6.1}$$

such that the $\mathbb{R}^3$-space is divided into two open regions: $R^- = \{\mathbf{x} \in \mathbb{R}^3 : \ h(\mathbf{x}) < 0\}$ and $R^+ = \{\mathbf{x} \in \mathbb{R}^3 : \ h(\mathbf{x}) > 0\}$; separated by a switching boundary defined by $\Sigma = \{\mathbf{x} \in \mathbb{R}^3 : \ h(\mathbf{x}) = z = 0\}$, where $\mathbf{x} = (x, y, z)$. We assume that the components of the two vector fields $\mathbf{F}^{\pm} : \mathbb{R}^3 \to \mathbb{R}^3$ are smooth functions denoted by $f_i^{\pm} : \mathbb{R}^3 \to \mathbb{R}$, for $i = 1, 2, 3$.

Remark 6.1. *The contact type of the vector fields* $\mathbf{F}^{\pm}$ *with* Σ *are provided by the directional Lie derivatives:* $L_{\mathbf{F}^{\pm}}h = \langle \nabla h, \mathbf{F}^{\pm} \rangle$*, where* $\nabla h = (0,0,1)$ *(gradient of smooth function* h*) and* $\langle .,. \rangle$ *denote the canonical inner product. The higher order Lie derivatives are given by* $L^n_{\mathbf{F}^{\pm}}h = \langle \nabla L^n_{\mathbf{F}^{\pm}}h, \mathbf{F}^{\pm} \rangle$ *for* $n = 2, 3, ...$ *So we get*

$$L_{\mathbf{F}^{\pm}}h = f_3^{\pm},$$
$$L^2_{\mathbf{F}^{\pm}}h = f_1^{\pm}\frac{\partial f_3^{\pm}}{\partial x} + f_2^{\pm}\frac{\partial f_3^{\pm}}{\partial y} + f_3^{\pm}\frac{\partial f_3^{\pm}}{\partial z},$$

which will be necessary for the course of this Chapter.

6.2.1 The unfolding of 1-degenerate two-fold systems

Generally there are two curves in $\mathbb{R}^3$-space where orbits of (6.1) are tangent to Σ, one for each involved vector field. We assume that the system (6.1) displays such tangency curves, which we denote by $T_{\pm}$. In this work, we are interested in systems whose tangency curves $T_{\pm}$ have a quadratic contact (non-transversal intersection) at a point of Σ, which we denote by $\widehat{\mathbf{x}}$, for a critical value of a parameter, let's say μ. In addition, for a small perturbation on μ, from its critical value $\mu = \mu_c$, $T_{\pm}$ are displaced passing to have two points of transversal intersection or no contact, like a fold bifurcation. Figure 6.1 illustrates this scenario in the Σ-plane. Moreover, we will analyze only the cases involving tangential singularities of the invisible fold type.

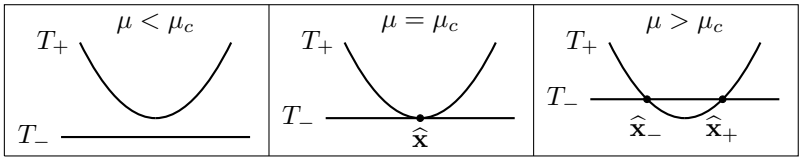

Figure 6.1: Fold bifurcation of double tangency points on Σ.

Note that the tangency conditions $L_{\mathbf{F}^{\pm}}h(x,y,0) = 0$ leads us to $f_3^{\pm}(x,y,0) = 0$. In this case, we assume that both the graphs of the implicit equations $f_3^{\pm}(x,y,0) = 0$ are smooth curves in the (x,y)-plane, and that both (or at least one) equations are dependent on one parameter, denoted by μ, and then we define

$$\widetilde{f}_{\mu}^{\pm}(x,y) = f_3^{\pm}(x,y,0).$$

The tangency points sets $T_{\pm}$ are, consequently, dependent on μ and determined by

$$T_{-}(\mu) = \{(x,y,z) \in \Sigma : \ \widetilde{f}_{\mu}^{-}(x,y) = 0\},$$
$$T_{+}(\mu) = \{(x,y,z) \in \Sigma : \ \widetilde{f}_{\mu}^{+}(x,y) = 0\}.$$

Then we established our hypothesis with respect to (6.1).

(H1) There is a point $(x,y,\mu) = (\widehat{x},\widehat{y},\mu_c)$, in the $(x,y,\mu)-$space, where is fulfilled $\frac{\partial \widetilde{f}_{\mu}^{\pm}(x,y)}{\partial (x,y)} \neq (0,0)$, $\frac{\partial \widetilde{f}_{\mu}^{+}(x,y)}{\partial \mu} \neq 0$ and/or $\frac{\partial \widetilde{f}_{\mu}^{-}(x,y)}{\partial \mu} \neq 0$. In addition, the equations

$$\widetilde{f}_{\mu}^{+}(x,y) = 0, \tag{6.2}$$
$$\widetilde{f}_{\mu}^{-}(x,y) = 0, \tag{6.3}$$
$$\frac{\partial \widetilde{f}_{\mu}^{+}}{\partial x}\frac{\partial \widetilde{f}_{\mu}^{-}}{\partial y}(x,y) - \frac{\partial \widetilde{f}_{\mu}^{+}}{\partial y}\frac{\partial \widetilde{f}_{\mu}^{-}}{\partial x}(x,y) = 0, \tag{6.4}$$

are satisfied at $(x,y,\mu) = (\widehat{x},\widehat{y},\mu_c)$ and $\mathrm{Det}\,[Q] \neq 0$ (determinant of Q), where Q is matrix Jacobian of the equations system (6.2)-(6.4). We assume, without loss of generality, that $(\widehat{x},\widehat{y},\mu_c) = (0,0,0)$.

The hypothesis **(H1)** ensures that for $\mu = 0$ occurs at the origin $(0,0)$ a non-transverse intersection between the tangency lines $T_{\pm}$, which are smooth curves at $(0,0)$. Moreover, the constraint $Det\,[Q] \neq 0$ ensures a single solution of the equations system (6.2)-(6.4) in the neighborhood of the origin of (x,y,μ)-space, and so the graphs of $\widetilde{f}_0^{+}(x,y) = 0$ are tangents with quadratic contact at $(x,y) = (0,0)$.

Then, T_+ and T_- are tangents with quadratic contact at $\mathbf{0}$ whenever $\mu = 0$ and system (6.1) has at $\mathbf{0}$ a 1-degenerate double tangency point. See Figure 6.2.

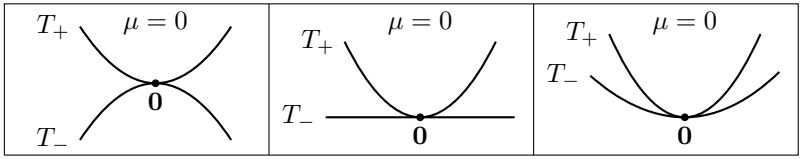

Figure 6.2: Illustrations of a 1-degenerate double tangency point at $\mathbf{0}$.

From here, we rewrite system (6.1) in a canonical form according to the following theorem.

Theorem 6.1. *Under hypothesis* ***(H1)*** *it is possible to write any system as* (6.1) *in the form*

$$(\dot{x}, \dot{y}, \dot{z}) = \begin{cases} \mathbf{F}_\mu^-(x, y, z), & \text{if } z < 0 \\ \mathbf{F}_\mu^+(x, y, z), & \text{if } z > 0, \end{cases} \tag{6.5}$$

with vector fields defined by

$$\mathbf{F}_\mu^-(\mathbf{x}) = \begin{bmatrix} c^- + p_\mu^-(\mathbf{x}) \\ b^- + q_\mu^-(\mathbf{x}) \\ \mu - y + e^- x^2 + r_\mu^-(\mathbf{x}) \end{bmatrix} \tag{6.6}$$

and

$$\mathbf{F}_\mu^+(\mathbf{x}) = \begin{bmatrix} c^+ + p_\mu^+(\mathbf{x}) \\ b^+ + q_\mu^+(\mathbf{x}) \\ \varepsilon\left(a\mu - y + e^+ x^2 + r_\mu^+(\mathbf{x})\right) \end{bmatrix}, \tag{6.7}$$

where $\varepsilon \neq 0$, $a \neq 1$, $e^+ \neq e^-$ *and* $p_\mu^\pm$, $q_\mu^\pm$ *and* $r_\mu^\pm$ *are polynomial functions of* (x, y, z) *and* μ*-parameter, such that* $p_0^\pm(\mathbf{0}) = q_0^\pm(\mathbf{0}) = r_\mu^\pm(\mathbf{0}) = 0$ *and* $\frac{\partial r_\mu^\pm}{\partial x} = \frac{\partial r_\mu^\pm}{\partial y} = \frac{\partial^2 r_\mu^\pm}{\partial x^2} = 0$ *for* $\mu = 0$ *and* $(x, y, z) = (0, 0, 0)$.

Proof. See Appendix 6.7. □

System (6.5)-(6.7) has at the origin of its state space a degenerate double tangency point, whenever $\mu = 0$. If $b^{\pm} \neq 0$ this double tangency point is classified as a singularity of the 1-degenerate two-fold type (or Q2-Singularity, see [118]). In addition, we can say that this system belongs to the family of 1-degenerate two-fold systems for $\mu = 0$ and to the its unfolding for $\mu \neq 0$.

We fix $\mu = 0$. Applying now the implicit function theorem to the equations

$$\begin{aligned} -y + e^{-}x^2 + r_0^{-}(x, y, 0) = 0, \\ -y + e^{+}x^2 + r_0^{+}(x, y, 0) = 0, \end{aligned}$$

we can parametrize the tangency lines in a neighborhood of $\mathbf{0}$, getting

$$\begin{aligned} T_{-}(0) = \left\{(x, y, z) \in \Sigma : \ y = e^{-}x^2 + \mathcal{O}(3)\right\}, \\ T_{+}(0) = \left\{(x, y, z) \in \Sigma : \ y = e^{+}x^2 + \mathcal{O}(3)\right\}. \end{aligned}$$

We observed three different cases with respect to the concavity of the tangency lines $T_{\pm}$ at the point of non-transverse intersection between them, as illustrated in Figure 6.2. Both cases are equivalent, so let's look only at the one where the tangency curves have opposite concavities at $\mathbf{0}$, that is, the cases where $e^{+}e^{-} < 0$.

We now look at the sliding and crossing regions on Σ, keeping $\mu = 0$. Figure 6.3 shows the four possible topological configurations on Σ according to the coefficients ε and $e^{\pm}$. Since the cases in Figures 6.3(b) and 6.3(d) have only one type of crossing region, they do not present first return map and are left for another works. The results for the case in Figure 6.3(c) can be obtained directly from the case in Figure 6.3(a) (or vice-versa), just take the time with opposite signal.

Figure 6.3(a) presents a configuration on the switching boundary Σ in a critical state. From this, the displacement of the tangency lines $T_{\pm}$ destroys the 1-degenerate two-fold point and a pair of regular two-fold points may arise, making possible the formation of the attractive

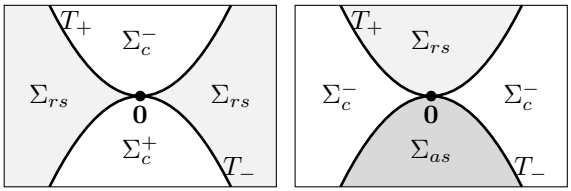

(a) $\varepsilon > 0$, $e^+ > 0$, $e^- < 0$ (b) $\varepsilon < 0$, $e^+ > 0$, $e^- < 0$

(c) $\varepsilon > 0$, $e^+ < 0$, $e^- > 0$ (d) $\varepsilon < 0$, $e^+ < 0$, $e^- > 0$

Figure 6.3: Possible configurations on Σ for 1-degenerate two-fold systems.

sliding region Σ_{as}. Figure 6.4 illustrates such scenario from the variation of the parameter μ, responsible for the displacement of $T_\pm$, being this the case of our interest in this Chapter. Here, we are considering $\varepsilon > 0$, $e^+ > 0$, $e^- < 0$ and $a < 0$, thus $\mathbf{0} \in \Sigma_{as}$ for $\mu > 0$ and $\mathbf{0} \in \Sigma_{rs}$ for $\mu < 0$, since $L_{\mathbf{F}_\mu^-} h(\mathbf{0}) = \mu$ and $L_{\mathbf{F}_\mu^+} h(\mathbf{0}) = \varepsilon a \mu$.

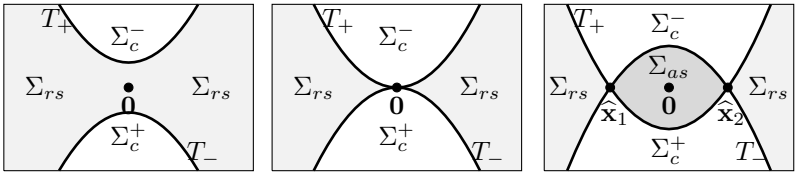

(a) $\mu < 0$ (b) $\mu = 0$ (c) $\mu > 0$

Figure 6.4: Attractive sliding region annihilation (generation).

Following with our analysis, we still want that the tangencies at the origin of (6.5)-(6.7), for $\mu = 0$, to be of the invisible fold type.

Then, we must have

$$L^2_{\mathbf{F}_0^+} h(\mathbf{0}) = -\varepsilon b^+ < 0,$$
$$L^2_{\mathbf{F}_0^-} h(\mathbf{0}) = -b^- > 0,$$

resulting in $\varepsilon b^+ > 0$ and $b^- < 0$. If we assume $\varepsilon > 0$, $b^+ > 0$ and $b^- < 0$, then $\mathbf{0}$ is a 1-degenerate T-singularity. In addition, we can say that there is a neighborhood of $\mathbf{0}$, for any $|\mu|$ small, where the tangency points at $T_\pm$ are of the invisible fold type. In this case, a pair of regular T-singularities arises for $\mu > 0$ (resp. $\mu < 0$), if $a < 1$ (resp. $a > 1$).

6.2.2 Regular and 1-degenerate T-singularities

In this subsection, we turn system (6.5)-(6.7) into a local canonical form of 1-degenerate two-fold systems and its unfolding, with invisible tangencies, according to the theorem below.

Theorem 6.2. *Consider the domain* $K = \{(x, y, z) \in \mathbb{R}^3 : x^2 + y^2 + z^2 < \delta\}$, *with* $\delta > 0$ *arbitrarily small. We assume* $e^+ > 0$, $e^- < 0$, $\varepsilon > 0$, $b^+ > 0$ *and* $b^- < 0$. *For any* $\mathbf{x} \in K$ *and* $|\mu|$ *small, system* (6.5)-(6.7) *can be rewritten as*

$$\dot{\mathbf{x}} = \begin{cases} \mathbf{F}_\mu^-(\mathbf{x}) & \text{if } z < 0 \\ \mathbf{F}_\mu^+(\mathbf{x}) & \text{if } z > 0 \end{cases}, \tag{6.8}$$

with the vector fields

$$\mathbf{F}_\mu^-(\mathbf{x}) = \begin{bmatrix} c_1 + p_1(\mathbf{x}) \\ -1 + q_1(\mathbf{x}) \\ \varepsilon_1 \left(\mu - y - x^2 + r_1(\mathbf{x})\right) \end{bmatrix} \tag{6.9}$$

and

$$\mathbf{F}_\mu^+(\mathbf{x}) = \begin{bmatrix} c_2 + p_2(\mathbf{x}) \\ 1 + q_2(\mathbf{x}) \\ \varepsilon_2 \left(-k\mu - y + kx^2 + r_2(\mathbf{x})\right) \end{bmatrix}, \tag{6.10}$$

acting on the switching boundary $\Sigma = \{\mathbf{x} \in K : h(\mathbf{x}) = z = 0\}$. *The functions* p_{12}, q_{12}, r_{12} *are polynomials of* (x, y, z), *such that* $p_{12}(\mathbf{0}) = q_{12}(\mathbf{0}) = r_{12}(\mathbf{0}) = 0$ *and* $\frac{\partial r_{12}(\mathbf{0})}{\partial x} = \frac{\partial^2 r_{12}(\mathbf{0})}{\partial x^2} = \frac{\partial r_{12}(\mathbf{0})}{\partial y} = 0$. *It is dependent on parameters:* $(c_1, c_2, \mu) \in \mathbb{R}^3$, $k > 0$, $\varepsilon_1 > 0$ *and* $\varepsilon_2 > 0$.

Proof. See Appendix 6.8. □

Proposition 6.1. *System* (6.8)-(6.10) *has a pair of T-singularities located at*

$$\widehat{\mathbf{x}}^{\pm}(\mu) = (\widehat{x}^{\pm}(\mu), \widehat{y}^{\pm}(\mu), 0), \tag{6.11}$$

such that

$$\widehat{x}^{\pm}(\mu) = \pm\sqrt{\mu} + \mathcal{O}(\mu), \tag{6.12}$$
$$\widehat{y}^{\pm}(\mu) = 0 + \mathcal{O}(\mu^{\frac{3}{2}}), \tag{6.13}$$

whenever $\mu \geq 0$.

Proof. All point $(x, y, 0)$ satisfying both equations

$$f_1(x, y) = \mu - y - x^2 + r_1(x, y, 0) = 0,$$
$$f_2(x, y) = -k\mu - y + kx^2 + r_2(x, y, 0) = 0,$$

it is a double tangency of (6.8)-(6.10). We rewrite the system above doing $f_1 - f_2 = 0$ and also $kf_1 + f_2 = 0$, getting

$$(1 + k)\mu = (1 + k)x^2 + (r_2 - r_1)(x, y, 0), \tag{6.14}$$
$$(1 + k)y = (kr_1 + r_2)(x, y, 0). \tag{6.15}$$

Since $k > 0$ and $r_{12}(\mathbf{0}) = \frac{\partial r_{12}(\mathbf{0})}{\partial x} = \frac{\partial^2 r_{12}(\mathbf{0})}{\partial x^2} = \frac{\partial r_{12}(\mathbf{0})}{\partial y} = 0$, then for any solution of (6.14)-(6.15) with $|x|$ small we can assure the expansions

$$\mu = x^2 + \mathcal{O}(x^3), \tag{6.16}$$
$$y = 0 + \mathcal{O}(x^3). \tag{6.17}$$

Note that there is real solution only for $\mu \geq 0$. It is easy to see that solutions of (6.16) that reach the origin when $\mu = 0$ are expressed by (6.12), for any $|\mu|$ small. Replacing (6.12) in (6.17) we obtain (6.13).

Double tangency points $\widehat{\mathbf{x}}^+(\mu)$ and $\widehat{\mathbf{x}}^-(\mu)$, defined for $\mu \geq 0$, are classified as T-singularities (invisible two-fold). This is expected because

$$L^2_{\mathbf{F}^-_\mu} h(x, y(x), 0) = \varepsilon_1 + s_1 x + \mathcal{O}(x^2) \approx \varepsilon_1 > 0,$$
$$L^2_{\mathbf{F}^+_\mu} h(x, y(x), 0) = -\varepsilon_2 + s_2 x + \mathcal{O}(x^2) \approx -\varepsilon_2 < 0,$$

where s_{12} are any real coefficients. So our proof is complete. □

Therefore, in system (6.8)-(6.10) there are two regular T-singularities for $\mu > 0$, with coordinates $\widehat{\mathbf{x}}^\pm(\mu)$ given in (6.12)-(6.13). For $\mu = 0$ both collide at the origin, that is, $\widehat{\mathbf{x}}^\pm(0) = (0, 0, 0)$. In this case, the origin of (6.8)-(6.10) is a 1-degenerate T-singularity.

6.2.3 Regions of sliding and crossing

The attractive/repulsive sliding regions and the crossing regions are denoted respectively by $\Sigma_{as}(\mu)$, $\Sigma_{rs}(\mu)$ and $\Sigma^\pm_c(\mu)$, both dependent as the parameter μ.

At point $(0, 0, 0)$ we have

$$L_{\mathbf{F}^-_\mu} h(0, 0, 0) = \varepsilon_1 \mu,$$
$$L_{\mathbf{F}^+_\mu} h(0, 0, 0) = -\varepsilon_2 k \mu,$$

therefore, $(0, 0, 0) \in \Sigma_{as}(\mu)$ for $\mu > 0$ and $(0, 0, 0) \in \Sigma_{rs}(\mu)$ for $\mu < 0$. This is an important result and from it we will explore the dynamics around the origin. First, we calculate the tangency lines T_- and T_+, in a neighborhood of the origin and for any $|\mu|$ small, namely

$$T_+(\mu) = \left\{(x, y, 0) \in K : y = k\left(-\mu + x^2\right) + \mathcal{O}(x^3)\right\}, \tag{6.18}$$

and

$$T_{-}(\mu) = \left\{(x, y, 0) \in K : y = \mu - x^2 + \mathcal{O}(x^3)\right\}. \tag{6.19}$$

After, to determine the regions of sliding and crossing on Σ, we disregard the terms of greater degree in the expansions of $T_{\pm}$.

So, the attractive sliding region can be represented as

$$\Sigma_{as}(\mu) = \left\{(x, y, 0) \in K : k\left(x^2 - \mu\right) < y < \mu - x^2\right\}, \tag{6.20}$$

defined only for $\mu > 0$ and such that $\mathbf{0} \in \Sigma_{as}(\mu)$. The repulsive sliding region is defined for any μ and is expressed as

$$\Sigma_{rs}(\mu) = \left\{(x, y, 0) \in K : -x^2 + \mu < y < k\left(-\mu + x^2\right)\right\}, \tag{6.21}$$

such that $\mathbf{0} \in \Sigma_{rs}(\mu)$ only for $\mu < 0$. If $\mu \geq 0$, then Σ_{rs} is defined in two sub regions on opposite sides of the y-axis. The crossing regions are defined for any μ and are given by

$$\Sigma_c^{+}(\mu) = \left\{(x, y, 0) \in K : y < k\left(x^2 - \mu\right) \text{ and } y < \mu - x^2\right\}, \tag{6.22}$$

$$\Sigma_c^{-}(\mu) = \left\{(x, y, 0) \in K : y > k\left(x^2 - \mu\right) \text{ and } y > \mu - x^2\right\}. \tag{6.23}$$

Origin is never a crossing point.

The two vector fields (6.9)-(6.10) calculated at the origin and for $\mu = 0$ turns out to be

$$\mathbf{F}_0^{-}(\mathbf{0}) = \begin{bmatrix} c_1 \\ -1 \\ 0 \end{bmatrix} \quad \text{and} \quad \mathbf{F}_0^{+}(\mathbf{0}) = \begin{bmatrix} c_2 \\ 1 \\ 0 \end{bmatrix}.$$

So that are anti-collinear whenever $c_2 = -c_1$. We can say then, that for $\mu = 0$ system (6.8)-(6.10) has a possible pseudo-equilibrium point at $\mathbf{0}$, along with a 1-degenerate T-singularity. Moreover, for $\mu \neq 0$ and $c_1 = -c_2$ such pseudo-equilibrium may remain at the origin or be moved to a nearby point, as we'll see in the Section 6.4.

6.3 Fold bifurcation of T-singularities

In this section we consider system (6.8)-(6.10) in a reduced form. Then we analyze the dynamics around the T-singularities points looking for bifurcations involving the collision between them, followed by the disappearance of the attractive sliding region (as illustrated in Figure 6.4). Our goal is to characterize the dynamics around a T-singularity, in the cases regular and 1-degenerate, from the analysis of bifurcations in the sliding vector field (sliding dynamics) and in the first return map (crossing dynamics).

For this, we assume in system (6.8)-(6.10) that $\varepsilon_{12} = k = 1$ and $p_{12}(\mathbf{x}) = q_{12}(\mathbf{x}) = r_{12}(\mathbf{x}) = 0$, and we redefine $c_1 = c_-$ and $c_2 = c_+$. The resulting system is

$$(\dot{x}, \dot{y}, \dot{z}) = \begin{cases} \mathbf{F}_\mu^-(x,y,z) = (c_-, -1, -y - x^2 + \mu), & \text{if } z < 0 \\ \mathbf{F}_\mu^+(x,y,z) = (c_+, 1, -y + x^2 - \mu), & \text{if } z > 0 \end{cases}, \quad (6.24)$$

where $\mathbf{x} = (x, y, z) \in \mathbb{R}^3$ is the state vector and $(c_+, c_-, \mu) \in \mathbb{R}^3$ is the vector of parameters.

6.3.1 Topological configuration on Σ

For the system (6.24) we have

$$L_{\mathbf{F}_\mu^-} h(x,y,0) = -y - x^2 + \mu,$$
$$L_{\mathbf{F}_\mu^+} h(x,y,0) = -y + x^2 - \mu.$$

There are two tangency lines on the Σ, whose graphs are parabolas defined by

$$T_-(\mu) = \{(x,y,z) \in \Sigma : \ y = -x^2 + \mu\}, \quad (6.25)$$
$$T_+(\mu) = \{(x,y,z) \in \Sigma : \ y = x^2 - \mu\}. \quad (6.26)$$

The tangency points $(x, y, 0) \in T_{\pm}$ are of the invisible fold type whenever the inequalities

$$L^2_{\mathbf{F}^-_\mu} h(x, y, 0) = 1 - 2c_- x > 0, \tag{6.27}$$

$$L^2_{\mathbf{F}^+_\mu} h(x, y, 0) = -1 + 2c_+ x < 0, \tag{6.28}$$

are fulfill.

The tangency sets $T_{\pm}$ intersect transversally at two points with coordinates

$$\widehat{\mathbf{x}}^{\pm}(\mu) = (\pm\sqrt{\mu}, 0, 0), \tag{6.29}$$

provided that $\mu > 0$. For $\mu = 0$ we have $\widehat{\mathbf{x}}^{+}(0) = \widehat{\mathbf{x}}^{-}(0) = (0, 0, 0)$, such that the contact between T_- and T_+ is quadratic (non-transverse) at the origin. And there is no contact for $\mu < 0$. In search of the T-singularities, we must ensure that inequalities (6.27)-(6.28) are fulfill at the points $\widehat{\mathbf{x}}^{\pm}(\mu)$ for $\mu \geq 0$. The trivial case occurs when $c_- = c_+ = 0$, since all point in $T_{\pm}$ is of the invisible fold type. In other cases we will assume $|\mu| < c$ depending on the positive value

$$c = \min\left\{\frac{1}{4c_-^2}, \frac{1}{4c_+^2}\right\}. \tag{6.30}$$

Thus the phase portrait of system (6.24) displays regular T-singularities at both points $\widehat{\mathbf{x}}^{\pm}(\mu)$ for $0 < \mu < c$ and 1-degenerate T-singularity at the origin $(0, 0, 0)$ for $\mu = 0$.

Note in Figure 6.4 that from the decreasing variation of the parameter μ through the critical value $\mu = 0$, occurs the collision between the two points $\widehat{\mathbf{x}}^{\pm}(\mu)$, followed by the disappearance of both, changing the sliding and crossing regions on the switching boundary Σ. We see the disappearance of the attractive sliding region (Σ_{as}) and the expansion of the repulsive sliding region (Σ_{rs}) that pass the contain the origin. The two crossing regions ($\Sigma^{\pm}_c$) persist for $\mu < 0$, but without transition points between them.

Defined only for $\mu > 0$, the attractive sliding region is given by

$$\Sigma_{as}(\mu) = \{(x, y, z) \in \Sigma : x^2 - \mu < y < -x^2 + \mu\}. \tag{6.31}$$

The region Σ_{as} contains the origin $(0, 0, 0)$ and is completely surrounded by tangential singularities of T_- in $y \geq 0$ and T_+ in $y \leq 0$. The points $\widehat{\mathbf{x}}^{\pm}$ are at the corners of Σ_{as}, so that they are the unique points of transition between the attractive and repulsive sliding regions. While the regions of repulsive sliding and crossing, given by

$$\Sigma_{rs}(\mu) = \{(x, y, z) \in \Sigma : -x^2 + \mu < y < x^2 - \mu\}, \tag{6.32}$$

and

$$\Sigma_c^+(\mu) = \{(x, y, z) \in \Sigma : y < -x^2 + \mu \text{ and } y < x^2 - \mu\}, \tag{6.33}$$
$$\Sigma_c^-(\mu) = \{(x, y, z) \in \Sigma : y > -x^2 + \mu \text{ and } y > x^2 - \mu\}, \tag{6.34}$$

respectively, are defined for all μ.

Following the literature of the area, as for example [26, 117, 118], we will analyze in next subsections (separately) the sliding and crossing dynamics, where the T-singularities are equivalent to the equilibria of sliding vector field and fixed points of first return map.

Remark 6.2. *In next subsections we assume in system* (6.24) *that* $c_\pm \neq 0$ *and* $|\mu| < c$ *with* c *given in* (6.30).

6.3.2 Sliding dynamics

It has been proven in [118] that the 1-degenerate T-singularity of systems as (6.24) is a saddle-node equilibrium of the sliding vector field and the center manifold is tangent to T_+ and to T_-. Here we also prove these facts. Moreover, we prove that the collision of two T-singularities produces in the sliding vector field an one-parameter bifurcation of saddle-node type.

The sliding vector field $\mathbf{F}_\mu^s$ associate to the system (6.24), calculated from the Filippov's method (see [51, 78]), is given by

$$\mathbf{F}_\mu^s(x,y,z) = \frac{1}{2(\mu - x^2)} \begin{bmatrix} (c_- + c_+)(\mu - x^2) + (c_- - c_+)y \\ -2y \\ 0 \end{bmatrix}.$$

Assuming $\mu > 0$, for all $(x,y,z) \in \Sigma_{as}(\mu)$ the inequality

$$2(\mu - x^2) = L_{\mathbf{F}_\mu^-} h(x,y,0) - L_{\mathbf{F}_\mu^+} h(x,y,0) > 0$$

is true.

The sliding dynamics is confined to plane $z = 0$, and so can be described by the planar sliding system

$$\frac{dx}{d\tau} = (c_- + c_+)(\mu - x^2) + (c_- - c_+)y, \tag{6.35}$$

$$\frac{dy}{d\tau} = -2y, \tag{6.36}$$

provided that $(x,y,0) \in \Sigma_{as}(\mu)$. According to [115], the sliding vector field can be smoothly extended to the boundary of Σ_{as}, and then we can expand the domain of (6.35)-(6.36) to its limits, $T_\pm$. To facilitate our analysis, it is appropriate to assume the system (6.35)-(6.36) defined throughout $\mathbb{R}^2$, remembering that for $(x,y,0) \in \Sigma_{rs}(\mu)$ we have the same vector field but with reversed time.

System (6.24) does not present pseudo-equilibria when we take $c_- \neq -c_+$, since the sliding vector field $\mathbf{F}_\mu^s$ has no equilibrium point for this parameter setting $c_\pm$. In addition, for $\mu > 0$ the sliding dynamics is governed only by the T-singularities $\widehat{\mathbf{x}}^\pm(\mu)$, whose reduced coordinates $(\pm\sqrt{\mu}, 0)$ are equilibria points of planar sliding system (6.35)-(6.36). These two equilibria points collide at the origin $(0,0)$ for $\mu = 0$ and then disappear of the phase portrait for $\mu < 0$.

Proposition 6.2. *Consider the planar sliding system* (6.35)-(6.36) *defined throughout* $\mathbb{R}^2$ *and with parameter* $c_\pm$ *fixed such that* $c_- \neq -c_+$.

Then, a Saddle-Node bifurcation occurs at the origin $(0,0)$ *when the parameter* μ *assumes the critical value* $\mu = 0$*. Moreover, the following statements hold.*

(i) *For* $\mu > 0$ *there are two hyperbolic equilibria points, of coordinates* $(\pm\sqrt{\mu}, 0)$*. Taking* $c_- < -c_+$ *(resp.* $c_- > -c_+$*), the point to the left (resp. right) of the origin is a stable node equilibrium and the point to the right (resp. left) is a saddle equilibrium.*

(ii) *For* $\mu = 0$ *the origin* $(0,0)$ *is the unique equilibrium, a non-hyperbolic of the saddle-node type.*

(iii) *For* $\mu < 0$ *there are no equilibria.*

Proof. The equilibria of system (6.35)-(6.36) must fulfill the equations

$$\begin{aligned}(c_- + c_+)(\mu - x^2) + (c_- - c_+)y = 0,\\ -2y = 0.\end{aligned}$$

It is easy to see that for $\mu > 0$ there are two equilibria, a with coordinates $(-\sqrt{\mu}, 0)$ (to the left of the origin) and another with coordinates $(\sqrt{\mu}, 0)$ (to the right of the origin). At critical value $\mu = 0$, both equilibria collide and the system now has a single equilibrium, at the origin $(0,0)$. And for $\mu < 0$ there are no equilibria, since $\mu - x^2 = 0$ has no real solution.

To evaluate the stability of the equilibria we consider the Jacobian matrix given by

$$J_{as}(\bar{x}(\mu), 0) = \begin{pmatrix} -2(c_- + c_+)\bar{x}(\mu) & c_- - c_+ \\ 0 & -2 \end{pmatrix},$$

where $\bar{x}(\mu)$ represents the $x-$coordinate of the equilibria, and whose eigenvalues are $\lambda_1 = -2 < 0$ and $\lambda_2(\bar{x}(\mu)) = -2(c_- + c_+)\bar{x}(\mu)$. Taking $c_- < -c_+$ and $\mu > 0$, for the equilibrium point to the left to the origin, i.e. with $\bar{x}(\mu) < 0$, we have $\lambda_2 < 0$ and therefore is a hyperbolic

stable node equilibrium. While the equilibrium point to the right, i.e. with $\bar{x}(\mu) > 0$, is a hyperbolic saddle equilibrium, since $\lambda_2 > 0$. Note that case $c_- > -c_+$ only reverses the sign of $\lambda_2(\bar{x}(\mu))$, and so, the node equilibrium is to the right of the origin and the saddle to the left. In the case $\mu = 0$ we have $\lambda_2(0) = 0$ and the origin $(0, 0)$ as a non-hyperbolic equilibrium point whose dynamic is a blend of saddle-node. So our proof is complete. □

In the Proposition 6.2 we assume (6.35)-(6.36) defined throughout $\mathbb{R}^2$ to simplify, since the attractive sliding dynamics is preserved. However, to extend the bifurcation results to the complete system (6.24) we must discard points in the crossing regions $\Sigma_c^{\pm}$ and change the sign of the time variable when in the repulsive sliding region Σ_{rs}. Then the Saddle-Node bifurcation proved in the Proposition 6.2 will involve only unstable equilibria when seen from the region Σ_{rs}.

Figure 6.5 illustrates the sliding dynamics on the switching boundary Σ of system (6.24), assuming $c_- < -c_+$ (fixed) and μ ranging from $\mu > 0$ to $\mu < 0$. This variation on the parameter μ destroys the attractive sliding region $\Sigma_{as}(\mu)$ along with the T-singularities points $\widehat{\mathbf{x}}^{\pm}(\mu)$. These phenomena create in the sliding vector field a Saddle-Node bifurcation that occurs at the 1-degenerate T-singularity located at $\widehat{\mathbf{x}}^{-}(0) = \widehat{\mathbf{x}}^{+}(0) = (0, 0, 0)$ for $\mu = 0$.

From the eigenvectors associated with the eigenvalues λ_1 and $\lambda_2^{\pm}$ of the planar sliding system (6.35)-(6.36), given by $\mathbf{v}_1 = (1, 0)$ and

$$\mathbf{v}_2^{\pm}(\mu) = \left(\frac{c_- - c_+}{\pm 2(c_- + c_+)\sqrt{\mu} - 2}, 1 \right),$$

respectively, we can observe that the eigenspaces generated by $\mathbf{v}_2^{-}(\mu)$ and $\mathbf{v}_2^{+}(\mu)$ extend through the crossing regions. In fact, since we are assuming $|\mu| < c$[1] and, then, $1/v_2^{\pm}(\mu) > 2\sqrt{\mu}$ and $1/v_2^{\pm}(\mu) < -2\sqrt{\mu}$, where $v_2^{\pm}$ denote the first coordinate of $\mathbf{v}_2^{\pm}$. While the eigenspace generated by $\mathbf{v}_1$, given by $S_1 = \{(x, y, z) \in \Sigma : y = 0\}$, is an invariant set

[1] With c given in (6.30)

being attractor for the part in Σ_{as} and repulsive in Σ_{rs}. Moreover, the center manifold for $\mu = 0$, defined by straight line S_1, is tangent to the parabolic lines $T_{\pm}(0)$ of tangency at the origin, since both curves have zero slope in it. See Figure 6.5.

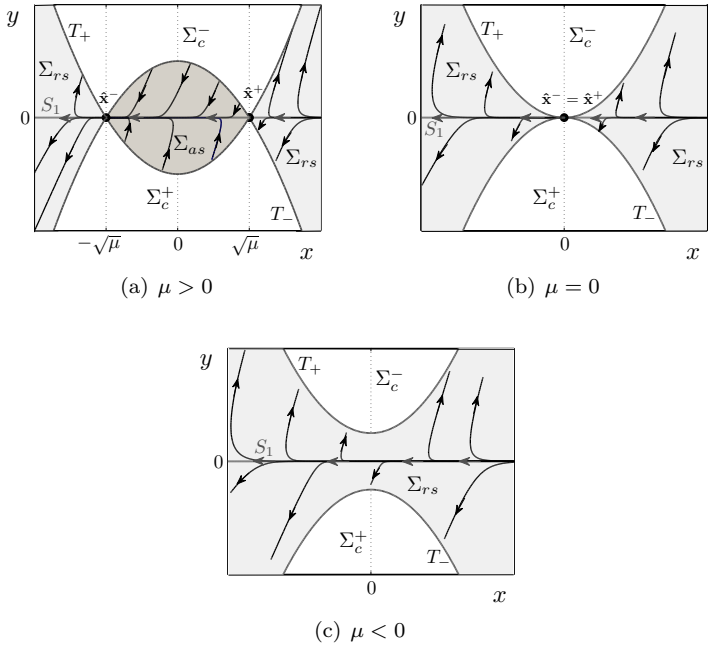

Figure 6.5: Saddle-Node sliding bifurcation in the system (6.24), assuming $c_- < -c_+$.

In the cases where $c_- = -c_+$, in the planar sliding system (6.35)-(6.36) there are infinite equilibria on the straight line $y = 0$. This situation is a critical point of stability exchange between the equilibria, since its eigenvalues are $\lambda_1 = -2 < 0$ and $\lambda_2^{\pm} = -2(c_- + c_+)(\pm\sqrt{\mu})$. So, for $c_- > -c_+$ the equilibrium point $(-\sqrt{\mu}, 0)$ is a saddle and $(\sqrt{\mu}, 0)$ is a stable node, and the opposite if $c_- < -c_+$ (see Proposition 6.2).

Based on the analysis performed so far, we can say that in 3D-Filippov systems with two T-singularities, the collision between them,

followed by the disappearance of the attractive sliding region and of the T-singularities themselves, creates a bifurcation of the type saddle-node in the sliding vector field. However this is only true when there are no pseudo-equilibria into the attractive sliding region, as in the case $c_- \neq -c_+$ here studied. In the Section 6.4 we will analyze what can happen in the sliding dynamics when there is a pseudo-equilibrium inside it.

6.3.3 Crossing dynamics and the first return map

In order to analyze the crossing dynamics of system (6.24), following [117] we use the associated first return map, which we know that T-singularities are fixed points on this map. For this, we consider an orbit of system (6.24) through the point $\mathbf{x}_0 \in \Sigma_c^+$ such that for $t = t_1 > 0$ the orbit transversally returns to Σ at the point $\mathbf{x}_1 \in \Sigma_c^-$. And its continuation through the point $\mathbf{x}_1 \in \Sigma_c^-$ such that for $t = t_2 > 0$ the orbit transversally returns to Σ at the point $\mathbf{x}_2 \in \Sigma_c^+$. The point $\mathbf{x}_1 = (x_1, y_1, 0)$ as a function of $\mathbf{x}_0 = (x_0, y_0, 0)$ is determined by the half-return map $(x_1, y_1) = P_+(x_0, y_0)$, and the point $\mathbf{x}_2 = (x_2, y_2, 0)$ as a function of $\mathbf{x}_1 = (x_1, y_1, 0)$ is determined by the half-return map $(x_2, y_2) = P_-(x_0, y_0)$. So, the first return map $(x_2, y_2) = P(x_0, y_0)$, which determines the point $\mathbf{x}_2$ as a function of $\mathbf{x}_0$, is obtained by $P_- \circ P_+$. See Figure 6.6.

The orbit-solution of system (6.24) for $z \geq 0$, with initial condition at the point $\mathbf{x}_0 = (x_0, y_0, 0) \in \Sigma_c^+$, is defined by flow Φ^+ of the vector field $\mathbf{F}^+$. Then, for all initial condition $\mathbf{x}_0$ we have

$$\Phi^+(t, \mathbf{x}_0) = \big(c_+ t + x_0, t + y_0, z^+(t, x_0, y_0)\big)$$

where

$$z^+(t, x_0, y_0) = \frac{1}{6} t \left[2c_+^2 t^2 + 3(2c_+ x_0 - 1)t + 6(x_0^2 - y_0 - \mu)\right].$$

To determine the return time of Φ^+ to the switching boundary Σ we

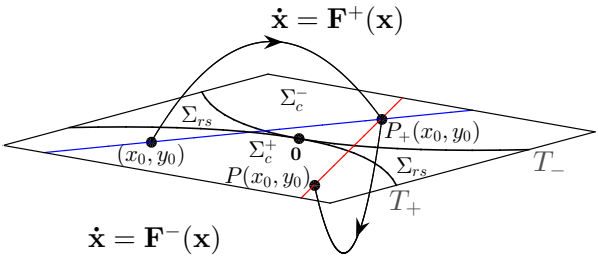

Figure 6.6: Determining the first return map.

solve the equation $z^+(t, x_0, y_0) = 0$ for $t \geq 0$. Denoted by t_1, the solution to the return equation is

$$t_1(x_0, y_0) = \frac{1/2 - c_+ x_0 - \sqrt{(1/2 - c_+ x_0)^2 - 4/3 c_+^2 (x_0^2 - y_0 - \mu)}}{2/3 c_+^2},$$

defined for all $(x_0, y_0) \in D_0 = \{(x, y) \in \mathbb{R}^2 : f(x) < y \leq x^2 - \mu\}$, where

$$f(x) = \frac{1}{16 c_+^2} \left(4 c_+^2 x^2 + 12 c_+ x - 3 - 16 c_+^2 \mu\right).$$

In this case, for $t = t_1(x_0, y_0)$ we have $\Phi^+(t_1, \mathbf{x}_0) = \mathbf{x}_1 = (x_1, y_1, 0)$ so that $(x_1, y_1) \in I_0 = \{(x, y) \in \mathbb{R}^2 : y \geq x^2 - \mu\}$.

The two-dimensional map $P_+ : D_0 \to I_0$ is give by

$$P_+(x_0, y_0) = (x_0 + c_+ t_1(x_0, y_0), y_0 + t_1(x_0, y_0)).$$

This map determines the points (x_1, y_1) of return of the orbits of system (6.24) to Σ, from the initial conditions (x_0, y_0), so that the equation

$$x_1 - c_+ y_1 = x_0 - c_+ y_0 \tag{6.37}$$

is satisfied. Furthermore, P_+ is dependent on the parameter μ, so that

for all (x_0, y_0, μ) in an neighbourhood of $(0, 0, 0)$ we can represent it by the expansions

$$\begin{aligned} x_1 &= x_0 - 2c_+ y_0 - 2c_+(\mu - x_0^2) + c_+ m(x_0, y_0, \mu) + \mathcal{O}(3), \\ y_1 &= -y_0 - 2(\mu - x_0^2) + m(x_0, y_0, \mu) + \mathcal{O}(3), \end{aligned}$$

where $m(x_0, y_0, \mu) = -\frac{4c_+}{3}(3x_0 - 2c_+(y_0 + \mu))(y_0 + \mu)$.

On the other hand, the orbit-solution of system (6.24) for $z \leq 0$, with initial condition at the point $\mathbf{x}_1 = (x_1, y_1, 0) \in \Sigma_c^-$, is defined by flow Φ^- of the vector field $\mathbf{F}^-$. Then, for all initial condition $\mathbf{x}_1$ we have

$$\Phi^-(t, \mathbf{x}_1) = \big(c_- t + x_1, -t + y_1, z^-(t, x_1, y_1)\big)$$

where

$$z^-(t, x_1, y_1) = -\frac{1}{6} t \left[2c_-^2 t^2 + 3(2c_- x_1 - 1)t + 6(x_1^2 + y_1 - \mu)\right].$$

To determine the return time of Φ^- to the Σ we solve the equation $z^-(t, x_1, y_1) = 0$ for $t \geq 0$. Denoted by t_2, the solution to the return equation is

$$t_2(x_1, y_1) = \frac{1/2 - c_- x_1 - \sqrt{(1/2 - c_- x_1)^2 - 4/3 c_-^2 (x_1^2 + y_1 - \mu)}}{2/3 c_-^2}, \tag{6.38}$$

defined for all $(x_1, y_1) \in D_1 = \{(x, y) \in \mathbb{R}^2 : -x^2 + \mu \leq y < g(x)\}$ with

$$g(x) = \frac{1}{16 c_-^2}\left(-4c_-^2 x^2 - 12 c_- x + 3 + 16 c_-^2 \mu\right).$$

In this case, for $t = t_2(x_1, y_1)$ we have $\Phi^-(t_2, \mathbf{x}_1) = \mathbf{x}_2 = (x_2, y_2, 0)$ so that $(x_2, y_2) \in I_1 = \{(x, y) \in \mathbb{R}^2 : y \leq -x^2 + \mu\}$.

The two-dimensional map $P_- : D_1 \to I_1$ is give by

$$P_-(x_1, y_1) = (x_1 + c_- t_2(x_1, y_1), y_1 - t_2(x_1, y_1)).$$

This map determines the points (x_2, y_2) of return of the orbits of system (6.24) to Σ, from the initial conditions (x_1, y_1), so that the equation

$$x_2 + c_- y_2 = x_1 + c_- y_1 \tag{6.39}$$

is satisfied. Furthermore, P_- is also dependent on the parameter μ, so that for all (x_1, y_1, μ) in an neighbourhood of $(0, 0, 0)$ we can represent it by the expansions

$$\begin{aligned} x_2 &= x_1 + 2c_- y_1 - 2c_-(\mu - x_1^2) - c_- n(x_1, y_1, \mu) + \mathcal{O}(3) \\ y_2 &= -y_1 + 2(\mu - x_1^2) + n(x_1, y_1, \mu) + \mathcal{O}(3) \end{aligned}$$

where

$$n(x_1, y_1, \mu) = -\frac{4c_-}{3}\left(3x_1 + 2c_-(y_1 - \mu)\right)(y_1 - \mu).$$

Both maps P_+ and P_- are involutions (see [116]) at T_+ and T_-, respectively, since $P_+(x_0, x_0^2 - \mu) = (x_0, x_0^2 - \mu)$, $P_-(x_1, -x_1^2 + \mu) = (x_1, -x_1^2 + \mu)$, $P_+^2(x_0, y_0) = (x_0, y_0)$, $P_-^2(x_1, y_1) = (x_1, y_1)$ and

$$\begin{aligned} \mathrm{Det}[DP_+(x_0, x_0^2 - \mu)] &= -1, \\ \mathrm{Det}[DP_-(x_1, -x_1^2 + \mu)] &= -1, \end{aligned}$$

where $DP_\pm$ denote the Jacobian matrices given by

$$DP_+(x_0, x_0^2 - \mu) = \begin{pmatrix} 1 + c_+\alpha(x_0) & -c_+(c_+\alpha(x_0) + 2) \\ \alpha(x_0) & -1 - c_+\alpha(x_0) \end{pmatrix}, \tag{6.40}$$

$$DP_-(x_1, -x_1^2 + \mu) = \begin{pmatrix} 1 + c_-\beta(x_1) & c_-(c_-\beta(x_1) + 2) \\ -\beta(x_1) & -1 - c_-\beta(x_1) \end{pmatrix}, \tag{6.41}$$

with $\alpha(x_0) = \frac{4x_0}{1 - 2c_+x_0}$ and $\beta(x_1) = \frac{4x_1}{1 - 2c_-x_1}$.

Based on the conditions stated above, we can ensure that there is an open set $D_{0c} \subset D_0$ in neighbourhood of (x_0, y_0) and $I_{0c} \subset I_0$ in neighbourhood of (x_1, y_1) such that $P_+(x_0, y_0) = (x_1, y_1) \in I_{0c}$ for all $(x_0, y_0) \in D_{0c}$. Analogously, we can ensure that there is an open set

$D_{1c} \subset D_1$ in neighbourhood of (x_1, y_1) and $I_{1c} \subset I_1$ in neighbourhood of (x_2, y_2) such that $P_-(x_1, y_1) = (x_2, y_2) \in I_{1c}$ for all $(x_1, y_1) \in D_{1c}$. In addition, we can establish $(x_0, y_0, 0) \in \Sigma_c^+$ and $(x_1, y_1, 0) \in \Sigma_c^-$, such that the points in D_{0c} and D_{1c} are crossing points. So, assuming $I_{0c} \subset D_{1c}$ we define the function that describes the first return map $P : (D_{0c}, \mathbf{p}^{\pm}) \to (I_{1c}, \mathbf{p}^{\pm})$ by composition $P = P_- \circ P_+$, where $\mathbf{p}^{\pm} = (\pm\sqrt{\mu}, 0)$. The explicit form for the first return map P is obtained by

$$P(x_0, y_0) = \begin{bmatrix} x_0 + c_+ t_1(x_0, y_0) + c_- t_2^0(x_0, y_0) \\ y_0 + t_1(x_0, y_0) - t_2^0(x_0, y_0) \end{bmatrix} \tag{6.42}$$

with $t_2^0 = t_2(P_+(x_0, y_0))$, which can be represented by the expansions

$$\begin{aligned} x_2 &= x_0 - 2(c_- + c_+)y_0 - 2(c_+ + 3c_-)(\mu - x_0^2) + \mathbf{r}_0^T H \mathbf{r}_0 + \mathcal{O}(3), \\ y_2 &= y_0 + 4(\mu - x_0^2) + \mathbf{r}_0^T G \mathbf{r}_0 + \mathcal{O}(3), \end{aligned} \tag{6.43}$$

for all (x_1, y_1, μ) in an neighbourhood of $(0, 0, 0)$, where $\mathbf{r}_0^T = \begin{bmatrix} x_0 & y_0 & \mu \end{bmatrix}$ and $H = (h_{ij})$ (resp. $G = (g_{ij})$), for $i = 1, 2, 3$, with $h_{1j} = g_{1j} = h_{23} = g_{23} = 0$ and

$$\begin{aligned} h_{21} &= -4(c_-^2 + 4c_- c_+ + c_+^2), \\ h_{22} &= \frac{8}{3}(c_-^3 + 3c_-^2 c_+ + 5c_- c_+^2 + c_+^3), \\ h_{31} &= -4(c_- + c_+)(3c_- + c_+), \\ h_{32} &= \frac{16}{3}(3c_-^3 + 6c_-^2 c_+ + 5c_- c_+^2 + c_+^3), \\ h_{33} &= \frac{8}{3}(3c_-^2 + 2c_- c_+ + c_+^2)(3c_- + c_+), \\ g_{21} &= 4(c_- + 3c_+), \\ g_{22} &= -\frac{8}{3}(c_-^2 + 3c_- c_+ + 4c_+^2), \\ g_{31} &= 12(c_- + c_+), \\ g_{32} &= -\frac{16}{3}(3c_-^2 + 6c_- c_+ + 4c_+^2), \end{aligned}$$

$$g_{33} = -\frac{8}{3}(9c_-^2 + 9c_-c_+ + 4c_+^2).$$

We consider the crossing dynamics of system (6.24) described by map P. The fixed points are displayed in the following proposition.

Proposition 6.3. *With respect to the fixed points of the first return map P, we have:*

i) *Assuming $c_- \neq -c_+$, for $\mu > 0$ there are two fixed points at $(-\sqrt{\mu}, 0)$ and $(\sqrt{\mu}, 0)$. In the critical case $c_- = -c_+$, for $\mu > 0$ there are infinite fixed points belonging to the ellipse defined by*

$$\Gamma = \{(x, y, z) \in \Sigma : 3x^2 + 4c_+^2 y^2 - 6c_+ xy - 3\mu = 0\}. \qquad (6.44)$$

ii) *For $\mu = 0$ there is a single fixed point at $(0, 0)$ and for $\mu < 0$ there are no fixed points, both cases for all $c_\pm$.*

Proof. The fixed points of map P must satisfy the equations $(x_0, y_0) = P(x_0, y_0)$, which can be reduced to

$$c_+ t_1(x_0, y_0) = -c_- t_2^0(x_0, y_0),$$
$$t_1(x_0, y_0) = t_2^0(x_0, y_0).$$

In this case we have two possibilities: (a) If $c_- \neq -c_+$ then the fixed points must satisfy the equations $t_1(x_0, y_0) = 0$ and $t_2^0(x_0, y_0) = 0$, that is, $y_0 = x_0^2 - \mu$ and $y_0 = -x_0^2 + \mu$, respectively. Therefore, there are two fixed points at $(-\sqrt{\mu}, 0)$ and $(\sqrt{\mu}, 0)$ for $\mu > 0$, a single fixed point at $(0, 0)$ for $\mu = 0$ and there are no fixed points for $\mu < 0$. (b) Now, if $c_- = -c_+$, then the fixed points must satisfy the equation $t_1(x_0, y_0) - t_2^0(x_0, y_0) = 0$, which can be reduced to equation in (6.44) provided that $\mu > 0$. Therefore the ellipse Γ determines on Σ an invariant set for the crossing dynamics. When μ assumes the critical value $\mu = 0$, this ellipse disappears and the origin becomes the only fixed point, since it is the only point to fulfill equation in (6.44). So our proof is complete. □

Remark 6.3. *The non-trivial fixed points* $(\pm\sqrt{\mu}, 0)$*, for* $\mu > 0$*, are equivalent to T-singularities of* (6.24) *with reduced coordinates, while for* $\mu = 0$ *the trivial fixed point is equivalent to 1-degenerate T-singularity with reduced coordinates. When* $c_- = -c_+$ *and* $\mu > 0$*, besides the fixed points equivalent to T-singularities, there are other infinite fixed points belonging to the set* Γ *which, except for points* $(\pm\sqrt{\mu}, 0)$*, is completely contained in the crossing regions for* $0 < \mu < \frac{3}{16c_+^2}$*.*

The stability of the non-trivial and trivial fixed points is proved in the following proposition. See Figure 6.9.

Proposition 6.4. *Assume* $c_- < -c_+$ *(resp.* $c_- > -c_+$*). With respect to the stability of the first return map* P*, we have:*

a) *For* $\mu > 0$ *the point fixed* $(-\sqrt{\mu}, 0)$ *is a saddle (resp. center) and* $(\sqrt{\mu}, 0)$ *is of center type (resp. saddle).*

b) *For* $\mu = 0$ *the origin is a parabolic fixed point originated by the collision between the two non-trivial fixed points of saddle and center types.*

Proof. We assume $c_- < -c_+$. Note that for the fixed points $(\pm\sqrt{\mu}, 0)$ and $(0, 0)$, we have $x_1 = x_0$ in the Jacobian matrices $DP_\pm$ given in (6.40)-(6.41). Then, the Jacobian matrix of the map P is defined by $DP(\hat{x}, 0) = DP_-(\hat{x}, 0) \cdot DP_+(\hat{x}, 0)$, applied at the point $(\hat{x}, 0)$, where $\hat{x}$ represents the x-coordinate of the fixed point. So, we get

$$DP(\hat{x}, 0) = \sigma(\hat{x}) \begin{pmatrix} 1 + 2\hat{x}(5c_- + c_+(1 + 2c_-\hat{x})) & -2(c_- + c_+(1 + 4c_-\hat{x})) \\ -8\hat{x}(1 + (c_- + c_+)\hat{x}) & 1 + 2\hat{x}(5c_+ + c_-(1 + 2c_+\hat{x})) \end{pmatrix}, \tag{6.45}$$

where $\sigma(\hat{x}) = \frac{1}{(1-2c_-\hat{x})(1-2c_+\hat{x})} > 0$, and then we calculate the corresponding determinant and trace, namely

$$\begin{aligned} \mathrm{Det}[DP(\hat{x}, 0)] &= 1, \\ \mathrm{Tr}[DP(\hat{x}, 0)] &= 2q(\hat{x}) = 2 + 16(c_- + c_+)\hat{x}\sigma(\hat{x}). \end{aligned}$$

In equation of trace, we have $q(0) = 1$, $0 < q(\sqrt{\mu}) < 1$ and $q(-\sqrt{\mu}) > 1$. Therefore, for $\mu > 0$ the non-trivial fixed point with $\hat{x} = -\sqrt{\mu} < 0$ is a saddle, since its eigenvalues are

$$\rho_{\pm}(\hat{x}) = q(\hat{x}) \pm \sqrt{q(\hat{x})^2 - 1}, \tag{6.46}$$

such that $\rho_{-}\rho_{+} = 1$, $0 < \rho_{-} < 1$ and $\rho_{+} > 1$. While the fixed point with $\hat{x} = \sqrt{\mu} > 0$ is of center type (elliptic), since its eigenvalues $\rho_{\pm}$ are complex conjugate such that $|\rho_{\pm}| = 1$. When the parameter μ assumes the critical value $\mu = 0$ both non-trivial fixed points, of the saddle and center types, collide at the origin. In this case the origin is the only fixed point of map P and its eigenvalues are $\rho_{\pm} = 1$. So, the trivial fixed point is parabolic, called 1:1 resonant. For the opposite assumption, $c_{-} > -c_{+}$, the exchange of stability occurs between the non-trivial fixed points. So our proof is complete. □

6.3.4 Invariant surfaces connected to T-singularity

Assuming $c_{-} = -c_{+}$ and $\mu = 0$ the map P has a single fixed point, located at the origin of its phase portrait, and Jacobian matrix with double eigenvalue 1. We take equations (6.37)-(6.39) and the straight line given by $\chi = \{(x, y, z) \in \Sigma : x = c_{+}y\}$, containing the trivial fixed point. Then, for all $(x_0, y_0, 0) \in \chi$ we have also $(x_1, y_1, 0) \in \chi$ and $(x_2, y_2, 0) \in \chi$. In this case, any trajectory of the system (6.24) started at the point $(x_0, y_0, 0) \in \chi$, crosses the switching boundary Σ a finite number of times circulating the origin, always at points belonging to the χ, until the point $(x_2, y_2, 0) \in \chi$ leaves the domain of P and so the trajectory not crosses the Σ anymore. On the straight line χ we can ensure, from the equation (6.43), that $y_2 - y_0 = -4c_{+}^2 y_0^2/3 + \mathcal{O}(3) < 0$ (remember that $y_0, y_2 < 0$) and, thus, any trajectory started at the point $(x, y, 0) \in \chi$ near the origin, moves away from the origin. See Figure 6.7.

In addition, for initial conditions outside χ, the evolution of the

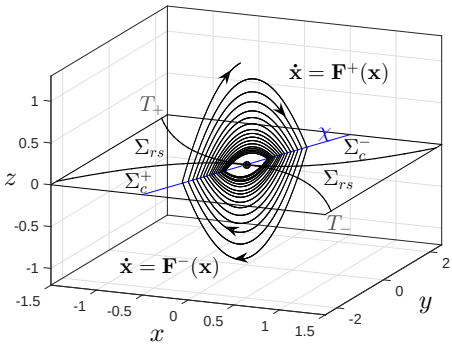

Figure 6.7: Phase portrait of system (6.24) for an initial condition at χ, with parameters $\mu = 0$ and $c_- = -c_+ = 1/4$.

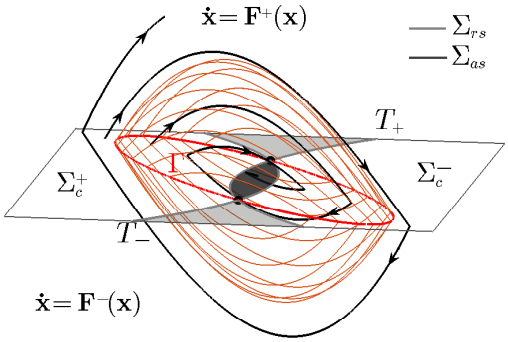

Figure 6.8: Invariant (non-smooth) ellipsoid present in the system (6.24) for $\mu > 0$ and $c_- = -c_+$.

map P occurs on parallel lines to χ. So, an trajectory of (6.24) through of any parallel line to χ that crosses the repulsive sliding region Σ_{rs}, spirals around the Σ_{rs} moving away from it.

Continuing with $c_- = -c_+$, for a small positive perturbation on the parameter μ from the critical value $\mu = 0$, the trivial fixed point bifurcates and gives rise to infinite fixed points belonging to the set Γ

given in (6.44). So, in addition to the fixed points $(\pm\sqrt{\mu}, 0) \in (T_- \cap T_+)$, there are other infinite fixed points belonging to crossing region Σ_c^+. A fixed point in the region Σ_c^+ implies the existence of its corresponding in the region Σ_c^-, and so there is a limit cycle that transversely crosses Σ at these two points. Crossing limit cycles in 3D-Filippov systems with an unique T-singularity have been recently studied in the works [26, 63].

In the case shown in Figure 6.8, the phase portrait of system (6.24) displays infinity CLCs through the Γ, with nonlinear center dynamics. These centers create an ellipsoid in the state space of the system (6.24), such that its interior determines the basin of attraction for Σ_{as}, and its surface is invariant to the flow of (6.24). The presence of attractive sliding region Σ_{as} inside and repulsive sliding region Σ_{rs} outside the ellipsoid, makes it unstable, as shown in Figures 6.8.

Now, taking fixed $c_\pm$ such that $c_- \neq c_+$, for a small positive perturbation on the parameter μ from the critical value $\mu = 0$, the trivial fixed point bifurcates and gives rise to two non-trivial fixed points, $(-\sqrt{\mu}, 0)$ and $(\sqrt{\mu}, 0)$, one is saddle and the other center (see Figure 6.9). The Jacobian matrix calculated at the fixed points, given in (6.45), has the eigenvalues $\rho_\pm(\hat{x})$ given in (6.46) and the eigenvectors $\mathbf{u}_\pm(\hat{x}) = (u_\pm(\hat{x}), 1)$, where

$$u_\pm(\hat{x}) = \frac{(c_+ - c_-)\hat{x} \pm \sqrt{(c_+ + c_-)(1 + 2c_-\hat{x})(1 + 2c_+\hat{x})\hat{x}}}{2\hat{x}(1 + (c_- + c_+)\hat{x})} \qquad (6.47)$$

and $\hat{x} = \hat{x}(\mu) \neq 0$ represents the x-coordinate for each fixed point. Note in the denominator of (6.47) that $1 + (c_- + c_+)\hat{x} > 0$, because we are assuming $0 < \mu < c$ (see Remark 6.2) which lead us to

$$\hat{x}(\mu) = \sqrt{\mu} < \sqrt{c} = \frac{1}{2|c_-|} < \frac{1}{|c_-| + |c_+|} \leq \frac{1}{|c_- + c_+|}, \qquad \text{for } c_- < -c_+,$$

$$\hat{x}(\mu) = -\sqrt{\mu} > -\sqrt{c} = \frac{-1}{2|c_-|} > \frac{-1}{|c_-| + |c_+|} \geq \frac{-1}{|c_- + c_+|}, \quad \text{for } c_- > -c_+,$$

provided that $|c_-| > |c_+|$ (if $|c_-| < |c_+|$ we must use $\sqrt{c} = \frac{1}{2|c_+|}$ in

the above expressions). From (6.47) it is possible to prove that the eigenvectors of the fixed point saddle are in the region of crossing Σ_c^+, just check that $u(\hat{x})^2 < \frac{1}{4\hat{x}^2}$ for all $0 < \mu < c$. In this case, one of the eigenvectors leaves the crossing region when the double tangential singularity is no longer of the invisible two-fold type.

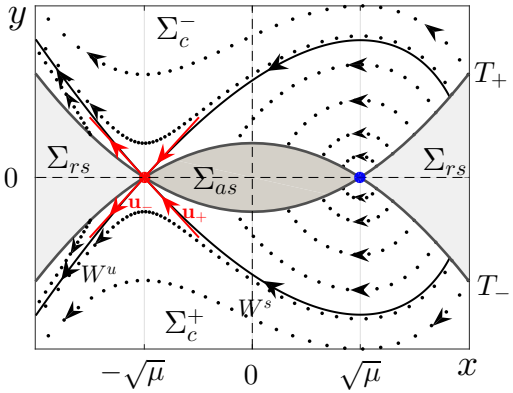

Figure 6.9: Crossing dynamics for $\mu > 0$, assuming $c_- < -c_+$.

Figure 6.9 illustrates the crossing dynamics described by first return map P, calculated from (6.42), presenting two fixed points for $\mu > 0$, one saddle and the other center. It is important to note the map P is defined only in the crossing region Σ_c^+. In order to get the crossing dynamics in Σ_c^- we must calculate the inverse map $P^{-1} = P_+ \circ P_-$. Both maps have same fixed points and with same stability, however, the stable (W^s) and unstable (W^u) invariant manifolds have their stability exchanged. In other words, the branch for the unstable manifold in region Σ_c^+, defines the stable manifold in region Σ_c^-, see [63, 68, 71].

For a neighborhood around the fixed point saddle, the map P_+ (resp. P_-) takes the branch of W^u from region Σ_c^+ (resp. Σ_c^-) to the branch of W^u in the region Σ_c^- (resp. Σ_c^+). Such connections between the branches of W^u in Σ_c^+ and Σ_c^-, produce an invariant cone with vertex at the T-singularity, which contains Σ_{rs} in its interior. While,

the connections between the branches of W^s in Σ_c^+ and Σ_c^-, produce an invariant cone containing Σ_{as} in its interior (see Figure 6.10). The existence and stability of this non-smooth cones is proved in [71], where we find that the cone surrounding the sliding region Σ_{as} is unstable while the other surrounding Σ_{rs} is stable, both asymptotically.

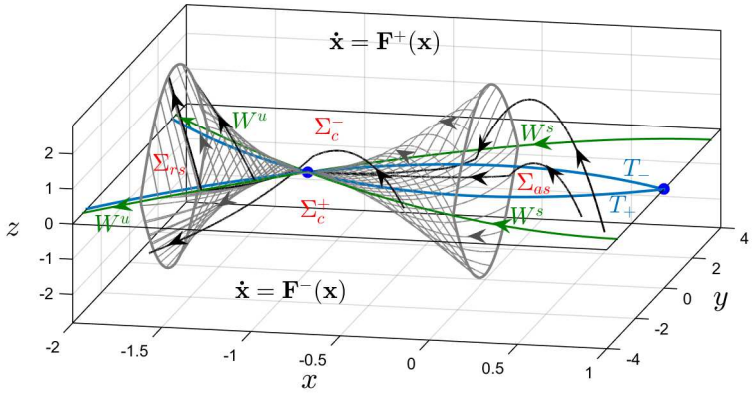

Figure 6.10: Invariant (non-smooth) cones present in the system (6.24) for $\mu = 1 > 0$ and $c_- = c_+ = -1/4$ ($c_- \neq -c_+$).

In the system (6.24) one of the two regular T-singularities is always related to the fixed point saddle for all $c_- \neq -c_+$ and $\mu > 0$. Therefore both stable and unstable cones persist for all $c_- \neq -c_+$, so that the point of connection between them exchange of T-singularity following the fixed point saddle from the exchange of the signal of $c_- + c_+$. In addition, when $c_- = -c_+$ and $\mu > 0$ the vector fields $\mathbf{F}_\mu^+$ and $\mathbf{F}_\mu^-$ are anti-collinear at the regular T-singularities, since

$$\mathbf{F}_\mu^+(\pm\sqrt{\mu}, 0, 0) = -\mathbf{F}_\mu^-(\pm\sqrt{\mu}, 0, 0) = (c_+, 1, -\mu),$$

so that a bifurcation occurs and the unstable and stable invariant cones (hyperbolic) give way to the unstable invariant ellipsoid (non-hyperbolic) connecting the two T-singularities.

We have seen in this section that the system (6.24) does not present isolated pseudo-equilibrium point in the sliding regions and also fixed point in the crossing regions. In this case, both sliding and crossing dynamics are governed only by T-singularities when they exist, such points being the equilibria of the planar sliding system and also of the first return map. If in system (6.24) we added terms of higher degree in the components of the vector fields $\mathbf{F}_\mu^\pm$, we can find pseudo-equilibrium points in the sliding regions and fixed points in the crossing regions. Such facts will be discussed in the following sections.

6.4 Two-parameter sliding bifurcations

Let us now see the bifurcations in the sliding vector field associated with the canonical form given in (6.8)-(6.10).

6.4.1 Equilibria of the sliding vector field

The dynamic behaviour of the system (6.8) at $z = 0$ is described by a sliding vector field, namely

$$\mathbf{F}^s(x,y,0) = \frac{1}{L(x,y)} \begin{bmatrix} \left(f_3^- f_1^+ - f_3^+ f_1^-\right)(x,y) \\ \left(f_3^- f_2^+ - f_3^+ f_2^-\right)(x,y) \\ 0 \end{bmatrix},$$

where $f_1^-(x,y) = c_1 + p_1(x,y,0)$, $f_1^+(x,y) = c_2 + p_2(x,y,0)$, $f_2^-(x,y) = -1 + q_1(x,y,0)$, $f_2^+(x,y) = 1 + q_2(x,y,0)$,

$$f_3^-(x,y) = \varepsilon_1\left(\mu - y - x^2 + r_1(x,y,0)\right),$$

$$f_3^+(x,y) = \varepsilon_2\left(-k\mu - y + kx^2 + r_2(x,y,0)\right),$$

and $L(x,y) = \left(f_3^- - f_3^+\right)(x,y) = (\varepsilon_1 + k\varepsilon_2)\mu - (1+k)x^2 + \varepsilon_1 r_1(x,y,0) - \varepsilon_2 r_2(x,y,0)$. As $f_3^-(x,y) = L^-_{\mathbf{F}_\mu} h(x,y,0)$ and $f_3^+(x,y) = L^+_{\mathbf{F}_\mu} h(x,y,0)$,

then we have $L(x,y) < 0$ for all $(x,y,0) \in \Sigma_{rs}$, $L(x,y) > 0$ for all $(x,y,0) \in \Sigma_{as}$ and $L(x,y) = 0$ only for $(x,y,0) \in T_+ \cap T_-$[2].

Following the standard analysis we take the first two components of $\mathbf{F}^s$ multiplied by singularity $L(x,y) > 0$ and write a two-dimensional system given by

$$\frac{dx}{d\tau} = \left(f_3^- f_1^+ - f_3^+ f_1^-\right)(x,y), \tag{6.48}$$

$$\frac{dy}{d\tau} = \left(f_3^- f_2^+ - f_3^+ f_2^-\right)(x,y), \tag{6.49}$$

where $d\tau = \frac{1}{L(x,y)}dt$, which has the same phase portrait that $\mathbf{F}^s$ in Σ_{as}. To simplify, let us consider the system (6.48)-(6.49) defined in the whole $\mathbb{R}^2$, looking for the possible equilibria bifurcations near the origin. We recall that for the repulsive sliding dynamics (in Σ_{rs}) we must take the equations (6.48)-(6.49) with reversed time.

It is important to remember that for $\mu > 0$ there are two points of double tangency in the system (6.8), and these points, with reduced coordinates, are equilibria of planar sliding system (6.48)-(6.49), because $f_3^-(x,y) = f_3^+(x,y) = 0$. We denote such equilibrium points by $\widehat{\mathbf{p}}^{\pm}$, so that $\widehat{\mathbf{p}}^{\pm}(\mu) = (\widehat{x}^{\pm}(\mu), \widehat{y}^{\pm}(\mu))$. For any $\mu \geq 0$ and small, coordinates of $\widehat{\mathbf{p}}^{\pm}$ in (x,y)-plane can be expressed by (6.12)-(6.13), as calculated in the previous subsection (see Proposition 6.1). Then, for $\mu = 0$ there are two equilibria colliding at the point $(0,0)$.

Remark 6.4. *We define here a new parameter,*

$$\nu = c_2 + c_1, \tag{6.50}$$

where c_1 is considered fixed and c_2 is a parameter that can be disturbed in system (6.8)*, as well as μ.*

We will show below the necessary and sufficient conditions to have a third equilibrium at $(0,0)$ such that for a small disturbance in

[2]The others possible zeros of the L function are located in crossing regions, not being important in this moment for the sliding dynamics.

vector of parameters (ν, μ), from the critical value $(\nu, \mu) = (0, 0)$, this equilibrium is moved (smoothly) from the origin to some point near of the origin.

We denoted by $(\widetilde{x}(\nu, \mu), \widetilde{y}(\nu, \mu))$ the equilibria manifold, which fulfills $(\widetilde{x}(0, 0), \widetilde{y}(0, 0)) = (0, 0)$ and equations

$$d_0(\nu)\mu + d_{11}\mu\widetilde{x} + d_{12}(\mu, \nu)\widetilde{y} + \mathcal{O}(2) = 0, \tag{6.51}$$

$$d_1\mu + d_{21}\mu\widetilde{x} + d_{22}(\mu)\widetilde{y} + \mathcal{O}(2) = 0, \tag{6.52}$$

where

$$\begin{aligned}
d_0(\nu) &= c_1(\varepsilon_2 k - \varepsilon_1) + \varepsilon_1\nu,\\
d_1 &= \varepsilon_1 - \varepsilon_2 k,\\
d_{11} &= \varepsilon_1\frac{\partial p_2}{\partial x}(0) + \varepsilon_2 k\frac{\partial p_1}{\partial x}(0),\\
d_{21} &= \varepsilon_1\frac{\partial q_2}{\partial x}(0) + \varepsilon_2 k\frac{\partial q_1}{\partial x}(0),\\
d_{12}(\nu, \mu) &= \left(\varepsilon_1\frac{\partial p_2}{\partial y}(0) + \varepsilon_2 k\frac{\partial p_1}{\partial y}(0)\right)\mu - \varepsilon_1\nu + c_1(\varepsilon_1 + \varepsilon_2),\\
d_{22}(\mu) &= -(\varepsilon_1 + \varepsilon_2) + \left(\varepsilon_1\frac{\partial q_2}{\partial y}(0) + \varepsilon_2 k\frac{\partial q_1}{\partial y}(0)\right)\mu.
\end{aligned}$$

Equations (6.51)-(6.52) is obtained from the (6.48)-(6.49), doing $(\frac{dx}{d\tau}, \frac{dy}{d\tau}) = (0, 0)$. We are presenting only the linear terms, but we also consider the quadratic and cubic terms.

Since $d_{22}(0) \neq 0$, then we can apply the implicit function theorem at $(\widetilde{x}, \widetilde{y}, \mu) = (0, 0, 0)$ to the equation (6.52), which does not depend on ν, we can assure for any solution with $|(\widetilde{x}, \mu)|$ small the expansion

$$\widetilde{y} = \frac{\varepsilon_1 - \varepsilon_2 k}{\varepsilon_1 + \varepsilon_2}\mu + \mathcal{O}(|(\widetilde{x}, \mu)|^2). \tag{6.53}$$

After, we substitute (6.53) in the equation (6.51), getting

$$\alpha\mu\nu + \kappa(\nu)\mu\widetilde{x} - \alpha\nu\widetilde{x}^2 + \sigma(\nu)\mu^2 + \mathcal{O}(|\widetilde{x}, \mu)|^3) = 0, \tag{6.54}$$

where

$$\alpha = \frac{\varepsilon_1\varepsilon_2(1+k)}{\varepsilon_1+\varepsilon_2} > 0,$$
$$\kappa(0) = \alpha\left(\frac{\partial(p_1+p_2)}{\partial x}(0) + c_1\frac{\partial(q_1+q_2)}{\partial x}(0)\right),$$
$$\sigma(0) = \alpha\frac{\varepsilon_1-\varepsilon_2 k}{\varepsilon_1+\varepsilon_2}\left(\frac{\partial(p_1+p_2)}{\partial y}(0) + c_1\frac{\partial(q_1+q_2)}{\partial y}(0)\right).$$

Assuming $\kappa_0 = \frac{\kappa(0)}{\alpha} \neq 0$ and $\mu \neq 0$, we can apply to (6.54) the implicit function theorem at $(\widetilde{x}, \nu, \mu) = (0,0,0)$ to solve for $\widetilde{x}$. Therefore, we get

$$\widetilde{x}(\nu,\mu) = -\frac{1}{\kappa_0}\nu - \sigma_0\mu + \mathcal{O}(|(\nu,\mu)|^2), \tag{6.55}$$

where $\sigma_0 = \frac{\sigma(0)}{\kappa(0)}$. The corresponding $\widetilde{y}(\nu,\mu)-$coordinate is directly obtained by substituting (6.55) in equation (6.53), namely

$$\widetilde{y}(\nu,\mu) = \frac{\varepsilon_1-\varepsilon_2 k}{\varepsilon_1+\varepsilon_2}\mu + \mathcal{O}(|(\nu,\mu)|^2). \tag{6.56}$$

For the case $\mu = 0$ the equation (6.54) is is reduced to

$$-\alpha\nu + \eta(\nu)\widetilde{x} + \mathcal{O}(\widetilde{x}^2) = 0,$$

such that $\eta(0) = -\kappa(0)$. Thus the coordinates $(\widetilde{x}(\nu,0), \widetilde{y}(\nu,0))$ can be directly obtained from (6.55) and (6.56) with $\mu = 0$.

Remark 6.5. *If $\varepsilon_1 = \varepsilon_2 k$ and $\nu = 0$, then $(\widetilde{x}(0,\mu), \widetilde{y}(0,\mu)) = (0,0)$ for all μ, because*

$$\mathbf{F}^-_\mu(\mathbf{0}) = \begin{bmatrix} c_1 \\ -1 \\ \varepsilon_2 k\mu \end{bmatrix} \quad \textit{and} \quad \mathbf{F}^+_{(0,\mu)}(\mathbf{0}) = \begin{bmatrix} -c_1 \\ 1 \\ -\varepsilon_2 k\mu \end{bmatrix}$$

are anti-collinear, being also transversal to Σ for $\mu \neq 0$ or tangent when $\mu = 0$.

We denote by $\widetilde{\mathbf{p}}(\nu,\mu) = (\widetilde{x}(\nu,\mu), \widetilde{y}(\nu,\mu))$ the equilibrium point

whose coordinates in (x, y)-plane are expressed by (6.55)-(6.56). Therefore, if the condition

$$\kappa_0 = \frac{\partial(p_1 + p_2)}{\partial x}(0) + c_1 \frac{\partial(q_1 + q_2)}{\partial x}(0) \neq 0 \tag{6.57}$$

is satisfied, then system (6.48)-(6.49) has at least three equilibrium points: $\widehat{\mathbf{p}}^{\pm}$ with coordinates given in (6.12)-(6.13) and defined for all $\mu \geq 0$; and also $\widetilde{\mathbf{p}}$, with coordinates given in (6.55)-(6.56) and defined for all (ν, μ) in a neighborhood of $(0, 0)$.

The following lemma summarizes the stability results of the equilibria of (6.48)-(6.49). We consider $\bar{\nu}^{\pm}$ and $\bar{\mu}$ defined by

$$\bar{\nu}^{\pm}(\mu) = \pm\kappa_0\sqrt{\mu} + \mathcal{O}(\mu)$$

for $\mu \geq 0$ and

$$\bar{\mu}(\nu) = \frac{1}{\kappa_0^2}\nu^2 + \mathcal{O}(\nu^3). \tag{6.58}$$

Lemma 6.1. *On the equilibria stability of system* (6.48)-(6.49)*.*

(a1) *If $\nu > \bar{\nu}^+(\mu)$, then $\widehat{\mathbf{p}}^-$ is a saddle equilibrium. If $\nu < \bar{\nu}^+(\mu)$, it is a stable node equilibrium.*

(a2) *If $\nu < \bar{\nu}^-(\mu)$, then $\widehat{\mathbf{p}}^+$ is a saddle equilibrium. If $\nu > \bar{\nu}^-(\mu)$, it is a stable node equilibrium.*

(a3) *Suppose $\kappa_0 > 0$ (resp. $\kappa_0 < 0$). If $\mu < \bar{\mu}(\nu)$, then $\widetilde{\mathbf{p}}$ is a stable node equilibrium (resp. saddle). If $\mu > \bar{\mu}(\nu)$, it is a saddle (resp. stable node).*

Proof. We already know the equilibria of the planar sliding system (6.48)-(6.49). We then proceed to the analysis of the hyperbolic stability of these equilibria.

From the Jacobian matrices of (6.48)-(6.49), denoted by J and applied at the equilibria $\widehat{\mathbf{p}}^{\pm}$ (existing only for $\mu \geq 0$), we get the equa-

tions of the determinant and trace, namely

$$\begin{aligned}\mathrm{Det}[J(\widehat{\mathbf{p}}^{\pm})] &= 2\varepsilon_1\varepsilon_2(1+k)\sqrt{\mu}\,[\pm\nu + (\kappa_0+\kappa_1\nu)\sqrt{\mu}\,] + \mathcal{O}(\mu^{\frac{3}{2}}),\\ \mathrm{Tr}[J(\widehat{\mathbf{p}}^{\pm})] &= -(\varepsilon_1+\varepsilon_2) + \mathcal{O}(\mu^{\frac{1}{2}}),\end{aligned}$$

respectively. Note that the trace is negative and that the eigenvalues are real (since $\mathrm{Tr}[J(\widehat{\mathbf{p}}^{\pm})]^2 - 4\mathrm{Det}[J(\widehat{\mathbf{p}}^{\pm})] > 0$) in a neighborhood of $(0,0)$, in the (ν,μ)-plane of parameters. Applying the implicit function theorem at $(\nu,\mu)=(0,0)$ to equations $\mathrm{Det}[J(\widehat{\mathbf{p}}^{\pm})]=0$, we can assure for any solution with $|\mu|$ small, the expansions $\nu = \bar{\nu}^{\mp}(\mu) = \mp\kappa_0\sqrt{\mu} + \mathcal{O}(\mu)$. Moreover, for $\nu < \bar{\nu}^{+}(\mu)$ (resp. $\nu > \bar{\nu}^{+}(\mu)$) and $\mu > 0$ we get $\mathrm{Det}[J(\widehat{\mathbf{p}}^{-})] > 0$ (resp. $\mathrm{Det}[J(\widehat{\mathbf{p}}^{-})] < 0$). Analogously, for $\nu > \bar{\nu}^{-}(\mu)$ (resp. $\nu < \bar{\nu}^{-}(\mu)$) and $\mu > 0$ we get $\mathrm{Det}[J(\widehat{\mathbf{p}}^{+})] > 0$ (resp. $\mathrm{Det}[J(\widehat{\mathbf{p}}^{+})] < 0$). From this, it is easy to see that the statements (a1) and (a2) of the Lemma 6.1 are true.

For the equilibrium point $\widetilde{\mathbf{p}}$, the equations of the determinant and trace are approximate in a neighborhood of $(\nu,\mu)=(0,0)$ by

$$\begin{aligned}\mathrm{Det}[J(\widetilde{\mathbf{p}})] &= -\varepsilon_1\varepsilon_2(1+k)\kappa_0\left(\mu - \frac{1}{\kappa_0^2}\nu^2\right) + \delta_{11}\nu\mu + \delta_{02}\mu^2 + \mathcal{O}(|(\nu,\mu)|^3),\\ \mathrm{Tr}[J(\widetilde{\mathbf{p}})] &= -(\varepsilon_1+\varepsilon_2) + \mathcal{O}(\nu,\mu),\end{aligned}$$

respectively. Note that, just as $\widehat{\mathbf{p}}^{\pm}$, the trace is negative ($\varepsilon_1+\varepsilon_2>0$) and the eigenvalues are real. Applying the implicit function theorem at $(\nu,\mu)=(0,0)$ to equation $\mathrm{Det}[J(\widetilde{\mathbf{p}})]=0$, we can assure for any solution with $|\nu|$ small, the expansion $\mu = \bar{\mu}(\nu) = \frac{1}{\kappa_0^2}\nu^2 + \mathcal{O}(\nu^3)$. Supposing $\kappa_0 < 0$, then: (i) for $\mu < \bar{\mu}(\nu)$ we get $\mathrm{Det}[J(\widetilde{\mathbf{p}})] < 0$; and (ii) for $\mu > \bar{\mu}(\nu)$ we get $\mathrm{Det}[J(\widetilde{\mathbf{p}})] > 0$. The case $\kappa_0 > 0$ has determinant with opposite sign. From this, it is easy to see that the statement (a3) of Lemma 6.1 is true. □

6.4.2 Bifurcations Analysis

In previous subsection we have analyzed the conditions of existence and stability of the equilibria $\widehat{\mathbf{p}}^{\pm}$ and $\widetilde{\mathbf{p}}$. From this, we can conclude about the bifurcations in system (6.48)-(6.49), as follows:

(b1) The equilibria $\widehat{\mathbf{p}}^{\pm}(\mu)$ are defined only for $\mu \geq 0$, and $\widehat{\mathbf{p}}^{+}(0) = \widehat{\mathbf{p}}^{-}(0) = (0,0)$, $\mathrm{Det}[J(0,0)] = 0$ and $\mathrm{Tr}[J(0,0)] < 0$. If $\mu > 0$ and $\nu < 0$ (resp. $\nu > 0$), then $\widehat{\mathbf{p}}^{-}$ is a stable node (resp. saddle) and $\widehat{\mathbf{p}}^{+}$ is a saddle (resp. stable node). If $\nu = 0$, then both equilibria are saddle for $\mu > 0$.

(b2) Assume $\nu < 0$ (resp. $\nu > 0$). The equilibria $\widehat{\mathbf{p}}^{-}(\mu)$ (resp. $\widehat{\mathbf{p}}^{+}$) and $\widetilde{\mathbf{p}}(\nu,\mu)$ are defined for all μ in a neighborhood of $\mu = \bar{\mu}(\nu)$, so that $\widehat{\mathbf{p}}^{-}(\bar{\mu}(\nu)) = \widetilde{\mathbf{p}}(\nu,\bar{\mu}(\nu)) = (-\nu/\kappa_0, 0) + \mathcal{O}(\nu^2)$, $\mathrm{Det}[J(\widehat{\mathbf{p}}^{-})] = 0$ and $\mathrm{Tr}[J(\widehat{\mathbf{p}}^{-})] < 0$. If $\mu < \bar{\mu}(\nu)$, then $\widehat{\mathbf{p}}^{-}$ (resp. $\widehat{\mathbf{p}}^{+}$) is a stable node and $\widetilde{\mathbf{p}}$ is a saddle. If $\mu > \bar{\mu}(\nu)$, then $\widehat{\mathbf{p}}^{-}$ (resp. $\widehat{\mathbf{p}}^{+}$) becomes a stable node and $\widetilde{\mathbf{p}}$ becomes a saddle.

(b3) Suppose $\nu = \gamma\mu$ with γ an any constant. For $\mu > 0$ we have that $\widehat{\mathbf{p}}^{\pm}$ are saddle equilibria, separated by $\widetilde{\mathbf{p}}$ which is a stable node equilibrium. For $\mu = 0$ these equilibria collide, so that $\widehat{\mathbf{p}}^{+}(0) = \widehat{\mathbf{p}}^{-}(0) = \widetilde{\mathbf{p}}(0,0) = (0,0)$, $\mathrm{Det}[J(0,0)] = 0$ and $\mathrm{Tr}[J(0,0)] < 0$. For $\mu < 0$ the equilibria $\widehat{\mathbf{p}}^{\pm}$ disappear, while $\widetilde{\mathbf{p}}$ persists and becomes a saddle.

From the statements listed above, it is clear that a Saddle-Node bifurcation occurs for $\mu = 0$ and a Transcritical bifurcation occurs for $\mu = \bar{\mu}(\nu)$, whenever $\nu \neq 0$. A combination of these two bifurcations occur for $(\nu,\mu) = (0,0)$, so that if we fix $\nu = \gamma\mu$, from the variation of the μ-parameter a Pitchfork bifurcation is observed at $\mu = 0$.

The set of bifurcations in the $(\nu,\mu)-$plane of parameters, shown in Figure 6.11 for the case $\kappa_0 < 0$, summarizes the results about the bifurcations in system (6.48)-(6.49), assuming $\|(\nu,\mu)\|$ small. The green

and brown lines indicate the Trancritical bifurcation (Tb) and Saddle-Node bifurcation (SNb), respectively. The black point at the origin indicates the Pitchfork bifurcation (Pb). The $(\nu, \mu)-$plane is divided into four regions around the origin, such that for each one we illustrate the dynamics involving the equilibria of (6.48)-(6.49). In these phase portraits the blue point represents the equilibrium $\widetilde{\mathbf{p}}$, while the red points represent the equilibria $\widehat{\mathbf{p}}^{-}$ (on the left) and $\widehat{\mathbf{p}}^{+}$ (on the right).

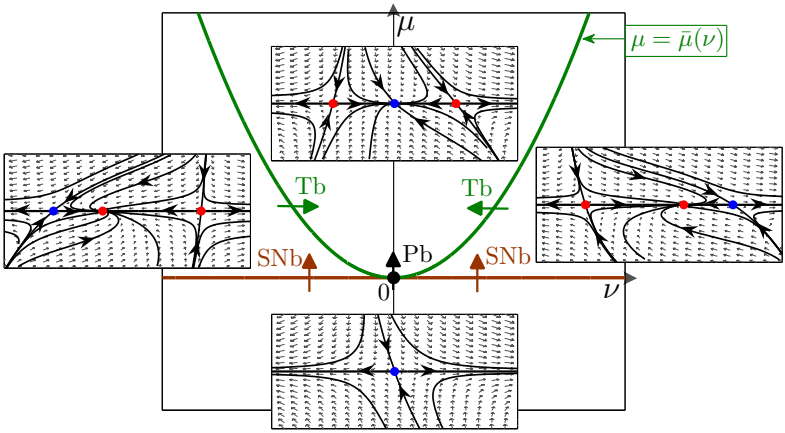

Figure 6.11: Bifurcations local set.

6.4.3 Stability at the pseudo-equilibrium point

The equilibrium point $\widetilde{\mathbf{p}}(\nu, \mu)$, of the planar sliding system (6.48)-(6.49), composes the first two coordinates of the pseudo-equilibrium $\widetilde{\mathbf{x}}(\nu, \mu)$ of system (6.8).

Theorem 6.3. *Assume $\kappa_0 \neq 0$ and that $\|(\nu, \mu)\| < \xi$ with ξ arbitrarily small. System (6.8) has at $\widetilde{\mathbf{x}} = (\widetilde{\mathbf{p}}, 0)$ a real pseudo-equilibrium point if $\mu \neq \bar{\mu}(\nu)$. Suppose $\kappa_0 < 0$ (resp. $\kappa_0 > 0$). If $\mu > \bar{\mu}(\nu)$, then $\widetilde{\mathbf{x}} \in \Sigma_{as}$ and is a stable pseudo-node (resp. pseudo-saddle). If $\mu < \bar{\mu}(\nu)$, then $\widetilde{\mathbf{x}} \in \Sigma_{rs}$ and is a pseudo-saddle (resp. unstable pseudo-node).*

Proof. Since

$$\begin{aligned} L_{F_\mu^-} h(\widetilde{\mathbf{x}}(\nu,\mu)) &= \alpha\,(\mu - \bar{\mu}(\nu)) + n_1\nu\mu + n_2\mu^2 + \mathcal{O}(3) \\ L_{F^+_{(\nu,\mu)}} h(\widetilde{\mathbf{x}}(\nu,\mu)) &= -\alpha\,(\mu - \bar{\mu}(\nu)) + n_3\nu\mu + n_4\mu^2 + \mathcal{O}(3) \end{aligned}$$

with $\bar{\mu}(\nu)$ given in (6.58), $\alpha > 0$ defined in previous subsection and n_i any coefficients, we can make the following statements. There is a neighborhood of $(0,0)$ in the (ν,μ)-plane of parameters, where:

(i) $\widetilde{\mathbf{x}}(\nu,\mu) \in \Sigma_{as}(\mu)$ for $\mu > \bar{\mu}(\nu)$;

(ii) $\widetilde{\mathbf{x}}(\nu,\mu) \in \Sigma_{rs}(\mu)$ for $\mu < \bar{\mu}(\nu)$.

Comparing the results listed above with the item (a3) of the Lemma 6.1, it is easy to see that item (c) of the Theorem 6.3 is also true. Recall that when the pseudo-equilibrium is in the repulsive region, its stability is the opposite to that found from system (6.48)-(6.49). □

Therefore, for $\mu = \bar{\mu}(\nu)$ the system (6.8) undergoes a pseudo-equilibrium transition from Σ_{as} to Σ_{rs} (or vice-versa). Moreover, the transition point is a regular T-singularity of coordinates

$$\widehat{\mathbf{x}}^+(\mu) = (\widehat{\mathbf{p}}^+(\mu), 0)$$

(or $\widehat{\mathbf{x}}^-(\mu) = (\widehat{\mathbf{p}}^-(\mu), 0)$) if $\nu \neq 0$. In the degenerate case $\mu = \nu = 0$, a collision between the pseudo-equilibrium and the pair of T-singularities occurs, so that for $\mu > 0$ the pseudo-equilibrium is in the attractive sliding region and for $\mu < 0$ it is in the repulsive sliding region.

Figure 6.12 shows a particular case, for $\varepsilon_1 = \varepsilon_2 k$, $\nu = 0$ and assuming $\kappa_0 < 0$. In this case, for $\mu > \bar{\mu}(0) = 0$ the origin is a stable pseudo-node in Σ_{as}, and a pseudo-saddle in Σ_{rs} when $\mu < 0$.

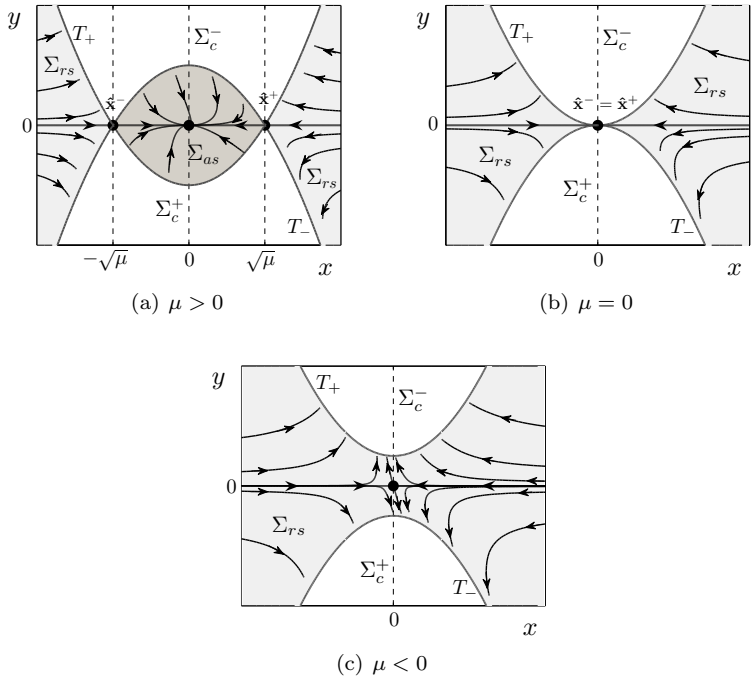

Figure 6.12: Topological configurations on Σ induced by the pitchfork sliding bifurcation.

6.5 A case study on crossing limit cycles

Let us now, by a simple example, apply the results of the previous section with respect to sliding bifurcations. From this, we associate such bifurcations with the birth of a limit cycle without sliding parts, that is, a crossing limit cycle (CLC).

The system used for the analysis is given by

$$\dot{\mathbf{x}} = \begin{cases} \mathbf{F}_{\mu}^{-}(\mathbf{x}), \text{ if } z < 0 \\ \mathbf{F}_{\mu,\nu}^{+}(\mathbf{x}), \text{ if } z > 0 \end{cases}, \tag{6.59}$$

with

$$\mathbf{F}^-_{\mu}(\mathbf{x}) = \begin{bmatrix} 1/4 \\ -1 \\ -y - x^2 + \mu \end{bmatrix}, \; \mathbf{F}^+_{\mu,\nu}(\mathbf{x}) = \begin{bmatrix} \nu - 1/4 - ax \\ 1 \\ -y - az + x^2 - \mu \end{bmatrix},$$

where $\mathbf{x} = (x, y, z) \in \mathbb{R}^3$, dependent on real parameters ν, μ and a. Note that (6.59) belongs to the family of systems with two T-singularities given in (6.8)-(6.10), already written in the canonical form. Thus, in a neighborhood of the origin the topological configuration of (6.59) at $z = 0$ is as in (6.8)-(6.10). Then for $\mu > 0$ and small, system (6.59) has two regular T-singularities at points $\widehat{\mathbf{x}}^{\pm}(\mu) = (\pm\sqrt{\mu}, 0, 0)$ and, at $\widehat{\mathbf{x}}^{\pm}(0) = (0, 0, 0)$ there exists a 1-degenerate T-singularity. Moreover, the tangency lines $T_{\pm}$, the sliding regions Σ_{as} and Σ_{rs}, and the crossing regions Σ^+_c and Σ^-_c, are defined as in (6.25), (6.26), (6.31), (6.32),(6.33) and (6.34), since the third component of the vector field in (6.59) and (6.24) are identical at $z = 0$.

6.5.1 Pseudo-equilibrium transition from Σ_{as} to Σ_{rs}

The system (6.59) has a pseudo-equilibrium point at $\widetilde{\mathbf{x}}(\nu) = (\nu/a, 0, 0)$ if, and only if, $a \neq 0$. This pseudo-equilibrium is real whenever $\frac{\nu^2}{a^2} - \mu \neq 0$, since thus the vectors

$$\mathbf{F}^-_{\mu}(\widetilde{\mathbf{x}}(\nu)) = \begin{bmatrix} \frac{1}{4} \\ -1 \\ -\frac{\nu^2}{a^2} + \mu \end{bmatrix} \quad \text{and} \quad \mathbf{F}^+_{(\nu,\mu)}(\mathbf{0}) = \begin{bmatrix} -\frac{1}{4} \\ 1 \\ \frac{\nu^2}{a^2} - \mu \end{bmatrix}$$

are anti-collinear and also transverse to Σ. The existence condition of pseudo-equilibrium point is also calculated from the coefficient κ_0 defined in (6.57), getting $\kappa_0 = -a \neq 0$. So, we can applied the Theorem 6.3 to the system (6.59), to obtain the stability and position of the pseudo-equilibrium point as follows:

i) Case $\kappa_0 = -a < 0$: For $\mu > \bar{\mu}(\nu) = \nu^2/a^2$ the point $\widetilde{\mathbf{x}}(\nu)$ is

a stable pseudo-node belonging to Σ_{as}, while for $\mu < \nu^2/a^2$ the point $\widetilde{\mathbf{x}}(\nu)$ is a pseudo-saddle belonging to Σ_{rs}.

ii) Case $\kappa_0 = -a > 0$: For $\mu > \nu^2/a^2$ the point $\widetilde{\mathbf{x}}(\nu)$ is a pseudo-saddle belonging to Σ_{as}, while for $\mu < \nu^2/a^2$ the point $\widetilde{\mathbf{x}}(\nu)$ is an unstable pseudo-node belonging to Σ_{rs}.

A transcritical bifurcation in the sliding dynamics occurs for all $\nu \neq 0$ and $\mu = \nu^2/a^2$. There are two bifurcation branches, as shown in Figure 6.11, with equations $\nu_{\pm} = \pm a\sqrt{\mu}$, for $\mu > 0$. This bifurcation is related to the pseudo-equilibrium transition from Σ_{as} to Σ_{rs} (or vice versa), being the transition point an equilibrium of the sliding dynamics located at one of double tangency points $\widehat{\mathbf{x}}^{\pm}(\mu) = (\pm\sqrt{\mu}, 0, 0)$. Since the double tangency points are invisible two-fold, then, from the transcritical bifurcation in the sliding dynamics, arises a CLC. In this case we say that (6.59) undergoes a *TS-bifurcation* for $\mu = \nu^2/a^2$ whenever $\nu \neq 0$.

Example 6.1. *Supposing $a = \mu = 1$, then a TS-bifurcation occurs when $\nu = -1$ and also when $\nu = 1$. Figure 6.13 shows a TS-bifurcation scenario in the system* (6.59)*, where for $\nu = -0.5 > -1$ the pseudo-equilibrium $\widetilde{\mathbf{x}}$ belongs to Σ_{as} and is stable (pseudo-node), being moved to Σ_{rs} when $\nu = -1.1 < -1$ and so becoming unstable (pseudo-saddle). Along with the pseudo-equilibrium in Σ_{rs}, arise in the state space of* (6.59) *a CLC with stable dynamics. For $\nu = -1$ occurs $\widetilde{\mathbf{x}}(-1) = \widehat{\mathbf{x}}^{-}(1) = (-1, 0, 0)$, so that the T-singularity point becomes a local attractor of* (6.59)*, revealing the stable nature of the CLC that arise from this point for $\nu < -1$.*

A pitchfork bifurcation in the sliding dynamics occurs for $(\nu, \mu) = (0, 0)$ whenever it is possible $\nu = \gamma\mu$, for an any constant γ. Such a bifurcation destroys (or creates) the attractive sliding region Σ_{as}, causing a pseudo-equilibrium transition from Σ_{as} to Σ_{rs} (or from Σ_{rs} to Σ_{as}). Here the transition point is a trivial equilibrium of the sliding dynamics located at a double tangency point classified as 1-degenerate

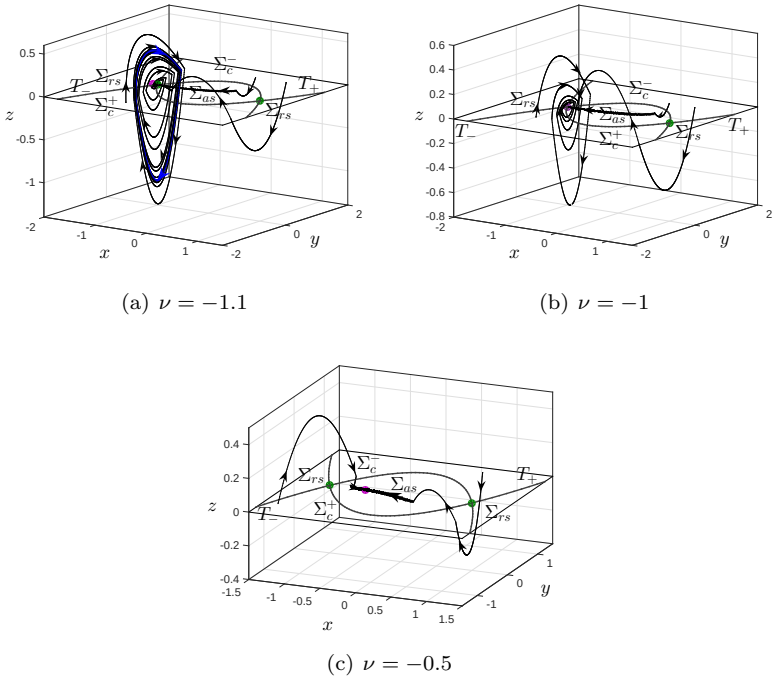

(a) $\nu = -1.1$

(b) $\nu = -1$

(c) $\nu = -0.5$

Figure 6.13: Simulation of system (6.59) in the states space and with parameters $a = \mu = 1$: An example of the *TS-bifurcation*. Green points are T-singularities, purple point is a pseudo-equilibrium and blue cycle, in figure (a), is a CLC.

T-singularity of system (6.59).

Example 6.2. *Supposing $\nu = 0$, then for all $\mu < 0$ the phase portrait of* (6.59) *has an unique pseudo-equilibrium point, located at $\widetilde{\mathbf{x}}(0) = (0, 0, 0) \in \Sigma_{rs}$ and with saddle dynamics if $a > 0$ (or unstable node if $a < 0$). In addition, there are no double tangency points and, consequently, there are no T-singularities and also attractive sliding region Σ_{as}. When $\mu = 0$ the vector fields of* (6.59) *become anti-collinear and tangent to Σ at the origin, so that the created double tangency point at the origin is classified as 1-degenerate T-singularity. Continuing, for*

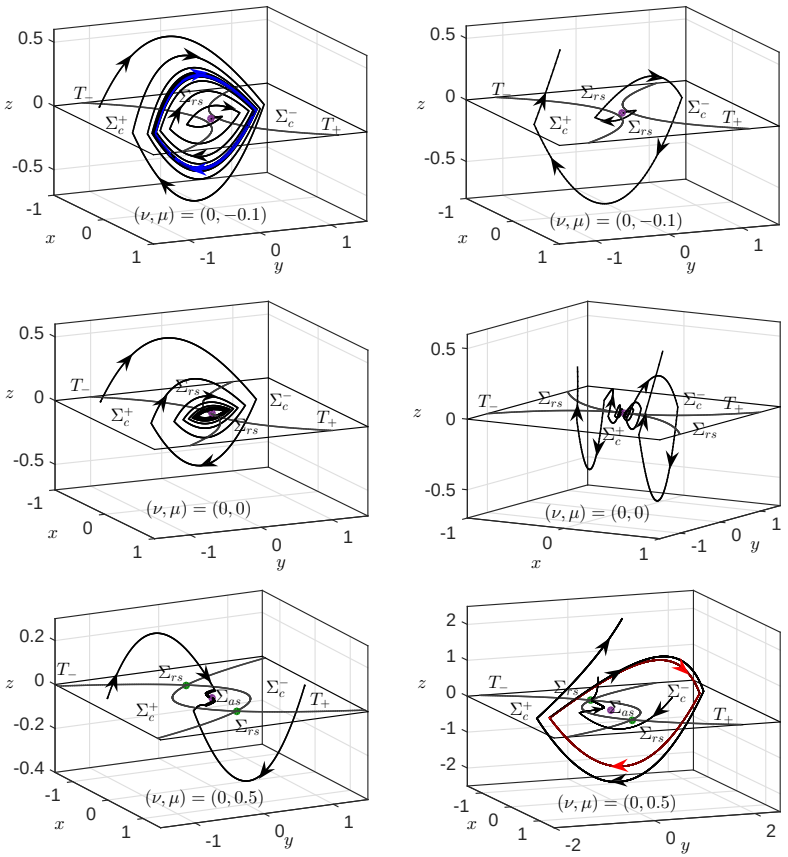

(a) $a = 1 > 0$ (b) $a = -1 < 0$

Figure 6.14: Simulation of system (6.59) in the state space: Examples of the *Double TS-bifurcation*. Green points are T-singularities, purple point is a pseudo-equilibrium and blue/red (stable/unstable) cycles are CLCs.

$\mu > 0$ the origin returns to be a pseudo-equilibrium, but now belonging to Σ_{as} and with stable node dynamics if $a > 0$ (or saddle if $a < 0$). With the disappearance of the 1-degenerate T-singularity and the appearance of two regular T-singularities, the attractive sliding region Σ_{as} finally emerges in Σ. See Figure 6.14.

The bifurcation that occurs in the system (6.59) when $(\nu, \mu) = (0, 0)$ is named here as *Double TS-bifurcation*. For both examples, $a = 1 > 0$ and $a = -1 < 0$, we see in Figure 6.14 the birth of a CLC. Such a CLC bifurcates from the 1-degenerate T-singularity and emerges around the Σ_{rs} (resp. Σ_{as}) for $\mu < 0$ (resp. $\mu > 0$), in the case $a > 0$ (resp. $a < 0$).

6.5.2 Analysis of limit cycles created from the TS-bifurcation

We use the method proposed in Chapter 4 to prove the existence and stability of the CLC, local to its birth and assuming the parameters $a = \mu = 1$. In addition, only one case is considered, which involves the T-singularity located at point $\widehat{\mathbf{x}}^{-}(1) = (-1, 0, 0)$, as in the example shown in Figure 6.13.

System (6.59) is rewrite in the canonical form according to Section 4.6 of Chapter 4, and the coefficients required for the analysis are calculated. We have listed below such coefficients:

$$v_{+} = \frac{1 + 4\nu}{\sqrt{3(5 + 4\nu)}}, \quad \varepsilon = -\frac{16(1 + \nu)}{3(5 + 4\nu)},$$

$$\sigma = 5.65, \qquad \rho = 3.55.$$

Following Theorem 4.4 of Chapter 4, a bifurcation occurs for $\varepsilon(\nu) = 0$, i.e., for $\nu = -1$, since $v_{+}(-1) < 0$. Moreover, for any ν such that $-5/4 < \nu < -1$, the constraint $\rho\varepsilon > 0$ is satisfied. Therefore the CLC arises in the phase portrait of (6.59) for $\nu < -1$. Since $\sigma > 0$ and $0 < 8\rho < \sigma^2$, the CLC is born with stable node dynamics. The stable CLC bifurcates of the T-singularity point at $(-1, 0, 0)$ when $\nu = -1$ and, exists to $\nu < -1$. This analysis is local, so that the obtained results are taken close enough to the bifurcation point, that is, for all ν such that $|\nu + 1| < \zeta$ with $\zeta > 0$ arbitrarily small.

We recall, as seen in the previous subsection, that for $\nu = -1$ a

Transcritical bifurcation occurs in sliding dynamics, associated to the pseudo-equilibrium transition from Σ_{as} (for $-1 < \nu < 1$) to Σ_{rs} (for $\nu < -1$). Simultaneously, a bifurcation of the Bogdanov-Takens type for maps occurs in the crossing dynamics, giving rise to two fixed points for $\nu < -1$, one in Σ_c^+ and the other in Σ_c^-, indicating the presence of a CLC.

6.5.3 Analysis of limit cycles created from the Double TS-bifurcation

In the following we analyze the stability and existence of CLCs bifurcating from the 1-degenerate T-singularity point of system (6.59). We set $\nu = 0$ to place the pseudo-equilibrium at the origin.

We consider an orbit of system (6.59) through the point $\mathbf{x}_0 \in \Sigma_c^+$ such that for $t = t_1 > 0$ the orbit transversally returns to Σ at the point $\mathbf{x}_1 \in \Sigma_c^-$. And its continuation through the point $\mathbf{x}_1 \in \Sigma_c^-$ such that for $t = t_2 > 0$ the orbit transversally returns to Σ at the point $\mathbf{x}_2 \in \Sigma_c^+$. See Figure 6.15.

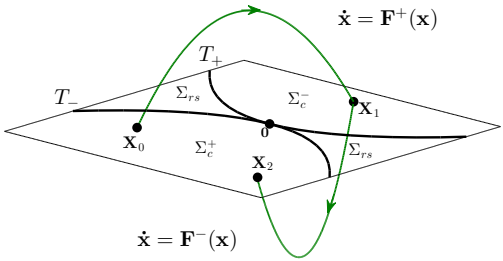

Figure 6.15: Determining the first return map.

Solution of $\dot{\mathbf{x}} = \mathbf{F}^+_{\mu,0}(\mathbf{x})$ with initial condition $(x_0, y_0, 0) \in \Sigma^+_c$ is

$$\begin{aligned} x(t) &= x_0 e^{-at} + \frac{1}{4} q(t), \\ y(t) &= t + y_0, \\ z(t) &= p(t) - \frac{e^{-at}}{2a} \left[q(t) + t\right] x_0 + q(t) \left[y_0 + \mu - e^{-at} x_0^2\right], \end{aligned}$$

where

$$p(t) = \frac{1 + 16a(1 - at) - 2a(8 + t)e^{-at} - e^{-2at}}{16a^3},$$

and

$$q(t) = \frac{e^{-at} - 1}{a}.$$

Suppose there is a $t = t_1 > 0$ such that $(x(t_1), y(t_1), z(t_1)) = (x_1, y_1, 0) \in \Sigma^-_c$. Then a half-return map is defined by $(x_1, y_1) = P_+(x_0, y_0, t_1)$ with

$$x_1 = x_0 e^{-at_1} + \frac{1}{4} q(t_1), \tag{6.60}$$

$$y_1 = t_1 + y_0, \tag{6.61}$$

$$0 = f(x_0, y_0, t_1) = \frac{z(t_1)}{q(t_1)}, \tag{6.62}$$

for all $t_1 = t_1(x_0, y_0) > 0$ fulfilling the third equation.

The division by $q(t_1)$ in the equation (6.62) eliminates the trivial solution $t_1 = 0$, since $q(0) = 0$. In this case $f(x_0, y_0, t_1) = 0$ is not defined at $t_1 = 0$ and $\lim_{t_1 \to 0^+} f(x_0, y_0, t_1) = 0$ only if $y_0 \to x_0^2 - \mu$, leading to $x_1 \to x_0$ and $y_1 \to y_0$. Therefore, all $(x_0, y_0, 0) \in \Upsilon_+ \subset T_+$ (Υ_+ is the set of invisible folds to $\mathbf{F}^+_{\mu,0}$) is a non-isolated fixed point for the P_+-map.

The P_+-map satisfy the conditions of involution (see [116]) at Υ_+, since

$$\begin{aligned} P_+(x_0, x_0^2 - \mu, 0) &= (x_0, x_0^2 - \mu), \\ P_+^2(x_0, y_0, 0) &= (x_0, y_0), \\ \lim_{t_1 \to 0^+} \mathrm{Det}[DP_+(x_0, y_0, t_1)] &= -1. \end{aligned}$$

This is an important property that should be checked. Here, DP_+ denotes the Jacobian matrix calculated by

$$DP_+(\mathbf{p}_0) = \frac{\partial P_+(\mathbf{p}_0)}{\partial(x_0, y_0)} - \frac{\partial P_+(\mathbf{p}_0)}{\partial t_1}\frac{\partial f(\mathbf{p}_0)}{\partial(x_0, y_0)}\left(\frac{\partial f(\mathbf{p}_0)}{\partial t_1}\right)^{-1}, \qquad (6.63)$$

where $\mathbf{p}_0 = (x_0, y_0, t_1)$ and

$$\begin{aligned}
\frac{\partial P_+(\mathbf{p}_0)}{\partial(x_0, y_0)} &= \begin{bmatrix} e^{-at_1} & 0 \\ 0 & 1 \end{bmatrix}, \\
\frac{\partial P_+(\mathbf{p}_0)}{\partial t_1} &= \begin{bmatrix} -\frac{1}{4}e^{-at_1}(1+4ax_0) & 1 \end{bmatrix}^T, \\
\frac{\partial f(\mathbf{p}_0)}{\partial(x_0, y_0)} &= \begin{bmatrix} \frac{e^{-at_1}}{2}\left(\frac{t_1}{1-e^{-at_1}} - \frac{1}{a} - 4x_0\right) & 1 \end{bmatrix}, \\
\frac{\partial f(\mathbf{p}_0)}{\partial t_1} &= \frac{-4(1+2ax_0)(1+4ax_0) + 16ae^{2at_1} + (1+4ax_0)^2 e^{-at_1}}{16a(e^{at_1}-1)^2} \\
&\quad + \frac{2 + 8a(x_0 - 2at_1 - 2) - 2at_1(1+4ax_0) + (1+4ax_0)^2}{16ae^{-at_1}(e^{at_1}-1)^2}.
\end{aligned}$$

Solution of $\dot{\mathbf{x}} = \mathbf{F}_\mu^-(\mathbf{x})$ with initial condition $(x_1, y_1, 0) \in \Sigma_c^-$ is

$$\begin{aligned}
x(t) &= \frac{1}{4}t + x_1, \\
y(t) &= -t + y_1, \\
z(t) &= -\frac{1}{48}t^3 + \frac{1}{4}(2 - x_1)t^2 - (y_1 + x_1^2 - \mu)t.
\end{aligned}$$

There exists a $t = t_2 > 0$ such that $(x(t_2), y(t_2), z(t_2)) = (x_2, y_2, 0) \in \Sigma_c^+$, given by

$$t_2 = 6(2 - x_1) - 2\sqrt{3}\sqrt{12(1 - x_1) - x_1^2 - 4(y_1 - \mu)},$$

whenever $y_1 < 3(1 - x_1) - \dfrac{x_1^2}{4} + \mu$. This $t_2 = t_2(x_1, y_1)$ determines the time spent by a trajectory, starting at $z = 0$, to return to the $z = 0$. We called of *return time* or *flight time*. To simplify the calculations, we leave the P_--map dependent on the return time $t_2 > 0$.

Given (x_1, y_1, μ) with $\mu - x_1^2 < y_1 < 3(1 - x_1) - \dfrac{x_1^2}{4} + \mu$, there is a $t = t_2 > 0$ such that $(x(t_2), y(t_2), z(t_2)) = (x_2, y_2, 0) \in \Sigma_c^+$. Then a Half-return map is defined by $(x_2, y_2) = P_-(x_1, y_1, t_2)$ with

$$x_2 = \frac{1}{4}t_2 + x_1, \tag{6.64}$$

$$y_2 = -t_2 + y_1, \tag{6.65}$$

$$0 = g(x_1, y_1, t_2) = -\frac{1}{48}t_2^2 + \frac{1}{4}(2 - x_1)t_2 - y_1 - x_1^2 + \mu, \tag{6.66}$$

for any $t_2 = t_2(x_1, y_1) \geq 0$ fulfilling the third equation and (x_1, y_1, μ) fulfilling the constraint $\mu - x_1^2 \leq y_1 < 3(1 - x_1) - \dfrac{x_1^2}{4} + \mu$. In this case $g(x_1, y_1, t_2) = 0$ is defined at $t_2 = 0$ and $g(x_1, y_1, 0) = 0$ only if $y_1 = -x_1^2 + \mu$, leading to $x_2 = x_1$ and $y_2 = y_1$. Therefore, all $(x_1, y_1, 0) \in \Upsilon_- \subset T_-$ (Υ_- is the set of invisible folds to $\mathbf{F}_\mu^-$) is a non-isolated fixed point for the P_--map.

Matrix DP_- denotes the Jacobian matrix calculated by

$$DP_-(\mathbf{p}_1) = \frac{\partial P_-(\mathbf{p}_1)}{\partial(x_1, y_1)} - \frac{\partial P_-(\mathbf{p}_1)}{\partial t_2}\frac{\partial g(\mathbf{p}_1)}{\partial(x_1, y_1)}\left(\frac{\partial g(\mathbf{p}_1)}{\partial t_2}\right)^{-1}, \tag{6.67}$$

where $\mathbf{p}_1 = (x_1, y_1, t_2)$ and

$$\frac{\partial P_-(\mathbf{p}_1)}{\partial(x_1, y_1)} = \begin{bmatrix} 1 & 0 \\ 0 & 1 \end{bmatrix}, \qquad \frac{\partial P_-(\mathbf{p}_1)}{\partial t_2} = \begin{bmatrix} \frac{1}{4} & -1 \end{bmatrix}^T$$
$$\frac{\partial g(\mathbf{p}_1)}{\partial(x_1, y_1)} = \begin{bmatrix} -\frac{t_2}{4} - 2x_1 & -1 \end{bmatrix}, \quad \frac{\partial g(\mathbf{p}_1)}{\partial t_2} = \frac{1}{24}(12 - t_2 - 6x_1)$$

The P_--map is a involution at Υ_-, since

$$P_-(x_1, -x_1^2 + \mu, 0) = (x_1, -x_1^2 + \mu),$$
$$P_-^2(x_1, y_1, 0) = (x_1, y_1),$$
$$\mathrm{Det}[DP_-(x_1, y_1, 0)] = -1.$$

Based on the conditions stated above, we can ensure that there is

an open set $D_0 \subset \Sigma_c^+$ in neighbourhood of $(x_0, y_0, 0) \in \Sigma_c^+$ and $I_0 \subset \Sigma_c^-$ in neighbourhood of $(x_1, y_1, 0) \in \Sigma_c^-$, where for all $(x_0, y_0, 0) \in D_0$ there is an unique $t = t_1 > 0$ such that $P_+(x_0, y_0, t_1) = (x_1, y_1)$ with $(x_1, y_1, 0) \in I_0$. Analogously, we can ensure that there is an open set $D_1 \subset \Sigma_c^-$ in neighbourhood of $(x_1, y_1, 0) \in \Sigma_c^-$ and $I_1 \subset \Sigma_c^+$ in neighbourhood of $(x_2, y_2, 0) \in \Sigma_c^+$, where for all $(x_1, y_1, 0) \in D_1$ there is an unique $t = t_2 > 0$ such that $P_-(x_1, y_1, t_2) = (x_2, y_2)$ with $(x_2, y_2, 0) \in I_1$.

In addition, we can establish $(x_0, y_0, 0) \in \Sigma_c^+$ and $(x_1, y_1, 0) \in \Sigma_c^-$, such that the points in D_0 and D_1 are crossing points. So, assuming $I_0 \subset D_1$ we define the function that describes the first return map $P : (D_0, \mathcal{T}) \to I_1$, by composition $P = P_- \circ P_+$, where $\mathcal{T}$ denoted the set of values possible for (t_1, t_2). The first return map P is obtained by

$$P(x_0, y_0, t_1, t_2) = \begin{bmatrix} x_0 e^{-at_1} + \frac{1}{4a}\left(at_2 + e^{-at_1} - 1\right) \\ y_0 + t_1 - t_2 \end{bmatrix}, \tag{6.68}$$

$$0 = f(x_0, y_0, t_1) \tag{6.69}$$

$$0 = g(x_1(x_0, t_1), y_1(y_0, t_1), t_2) = \widetilde{g}(x_0, y_0, t_1, t_2) \tag{6.70}$$

for all $(x_0, y_0, 0) \in D_0$ and $(t_1, t_2) \in \mathcal{T}$.

A point $(\widehat{x}_0, \widehat{y}_0)$ is a fixed point of P-map if there are $\widehat{t}_1 = t_1(\widehat{x}_0, \widehat{y}_0) \geq 0$ and $\widehat{t}_2 = t_2(\widehat{x}_0, \widehat{y}_0) \geq 0$ satisfying the equations (6.69)-(6.70), such that $(\widehat{x}_0, \widehat{y}_0) = P(\widehat{x}_0, \widehat{y}_0, \widehat{t}_1, \widehat{t}_2)$. Trivial fixed points occur for $\widehat{t}_1 = \widehat{t}_2 = 0$ and are located at the intersections of the tangency lines T_+ and T_-. More precisely, if $\mu > 0$ there are two trivial fixed points, located at the regular T-singularities of coordinates $(\pm\sqrt{\mu}, 0, 0)$; if $\mu = 0$ there is only one trivial fixed point, located at the 1-degenerate T-singularity of coordinates $(0, 0, 0)$; and if $\mu < 0$ there are no trivial fixed points. In fact, since $P(x_0, y_0, 0, 0) = (x_0, y_0)$,

$$\lim_{t_1 \to 0} f(x_0, y_0, t_1) = y_0 - x_0^2 + \mu = 0,$$

$$\widetilde{g}(x_0, y_0, 0, 0) = -y_0 - x_0^2 + \mu = 0,$$

that is, the trivial fixed points have coordinates $(\sqrt{\mu}, 0)$ and $(-\sqrt{\mu}, 0)$, whenever $\mu \geq 0$. Any other fixed point $(\widehat{x}_0, \widehat{y}_0)$ of P-map, with $\widehat{t}_1 > 0$ and $\widehat{t}_2 > 0$, must meet $(\widehat{x}_0, \widehat{y}_0, 0) \in \Sigma_c^+$. Such a fixed point in the crossing region indicates the presence of a CLC in the phase portrait of system (6.59).

Remark 6.6. *If $(\widehat{x}_0, \widehat{y}_0)$ is a fixed point of the map $P = P_- \circ P_+$ and $\widehat{\mathbf{x}}_0 = (\widehat{x}_0, \widehat{y}_0, 0) \in \Sigma_c^+$, then $\widehat{\mathbf{x}}_0$ is a crossing point of the CLC with the plane $z = 0$. Consequently, $(\widehat{x}_1, \widehat{y}_1)$ is a fixed point of the map $P = P_+ \circ P_-$ such that $\widehat{\mathbf{x}}_1 = (\widehat{x}_1, \widehat{y}_1, 0) \in \Sigma_c^-$ is the another crossing point of the CLC with the plane $z = 0$.*

Proposition 6.5. *We defined the set*

$$\Omega = \{(a, \tau) \in \mathbb{R}^2 : \tau > 0, a \neq 0, \psi_1(a, \tau) < 0 < \psi_2(a, \tau)\},$$

where

$$\psi_1(a, \tau) = -\frac{1}{a} + \frac{1 - 8a}{8a(1 - e^{a\tau})}\tau + \frac{1 + e^{a\tau}}{16(e^{a\tau} - 1)^2}\tau^2, \tag{6.71}$$

$$\psi_2(a, \tau) = 24 + \frac{3}{a} + \frac{1 + 2e^{a\tau}}{1 - e^{a\tau}}\tau. \tag{6.72}$$

For each $(a, \tau) \in \Omega$ there is a $\mu = \widehat{\mu}(a, \tau)$, where

$$\widehat{\mu}(a, \tau) = \frac{6 + a(48 + a\tau^2) - 3a(1 + 8a)\tau coth[\frac{a\tau}{2}]}{96a^2}, \tag{6.73}$$

so that the phase portrait of system (6.59) has a CLC transversely intersecting the plane $z = 0$ at the points $\widehat{\mathbf{x}}_0 = (\widehat{x}_0, \widehat{y}_0, 0) \in \Sigma_c^+$ and $\widehat{\mathbf{x}}_1 = (\widehat{x}_1, \widehat{y}_1, 0) \in \Sigma_c^-$, with coordinates expressed by parametric equations

$$\widehat{x}_0(a, \tau) = \frac{1 + (a\tau - 1)e^{a\tau}}{4a(e^{a\tau} - 1)}, \tag{6.74}$$

$$\widehat{y}_0(a, \tau) = \frac{48 - 3(1 - 24a)\tau - a\tau^2 - 4e^{a\tau}(24 + 24a\tau + a\tau^2)}{96a(e^{a\tau} - 1)^2} + \tag{6.75}$$

$$+\frac{e^{2a\tau}(48+3(1+8a)\tau-a\tau^2)}{96a(e^{a\tau}-1)^2},$$

$$\widehat{x}_1(a,\tau)=-\tau/4+\widehat{x}_0(a,\tau), \tag{6.76}$$

$$\widehat{y}_1(a,\tau)=\tau+\widehat{y}_0(a,\tau). \tag{6.77}$$

Proof. Assume that for given $a\neq 0$ and μ the system (6.59) has a CLC transversely intersecting the plane $z=0$ at points $\widehat{\mathbf{x}}_1\in\Sigma_c^-$ and $\widehat{\mathbf{x}}_0\in\Sigma_c^+$, with *return times* $\widehat{t}_1>0$ and $\widehat{t}_2>0$ in the zones $z>0$ and $z<0$, respectively. Then, the values $\widehat{x}_0$, $\widehat{y}_0$, $\widehat{x}_1$, $\widehat{y}_1$, $\widehat{t}_1$ and $\widehat{t}_2$ satisfy the closing equations

$$\begin{aligned}(x_1,y_1)&=P_+(x_0,y_0,t_1),\\ 0&=f(x_0,y_0,t_1)\\ (x_0,y_0)&=P_-(x_1,y_1,t_2),\\ 0&=g(x_1,y_1,t_2).\end{aligned}$$

Note from (6.61), (6.64) and (6.65) that $t_1=t_2=y_1-y_0=4(x_0-x_1)$. Then we defined $\tau=\widehat{t}_1=\widehat{t}_2$ and consequently $\widehat{x}_1=-\tau/4+\widehat{x}_0$ and $\widehat{y}_1=\tau+\widehat{y}_0$. We use $\tau>0$ as auxiliary parameter and we solve the equations

$$\begin{aligned}\widehat{x}_0-\frac{1}{4}\tau&=\widehat{x}_0e^{-a\tau}+\frac{1}{4}q(\tau),\\ 0&=\frac{p(\tau)}{q(\tau)}-\frac{e^{-a\tau}}{2a}\left[1+\frac{\tau}{q(\tau)}\right]\widehat{x}_0+\widehat{y}_0+\widehat{\mu}-e^{-a\tau}\widehat{x}_0^2,\\ 0&=-\frac{1}{48}\tau^2+\frac{1}{4}(\widehat{x}_0-2)\tau-\widehat{y}_0-\widehat{x}_0^2+\widehat{\mu},\end{aligned}$$

to $(\widehat{x}_0,\widehat{y}_0,\widehat{\mu})$ and so we get the searched solutions (6.73), (6.74) and (6.75), defined for $a\neq 0$ and $\tau>0$. The constraint $\widehat{\mathbf{x}}_0\in\Sigma_c^+$ is violated when $L_{\mathbf{F}_\mu^-}h(\widehat{\mathbf{x}}_0)=0$ and the constraint $\widehat{\mathbf{x}}_1\in\Sigma_c^-$ is violated when $L_{\mathbf{F}_{\mu,0}^+}h(\widehat{\mathbf{x}}_1)=0$. So, to have $\widehat{\mathbf{x}}_0\in\Sigma_c^+$ and $\widehat{\mathbf{x}}_1\in\Sigma_c^-$ is necessary $L_{\mathbf{F}_{\mu,0}^+}h(\widehat{\mathbf{x}}_1)<0<L_{\mathbf{F}_\mu^-}h(\widehat{\mathbf{x}}_0)$. As $L_{\mathbf{F}_\mu^-}h(\widehat{\mathbf{x}}_0)=\frac{\tau}{48}\psi_2(a,\tau)$ and $L_{\mathbf{F}_{\mu,0}^+}h(\widehat{\mathbf{x}}_1)=\psi_1(a,\tau)$, then $\widehat{\mathbf{x}}_0\in\Sigma_c^+$ and $\widehat{\mathbf{x}}_1\in\Sigma_c^-$ for all $a\neq 0$ and

$\tau > 0$ fulfilling $\psi_1(a,\tau) < 0 < \psi_2(a,\tau)$. Therefore, for each $(a,\tau) \in \Omega$ there is a $\mu = \widehat{\mu}(a,\tau)$ (see equation (6.73)) for which system (6.59) presents a CLC in its phase portrait. All CLC has period 2τ and transversely intersect the plane $z = 0$ at the points $\widehat{\mathbf{x}}_1 \in \Sigma_c^-$ and $\widehat{\mathbf{x}}_0 \in \Sigma_c^+$, whose coordinates are expressed by parametric equations (6.74)-(6.77). □

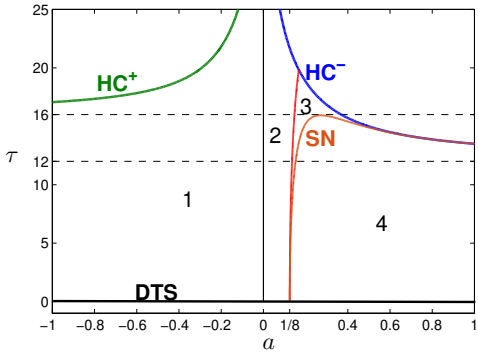

Figure 6.16: Ω-Domain of CLCs in the (a,τ)-plane. Regions 1, 2, 3 and 4 are demarcated by solid lines. The curves of green and blue color indicate a *non-standard* homoclinic bifurcation, denoted by HC^+ and HC^-, respectively; the curve of orange color indicates a saddle-node bifurcation, denoted by SN; the horizontal black line indicates a double TS-bifurcaton, denoted by DTS.

The set Ω defined in Proposition 6.5 is geometrically represented in the (a,τ)-plane of the Figure 6.16, from the regions 1, 2 3 and 4, including the borders 2-3 and 3-4. The regions are defined by

$$\Omega_1 = \{\tau > 0,\ a < 0 \text{ and } \psi_1(a,\tau) < 0\},$$
$$\Omega_2 = \{\tau > 0,\ a > 0,\ \psi_2(a,\tau) > 0 \text{ and } \widehat{\mu}(a,\tau) \geq 0\},$$
$$\Omega_3 = \{\tau > 0,\ a > 0,\ \psi_2(a,\tau) > 0 \text{ and } \widehat{\mu}(a,\tau) \leq 0 < \frac{\partial \widehat{\mu}}{\partial \tau}(a,\tau)\},$$
$$\Omega_4 = \{\tau > 0,\ a > 0, \text{ and } \frac{\partial \widehat{\mu}}{\partial \tau}(a,\tau) < 0\},$$

and, its borders, are defined by

$$\begin{aligned} HC^+ &= \{\tau > 0,\ a < 0\ : \psi_1(a,\tau) = 0\},\\ HC^- &= \{\tau > 0,\ a > 0\ : \psi_2(a,\tau) = 0\},\\ SN &= \{\tau > 0,\ a > 0\ : \frac{\partial \widehat{\mu}}{\partial \tau}(a,\tau) = 0\}. \end{aligned}$$

In Figure 6.16, for any point (a,τ) taken in regions 1, 2, 3 and 4, including the borders 2-3 and 3-4, there is a CLC. For any point (a,τ) on the green curve, of equation $\psi_1(a,\tau) = 0$, the CLC touches the tangency line T_+ at a visible fold point and then appears a type of homoclinic loop which is associated with the vanishing (or birth) of this CLC[3]. For any point (a,τ) on the blue curve, of equation $\psi_2(a,\tau) = 0$, the CLC touches the tangency line T_- at a visible fold point and then appears a type of homoclinic loop which is associated with the vanishing (or birth) of this CLC[4]. For any (a,τ) on the red curve occurs $\widehat{\mu}(a,\tau) = 0$, being $\widehat{\mu} < 0$ in regions 1 and 2 and $\widehat{\mu} > 0$ in 3 and 4. For any point (a,τ) on the orange curve we obtain $\frac{\partial \widehat{\mu}}{\partial \tau}(a,\tau) = 0$, that is, this curve indicates a saddle-node bifurcation of CLCs.

We assume $(a,\tau) \in \Omega = \Omega_1 \cup \Omega_2 \cup \Omega_3 \cup \Omega_4 \cup SNB$. The Jacobian matrix of (6.68), denoted by DP, is defined by

$$DP(a,\tau) = DP_-(\widehat{\mathbf{p}}_1(a,\tau)) \cdot DP_+(\widehat{\mathbf{p}}_0(a,\tau)),$$

where

$$\widehat{\mathbf{p}}_1(a,\tau) = (\widehat{x}_1(a,\tau), \widehat{y}_1(a,\tau), \tau)$$

and

$$\widehat{\mathbf{p}}_0(a,\tau) = (\widehat{x}_0(a,\tau), \widehat{y}_0(a,\tau), \tau).$$

Matrices DP_+ and DP_- are given in (6.63) and (6.67), respectively. We denote by $\rho_{1,2}$ the eigenvalues of DP. It is easy to numerically verify the following statements.

[3]The fixed point (x_1, y_1) leaves the region Σ_c^- by a visible fold point at T_+.
[4]The fixed point (x_0, y_0) leaves the region Σ_c^+ by a visible fold point at T_-.

(a) For all $(a,\tau) \in \Omega$ the eigenvalues $\rho_{1,2}(a,\tau)$ are real, i.e., CLC with saddle or node dynamics.

(b) For all $(a,\tau) \in \Omega_1$ we obtain $\rho_{1,2}(a,\tau) > 1$, i.e., unstable (node) CLC.

(c) For all $(a,\tau) \in \Omega_2 \cup \Omega_3$ we obtain $\rho_1(a,\tau) < 1$ and $\rho_2(a,\tau) > 1$, i.e., unstable (saddle) CLC.

(d) For all $(a,\tau) \in \Omega_4$ we obtain $\rho_{1,2}(a,\tau) < 1$, i.e., stable (node) CLC.

(e) For all $(a,\tau) \in SN$ we obtain $\rho_1(a,\tau) < 1$ and $\rho_2(a,\tau) = 1$, i.e., semi-stable (saddle-node) CLC, created by the collision between a CLC of the stable node type and other of the saddle type.

(f) For any $a \neq 0$ we obtain $\lim_{\tau\to 0^+} \rho_{1,2}(a,\tau) = 1$.

Example 6.3. *There is a stable (node) CLC in system* (6.59) *when* $\nu = 0$, $a = 1$ *and* $\mu = -0.1$, *as shown in Figure 6.14(a). We solve numerically the equation* $\widehat{\mu}(1,\tau) = -0.1$ *and we find* $\tau = 1.71$ *as unique solution*[5]. *Consequently, we obtain the eigenvalues* $\rho_1(1,1.71) = 0.18$ *and* $\rho_2(1,1.71) = 0.37$. *So, this CLC has dynamics of the stable node type. The same can be done to verify the stability of the CLC shown in Figure 6.14(b), now for* $a = -1$ *and* $\mu = 0.5$. *In this case we find* $\tau = 3.49$ *as unique solution and, consequently, the eigenvalues* $\rho_1(-1,3.49) = 14.3$ *and* $\rho_2(-1,3.49) = 34.7$. *So, this CLC has dynamics of the unstable node type.*

From the branch solutions

$$\xi_a(\tau) = (\widehat{x}_0(a,\tau), \widehat{y}_0(a,\tau), \widehat{x}_1(a,\tau), \widehat{y}_1(a,\tau), \widehat{\mu}(a,\tau)),$$

dependent on the parameter $a \neq 0$, we calculate $\lim_{\tau\to 0^+} \xi_a(\tau) = (0,0,0,0,0)$. So, when $\tau \to 0^+$ the CLC is approaching its point of birth, located at the point $(0,0,0) \in \Sigma$ for $\mu = 0$ (i.e., located at the

[5]Approximated values of τ and ρ_{12}.

1-degenerate T-singularity). We assume $|\mu|$ small, then a CLC is born for $\mu > 0$ if $a \leq \frac{1}{8}$ and for $\mu < 0$ if $a > \frac{1}{8}$, since

$$\begin{aligned}
\lim_{\tau\to 0^+} \widehat{\mu}(a,\tau) &= 0,\\
\lim_{\tau\to 0^+} \frac{\partial\widehat{\mu}}{\partial\tau}(a,\tau) &= 0,\\
\lim_{\tau\to 0^+} \frac{\partial^2\widehat{\mu}}{\partial\tau^2}(a,\tau) &= \frac{1-8a}{96},\\
\lim_{\tau\to 0^+} \frac{\partial^3\widehat{\mu}}{\partial\tau^3}(1/8,\tau) &= 0,\\
\lim_{\tau\to 0^+} \frac{\partial^4\widehat{\mu}}{\partial\tau^4}(1/8,\tau) &= \frac{1}{15360} > 0.
\end{aligned}$$

But until when the CLC persists, ie, what is the interval for μ such that there is a CLC? Is there only one, or can there be more than one CLC simultaneously for same μ value?

In order to answer this questions asked above, let us look at Figure 6.16. Taking $a < 0$ there is a $\tau = \tau_{max}(a)$ satisfying $\psi_1(a, \tau_{max}) = 0$, so that $\tau_{max} \to \infty$ when $a \to 0^-$ and for $a \to -\infty$ we have $\tau_{max}(a) \to 16$. So, if $a < 0$ for all τ fulfilling $0 < \tau < \tau_{max}(a)$ there is a CLC defined. This CLC is unique since $\widehat{\mu}(a,\tau) > 0$ and $\frac{\partial\widehat{\mu}}{\partial\tau}(a,\tau) > 0$ for all $(a,\tau) \in \Omega_1$. In this case, if $a < 0$ then there is only one CLC for all $\mu \in (0, \mu_{g^+}(a))$, where $\mu_{g^+}(a) = \widehat{\mu}(a, \tau_{max}(a))$.

Taking $a > 0$ there is a $\tau = \tau_{max}(a)$ satisfying $\psi_2(a, \tau_{max}) = 0$, so that for each $\tau \in (0, \tau_{max})$ a CLC is defined. In addition, for $a \to +\infty$ we have $\tau_{max}(a) \to 12$ and for $a \to 0^+$ we have $\tau_{max}(a) \to +\infty$. However, if $a > \frac{1}{8}$ then there is $\tau = \tau_{sn}(a) \in (0, \tau_{max}(a))$ satisfying $\frac{\partial\widehat{\mu}}{\partial\tau}(a,\tau_{sn}) = 0$, $\frac{\partial^2\widehat{\mu}}{\partial\tau^2}(a,\tau_{sn}) > 0$ and $\widehat{\mu}(a,\tau_{sn}) < 0$. We defined $\mu_{sn}(a) = -\widehat{\mu}(a,\tau_{sn}) > 0$ and then we ensure that for a $\mu > -\mu_{sn}$ and close to the critical value $-\mu_{sn}$, two CLCs coexist. Both collide when $\mu = -\mu_{sn}$ and disappear for $\mu < -\mu_{sn}$, as in a Saddle-Node bifurcation of limit cycles.

Example 6.4. *If we fixed $a = -1$, from the equation $\psi_1(-1, \tau_{max}) = 0$ we obtain $\tau_{max} = 17.06$ and then $\mu_{g^+} = \widehat{\mu}(-1, 17.06) = 6.33$, that is,*

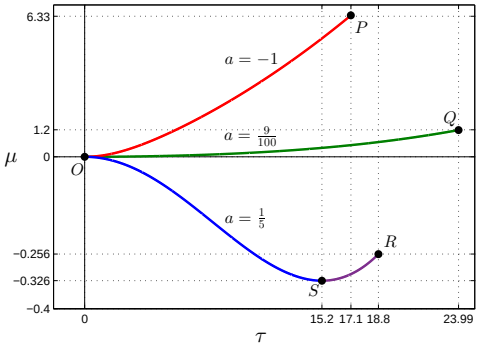

Figure 6.17: Bifurcations diagram in the (τ, μ)-plane, being $\tau = \widehat{y}_1 - \widehat{y}_0 = -4(\widehat{x}_1 - \widehat{x}_0)$. The branches are obtained by $\mu = \widehat{\mu}(-1, \tau)$ (red), $\mu = \widehat{\mu}(0.09, \tau)$ (green) and $\mu = \widehat{\mu}(0.2, \tau)$ (blue-purple), for $\tau \in (0, \tau_{max})$. A double TS-bifurcation occurs at point $O(0, 0)$. At points $P(\tau_{max}, \mu_{g^+})$, $Q(\tau_{max}, \mu_{g^-})$ and $R(\tau_{max}, \mu_{g^-})$, the CLC collapses in the tangency line T_-. At $S(\tau_{sn}, \mu_{sn})$ a saddle-node bifurcation occurs.

for all $\mu \in (0, 6.33)$ the system (6.59) has a CLC[6]. This CLC is unstable with node dynamics, since $(-1, \tau) \in \Omega_1$. See Figure 6.17, where the red color curve segment indicates the range of μ for which there is a CLC. Note in Figure 6.18(a), of stability analysis, that both eigenvalues (real) have an absolute value greater than 1.

Example 6.5. *Another unstable CLC is found if $a = 0.09$. From the equation $\psi_2(0.09, \tau_{max}) = 0$ we obtain $\tau_{max} = 23.99$ and then $\mu_{g^-} = \widehat{\mu}(0.09, 23.99) = 1.2$, that is, for all $\mu \in (0, 1.2)$ the system (6.59) has a CLC. This CLC is unstable with saddle dynamics, since $(0.09, \tau) \in \Omega_2$. See Figure 6.17, where the green color curve segment indicates the range of μ for which there is a CLC. The stability analysis shown in Figure 6.18(b), reveals positive eigenvalues one with absolute value greater than 1 and the other less than 1.*

[6]Approximated values of τ_{max} and $\mu_g^{\pm}$. We use Figure 6.16 for an initial condition choice in the resolution of the equations $\psi_1(-1, \tau_{max}) = 0$, $\psi_2(0.09, \tau_{max}) = 0$, $\psi_2(0.2, \tau_{max}) = 0$ and $\frac{\partial \widehat{\mu}}{\partial \tau}(0.2, \tau_{sn}) = 0$.

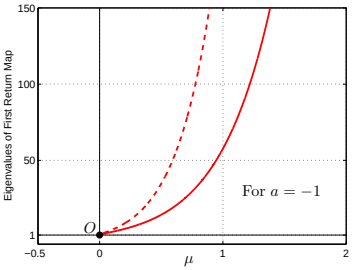

(a) For $a = -1$.

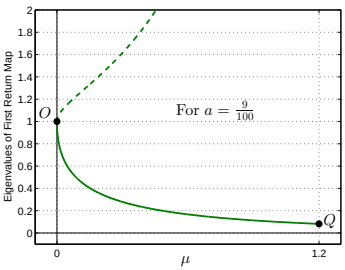

(b) For $a = \frac{9}{100}$.

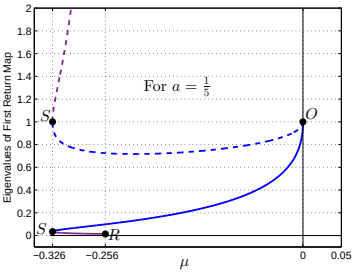

(c) For $a = \frac{1}{5}$.

Figure 6.18: Numerical analysis of stability. The branches are obtained by vector equations $\vec{r}_1(\tau) = (\bar{\mu}(\tau), \bar{\rho}_1(\tau))$ (solid branches) and $\vec{r}_2(\tau) = (\bar{\mu}(\tau), \bar{\rho}_2(\tau))$ (dashed branches), where $\bar{\rho}_1(\tau) = \rho_1(a, \tau)$, $\bar{\rho}_2(\tau) = \rho_2(a, \tau)$ and $\bar{\mu}(\tau) = \widehat{\mu}(a, \tau)$ for the constants $a = -1$, $a = \frac{9}{100}$ or $a = \frac{1}{5}$ and for all $\tau \in (0, \tau_{max})$.

Example 6.6. *More special case, occurring a Saddle-Node bifurcation of CLCs, is obtained by taking* $a = \frac{1}{5}$. *From the equations* $\frac{\partial \widehat{\mu}}{\partial \tau}(0.2, \tau_{sn}) = 0$ *and* $\psi_2(0.2, \tau_{max}) = 0$ *we obtain* $\tau_{sn} = 15.2$ *and* $\tau_{max} = 18.8$. *The critical values* $\mu_{sn} = \widehat{\mu}(0.2, 15.2) = -0.326$ *and* $\mu_{g^-} = \widehat{\mu}(0.2, 15.2) = -0.256$ *are obtained. There is a stable CLC with node dynamics for all* $\mu \in (0, \mu_{sn})$, *since* $(0.2, \tau) \in \Omega_3$ *whenever* $0 < \tau < \tau_{sn}$. *Also there is an unstable CLC with saddle dynamics for all* $\mu \in (\mu_{g^-}, \mu_{sn})$, *since* $(0.2, \tau) \in \Omega_4$ *whenever* $\tau_{sn} < \tau < \tau_{max}$.

In Figure 6.17 the blue (purple) color curve segment indicates

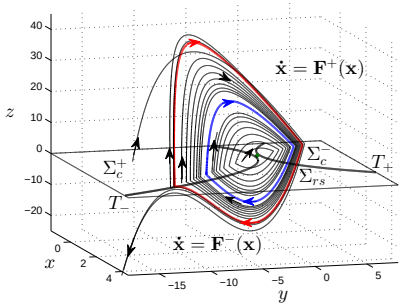

(a) For $a = 0.2$, $\nu = 0$ and $\mu = -0.29$.

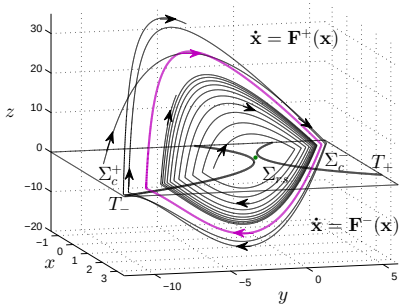

(b) For $a = 0.2$, $\nu = 0$ and $\mu = -0.326$.

Figure 6.19: Simulations of system (6.59) in state space. In (a) we visualized two CLCs, an unstable of the saddle type (red) and another stable of the node type (blue), and in (b) a semi-stable CLC of the saddle-node type (purple). In both, the green point in Σ_{rs} represents the trivial pseudo-saddle.

the range of μ for which there is a stable (unstable) CLC. Note that for two different values of τ, near to τ_{sn}, we obtain a same value for μ, thus indicating the presence of two CLCs, simultaneously, in the phase portrait of the system (6.59)*. The stability analysis shown in Figure 6.18(c), reveals two pair of positive eigenvalues, one pair with both eigenvalues less than 1 and the other pair with one eigenvalue greater than 1 and other less than 1.*

A Saddle-Node bifurcation of CLCs occurs in system (6.59)[7] for any $a > \frac{1}{8}$ and $\mu = \mu_{sn}(a)$, where $\mu_{sn}(a) = \widehat{\mu}(a, \tau_{sn}(a))$. Figure 6.19 shows simulations of system (6.59) in state space, where we visualize, for $\mu = -0.29 > \mu_{sn}(0.2)$, the coexistence of two CLCs of opposite stabilities and then, for $\mu = -0.326 = \mu_{sn}(0.2)$, the collision of these CLCs. Soon after, for $\mu < \mu_{sn}(0.2)$, there are no more CLCs in the phase portrait of (6.59).

To conclude this section, from the results of the existence and stability analysis of CLCs for system (6.59) held here, we state the following lemma.

Lemma 6.2. *We defined the values* $\mu_{sn}(a) = -\widehat{\mu}(a, \tau_{sn}(a)) > 0$ *for any* $a \neq 0$ *and* $\tau_{sn}(a) > 0$ *satisfying* $\frac{\partial \widehat{\mu}}{\partial \tau}(a, \tau_{sn}) = 0$, $\mu_{g^+}(a) = \widehat{\mu}(a, \tau_{max}(a))$ *for any* $a < 0$ *and* $\tau_{max}(a) > 0$ *satisfying* $\psi_1(a, \tau_{max}) = 0$, *and* $\mu_{g^-}(a) = \widehat{\mu}(a, \tau_{max}(a))$ *for any* $a > 0$ *and* $\tau_{max}(a) > 0$ *satisfying* $\psi_2(a, \tau_{max}) = 0$, *where* $\psi_1(a, \tau)$, $\psi_2(a, \tau)$ *and* $\widehat{\mu}(a, \tau)$ *are given in* (6.71), (6.72) *and* (6.73), *respectively. With regard to the phase portrait of system* (6.59), *we can state the following.*

(a) If $a < 0$ *then for all* $\mu \in (0, \mu_{g^+}(a))$ *there is an unstable CLC with node dynamics.*

(b) If $0 < a \leq \frac{1}{8}$ *then for all* $\mu \in (0, \mu_{g^-}(a))$ *there is an unstable CLC with saddle dynamics.*

(c) If $a > \frac{1}{8}$ *then,*

(c.1) for all $\mu \in (-\mu_{sn}(a), 0)$ *there is a stable CLC with node dynamics.*

(c.2) for all $\mu \in (-\mu_{sn}(a), \mu_{g^-}(a))$ *there is an unstable CLC with saddle dynamics.*

(c.3) both stable node and saddle CLCs coexist for all $\mu \in (-\mu_{sn}(a), 0)$ *if* $\mu_{g^-}(a) \geq 0$, *or for all* $\mu \in (-\mu_{sn}(a), \mu_{g^-}(a))$ *if* $\mu_{g^-}(a) < 0$.

[7] Keeping $\nu = 0$.

6.6 Conclusion

The analysis performed along the Chapter shows that systems with two T-singularities can present interesting bifurcations as the fold bifurcation of T-singularities, the TS-bifurcation and the double TS-bifurcation. Such bifurcations are said to be *compound*, since they are characterized by standard bifurcations occurring simultaneously in the sliding vector field and in the first return map. We have presented a detailed analysis of the sliding and crossing dynamics around the T-singularities, regular or degenerate, and also the sliding dynamics at the pseudo-equilibrium. From the case study, we have proved the existence of up to two CLCs, the stability and bifurcations involving such CLCs.

6.7 Appendix A: Proof of Theorem 6.1

We represent the state variables of system (6.1) as $\mathbf{x} = (x_1, x_2, x_3)$. From the hypothesis **(H1)** we write

$$\widetilde{f}_{\mu}^{+}(x_1, x_2) = a_0^{+}\mu + a_{10}^{+}x_1 + a_{01}^{+}x_2 + \sigma_{\mu}^{+}(x_1, x_2),$$
$$\widetilde{f}_{\mu}^{-}(x_1, x_2) = \mu + a_{10}^{-}x_1 + a_{01}^{-}x_2 + \sigma_{\mu}^{-}(x_1, x_2),$$

where $\sigma_{\mu}^{\pm}$ are polynomial functions of (x_1, x_2), may be dependent on the parameter μ, and such that $\sigma_{\mu}^{\pm}(\mathbf{0}) = \frac{\partial \sigma_0^{\pm}(\mathbf{0})}{\partial x_1} = \frac{\partial \sigma_0^{\pm}(\mathbf{0})}{\partial x_2} = 0$. Note that $\sigma_{\mu}^{\pm}$ represent the non linear parts of $\widetilde{f}_{\mu}^{\pm}$. Moreover, the coefficients of linear part of $\widetilde{f}_{\mu}^{\pm}$ must satisfy

$$a_{10}^{+}a_{01}^{-} = a_{01}^{+}a_{10}^{-}.$$

The matrix Q of **(H1)** is

$$Q = \begin{pmatrix} a_{10}^{+} & a_{01}^{+} & a_0^{+} \\ a_{10}^{-} & a_{01}^{-} & 1 \\ a_1 & a_2 & a_3 \end{pmatrix},$$

where $a_1 = \frac{\partial n}{\partial x_1}(\mathbf{0})$, $a_2 = \frac{\partial n}{\partial x_2}(\mathbf{0})$ and $a_3 = \frac{\partial n}{\partial \mu}(\mathbf{0})$, and $n(x_1, x_2, \mu) = \frac{\partial \widetilde{f}_{\mu}^{+}}{\partial x_1}\frac{\partial \widetilde{f}_{\mu}^{-}}{\partial x_2} - \frac{\partial \widetilde{f}_{\mu}^{-}}{\partial x_1}\frac{\partial \widetilde{f}_{\mu}^{+}}{\partial x_2}$. Since, $\mathrm{Det}[Q] \neq 0$ then the linear part of $\widetilde{f}_{\mu}^{\pm}$ must be non null. So, we assume that $a_{01}^{-} \neq 0$.

The new state variables are:

$$y = -a_{10}^{-}x_1 - a_{01}^{-}x_2, \tag{6.78}$$
$$x = x_1. \tag{6.79}$$

From this change of variables, we rewrite $\widetilde{f}_{\mu}^{\pm}$ as

$$\widetilde{\widetilde{f}}_{\mu}^{+}(x, y) = a\varepsilon\mu - \varepsilon y + \widetilde{\sigma}_{\mu}^{+}(x, y),$$
$$\widetilde{\widetilde{f}}_{\mu}^{-}(x, y) = \mu - y + \widetilde{\sigma}_{\mu}^{-}(x, y),$$

where $\varepsilon = \frac{a_{01}^+}{a_{01}^-} \neq 0$ and $a = \frac{a_0^+}{\varepsilon}$. Note that $\varepsilon \neq 0$, since the hypothesis **(H1)** ensures that both the graphs of the implicit equations $\widetilde{\widetilde{f}}_\mu^{\pm}(x,y) = 0$ are smooth curves at $(x,y,\mu) = (0,0,0)$, that is, $\frac{\partial \widetilde{\widetilde{f}}_0^{\pm}(0,0)}{\partial(x,y)} \neq (0,0)$.

We recalculate the matrix Q and its determinant, and we get

$$\widetilde{Q} = \begin{pmatrix} 0 & -\varepsilon & a\varepsilon \\ 0 & -1 & 1 \\ \widetilde{a}_1 & \widetilde{a}_2 & \widetilde{a}_3 \end{pmatrix}$$

and $\mathrm{Det}[\widetilde{Q}] = \varepsilon(a-1)\widetilde{a}_1 \neq 0$. Therefore, we must have $a \neq 1$ and $\widetilde{a}_1 = \varepsilon(e^- - e^+) \neq 0$, that is, $e^- \neq e^+$, where $e^- = \frac{\partial^2 \widetilde{\sigma}_\mu^-}{\partial x^2}$ and $e^+ = \frac{1}{\varepsilon}\frac{\partial^2 \widetilde{\sigma}_\mu^+}{\partial x^2}$ for $(x,y,\mu) = (0,0,0)$.

Finally, by applying the change of variables given in (6.78)-(6.79) to the system (6.1), we rewrite it in a form as in (6.5)-(6.7) of Theorem 6.1.

6.8 Appendix B: Proof of Theorem 6.2

Consider the system (6.5)-(6.7) rewrite as

$$\frac{d}{d\tau}(x_1,x_2,x_3) = \begin{cases} \mathbf{F}_u^-(x_1,x_2,x_3), & \text{if } x_3 < 0 \\ \mathbf{F}_u^+(x_1,x_2,x_3), & \text{if } x_3 > 0, \end{cases}$$

with vector fields defined by

$$\mathbf{F}_u^-(\mathbf{x}) = \begin{bmatrix} c^- + p_u^-(\mathbf{x}) \\ b^- + q_u^-(\mathbf{x}) \\ u - x_2 + e^- x_1^2 + r_u^-(\mathbf{x}) \end{bmatrix}$$

and

$$\mathbf{F}_u^+(\mathbf{x}) = \begin{bmatrix} c^+ + p_u^+(\mathbf{x}) \\ b^+ + q_u^+(\mathbf{x}) \\ \varepsilon\left(au - x_2 + e^+ x_1^2 + r_u^+(\mathbf{x})\right) \end{bmatrix},$$

for all $\mathbf{x} = (x_1, x_2, x_3) \in K$ and $|u|$ small. We assume that $\varepsilon > 0$, $e^- < 0$, $e^+ > 0$, $b^+ > 0$ and $b^- < 0$, and we defined the coefficients

$$\alpha = \frac{1-a}{1+k} \neq 0,$$
$$\beta = \frac{a+k}{1+k}.$$

To write the system (6.5)-(6.7) in the local canonical form given in (6.8)-(6.10), just apply the change of variables of the state and time, besides the definition of new parameters according to Table 6.1. The new polynomial functions are get by $p_1 = \frac{p_0^-}{-b^-\sqrt{-e^-}}$, $p_2 = \frac{p_0^+}{b^+\sqrt{-e^-}}$, $q_1 = \frac{q_0^-}{-b^-}$, $q_2 = \frac{q_0^+}{b^+}$, $r_1 = \frac{r_0^-}{-b^-}$ and $r_2 = \frac{r_0^+}{b^+}$.

State and time variables	Parameters
$t = -b^-\tau$ for $z < 0$	$c_1 = \frac{c^-}{-b^-\sqrt{-e^-}}$
$t = b^+\tau$ for $z > 0$	$\varepsilon_1 = \frac{1}{-b^-} > 0$
$x = \sqrt{-e^-}x_1$	$c_2 = \frac{c^+}{b^+\sqrt{-e^-}}$
$y = x_2 - \beta u$	$\varepsilon_2 = \frac{\varepsilon}{b^+} > 0$
$z = x_3$	$k = -\frac{e^+}{e^-} > 0$
	$\mu = \alpha u$

Table 6.1: Normalization

Chapter 7

Boundary Equilibrium Bifurcations in a Family of 3D-DPWL Systems

In this Chapter we study a family of discontinuous piecewise-smooth systems in $\mathbb{R}^3$ whose vector fields are linear on both sides of the switching boundary, which we call 3D-DPWL systems. Furthermore, we are interested in systems with two parallel tangency lines containing a cusp point each. This configuration is observed in piecewise-linear control systems in which the control action is discontinuous such as the Sliding Mode Control (SMC). We consider a general system of this class and then derive a canonical form to reduce the number of system parameters. The general objective in this Chapter is, from the canonical form, to perform an analysis of the equilibria, stability, sliding dynamics and boundary equilibrium bifurcations (BEBs). The main result is the classification of the BEBs and its unfoldings in the sliding vector field. This and others results obtained on the existence and stability of equilibria are applied in two practical examples involving the SMC of dc-dc buck power converters.

7.1 Introduction

Bifurcations in DPWS systems (or Filippov systems) have motivated many works over the years. We highlight here the so-called *Boundary Equilibrium Bifurcations* (BEBs), see for instance [13, 44, 45, 55, 67, 78]. The BEBs are part of the *Discontinuous-Induced Bifurcations* (DIBs), occurring generically by varying one single parameter (codimension-one local bifurcation). The DIBs are unique bifurcations of piecewise-smooth systems. Such bifurcations occur when an invariant set of the system (equilibrium point, limit cycle, etc), crosses or touches tangentially the switching boundary Σ of this system, see [42] and references therein.

The BEBs can trigger varied and complex phenomena, such as the birth of periodic orbits with a sliding part or even strange attractors, see for instance [61]. But, with regard to the position of the equilibria involved[1], in relation to the boundaries of their respective vector fields, there are two generic scenarios according to [37, 93], both occurring by a one-parameter bifurcation:

(i) The *persistence* scenario is observed when a natural equilibrium turns into a pseudo-equilibrium. In this case, if the natural equilibrium is real (resp. virtual), then the pseudo-equilibrium is virtual (resp. real).

(ii) The *nonsmooth fold* scenario is observed when both a natural equilibrium and a pseudo-equilibrium collide and disappear. In this case, if the natural equilibrium is real (resp. virtual), then the pseudo-equilibrium is also.

The persistence of a single equilibrium indicates that both natural and pseudo equilibria do not coexist, as shown in Figure 7.1. In the nonsmooth fold scenario they collide and disappear, so that they can co-

[1] See definitions of the typical equilibria of DPWS systems in the preliminary Chapter 2, Section 2.3: natural equilibrium, pseudo-equilibrium and boundary equilibrium.

exist. Undoubtedly, persistence scenario with a real pseudo-equilibrium is ideal for the applications in sliding mode control systems, however this is not always possible. To determine which situation occurs for a given BEB in a DPWS system, we use Theorem 1 statement in [45], page 1382.

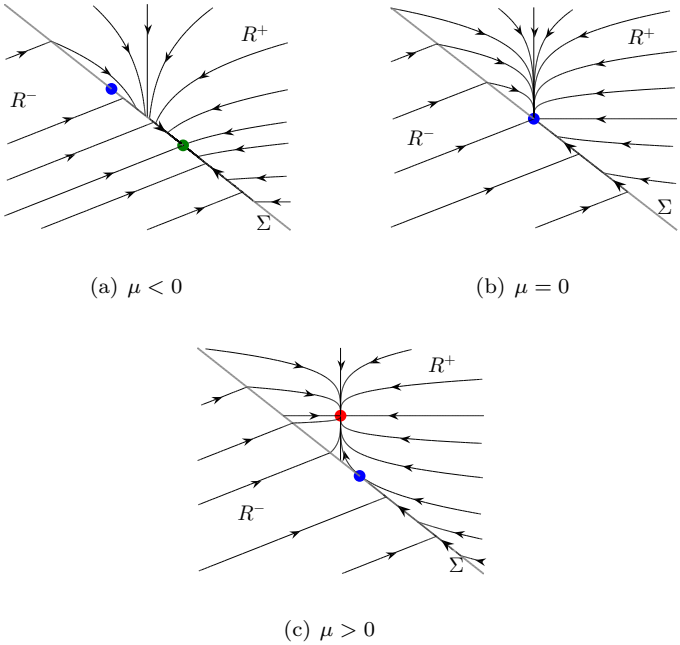

(a) $\mu < 0$ (b) $\mu = 0$

(c) $\mu > 0$

Figure 7.1: Boundary node collision in a persistence scenario of BEBs in system 7.1. The switching boundary is $\Sigma = \{(x, y) \in \mathbb{R}^2 : x + y = 0\}$, dividing the plane into two open regions: $R^+ = \{(x, y) \in \mathbb{R}^2 : x + y > 0\}$ and $R^- = \{(x, y) \in \mathbb{R}^2 : x + y < 0\}$. The green and blue dots in (a) are, respectively, the pseudo-equilibrium (real) and the invisible fold. The blue dot, in (b), is the boundary equilibrium. The red and blue dots in (c) are, respectively, the natural equilibrium (real) and the visible fold.

For two-dimensional dynamical systems we now know all the unfolding dynamics of the BEBs, having a total of twelve topologically distinct cases. The first classification of BEBs was given by Filippov

in [51], where were determined eight topologically distinct cases for the generic local dynamics at a boundary equilibrium. An almost complete list of their unfoldings of codimension-one, with ten cases, were described by Kuznetsov *et al.* in [78] and, the missing cases, have only recently been revealed by Hogan *et al.* in [67]. Other works with important results that deserve highlight are [22, 35, 45, 60, 64, 93].

Example 7.1. *In Figure 7.1 we see one of twelve distinct cases of BEBs. Such a generic unfolding is obtained, for example, by the variation of the parameter μ in the system*

$$(\dot{x},\dot{y}) = \begin{cases} \mathbf{F}^+(x,y) = (-4x, -y+\mu) & \text{if } x+y>0 \\ \mathbf{F}^-(x,y) = (2,1) & \text{if } x+y<0 \end{cases}. \tag{7.1}$$

For $\mu = 0$ a BEB persistence occurs at the boundary equilibrium located at $(0,0)$. Moreover, this BEB has as characteristic the persistence of the natural stable node equilibrium for $\mu > 0$ and of the stable pseudo-equilibrium for $\mu < 0$ (see BN_1 case in [78]). The nonsmooth fold scenario can be also observed at a boundary node equilibrium, if we take -1 instead of 1 in the second component of the constant vector field $\mathbf{F}^-$ (see Remark 4.2 in [64]).

There are few studies related to BEBs in $\mathbb{R}^3$, and the number of topologically distinct cases of BEBs in 3D-Filippov systems is not yet known. We highlight here the recent study of Simpson in [105], where a new normal form is proposed for BEBs in systems of any number of dimensions, and are provided numerical evidence for the emergence of chaotic attractors from BEBs. Another recent study, made by Glendinning in [61], have shown that the Shilnikov mechanism appears naturally in the unfolding of BEBs in $\mathbb{R}^3$, which are associated with the creation of complex orbits near other bifurcations of piecewise smooth systems.

The bifurcation theory for piecewise-smooth systems is still in evolution, and in this Chapter we intend to contribute to its development by presenting new results with respect to BEBs in $\mathbb{R}^3$. For

this, we derive a canonical form for 3D-DPWS systems of our interest and we perform a two-parameter analysis on the dynamic behaviour of these systems. In addition, we given the conditions on the parameters of the canonical form for a BEB to occur, classifying into *persistence* or *nonsmooth fold*. We also given a complete classification of the sliding dynamics at the pseudo-equilibrium (even when it becomes a boundary equilibrium), thus obtaining all the unfolding dynamics of the BEBs, persistence and nonsmooth fold, in the sliding vector field of systems reducible to canonical form in study.

The results obtained are applied in two practical examples involving the sliding mode control of dc-dc buck power converters. For a first application we use the model of a buck converter with sliding mode control and washout filter, where the stability and bifurcation of the pseudo-equilibrium, desired operation point for the converter, are completely determined from the canonical form. In our second application we used the model of a bidirectional buck converter feeding a constant power load, in which case the vector fields involved are nonlinear. From the linear version of this system around the boundary equilibrium point, we analyse the BEBs by applying the results obtained with the canonical form. For this second application we also present a partial analysis of other bifurcations of equilibria and limit cycles that may occur.

This Chapter is organized as follows. In the Section 7.2 we present the system model which will be the object of study in this chapter, ours objectives and also main results. In Section 7.3 we derive a canonical form for 3D-DPWS systems of our interest and then we describe the associated sliding vector field as well as dynamic characteristics on the switching boundary. Moreover, we analyse the existence of natural equilibria, pseudo-equilibria and boundary equilibria. The sliding dynamics at a pseudo-equilibrium point is investigated in Section 7.4. In Section 7.5 we study the BEBs and classify the different types of boundary equilibria with respect to the sliding dynamics in its neighborhood. The Sections 7.6 and 7.7 are dedicated to applications of the results obtained in previous sections.

Previous results on Filippov theory in Chapter 2 are important for the development that follows.

7.2 Setting the problem and main results

DPWS systems are often used as models of discontinuous control systems in various fields of science and engineering such as mechanical, electrical, biology, among others, see for instance [31, 80, 103, 123, 125].

In this chapter we study a particular class of 3D-DPWS systems that describe the dynamics of control systems of the form

$$\dot{\mathbf{x}} = P\mathbf{x} + \mathbf{n}u, \tag{7.2}$$

where $\mathbf{x}, \mathbf{n} \in \mathbb{R}^3$, P is a matrix of order 3 and the control signal u is supposed to be a scalar discontinuous function, piecewise-constant, as

$$u = \begin{cases} u^- & \text{if } h(\mathbf{x}) < 0 \\ u^+ & \text{if } h(\mathbf{x}) > 0 \end{cases}, \tag{7.3}$$

such that $u^- \neq u^+$. The scalar function $h : \mathbb{R}^3 \to \mathbb{R}$ must be designed to meet the control objectives, being usually defined as $h(\mathbf{x}) = \mathbf{k}^T(\mathbf{x}-\mathbf{x}_r)$, where $\mathbf{x}_r$ is the reference vector and $\mathbf{k}$ is the control parameter vector. The control theory for these variable structure systems is well known and is named as Sliding Mode Control (SMC), see [122].

System (7.2)-(7.3) in closed loop is rewritten as the discontinuous piecewise-linear system (DPWL system) given in (7.4). An important feature of these systems is that they have linear sliding vector field and thus exhibit, under certain conditions, only a pseudo-equilibrium. Even presenting linear vector fields, DPWL systems are rich in non-linear phenomena developed by the interaction of such vector fields with the discontinuity surface (switching boundary) $\Sigma = \{\mathbf{x} \in \mathbb{R}^3 : h(\mathbf{x}) = 0\}$. DPWL systems are widely used in SMC applications, in general for the study of its dynamic behaviour. Undoubtedly, the bifurcation theory

[37, 77] presents powerful tools for the analysis of nonlinear dynamics. From the analysis of bifurcations we can, for example, to determine the region in the space of system and control parameters where the control objectives are met, and thus design more efficient controllers capable of inhibiting the undesired dynamics caused by bifurcations; see for instance [29, 92].

The desired operating point of discontinuous control systems as (7.2)-(7.3), is a pseudo-equilibrium. In this sense, it is necessary to ensure, besides stability, that this pseudo-equilibrium point is real (admissible) and that it remains so after the variation in some system parameter. BEBs are responsible for the transition from real to virtual pseudo-equilibrium, and therefore the BEBs analysis should be considered as an important part of the control project, in order to prevent in order to prevent the occurrence of such undesired phenomenon.

Our objectives in this chapter are: (i) to describe the dynamic behaviour of discontinuous control systems as (7.2)-(7.3), reducible to a canonical form (see (7.5) at the next section); (ii) to establish the stability conditions at the pseudo-equilibrium point; (iii) to determine bifurcation mechanisms associated with BEBs in $\mathbb{R}^3$ and to classify the different unfoldings in the sliding dynamics; (iv) to apply the results obtained in power electronics systems involving the control of dc-dc buck converters.

Results obtained with respect to the existence, position, stability and bifurcations of equilibria in canonical form (7.5) can be applied to any given system of form (7.4), fulfilling the required hypotheses (see **(H1)** and **(H2)** in Section 7.3). The methodology of application in a given system (see Section 7.6) passes through the verification of the required hypotheses, the calculation of the new coefficients and parameters from of those that are given (see Theorem 7.1 and Lemma 7.1) and transcription of the general results for the given system (whenever the required conditions on coefficients and parameters are satisfied).

Our main results in this chapter are: (i) the classification of BEBs in 3D-DPWL systems of the form (7.4), giving explicit conditions on the system parameters for the occurrence of each of the two scenarios, persistence and nonsmooth fold (see Theorem 7.3 and Figure 7.5), and also the characterization of the dynamics of its unfoldings in the sliding vector field (see Table 7.1); (ii) the canonical form and the pathways to get it, from which it is possible to obtain, following our results, different types of BEBs, as we will do in the Section 7.5 through the study of a few examples; (iii) the description of the sliding dynamics, providing the conditions on the system parameters to obtain each of the types (saddle, node, focus, center) of pseudo-equilibrium and boundary equilibrium (see Theorem 7.2 and Table 7.1); (iv) the numerical results obtained from 4 examples, where we have presented the phase portraits associated to different types of BEBs and, in our main example, we show the birth (or vanishing) of a limit cycle (with sliding part) from a BEB persistence which involves an unstable pseudo-focus and a natural stable node equilibrium. Such results of sliding dynamics, along with the results of the BEBs analysis, allow us to choose properly the parameters for a correct operation of the control system, even with small uncertainties and perturbations in its parameters.

Proof of the existence of BEBs in power converters under a SMC strategy, identification (from the simulated results, guided by the local analysis of bifurcations) of a stable limit cycle in $\mathbb{R}^3$ with a sliding segment (from a boundary focus collision) and also the identification of a *Grazing* bifurcation of limit cycle, are important results in DIBs applications for 3D-DPWS systems.

7.3 Introducing a relevant canonical form

Consider given a 3D-DPWL system of form

$$\dot{\mathbf{x}} = \begin{cases} P\mathbf{x} + \mathbf{n}^-, & \text{if } h(\mathbf{x}) < 0 \\ P\mathbf{x} + \mathbf{n}^+, & \text{if } h(\mathbf{x}) > 0 \end{cases}, \tag{7.4}$$

where the dot denotes derivative respect to the time t, $\mathbf{x} = (x, y, z) \in \mathbb{R}^3$ is the state vector, $P = (p_{ij})_3$ for $i, j \in \{1, 2, 3\}$ and $\mathbf{n}^{\pm} = (n_1^{\pm}, n_2^{\pm}, n_3^{\pm})$ are matrix and vector of parameters, and h is a switching scalar function.

We define the switching boundary Σ of (7.4) as being the third coordinate plane:

$$\Sigma = \{(x, y, z) \in \mathbb{R}^3 : h(\mathbf{x}) = z = 0\}.$$

More general situations can be recast to this situation after some elementary transformation. The $\mathbb{R}^3$-space is divided by Σ in two open regions: $R^- = \{(x, y, z) \in \mathbb{R}^3 : \ z < 0\}$ and $R^+ = \{(x, y, z) \in \mathbb{R}^3 : z > 0\}$; and the state space of (7.4) is formed by $R^+ \cup R^- \cup \Sigma$. We define $\mathcal{F}^-(\mathbf{x}) = P\mathbf{x} + \mathbf{n}^-$ as the linear vector field acting on the zone R^- ($z < 0$) and $\mathcal{F}^+(\mathbf{x}) = P\mathbf{x} + \mathbf{n}^+$ on R^+ ($z > 0$), both interacting on Σ ($z = 0$).

Switching boundary Σ can be divided into up to three regions in which the system (7.4), among Σ_{as}, Σ_{rs} and $\Sigma_c^{\pm}$; in which the system (7.4) displays sliding or crossing dynamics. The transition between the crossing and sliding modes occurs over two parallel straight lines, where the orbits of (7.4) are tangents to Σ. Both tangency lines, denoted by T_- with respect to the vector field $\mathcal{F}^-$ and T_+ to $\mathcal{F}^+$, are generally formed by two half-lines of fold singularities (invisible on one branch and visible on the other) connected by a cusp singularity. See Figure 7.2 where we visualize a possible scenario of the dynamics of system (7.4) in the neighborhood of Σ.

Analysis of dynamics and bifurcations in systems modelled by (7.4), with configurations on Σ described in the previous paragraph and the one in which the Σ_{as} is present, are the objective of our study in this chapter. To begin, below we present conditions on the parameters of general system (7.4) to obtain such behaviour[2].

[2]See definitions of sliding regions and tangential singularities in background Chapter 2.

(H1) The conditions $p_{31} \neq 0$ and/or $p_{32} \neq 0$, and $n_3^- - n_3^+ > 0$ hold. In this way, there are tangency lines

$$T_\pm = \{(x, y, 0) \in \Sigma : p_{31}x + p_{32}y + n_3^\pm = 0\},$$

and the attractive sliding region Σ_{as} between them is given by

$$\Sigma_{as} = \{(x, y, 0) \in \Sigma : -n_3^- < p_{31}x + p_{32}y < -n_3^+\}.$$

(H2) There are two points $\mathbf{x}_c^\pm$, one for each vector field $\mathcal{F}^\pm(\mathbf{x})$, such that

$$h(\mathbf{x}_c^\pm) = L_{\mathcal{F}^\pm}h(\mathbf{x}_c^\pm) = L^2_{\mathcal{F}^\pm}h(\mathbf{x}_c^\pm) = 0$$

and $\mathrm{Det}\,[Q] \neq 0$, where

$$Q = \begin{bmatrix} \nabla h(\mathbf{x}_c^\pm) \\ \nabla L_{\mathcal{F}^\pm}h(\mathbf{x}_c^\pm) \\ \nabla L^2_{\mathcal{F}^\pm}h(\mathbf{x}_c^\pm) \end{bmatrix}.$$

(H3) At $\mathbf{x}_c^\pm$ we have $L^3_{\mathcal{F}^\pm}h(\mathbf{x}_c^\pm) = \mathrm{Det}\,[R^\pm]$ not identically zero, where

$$R^\pm = \begin{bmatrix} p_{11} & p_{12} & n_1^\pm \\ p_{21} & p_{22} & n_2^\pm \\ p_{31} & p_{32} & n_3^\pm \end{bmatrix}.$$

Remark 7.1. *Note that* $L_{\mathcal{F}^-}h(x, y, 0) - L_{\mathcal{F}^+}h(x, y, 0) = n_3^- - n_3^+ > 0$, *then* $L_{\mathcal{F}^-}h(x, y, 0) > L_{\mathcal{F}^+}h(x, y, 0)$ *for all* $(x, y, 0) \in \Sigma$.

The next step is to rewrite system (7.4) in a canonical form, with reduced number of parameters, where all tangency point of T_+ and of T_- have coordinates $(1, y, 0)$ and $(-1, y, 0)$ with $y \in \mathbb{R}$, respectively. Still with respect to the tangency lines $T_\pm$, at the points $(1, 0, 0)$ and $(-1, 0, 0)$ a change between visible and invisible fold singularities occur. Moreover, the attractive sliding region Σ_{as} is present between such parallel lines, that is, if $-1 < x < 1$ then $(x, y, 0) \in \Sigma_{as}$ (see Figure

7.2). This canonical form is given below (see Equation (7.5)) and will be analysed in the next sections, in order to characterize the present dynamics and the possible BEBs. For simplicity, let us use the same notation for the coordinates of the new state space, as well as for the time variable.

The canonical form considered is described by

$$\dot{\mathbf{x}} = \begin{cases} A\mathbf{x} + \mathbf{b}^-, & \text{if } z < 0 \\ A\mathbf{x} + \mathbf{b}^+, & \text{if } z > 0 \end{cases}, \tag{7.5}$$

where

$$A = \begin{bmatrix} a_{11} & 1 & 0 \\ a_{21} & a_{22} & a_{23} \\ 1 & 0 & 0 \end{bmatrix}, \quad \mathbf{x} = \begin{bmatrix} x \\ y \\ z \end{bmatrix}, \quad \mathbf{b}^- = \begin{bmatrix} a_{11} \\ b_2^- \\ 1 \end{bmatrix} \text{ and } \mathbf{b}^+ = \begin{bmatrix} -a_{11} \\ b_2^+ \\ -1 \end{bmatrix},$$

for some parameters a_{11}, a_{21}, a_{22}, a_{23} and $b_2^{\pm}$. Switching boundary Σ remains the same, given by the plane $z = 0$. The linear vector fields which interact with Σ are defined by $\mathbf{F}^{\pm}(\mathbf{x}) = A\mathbf{x} + \mathbf{b}^{\pm}$.

Theorem 7.1. *Consider the hypotheses* **(H1)** *and* **(H2)** *with respect to system* (7.4)*. Then, there are a linear transformation of coordinates and a rescaling of time, such that the state portrait of* (7.4) *is mapped onto the state portrait of* (7.5)*, preserving orientation of all the orbits, including sliding orbits.*

Proof. See Appendix 7.9. □

Remark 7.2. *All results obtained from the canonical form* (7.5) *are also observed in the general system* (7.4)*. This is our goal. From the analysis of the canonical form* (7.5)*, we know the dynamics of the general system* (7.4)*.*

Figure 7.2 shows the switching boundary Σ of system (7.5) and illustrates the behaviour of their orbits through Σ. In the next subsections we will study this system, determining its main characteristics,

equilibrium points, stability and sliding dynamics.

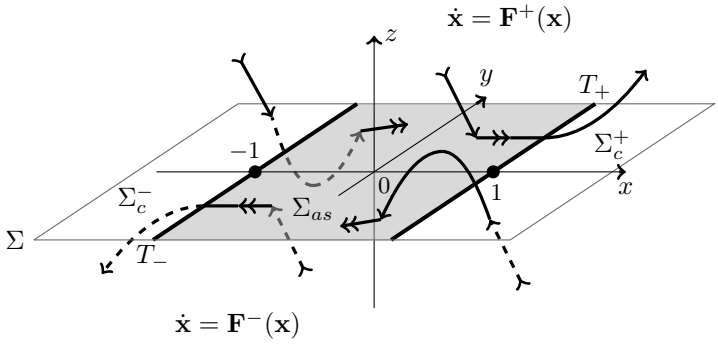

Figure 7.2: Switching boundary of system (7.5).

7.3.1 Topological configuration on switching boundary Σ

In order to analyse the dynamic behaviour of system (7.5) on Σ, we recalculated the Lie derived of first, second and third order of the scalar function $h(x, y, z) = z$ with respect to its vector fields, getting

$$L_{\mathbf{F}^+} h(x, y, 0) = x - 1, \tag{7.6}$$

$$L^2_{\mathbf{F}^+} h(1, y, 0) = y, \tag{7.7}$$

$$L^3_{\mathbf{F}^+} h(1, 0, 0) = a_{21} + b_2^+, \tag{7.8}$$

and

$$L_{\mathbf{F}^-} h(x, y, 0) = x + 1, \tag{7.9}$$

$$L^2_{\mathbf{F}^-} h(-1, y, 0) = y, \tag{7.10}$$

$$L^3_{\mathbf{F}^-} h(-1, 0, 0) = -a_{21} + b_2^-. \tag{7.11}$$

The above equations are used to classify the behaviour on Σ, as follow.

The vector fields $\mathbf{F}^-$ and $\mathbf{F}^+$ are tangents to Σ at the points of

the (parallel) straight lines

$$T_- = \{(x, y, z) \in \mathbb{R}^3 : \ z = 0 \text{ and } x = -1\}$$

and

$$T_+ = \{(x, y, z) \in \mathbb{R}^3 : \ z = 0 \text{ and } x = 1\},$$

respectively. Regarding to the tangency lines $T_\pm$, the following classifications hold.

(i) On the tangential singularities at $(-1, y, 0) \in T_-$: *invisible fold* for all $y > 0$; *visible fold* for all $y < 0$; and a *cusp* tangency for $y = 0$, whenever $a_{21} \neq b_2^-$.

(ii) On the tangential singularities at $(1, y, 0) \in T_+$: *visible fold* for all $y > 0$; *invisible fold* for all $y < 0$; and a *cusp* tangency for $y = 0$, whenever $a_{21} \neq -b_2^+$.

The *cusp* tangencies are important points of system (7.5) for our study, which we denoted by

$$\mathbf{x}_c^\pm = (\pm 1, 0, 0).$$

The switching boundary Σ is divided into three regions of different dynamical behaviour. Two crossing regions, namely

$$\Sigma_c^- = \{(x, y, z) \in \mathbb{R}^3 : \ z = 0 \text{ and } x < -1\},$$

where future orbits of (7.5) crosses the plane $z = 0$ towards of $z > 0$ to $z < 0$; and

$$\Sigma_c^+ = \{(x, y, z) \in \mathbb{R}^3 : \ z = 0 \text{ and } x > 1\},$$

where future orbits of (7.5) crosses the plane $z = 0$ towards of $z < 0$ to $z > 0$. Also, one attractive sliding region, namely

$$\Sigma_{as} = \{(x, y, z) \in \mathbb{R}^3 : \ z = 0 \text{ and } -1 < x < 1\},$$

such that all future orbit of (7.5) that intersects the plane $z = 0$ in this region, remains confined to it, sliding according the dynamics of the vector field

$$\mathbf{F}^s(x, y, 0) = \frac{1}{2}\begin{bmatrix} 2y \\ (2a_{21} - b_2^- + b_2^+)x + 2a_{22}y + b_2^- + b_2^+ \\ 0 \end{bmatrix}. \tag{7.12}$$

7.3.2 Natural equilibria, pseudo-equilibria and boundary equilibria

The vectors fields $\mathbf{F}^-$ and $\mathbf{F}^+$ has a single equilibrium point each, if and only if,

$$\mathrm{Det}\,[A] = a_{23} \neq 0. \tag{7.13}$$

For simplify we define two new parameters, μ and ν, such that

$$\mu = -L^3_{\mathbf{F}^+} h(1, 0, 0) = -a_{21} - b_2^+, \tag{7.14}$$

$$\nu = -L^3_{\mathbf{F}^-} h(-1, 0, 0) = a_{21} - b_2^-. \tag{7.15}$$

This way, the equilibrium point of $\mathbf{F}^-$ has coordinates

$$\overline{\mathbf{x}}^- = \left(-1, 0, \frac{\nu}{a_{23}}\right). \tag{7.16}$$

Such point is a real equilibrium for $a_{23}\nu < 0$, a virtual equilibrium for $a_{23}\nu > 0$, or a boundary equilibrium when $\nu = 0$.

On the other hand, the equilibrium point of $\mathbf{F}^+$ has coordinates

$$\overline{\mathbf{x}}^+ = \left(1, 0, \frac{\mu}{a_{23}}\right). \tag{7.17}$$

Such point is a real equilibrium for $a_{23}\mu > 0$, virtual equilibrium for $a_{23}\mu < 0$, or a boundary equilibrium when $\mu = 0$.

Proposition 7.1. *The natural equilibria* $\overline{\mathbf{x}}^{\pm}$ *of system* (7.5) *have the same stability, being hyperbolic and asymptotically stable iff*

$$\begin{aligned} a_{23} &< 0, \\ a_{11} + a_{22} &< 0, \\ (a_{11} + a_{22})(a_{21} - a_{11}a_{22}) + a_{23} &> 0. \end{aligned}$$

Proof. Such conditions above are obtained through the direct application of Routh-Hurwitz stability criterion to characteristic polynomials of third degree. □

Sliding vector field $\mathbf{F}^s$, given in (7.12), is linear and therefore the system (7.5) has a single pseudo-equilibrium point at

$$\widetilde{\mathbf{x}} = \left(\frac{\nu + \mu}{\nu - \mu}, 0, 0 \right), \tag{7.18}$$

iff $\nu \neq \mu$. The point $\widetilde{\mathbf{x}}$ is the equilibrium of sliding vector field $\mathbf{F}^s$, and is a real equilibrium[3] for $\mu\nu < 0$; virtual equilibrium for $\mu\nu > 0$; and becomes a boundary equilibrium for $\mu = 0$ or for $\nu = 0$.

System (7.5) has only one boundary equilibrium, located at the point

$$\mathbf{x}_b^- = (-1, 0, 0) \tag{7.19}$$

if $\nu = 0$ and $\mu \neq 0$; or at point

$$\mathbf{x}_b^+ = (1, 0, 0) \tag{7.20}$$

if $\mu = 0$ and $\nu \neq 0$. Note that, the boundary equilibrium $\mathbf{x}_b^-$ comes up when the equilibrium of vector field $\mathbf{F}^-$ collides with the switching boundary $\Sigma = \{z = 0\}$, such that $\mathbf{x}_b^- = \overline{\mathbf{x}}^- = \widetilde{\mathbf{x}}$ is equilibrium of $\mathbf{F}^-$ and also of the sliding vector field $\mathbf{F}^s$. Analogously, the boundary equilibrium $\mathbf{x}_b^+$ comes up when the equilibrium of $\mathbf{F}^+$ collides with the

[3]Note that $\left|\frac{\nu+\mu}{\nu-\mu}\right| < 1$ has as solution the region in (ν, μ)-plane defined by $\mu\nu < 0$.

switching boundary, such that $\mathbf{x}_b^+ = \overline{\mathbf{x}}^+ = \widetilde{\mathbf{x}}$ is equilibrium of $\mathbf{F}^+$ and also of $\mathbf{F}^s$. In the degenerate case, when $\nu = \mu = 0$, the system (7.5) has the two boundary equilibrium points $\mathbf{x}_b^\pm$, coexistent. But, the sliding vector field $\mathbf{F}^s$ has an infinite number of equilibria on the straight line segment (contained in Σ) that joining the points $\mathbf{x}_b^\pm$.

Remark 7.3. *Note that the boundary equilibria $\mathbf{x}_b^\pm$ have the same coordinates as the cusp singularities $\mathbf{x}_c^\pm$. What happens, is that at the point $(-1,0,0)$ we have a cusp singularity if $\nu \neq 0$, and a boundary equilibrium if $\nu = 0$. Similarly, at the point $(1,0,0)$ we have a cusp singularity if $\mu \neq 0$, and a boundary equilibrium if $\mu = 0$.*

7.4 Sliding vector field dynamics

The sliding vector field (7.12) is defined for all $(x,y) \in \mathbb{R}^2$ and $z = 0$, but only makes sense for $(x,y) \in \Sigma_{as}$, allowing it to be extended to its borders that are defined by T_- and T_+. Following the standard analysis of the sliding vector field, we taking only the two first coordinates of (7.12) and write a two-dimensional linear system, whose dynamics is topologically equivalent to (7.12) in Σ_{as}. So, the sliding dynamics will be analysed by

$$\dot{\mathbf{x}} = J(\nu,\mu)\mathbf{x} + C(\nu,\mu), \tag{7.21}$$

where $\mathbf{x} = (x,y)$,

$$J(\nu,\mu) = \begin{bmatrix} 0 & 1 \\ \frac{(\nu-\mu)}{2} & a_{22} \end{bmatrix}, \quad C(\nu,\mu) = \begin{bmatrix} 0 \\ -\frac{(\nu+\mu)}{2} \end{bmatrix},$$

and μ and ν defined in (7.14) and (7.15), respectively.

There is only one pseudo-equilibrium point in the 3D-DPWL system (7.5), denoted by $\widetilde{\mathbf{x}}$ and given in (7.18). This point is the equilibrium of sliding vector field (7.12) and, therefore, also is the equilibrium of planar sliding system (7.21) (only considering the (x,y)-coordinates). Dynamics at the pseudo-equilibrium $\widetilde{\mathbf{x}}$ is then investigated from the

planar sliding system (7.21), based in the eigenvalues of J, given by

$$\lambda^{\pm} = \frac{1}{2}\left(a_{22} \pm \sqrt{a_{22}^2 + 2(\nu - \mu)}\right).$$

Theorem 7.2. *Assume $\mu \neq \nu$. System (7.5) has a single pseudo-equilibrium point, namely*

$$\widetilde{\mathbf{x}} = \left(\frac{\nu + \mu}{\nu - \mu}, 0, 0\right).$$

Moreover, the following statements hold.

a) *If $\nu\mu < 0$, then the pseudo-equilibrium $\widetilde{\mathbf{x}}$ is real. In the opposite case it is virtual.*

b) *If $\nu > \mu$, then $\widetilde{\mathbf{x}}$ is a pseudo-saddle.*

c) *Assume $a_{22} < 0$ (resp. $a_{22} > 0$). If $\nu < \mu \leq \nu + \frac{a_{22}^2}{2}$, then $\widetilde{\mathbf{x}}$ is a stable pseudo-node (resp. unstable); if $\mu > \nu + \frac{a_{22}^2}{2}$, then it is a stable pseudo-focus (resp. unstable).*

d) *If $a_{22} = 0$ and $\nu < \mu$, then $\widetilde{\mathbf{x}}$ is a pseudo-center.*

Remark 7.4. *An important feature of system (7.5) is that the pseudo-equilibrium manifold, given by*

$$\mathcal{M} = \{(x, y, 0) \in \Sigma : y = 0\},$$

is transverse to the tangency lines $T_{\pm}$ at the cusp points $\mathbf{x}_c^{\pm} = (\pm 1, 0, 0)$, as shown in the Figure 7.3. Moreover, the sliding vector field is tangent to T_- at $\mathbf{x}_c^-$ and T_+ at $\mathbf{x}_c^+$, and in the other points of $T_{\pm}$ it is transversal, see Lemma 2.1 and 2.2. More specifically, all point in T_- such that $y > 0$ (invisible fold points), is an entry point of $\mathbf{F}^s$; while for $y < 0$ (visible fold points) it is an exit point of $\mathbf{F}^s$. On the other hand, all point in T_+ such that $y < 0$ (invisible fold points), is an entry point of $\mathbf{F}^s$; while for $y > 0$ (visible fold points) it is an exit point of $\mathbf{F}^s$.

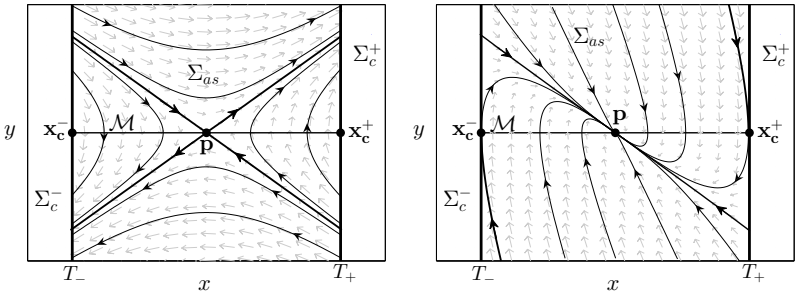

(a) pseudo-saddle

(b) stable pseudo-node

(c) stable pseudo-focus

Figure 7.3: Dynamics of sliding vector field, assuming $a_{22} < 0$ and $\nu\mu < 0$.

In Figure 7.3 we see some phase portraits of $\mathbf{F}^s$, in the cases where $\widetilde{\mathbf{x}}$ is a real hyperbolic pseudo-equilibrium. The eigenvectors $\mathbf{v}_\pm = (1, \lambda^\pm/2)$ are associated with eigenvalues $\lambda^\pm$, so that the straight lines generated by $\mathbf{v}_+$ and $\mathbf{v}_-$ have slope with opposite signs whenever $\widetilde{\mathbf{x}}$ is a pseudo-saddle, and slope of the same signal whenever $\widetilde{\mathbf{x}}$ is a pseudo-node.

7.5 Two-parameter bifurcation analysis of equilibria

A boundary equilibrium arises in state space of the system (7.5) when one of its natural equilibria collides with the switching boundary Σ. More specifically, this critical point arises from the collision between three particular points: a natural equilibrium, a pseudo-equilibrium and a cusp singularity. The appearance of a boundary equilibrium in a 3D-DPWS system represents a codimension-one DIB known as BEB, and is classified according to two possible scenarios: *persistence* and *nonsmooth fold*. Equilibria analysis in Subsection 7.3.2 indicates the existence of generic BEBs in system (7.5). Here we will analyse in detail these bifurcations and the sliding dynamics at the boundary equilibrium.

First we analyse the BEBs involving the equilibrium $\overline{\mathbf{x}}^+$ of the vector field $\mathbf{F}^+$, taking μ as the bifurcation parameter and the remaining fixed. The equilibrium point $\overline{\mathbf{x}}^+$ moves on a straight line in $\mathbb{R}^3$ with vector equation $\overline{\mathbf{x}}^+(\mu) = \left(1, 0, \frac{\mu}{a_{23}}\right)$, from the variation of the parameter μ. Along, the pseudo-equilibrium point $\widetilde{\mathbf{x}}$ moves on a straight line in Σ with vector equation $\widetilde{\mathbf{x}}(\mu) = \left(\frac{\nu+\mu}{\nu-\mu}, 0, 0\right)$, also according to the parameter μ. The manifold equilibria defined by $\overline{\mathbf{x}}^+(\mu)$ and $\widetilde{\mathbf{x}}(\mu)$ are passing through the cusp tangency point of coordinates $\mathbf{x}_c^+ = (1, 0, 0)$, so that for $\mu = 0$ the equilibrium points $\overline{\mathbf{x}}^+$ and $\widetilde{\mathbf{x}}$ collide with the cusp point $\mathbf{x}_c^+$, giving rise to the boundary equilibrium $\mathbf{x}_b^+ = \overline{\mathbf{x}}^+(0) = \widetilde{\mathbf{x}}(0) = \mathbf{x}_c^+$. Therefore, for $\mu = 0$ the system (7.5) undergoes, possibly, a BEB.

After, we analyse the BEBs involving the equilibrium $\overline{\mathbf{x}}^-$ of the vector field $\mathbf{F}^-$, taking ν as the bifurcation parameter and the remaining fixed. The equilibrium point $\overline{\mathbf{x}}^-$ moves on a straight line in $\mathbb{R}^3$ with vector equation $\overline{\mathbf{x}}^-(\nu) = \left(-1, 0, \frac{\nu}{a_{23}}\right)$, from the variation of the parameter ν. Along, the pseudo-equilibrium point $\widetilde{\mathbf{x}}$ moves on a straight line in Σ with vector equation $\widetilde{\mathbf{x}} = \widetilde{\mathbf{x}}(\nu)$, now according to the parameter ν. The manifold equilibria defined by $\overline{\mathbf{x}}^-(\nu)$ and $\widetilde{\mathbf{x}}(\nu)$ are passing

through the cusp tangency point of coordinates $\mathbf{x}_c^- = (-1, 0, 0)$, so that for $\nu = 0$ the equilibrium points $\overline{\mathbf{x}}^-$ and $\widetilde{\mathbf{x}}$ collide with cusp point $\mathbf{x}_c^-$, giving rise to the boundary equilibrium $\mathbf{x}_b^- = \overline{\mathbf{x}}^-(0) = \widetilde{\mathbf{x}}(0) = \mathbf{x}_c^-$ (see Figure 7.4). Therefore, for $\nu = 0$ the system (7.5) undergoes, possibly, a BEB.

Theorem 7.3 confirms the existence of BEBs in system (7.5), and provides the required conditions on the system parameters for the occurrence of the persistence or nonsmooth fold scenario.

Theorem 7.3. *Assume $a_{23} \neq 0$ and $\nu \neq \mu$. Then system (7.5) undergoes a BEB for $\nu = 0$ if $\mu \neq 0$ or for $\nu = 0$ if $\mu \neq 0$. In addition, the following statements hold.*

(a) *The BEB at $\mu = 0$ corresponds to persistence scenario if $a_{23}\nu > 0$, and to nonsmooth fold if $a_{23}\nu < 0$.*

(b) *The BEB at $\nu = 0$ corresponds to persistence scenario if $a_{23}\mu < 0$, and to nonsmooth fold if $a_{23}\mu > 0$.*

Proof. The proof is obtained from the application of the Theorem 2.1 (given in Chapter 2) to the system (7.5).

(a) We obtain $N - C^T A^{-1} M = 1/a_{23} \neq 0$ and $-C^T A^{-1} B = \nu/a_{23} \neq 0$. Then, $a_{23}\nu > 0$ implies in the persistence case and $a_{23}\nu < 0$ implies in the nonsmooth fold case.

(b) We obtain $N - C^T A^{-1} M = 1/a_{23} \neq 0$ and $C^T A^{-1} B = -\mu/a_{23} \neq 0$. Then, $a_{23}\mu < 0$ implies in the persistence case and $a_{23}\mu > 0$ implies in the nonsmooth fold case.

In Figure 7.4 the two BEBs, persistence and nonsmooth fold, are illustrated. This BEBs involve the natural equilibrium $\overline{\mathbf{x}}^-$ and the pseudo-equilibrium $\widetilde{\mathbf{x}}$. Note the triple collision between the natural equilibrium $\overline{\mathbf{x}}^-$, the pseudo-equilibrium $\widetilde{\mathbf{x}}$ and the cusp singularity $\mathbf{x}_c^-$, turning this last point into the boundary equilibrium $\mathbf{x}_b^-$. □

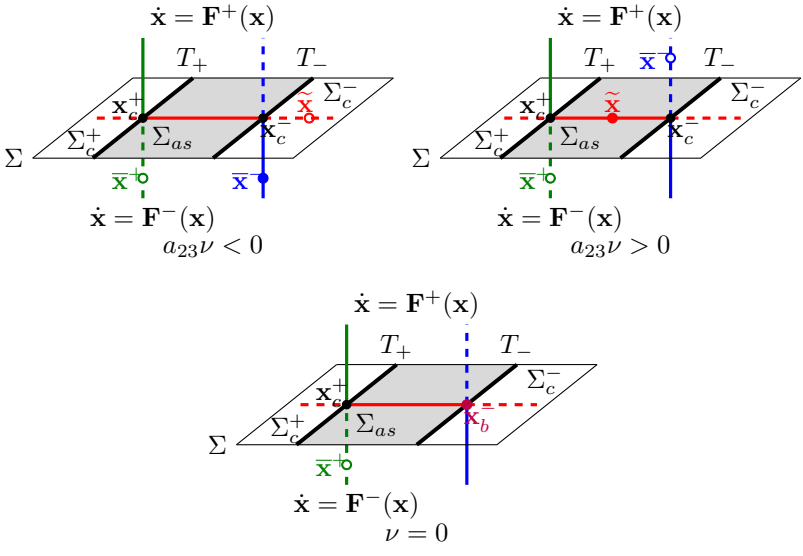

(a) Persistence if $a_{23}\mu < 0$.

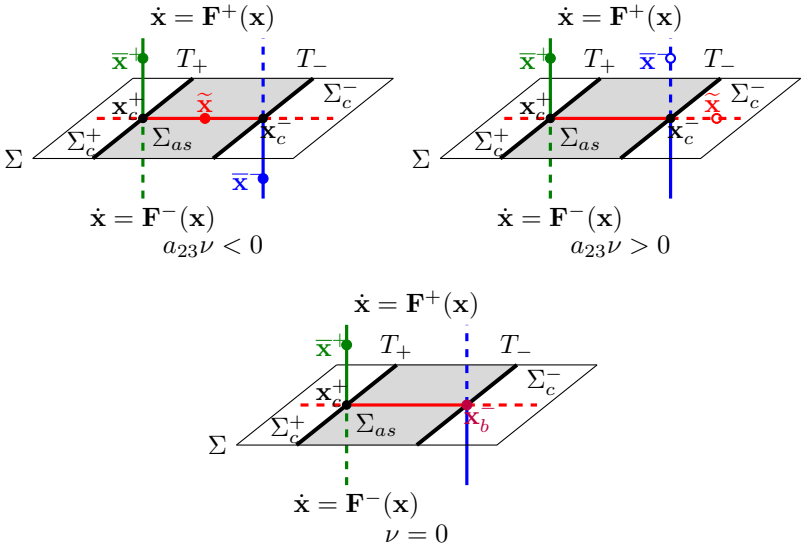

(b) Nonsmooth fold if $a_{23}\mu > 0$.

Figure 7.4: BEBs in system (7.5) involving the natural equilibrium $\overline{\mathbf{x}}^-$ (blue) and the pseudo-equilibrium $\widetilde{\mathbf{x}}$ (red). The point $\mathbf{x}_c^-$ represent the cusp singularity of vector filed $\mathbf{F}^-$ and $\mathbf{x}_b^-$ (purple) the boundary equilibrium.

Remark 7.5. *An important finding here is that the other natural equilibrium, that is* $\overline{\mathbf{x}}^+$*, is virtual when the BEB at* $\mathbf{x}_b^-$ *is of the persistence type and it real when is of the nonsmooth fold type. Moreover, the natural equilibria and pseudo-equilibria can be simultaneously real but never simultaneously virtual.*

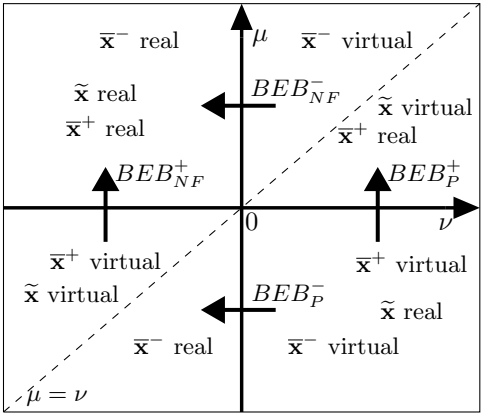

Figure 7.5: BEBs in the (ν, μ)-plane of parameters, assuming $a_{23} > 0$. $BEB_{NF}^{\pm}$ and $BEB_P^{\pm}$ denote the nonsmooth fold and the persistence scenarios, respectively, for the vector field $\mathbf{F}^{\pm}$.

Figure 7.5 summarizes our analysis of BEBs in the (ν, μ)-plane of parameters, where we assume $a_{23} > 0$. Parameter μ is responsible for a BEB involving the equilibrium of the vector field $\mathbf{F}^+$, occurring for $\mu = 0$ and being of the nonsmooth fold type if $\nu < 0$, or persistence if $\nu > 0$. The parameter ν is responsible for a BEB involving the equilibrium of the vector field $\mathbf{F}^-$, occurring for $\nu = 0$ and being of the nonsmooth fold type if $\mu > 0$, or persistence if $\mu < 0$. In the case $a_{23} < 0$ the scenarios are the same but occur for opposite values of μ and ν (simply replace the quadrants 1 with 3, and 2 with 4, in Figure 7.5).

The boundary equilibrium $\overline{\mathbf{x}}_b^-$ (resp. $\overline{\mathbf{x}}_b^+$) is also an equilibrium of sliding vector field, so that the sliding dynamics at this point is

BE	SD		$a_{23} > 0$	$a_{23} < 0$
$\overline{\mathbf{x}}_b^+ = (1,0,0)$ $\mu = 0$ $\nu \neq 0$ $a_{23} \neq 0$	Saddle	$\nu > 0$	P	NF
	Node $a_{22} \neq 0$	$-\frac{a_{22}^2}{2} \leq \nu < 0$	NF	P
	Focus $a_{22} \neq 0$	$\nu < -\frac{a_{22}^2}{2}$	NF	P
	Center $a_{22} = 0$	$\nu < 0$	NF	P
$\overline{\mathbf{x}}_b^- = (-1,0,0)$ $\nu = 0$ $\mu \neq 0$ $a_{23} \neq 0$	Saddle	$\mu < 0$	P	NF
	Node $a_{22} \neq 0$	$0 < \mu \leq \frac{a_{22}^2}{2}$	NF	P
	Focus $a_{22} \neq 0$	$\mu > \frac{a_{22}^2}{2}$	NF	P
	Center $a_{22} = 0$	$\mu > 0$	NF	P

Table 7.1: Classification of boundary equilibrium points with respect to the sliding dynamics and the type of BEB present. Legend: P indicates the persistence scenario, NF indicates the nosmooth fold scenario, BE means boundary equilibrium and SD means sliding dynamics.

equivalent to the dynamics at the pseudo-equilibrium, described in the Theorem 7.2. In Table 7.1 we present the required conditions on the system parameters to obtain in the phase portrait of (7.5) a boundary equilibrium with sliding dynamics: saddle, node, focus or center[4]. For each of them, the BEB can be of the nonsmooth fold or persistence type, depending on the signal of parameter a_{23}. In addition, if $a_{22} < 0$ (resp. $a_{22} > 0$) then the node/focus boundary equilibrium is asymptotically stable (resp. unstable) from the sliding vector field $\mathbf{F}^s$.

[4]We have included the non-hyperbolic case involving a pseudo-center. This result can be used in the study of Hopf bifurcation in 3D-DPWS systems where the sliding vector field has the linear part of the form given in (7.21).

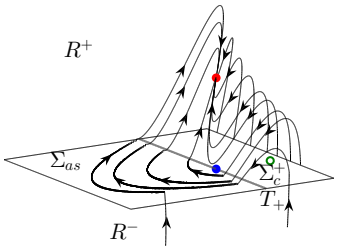

(a) $\mu < 0$

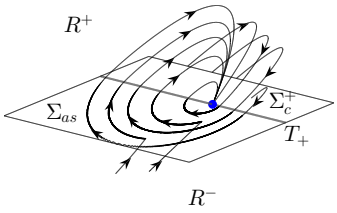

(b) $\mu = 0$

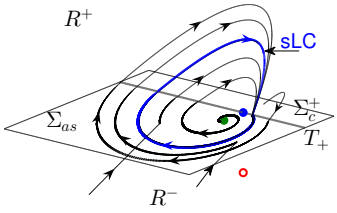

(c) $\mu > 0$

Figure 7.6: Persistence BEB with an unstable pseudo-focus and a stable node (natural) equilibrium. The red dot represents the natural equilibrium point, the green dot represents the pseudo-equilibrium point and the blue dot represents the boundary equilibrium point when $\mu = 0$ and the cusp point for $\mu \neq 0$. The small circle indicates that the equilibrium is virtual. sLC denotes the stable limit cycle, shown in blue color.

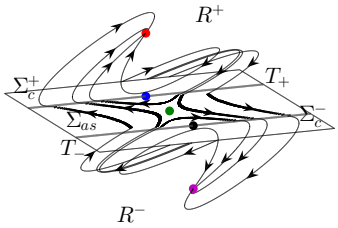

(a) $\mu < 0$

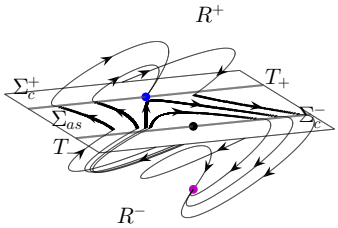

(b) $\mu = 0$

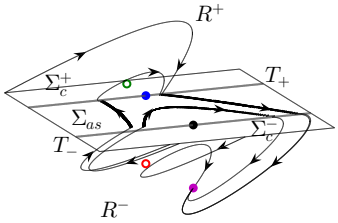

(c) $\mu > 0$

Figure 7.7: Nonsmooth Fold BEB with a pseudo-saddle and a stable node (natural) equilibrium. The red and purple dots represent the natural equilibrium points, the green dot represents the pseudo-equilibrium point, the black dot represents cusp point of $\mathbf{F}^-$, the blue dot represents the cusp point of $\mathbf{F}^+$ for $\mu \neq 0$ and a boundary equilibrium point when $\mu = 0$. The small circle indicates that the equilibrium is virtual.

Example 7.2. Boundary Node-Focus: ***persistence scenario.*** *Consider in system* (7.5) *that* $a_{22} = 0.5$, $a_{11} = -6.5$, $a_{21} = -14.25$, $a_{23} = -6 < 0$, $b_2^- = -13.25$ (*implies in* $\nu = -1 < 0$) *and* $b_2^+ = 14.25 - \mu$, *for* $|\mu|$ *small. Thus the natural equilibria are stable and have node dynamics, while the pseudo-equilibrium is unstable with focus dynamics* (*since* $\mu > -0.875$). *In this study case, a BEB occurs for* $\mu = 0$, *involving the pseudo-focus* (*equilibrium of* $\mathbf{F}^s$) *and the node equilibrium of* $\mathbf{F}^+$. *As* $a_{23}\nu > 0$, *then the persistence scenario is observed. A nonsmooth limit cycle with sliding part arises from the boundary equilibrium point for* $\mu > 0$. *This limit cycle is composed of an orbit segment of* $\mathbf{F}^+$ *and a sliding orbit segment of* $\mathbf{F}^s$. *In addition, it is stable and develops around unstable* (*real*) *pseudo-focus. See Figure 7.6.*

Example 7.3. Boundary Node-Saddle: ***nonsmooth fold scenario.*** *Consider in system* (7.5) *that* $a_{22} = 0.5$, $a_{11} = -6.5$, $a_{21} = -14.25$, $a_{23} = -6 < 0$, $b_2^- = -15.25$ (*implies in* $\nu = 1 > 0$) *and* $b_2^+ = 14.25 - \mu$, *for* $\mu < 1$. *Thus the natural equilibria are stable and have node dynamics, while the pseudo-equilibrium is unstable with saddle dynamics. In this study case, a BEB occurs for* $\mu = 0$, *involving the pseudo-saddle* (*equilibrium of* $\mathbf{F}^s$) *and the node equilibrium of* $\mathbf{F}^+$. *As* $a_{23}\nu < 0$, *then the nonsmooth fold scenario is observed. We have chosen here to consider the phase portraits showing the global dynamics, involving all system equilibria and the unfoldings of the nonsmooth fold BEB. See Figure 7.7.*

Generically, BEBs are of codimension-one, but degenerate cases of larger codimension also can occur in the system (7.5). A codimension-two BEB occurs for $\mu = \nu = 0$, provided that $a_{23} \neq 0$. In this case both natural equilibria become boundary equilibria (in [93] a double boundary equilibrium analysis in two-dimensional systems is introduced). Another codimension-two BEB occurs when the boundary equilibrium is a center with respect to the sliding dynamics, that is, for $a_{22} = \mu = 0$, provided that $a_{23} \neq 0$ and $\nu < 0$. In the following we introduce two examples with non-hyperbolic BEBs (see case studies of two-dimensional

systems in [45]). In both, the boundary equilibrium has node dynamics with respect to $\mathbf{F}^+$ and center dynamics with respect to $\mathbf{F}^s$. But, in the first example we observed the persistence scenario and, in the second, the nonsmooth fold scenario is observed.

Example 7.4. Boundary Node-Center: ***persistence scenario.*** *Consider in system* (7.5) *that* $a_{22} = 0$, $a_{11} = -6$, $a_{21} = -11$, $a_{23} = -6 < 0$, $b_2^- = 1$ (*implies in* $\nu = -12 < 0$) *and* $b_2^+ = 11 - \mu$. *Thus the natural equilibria are stable and have node dynamics, while the pseudo-equilibrium has center dynamics. In this study case, a BEB occurs for* $\mu = 0$, *involving the pseudo-center* (*equilibrium of* $\mathbf{F}^s$) *and the node equilibrium of* $\mathbf{F}^+$. *As* $a_{23}\nu > 0$, *then the persistence scenario is observed. See Figure 7.8.*

Example 7.5. Boundary Node-Center: ***nonsmooth fold scenario.*** *Consider in system* (7.5) *that* $a_{22} = 0$, $a_{11} = 6$, $a_{21} = -11$, $a_{23} = 6 > 0$, $b_2^- = 1$ (*implies in* $\nu = -12 < 0$) *and* $b_2^+ = 11 - \mu$. *In this example remain the pseudo-center and the natural node equilibria, but now the node equilibria are unstable. Thus, a BEB occurs for* $\mu = 0$ *and, as* $a_{23}\nu < 0$, *the nonsmooth fold scenario is observed. See Figure 7.9.*

We conclude this section by giving below the main parameters of the canonical form (7.5), calculated according to the parameters of the original system (7.4), thus facilitating the process of applying the obtained results.

Lemma 7.1. *The parameters* a_{23} *and* a_{22}, *the first responsible for the existence of natural equilibria and the second for the stability in sliding dynamics, are given by*

$$a_{23} = \frac{8Det[P]}{(n_3^- - n_3^+)^3}, \tag{7.22}$$

$$a_{22} = \frac{2((n_3^- - n_3^+)(p_{11} + p_{22}) - (n_1^- - n_1^+)p_{31} - (n_2^- - n_2^+)p_{32})}{(n_3^- - n_3^+)^2}, \tag{7.23}$$

as functions of the parameters of system (7.4).

The pair of parameters (ν, μ)*, responsible for the boundary equilibrium bifurcations predicted by Theorem 7.3, is ruled by the values*

$$\mu = -\frac{8Det[R^+]}{(n_3^- - n_3^+)^3}, \tag{7.24}$$

$$\nu = -\frac{8Det[R^-]}{(n_3^- - n_3^+)^3}, \tag{7.25}$$

where

$$R^{\pm} = \begin{bmatrix} p_{11} & p_{12} & n_1^{\pm} \\ p_{21} & p_{22} & n_2^{\pm} \\ p_{31} & p_{32} & n_3^{\pm} \end{bmatrix}.$$

Proof. For the values of a_{23} and a_{22} we have proved in Appendix 7.9 from the normalization of system (7.4) to form (7.5). Parameters μ and ν are defined in (7.14) and (7.15), respectively. From this, we write

$$-L^3_{\mathbf{F}^{\pm}} h(\pm 1, 0, 0) = -\frac{8L^3_{\mathcal{F}^{\pm}} h(\mathbf{x}_c^{\pm})}{(n_3^- - n_3^+)^3} = -\frac{8\mathrm{Det}\,[R^{\pm}]}{(n_3^- - n_3^+)^3},$$

thus obtaining the equations (7.24)-(7.25). □

7.6 Application 1: The buck converter under a SMC strategy

In this section we consider a 3D-DPWL system that describes the dynamics of the dc-dc buck converter under a sliding mode control strategy. We will use the results of stability and bifurcations obtained from the canonical form (7.5), in previous section, to study the dynamic behaviour and possible BEBs in the control system proposed for the buck converter. This analysis provides us with important information about the dynamics of this control system.

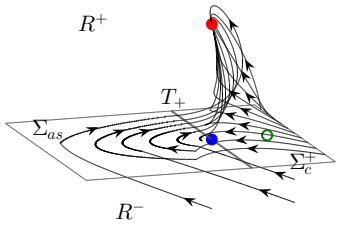

(a) $\mu < 0$

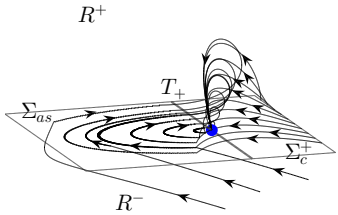

(b) $\mu = 0$

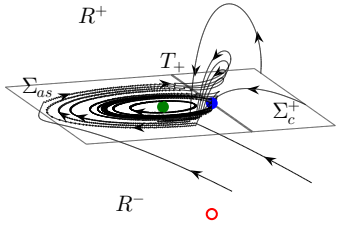

(c) $\mu > 0$

Figure 7.8: Persistence BEB with pseudo-center and stable node (natural) equilibrium. The red dot represent the natural equilibrium point, the green dot represents the pseudo-equilibrium point, the blue dot represents the cusp point of $\mathbf{F}^+$ for $\mu \neq 0$ and a boundary equilibrium point when $\mu = 0$. The small circle indicates that the equilibrium is virtual.

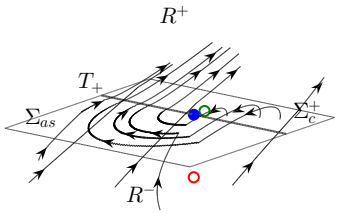

(a) $\mu < 0$

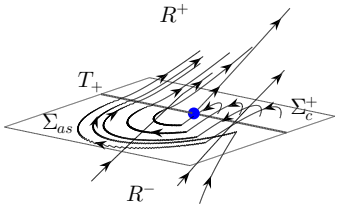

(b) $\mu = 0$

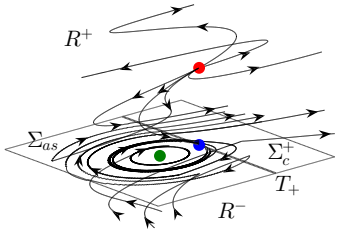

(c) $\mu > 0$

Figure 7.9: Nonsmooth fold BEB with pseudo-center and unstable node equilibrium. The red dot represent the natural equilibrium point, the green dot represents the pseudo-equilibrium point, the blue dot represents the cusp point of $\mathbf{F}^+$ for $\mu \neq 0$ and a boundary equilibrium point when $\mu = 0$. The small circle indicates that the equilibrium is virtual.

7.6.1 Closed loop control system modelling

The basic topology of a DC-DC buck converter is shown in Figure (7.10)(a), where R, L, C, r_L and V_{in}, are the resistive load, the inductance, the capacitance, the inductor resistance and the voltage source, respectively. The voltage $v_{out} = v_C$ (ideal case) passing through R is the system output, which must be conducted to a desired value $v_C = V_{ref} < V_{in}$ in steady state. To obtain the desired voltage value at the output, a control strategy by sliding modes based on the use of a *washout* filter is implemented, as illustrated in Figure (7.10)(b)-(c), in order to reject load perturbations, mainly the changes produced by load changes of R.

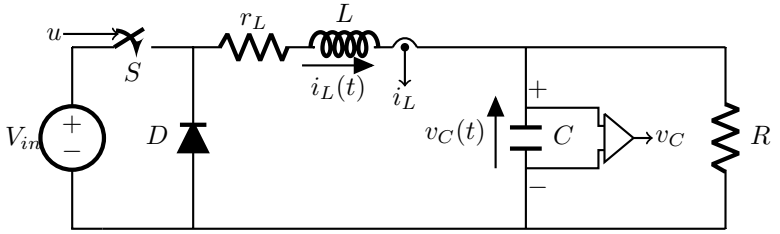

(a) DC-DC *buck* converter.

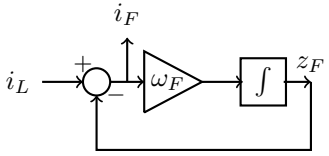

(b) Washout filter.

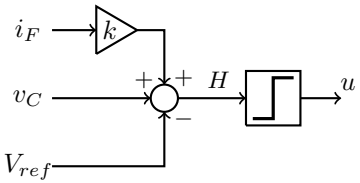

(c) Sliding mode controller.

Figure 7.10: Topology of a buck converter with Sliding Mode Control (SMC) and a washout filter. The control function is $u = \frac{1}{2}(1 - \text{sign}[H])$. In the schemes, the filtered inductor current given by $i_F = i_L - z_F$ represents the difference between the inductor current i_L and the filtered signal z_F.

The model of the buck converter with washout filter, operating in Continuous Conduction Mode (CCM), is given by

$$L\frac{di_L}{dt} = uV_{in} - r_L i_L - v_C \tag{7.26}$$

$$C\frac{dv_C}{dt} = i_L - \frac{v_C}{R} \tag{7.27}$$

$$\frac{dz_F}{dt} = \omega_F(i_L - z_F), \tag{7.28}$$

where $v_C > 0$ and $i_L > 0$ are the instantaneous capacitor voltage and inductor current, respectively. The filtered inductor current, denoted by the new variable z_F, is the output of the washout filter modelled by equation (7.28), where ω_F is the cut-off filter frequency should be assigned with the natural frequency of the system (see [91, 111]).

The control law is defined as

$$u = \frac{1}{2}(1 - \text{sign}[H]), \tag{7.29}$$

such that $u = 0$ implies that the S switch, in Figure 7.10(a), is off and $u = 1$ it is on. From this, the control surface is chosen as

$$H(i_L, v_C, z_F) = v_C - V_{ref} + K(i_L - z_F), \tag{7.30}$$

where $V_{ref} < V_{in}$ is the reference voltage (desired voltage value at the output) and $K > 0$ is the control parameter, which must be adjusted properly to ensure stability (at least local) of the desired operating point.

Looking for a simplified model with the horizontal planar switching surface, the equations (7.26)-(7.28) are normalized by applying the change of variables, time and parameters, given by Table 7.2. The switch position function is invariant with respect to the normalization. In this way, we obtain a dimensionless dynamical system, which we represent as a DPWL dynamical system of form

$$(\dot{x},\dot{y},\dot{z}) = \begin{cases} \mathcal{F}^+(x,y,z) = P\mathbf{x} + \mathbf{n}^+, \text{ if } z > 0 \\ \mathcal{F}^-(x,y,z) = P\mathbf{x} + \mathbf{n}^-, \text{ if } z < 0 \end{cases}, \tag{7.31}$$

where $(x,y,z) \in \mathbb{R}^3$ are the new state variables and

$$P = \begin{bmatrix} -b & -1 & 0 \\ 1 & -a & 0 \\ 1-bk & \omega - a - k & -\omega \end{bmatrix}, \quad \mathbf{x} = \begin{bmatrix} x \\ y \\ z \end{bmatrix},$$

$$\mathbf{n}^+ = \begin{bmatrix} 0 \\ 0 \\ -\omega y_r \end{bmatrix} \text{ and } \mathbf{n}^- = \begin{bmatrix} 1 \\ 0 \\ k - \omega y_r \end{bmatrix}.$$

The new parameters are $\omega \in (0,1]$, $0 < y_r < 1$, $a > 0$, $b > 0$ and $k > 0$. The dot " $\cdot$ " indicates $\frac{d}{d\tau}$. We highlight that $x > 0$ is the normalized inductor current, $y > 0$ is the normalized capacitor voltage and $a > 0$ is the normalized load parameter.

The vector field $\mathcal{F}^+$ has a equilibrium point at

$$\overline{\mathbf{x}}^+ = (0,0,-y_r),$$

being always virtual. This equilibrium point not belong to the region of interest $x > 0$ and $y > 0$, and so we leave out of our study. On the other hand, the vector field $\mathcal{F}^-$ has a equilibrium at point

$$\overline{\mathbf{x}}^- = (a\bar{y}, \bar{y}, \bar{y} - y_r),$$

where

$$\bar{y} = \frac{1}{1+ab}.$$

This natural equilibrium of (7.31) is classified as a real equilibrium for $y_r > \bar{y}$ and a virtual equilibrium for $y_r > \bar{y}$. The eigenvalues of matrix P are $\left\{\frac{1}{2}\left(-a-b \pm \sqrt{(a-b)^2-4}\right), -\omega\right\}$, which have negative real part. In this way, $\overline{\mathbf{x}}^-$ is a stable hyperbolic equilibrium.

State and Time Variables	Parameters
$i_L = V_{in}\sqrt{\frac{C}{L}}x$	$V_{ref} = y_r V_{in}$
$v_C = V_{in} y$	$R = \frac{1}{a}\sqrt{\frac{L}{C}}$
$z_F = i_L + \frac{v_C - V_{ref} - V_{in} z}{K}$	$K = k\sqrt{\frac{L}{C}}$
$t = \sqrt{CL}\tau$	$r_L = b\sqrt{\frac{L}{C}}$
	$\omega_F = \frac{\omega}{\sqrt{LC}}$

Table 7.2: Normalization.

7.6.2 Stability conditions at the pseudo-equilibrium

The desired operating point for the buck converter is a equilibrium of sliding vector field (pseudo-equilibrium of (7.31)), denoted by $\mathbf{p}$, which is expected to have coordinates $\mathbf{p} = (ay_r, y_r, 0)$. In order to report the sliding dynamics and stability of $\mathbf{p}$, we will use the results obtained in the previous section, from the canonical form (7.5).

We assume in system (7.31) that $k \neq 1/b$ (usually $k < 1/b$). Then, in system (7.31) we have $p_{31} = 1 - bk \neq 0$ and $n_3^- - n_3^+ = k > 0$. Moreover, the parameters (a, k, b, ω) are easily selected so that

$$\mathrm{Det}\,[Q] = -bka^2 + f(k, b, \omega)a + g(k, b, \omega) \neq 0,$$

where $f(k, b, \omega) = -k + \omega + b(-1 + k(b - k + \omega))$ and $g(k, b, \omega) = -1 - (k - \omega)^2 - b^2 k\omega + b(k + \omega)$. Following the Theorem 7.1, we can write the system (7.31) in the canonical form (7.5), and so we get from the Lemma 7.1 the main parameters:

$$a_{22} = -\frac{2(1 + ak)}{k^2} < 0,$$
$$a_{23} = -\frac{8(1 + ab)\omega}{k^3} < 0,$$

$$\mu = -a_{23} y_r > 0,$$
$$\nu = a_{23}\left(\frac{1}{1+ab} - y_r\right) = a_{23}(\bar{y} - y_r).$$

The pseudo-equilibrium point for the buck converter in canonical form (7.5) has coordinates given by

$$\widetilde{\mathbf{x}} = \begin{bmatrix} \frac{\nu+\mu}{\nu-\mu} \\ 0 \\ 0 \end{bmatrix} = \begin{bmatrix} 1 - 2y_r(1+ab) \\ 0 \\ 0 \end{bmatrix}.$$

Using the change of coordinates (7.36) proposed in Appendix 7.9, we calculate the coordinates of this point referring to the model of buck converter given in (7.31). In this way, we obtain

$$\mathbf{p} = T\widetilde{\mathbf{x}} + C = \begin{bmatrix} ay_r \\ y_r \\ 0 \end{bmatrix},$$

with matrices T and C given in Appendix 7.9.

Since $a_{23} < 0$, $a_{22} < 0$, $\mu = \nu - a_{23}\bar{y} > \nu$ and

$$\mu\nu = -a_{23}^2 y_r(\bar{y} - y_r),$$
$$\mu - \nu - \frac{a_{22}^2}{2} = \frac{4k\omega - 2(1+ak)^2}{k^4},$$

from the Proposition 7.2 we can conclude that:

(i) if $y_r < \bar{y} = \frac{1}{1+ab}$ then $\mathbf{p}$ is a real pseudo-equilibrium, that is, $\mathbf{p} \in \Sigma_{as}$;

(ii) $\mathbf{p}$ is a stable pseudo-node for $a \geq \frac{-1+2\sqrt{k\omega}}{k}$ and a stable pseudo-focus for $a < \frac{-1+2\sqrt{k\omega}}{k}$.

It is important to note that there is a threshold for reference parameter y_r, given by $y_r = \bar{y}$, so that just for $y_r < \bar{y}$ the proposed control keeps the buck converter working at the required point $\mathbf{p}$. Figure 7.11

shows some phase portraits of the buck converter controlled by SMC-washout, from of simulations of system (7.31), where is observed that from the breach of this threshold the buck converter pass to operate at the natural equilibrium $\overline{\mathbf{x}}^{-}$.

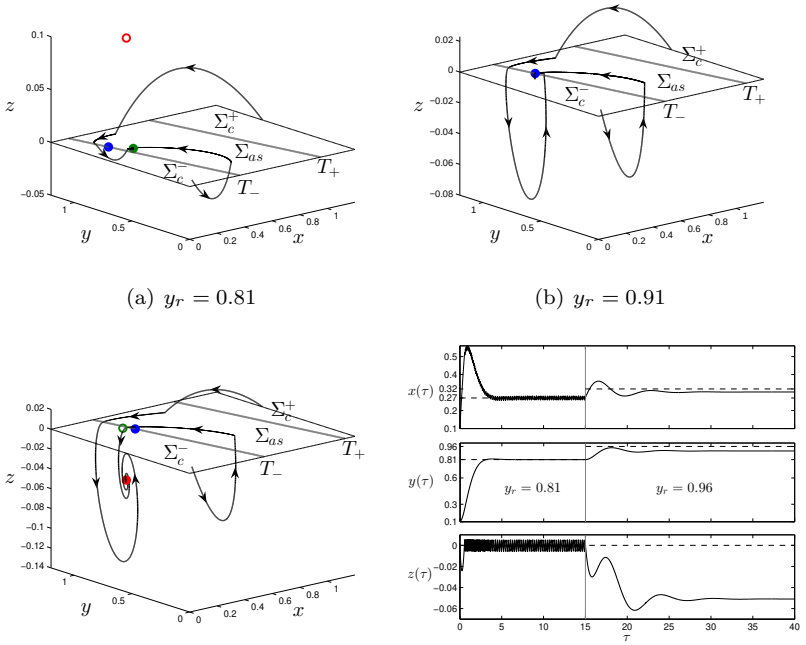

(a) $y_r = 0.81$

(b) $y_r = 0.91$

(c) $y_r = 0.96$

(d) Response time.

Figure 7.11: The persistence BEB in a buck converter. System (7.31) simulated with $b = 0.3$, $k = 1/2$, $\omega = 1$, $a = 1/3$ and for differents values of y_r. In (a), (b) and (c) we have the solution in state space and in (d) we have the solution in time. The blue point refers to the natural equilibrium, virtual in (a) and real in (c). The red point refers to the pseudo-equilibrium, real in (a) and virtual in (c). The green point refers to the cusp singularity in (a) and (c), but in (b), it refers to the boundary equilibrium. In (d), the dashed line indicates the operating point required for the converter, but not reached when the normalized reference voltage (y_r) exceeds the value 0.91.

Natural equilibrium $\overline{\mathbf{x}}^-$ and pseudo-equilibrium $\mathbf{p}$ do not coexist for $y_r \neq \bar{y}$. In this case, the *persistence* scenario of a BEB is observed in system (7.31), as shown in the Figure 7.11. In addition, for $y_r < \bar{y}$ the natural equilibrium $\overline{\mathbf{x}}^-$ is real and the pseudo-equilibrium $\mathbf{p}$ is virtual; and for $y_r > \bar{y}$ we have that $\overline{\mathbf{x}}^-$ is virtual and $\mathbf{p}$ is real. Applying Theorem 7.3 we prove this statements.

To conclude our analysis of the buck converter with a SMC strategy, modelled by 3D-DPWL system (7.31), we summarize the results of stability and bifurcation of their equilibrium points with respect to the parameters of reference y_r and resistive load a, showed in Figure 7.12. Natural equilibrium $\overline{\mathbf{x}}^-$ and pseudo-equilibrium $\mathbf{p}$ are stable (node or focus), as well as the natural equilibrium $\overline{\mathbf{x}}^+$ which we leave out because it is never present in the phase portrait of (7.31) (it is always virtual). For all pair of parameters (a, y_r) taken below the persistence bifurcation curve, that is, $y_r < \bar{y} = \frac{1}{1+ab}$, then $\mathbf{p} \in \Sigma_{as}$ is the unique equilibrium point present in the phase portrait of (7.31).

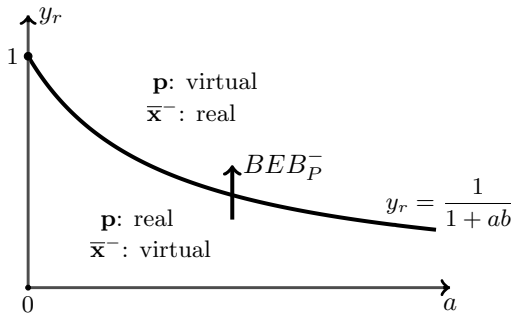

Figure 7.12: The persistence BEB in the (a, y_r)-plane of parameters.

7.7 Application 2: The buck converter feeding a nonlinear load of CPL-type

Results of the BEBs analysis performed in Section 7.5 can be applied to the 3D-DPWS systems where the vector fields involved are nonlinear, as we will see in this current section. For this, we consider the model of the buck converter connected to a constant power load and to regulate the output voltage of the converter we use sliding mode controller based on a washout filter. We also present a summary analysis of other bifurcations (classical and DIBs) of equilibria and limit cycles.

7.7.1 Closed loop control system modelling

In typical dc distribution systems with a cascaded converter architecture, loads connected to the bus by an electronic converter behave as constant power drawn from the feeder, and can be modelled as a constant power load (CPL, for short), see [111] and references therein. For this application we will use a 3D-DPWS system that models the voltage control process at the output of the bidirectional buck converter by feeding a CPL, see Figure 7.13.

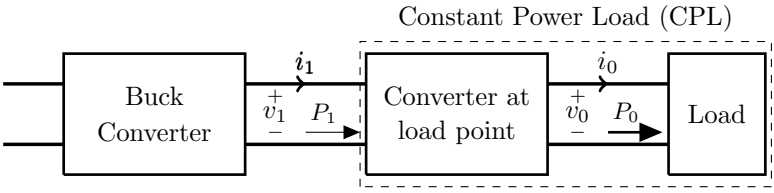

Figure 7.13: A converter at the load point behaves as a constant power load for the feeder (buck) converter. Both P_1, P_0, v_0 and i_0 are constants and $P_1 = P_0$, see [112].

We start from the system already written in the normalized form which is obtained from the change of coordinates and time variable

proposed in Table 7.2, adding $P = V_{in}^2\sqrt{\frac{C}{L}}d$, where P denotes the original CPL load parameter and d denotes the normalized CPL load parameter. In addition, to simplify, we assume this system without the presence of constant impedance loads (linear loads).

In this way, we consider the system given by

$$(\dot{x},\dot{y},\dot{z}) = \begin{cases} \mathcal{F}^+(x,y,z), \text{ if } z > 0 \\ \mathcal{F}^-(x,y,z), \text{ if } z < 0 \end{cases}, \tag{7.32}$$

composed by the nonlinear vector fields

$$\mathcal{F}^+(x,y,z) = \begin{bmatrix} -bx - y \\ x - d/y \\ f_3(x,y,z) \end{bmatrix} \quad \text{and} \quad \mathcal{F}^-(x,y,z) = \begin{bmatrix} 1 - bx - y \\ x - d/y \\ f_3(x,y,z) + k \end{bmatrix},$$

where

$$f_3(x,y,z) = (1-kb)x + (\omega - k)y - d/y - \omega z - \omega y_r,$$

$x \in (-x_{max}, x_{max})$, $y \in (0, y_{max})$ and $z \in \mathbb{R}$ are the normalized variables of inductor current, capacitor voltage and filter, respectively. The normalized parameters $d \in \mathbb{R}$, $b > 0$, $\omega \in (0,1]$, $k > 0$ and $0 < y_r < 1$ correspond to the CPL, inductor resistance, filter cut-off frequency, control parameter and reference voltage (desired voltage value at the output), respectively. Switching plane is defined by $\Sigma = \{(x,y,z) \in \mathbb{R}^3 : h(x,y,z) = z = 0\}$.

Tangency lines on the plane $z = 0$ are given by equations $L_{\mathcal{F}^+}h(x,y,0) = f_3(x,y,0) = 0$ and $L_{\mathcal{F}^-}h(x,y,0) = f_3(x,y,0) + k = 0$. In addition, there is an attractive sliding region (Σ_{as}) whenever $k > 0$, given by

$$\Sigma_{as} = \{(x,y,0) \in \Sigma : -k < f_3(x,y,0) < 0\}.$$

At Σ_{as} the sliding dynamics is described by system $(\dot{x},\dot{y},\dot{z}) = ky\mathcal{F}^s(x,y,0)$,

where $\mathcal{F}^s$ is the sliding vector field of system (7.32) and

$$\begin{aligned}\dot{x} &= -xy - \omega y(y - y_r) + d,\\ \dot{y} &= k(xy - d),\\ \dot{z} &= 0.\end{aligned}$$

System (7.32) has a pseudo-equilibrium point (equilibrium of $\mathcal{F}^s$) at $\widetilde{\mathbf{x}}(d) = (d/y_r, y_r, 0)$, for all $d \in \mathbb{R}$. This is the desired operating point in the state space of our control system under analysis. Natural equilibrium points of (7.32), that is, equilibria of $\mathcal{F}^{\pm}$, can coexist with the pseudo-equilibrium $\widetilde{\mathbf{x}}$. Points $\overline{\mathbf{x}}_{12}^{-} = \left(\frac{1\pm\gamma}{2b}, \frac{1\mp\gamma}{2}, \frac{1-2y_r\mp\gamma}{2b}\right)$, with $\gamma = \sqrt{1-4bd}$, are the equilibria of the vector field $\mathcal{F}^-$, being $\overline{\mathbf{x}}_1^- = \overline{\mathbf{x}}_1^-(d)$ defined for all $0 < d \leq 1/4b$ and $\overline{\mathbf{x}}_2^- = \overline{\mathbf{x}}_2^-(d)$ for all $d \leq 1/4b$, and such that $\overline{\mathbf{x}}_1^-(1/4b) = \overline{\mathbf{x}}_2^-(1/4b)$. While that $\mathcal{F}^+$ has a equilibrium point at $\overline{\mathbf{x}}^+(d) = \left(-\sqrt{\frac{-d}{b}}, \sqrt{-bd}, \sqrt{-bd} - y_r\right)$, defined for all $d \leq 0$. We next evaluate the stability and robustness of system (7.32) based on the study of bifurcations and numerical simulation.

7.7.2 On bifurcations and limit cycles

Both vector fields of system (7.32), $\mathcal{F}^{\pm}$ and also $\mathcal{F}^s$, determine smooth nonlinear dynamical systems so that we can find classical bifurcations of smooth systems in system (7.32). Furthermore, we can also find in system (7.32) different types of DIBs.

We start with a DIB known as BEB, based on the previously results of this Chapter. We chose the parameter d as the BEB bifurcation parameter. Taking $z = 0$ and solving the equations $\mathcal{F}^+(x, y, z, d) = \mathbf{0}$ and $\mathcal{F}^-(x, y, 0, d) = \mathbf{0}$ with respect to (x, y, z, d), we get

$$\left(\overline{\mathbf{x}}_b^-, d_B^-\right) = \left(-\frac{y_r}{b}, y_r, 0, \frac{(1-y_r)y_r}{b}\right), \tag{7.33}$$

$$\left(\overline{\mathbf{x}}_b^+, d_B^+\right) = \left(\frac{1-y_r}{b}, y_r, 0, -\frac{y_r^2}{b}\right), \tag{7.34}$$

respectively, where $\overline{\mathbf{x}}_b^{\pm}$ denote the boundary equilibrium of (7.32), related to the vector field $\mathcal{F}^{\pm}$, and appearing for the critical value $d = d_B^{\pm}$ of the load parameter.

Then, a piecewise-linear version of (7.32) at a boundary equilibrium point $(\overline{\mathbf{x}}_b, d_B)$ is obtained and represented by

$$\dot{\mathbf{x}} = \begin{cases} P\mathbf{x} + \mathbf{n}^-, & \text{if } z < 0 \\ P\mathbf{x} + \mathbf{n}^+, & \text{if } z > 0 \end{cases}, \tag{7.35}$$

where

$$\mathbf{x} = \begin{bmatrix} x \\ y \\ z \end{bmatrix}, \quad P = \begin{bmatrix} -b & -1 & 0 \\ 1 & d_B/y_r^2 & 0 \\ 1-bk & d_B/y_r^2 + \omega - k & -\omega \end{bmatrix},$$

$$\mathbf{n}^- = \begin{bmatrix} 1 \\ -(d+d_B)/y_r \\ -(d+d_B)/y_r + k - \omega y_r \end{bmatrix}, \quad \mathbf{n}^+ = \begin{bmatrix} 0 \\ -(d+d_B)/y_r \\ -(d+d_B)/y_r - \omega y_r \end{bmatrix},$$

with $d_B = d_B^- = \frac{(1-y_r)y_r}{b}$ if $\overline{\mathbf{x}}_b = \overline{\mathbf{x}}_b^-$ (boundary equilibrium related to $\mathcal{F}^-$) or $d_B = d_B^+ = -\frac{y_r^2}{b}$ if $\overline{\mathbf{x}}_b = \overline{\mathbf{x}}_b^+$ (boundary equilibrium related to $\mathcal{F}^+$).

System (7.35) meets the hypotheses **(H1)** and **(H2)** described in Section 7.3. The first is simple to check: $p_{31} = 1 - bk \neq 0$ and $n_3^- - n_3^+ = k > 0$. We can assume this, since usually $0 < k < 1/b$. For the second hypothesis, it is necessary to calculate the matrix Q applied at the points $d_B^{\pm}$ given in (7.33) and (7.34). Then, the parameters (y_r, k, b, ω) are easily selected so that $\mathrm{Det}\left[Q(d_B^{\pm})\right] = -p_{31}^2 - p_{32}^2 + (b + p_{22})p_{31}p_{32} \neq 0$.

Following the Theorem 7.1, we can write the system (7.35) in the canonical form (7.5), and so get the canonical system parameters (for each of the values $d = d_B^{\pm}$)

$$a_{23}(d) = \frac{8\omega b(d + d_B^+)}{k^3 y_r^2},$$

$$\nu(d) = \frac{8\omega b(d - d_B^-)}{k^3 y_r},$$
$$\mu(d) = \frac{8\omega b(d - d_B^+)}{k^3 y_r},$$

from the Lemma 7.1, which are responsible for the BEBs. Note that $\mu = \nu + \frac{8\omega}{k^3} > \nu$. Finally, we can prove the occurrence of persistence and nonsmooth fold bifurcations of boundary equilibria in the buck converter model considered, using the Theorem 7.3. The analysis proceeds in two stages, one for each vector field involved, $\mathcal{F}^{\pm}$.

Regarding the vector field $\mathcal{F}^+$, we have

$$\mu(d_B^+) = 0,$$
$$a_{23}(d_B^+)\nu(d_B^+) = \frac{128\omega^2}{k^6} > 0.$$

Therefore, for $d = d_B^+$ the system (7.32) undergoes a boundary equilibrium bifurcation of the *persistence* type (see item (a) of Theorem 7.3). Such a bifurcation involves the points of natural equilibrium $\overline{\mathbf{x}}^+$ and pseudo-equilibrium $\widetilde{\mathbf{x}}$.

Now, we pass to the boundary equilibrium of the vector field $\mathcal{F}^-$. In this case, we have

$$\nu(d_B^-) = 0,$$
$$a_{23}(d_B^-)\mu(d_B^-) = \frac{64\omega^2(1 - 2y_r)}{k^6 y_r} \neq 0 \text{ if } y_r \neq 1/2.$$

Therefore, if $y_r > 1/2$ the *persistence* BEB is observed at the boundary equilibrium point $\overline{\mathbf{x}}_b^-$; or in otherwise, if $y_r < 1/2$ the *nonsmooth fold* BEB is observed (see item (b) of Theorem 7.3). First case involves the equilibria points $\overline{\mathbf{x}}_1^-$ and second case involves $\overline{\mathbf{x}}_2^-$.

Figure 7.14 shows a (y_r, d)-plane of parameters, where the black parabolic curves indicate occurrence of the boundary equilibrium bifurcations. At the complete parabolic curve of equation

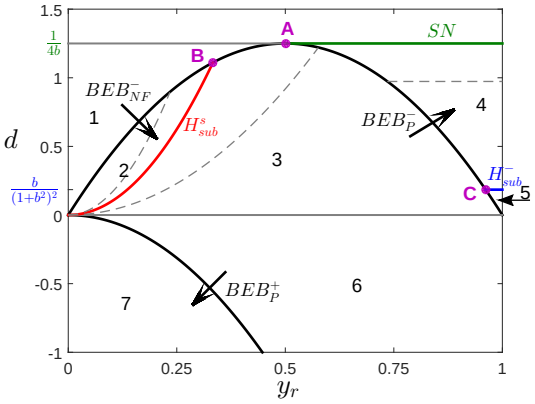

Figure 7.14: Equilibria bifurcations set in the (y_r, d)-plane of parameters, assuming $b = 0.2$, $k = 0.1$ and $\omega = 1$.

$$d = d_B^-(y_r) = \frac{(1 - y_r)y_r}{b},$$

the left branch refers to the *nonsmooth fold* BEB involving the equilibrium $\overline{\mathbf{x}}_1^-$ of the vector field $\mathcal{F}^-$ (BEB^-_{NF}). While that, the right branch refers to the *persistence* BEB involving the equilibrium $\overline{\mathbf{x}}_2^-$, also equilibrium of $\mathcal{F}^-$ (BEB^-_P). The half-parabola of equation

$$d = d_B^+(y_r) = -\frac{y_r^2}{b},$$

refers to the *persistence* BEB involving the equilibrium $\overline{\mathbf{x}}^+$ of the vector field $\mathcal{F}^+$ (BEB^+_P). The black arrows in this figure, indicates the side of the parabolic curve where the equilibrium of $\mathcal{F}^\pm$ is real, consequently, in the opposite side is virtual.

The vector fields involved $\mathcal{F}^\pm$ and also $\mathcal{F}^s$ exhibit some classical bifurcations such as (i) saddle-node bifurcation of the equilibria $\overline{\mathbf{x}}_{12}^-$, indicated by the green straight line segment (SN) in Figure 7.14 and occurring to

$$d = \frac{1}{4b};$$

Regions	$\overline{\mathbf{x}}^{+}$	$\overline{\mathbf{x}}_1^{-}$	$\overline{\mathbf{x}}_2^{-}$	$\widetilde{\mathbf{x}}$
1	-	virtual	virtual	virtual
2	-	real saddle	virtual	real unstable node/focus
3	-	real saddle	virtual	real stable node/focus
4	-	real saddle	real unstable node/focus	virtual
5	-	real saddle	real stable focus	virtual
6	virtual	-	virtual	real stable node
7	real stable node	-	virtual	real stable node

Table 7.3: Equilibria stability according to the Figure 7.14.

(ii) the subcritical Hopf bifurcations of the equilibrium $\overline{\mathbf{x}}_2^-$ and pseudo-equilibrium $\widetilde{\mathbf{x}}$, indicated by the blue straight line segment (H_{sub}^-) and red parabolic curve segment (H_{sub}^s), and occurring to

$$d = \frac{b}{(1+b^2)^2} \quad \text{and} \quad d = \frac{y_r^2}{k},$$

respectively. Moreover, in Figure 7.14 the points $A(1/2, 1/(4b))$, $B(k/(b+k), k/(b+k)^2)$ and $C(1/(1+b^2), b/(1+b^2)^2)$ indicate bifurcations of codimension two where the saddle-node or Hopf bifurcations are occurring simultaneously to a BEB.

The results of stability and bifurcations of equilibria in system (7.32), according to the region in the (y_r, d)-plane defined in Figure 7.14, are summarized in the Table 7.3. These regions are demarcated by solid lines and the dashed lines indicate the node/focus dynamics transition of equilibria. So, choosing a point (y_r, d) in the bifurcations set of Figure 7.14, we know the dynamics involving the equilibria.

Example 7.6. Boundary Focus Bifurcations: *persistence case with stable pseudo-node and unstable focus.* *Consider $y_r = 0.9$. If d is disturbed around the critical value $d = d_B^- = 0.45$, so that we moved from region 3 to the region 4 in Figure 7.14, then persistence BEB involving the unstable focus equilibrium $\mathbf{e}_2^-$ and the stable pseudo-node $\mathbf{p}$, is observed in system* (7.32)*. This dynamic scenario is simulated and shown in Figure 7.15, where the points of focus equilibrium, pseudo-node and boundary equilibrium are represent by red, green and blue dots, respectively. A stable limit cycle with sliding part arises in the state space for $d > d_B^- = 0.45$.*

Boundary focus bifurcations in planar Filippov systems were studied in [78], from which it was proved the existence of five generic critical cases. These BEBs involving a natural focus equilibrium, a pseudo-equilibrium and a fold singularity. In the case where the natural equilibrium is an unstable focus, the pseudo-equilibrium is stable we have a persistence BEB. Such a bifurcation produce a stable limit cycle that

is composed of two segments of orbits, one defined by the sliding vector field $\mathcal{F}^s$ and the other by vector field $\mathcal{F}^-$ (or $\mathcal{F}^+$). In addition, this limit cycle is present in the state space when the focus is a real equilibrium close to the Σ, the pseudo-equilibrium is virtual and the fold singularity is visible.

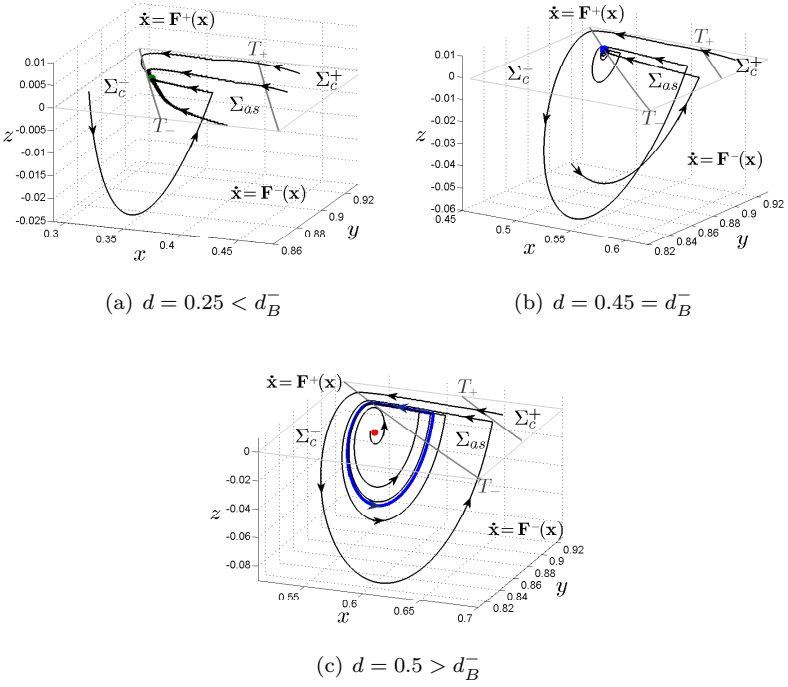

(a) $d = 0.25 < d_B^-$

(b) $d = 0.45 = d_B^-$

(c) $d = 0.5 > d_B^-$

Figure 7.15: Simulation results of Buck-SMC-Washout system (7.32) with parameters $b = 0.2$, $\omega = 1$, $k = 0.1$ and $y_r = 0.9$.

Figure 7.15 shows an $\mathbb{R}^3$ version for the boundary focus collision in a Filippov system, from simulation results of the buck converter system (7.32). As in the two-dimensional case, a stable limit cycle with sliding part arises from a boundary equilibrium of dynamic unstable focus for $\mathcal{F}^-$ and stable node for $\mathcal{F}^s$. In $\mathbb{R}^3$, the tangential singularity involved is of the cusp type and divided the line of tangency into fold visible and

invisible. In addition, this limit cycle is present in the state space when the focus is a real equilibrium close to the Σ, the pseudo-equilibrium is virtual and the cusp singularity is "visible" (that is, $L^3_{\mathcal{F}^-}h(\mathbf{x}_c^-) < 0$ at the cusp point).

Example 7.7. Grazing Bifurcation. *Consider in system* (7.32) *that* $b = \sqrt{1/3}$, $\omega = 1$, $k = 0.5$, $y_r = 0.937$ *and* $d = 0.305$. *In this case there is an unstable limit cycle around the real focus equilibrium of the vector field* $\mathcal{F}^-$, *tangent to the switching boundary* Σ, *see Figure 7.16. For a small perturbation in parameter* d *(for* $d < 0.305$*) this limit cycle is destroyed. Then we have a Grazing bifurcation occurring in system* (7.32).

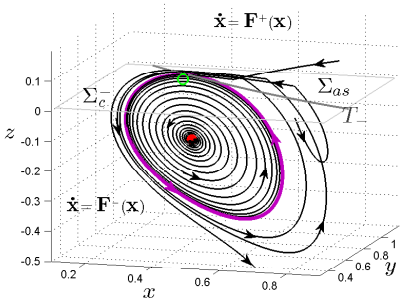

Figure 7.16: Simulation results of Buck-SMC-Washout system (7.32) with parameters $b = \sqrt{1/3}$, $\omega = 1$, $k = 0.5$, $y_r = 0.937$ and $d = 0.305$.

7.8 Conclusion

In this Chapter we have studied a canonical form to 3D-DPWL systems with parallel tangency lines containing the singularity cusp each. Such an adopted model often appears in problems of engineering and it is used to describe the dynamics of discontinuous control systems such as the SMC. For this family of systems, we have determined the specific conditions on the system parameters for a BEB to

occur, classifying it into persistence or nonsmooth fold. Furthermore, we have provided a complete classification of the sliding dynamics at the pseudo-equilibrium, which is valid for when it becomes a boundary equilibrium. From the combination of the results on the BEBs and sliding dynamics, we then exhibit all the unfolding dynamics of the BEBs in the sliding vector field.

Two applications were considered. In both we used the buck converter with sliding mode control and washout filter, but in the first application we take the converter connected to a resistive load, while in the second we considered a CPL load. In the system with CPL load we have identified other bifurcations of equilibria (saddle-node, Hopf and sliding Hopf) and of limit cycles (Grazing bifurcation). In addition to these, we highlight the case study done on the boundary focus bifurcation in $\mathbb{R}^3$, which is associated with the birth of a nonsmooth limit cycle with a sliding segment.

7.9 Appendix: Proof of Theorem 7.1

Linear transformation of the state space of system (7.4) on the state space of system (7.5), provided by Theorem 7.1, is obtained by applying the change of coordinates

$$\mathbf{y} = T\mathbf{x} + C, \tag{7.36}$$

where $T = T_1T_2T_3$ is an invertible matrix, $C = T_1N_2 + N_1$, $\mathbf{y}$ denotes the state vector of (7.4) and $\mathbf{x}$ denotes the state vector of (7.5); with

$$T_1 = \begin{bmatrix} \frac{n_3^- - n_3^+}{2p_{31}} & \frac{p_{32}}{\mathrm{Det}[Q]} & -\frac{p_{33}}{p_{31}} \\ 0 & -\frac{p_{31}}{\mathrm{Det}[Q]} & 0 \\ 0 & 0 & 1 \end{bmatrix}, \quad T_2 = \begin{bmatrix} 1 & 0 & 0 \\ r & -\frac{(n_3^- - n_3^+)^2}{4} & q \\ 0 & 0 & 1 \end{bmatrix},$$

$$T_3 = \begin{bmatrix} 1 & 0 & 0 \\ \frac{2}{(n_3^- - n_3^+)^2}s & 1 & 0 \\ 0 & 0 & 1 \end{bmatrix},$$

$$N_1 = \begin{bmatrix} -\frac{n_3^- + n_3^+}{2p_{31}} \\ 0 \\ 0 \end{bmatrix}, \quad N_2 = \begin{bmatrix} 0 & 0 & 0 \\ \frac{p_{31}}{2} & \frac{p_{32}}{2} & \frac{-p_{11}p_{31} - p_{21}p_{32}}{2p_{31}} \\ 0 & 0 & 0 \end{bmatrix} \begin{bmatrix} n_1^- + n_1^+ \\ n_2^- + n_2^+ \\ n_3^- + n_3^+ \end{bmatrix},$$

$$q = p_{13}p_{31} + p_{23}p_{32} - \frac{p_{33}}{p_{31}}(p_{11}p_{31} + p_{21}p_{32}),$$

$$r = \frac{(n_3^- - n_3^+)(p_{21}p_{32} + p_{31}(p_{11} + p_{33}))}{2p_{31}},$$

$$s = \begin{bmatrix} p_{31} & p_{32} & p_{33} \end{bmatrix} \begin{bmatrix} n_1^- - n_1^+ \\ n_2^- - n_2^+ \\ n_3^- - n_3^+ \end{bmatrix}.$$

We are assume that in hypothesis **(H1)** the condition $p_{31} \neq 0$ hold, while p_{32} can be null or not. For the change in the time scale, we use the relation

$$t = \frac{2}{n_3^- - n_3^+}\tau, \tag{7.37}$$

where t denotes the time variable of (7.4) and τ denotes the time variable of (7.5).

The proposed transformation is done in two steps, as follow.

First change of coordinates is given by $\mathbf{y} = T_1\mathbf{x}_1 + N_1$. From it, tangency lines T_- and T_+ are moved to the vertical lines at $(-1, v, 0)$ and $(1, v, 0)$, for $v \in \mathbb{R}$, respectively. Moreover, the new system always has a point in $T_\pm$ connecting the half-line of visible folds with the half-line of invisible folds. These connection points are generically singularities cusp. Then the time variable is changed by applying (7.37). Note that, from **(H1)** we have $n_3^- - n_3^+ > 0$. In this way, the time normalization eliminates cases where the sliding region is repulsive, thus obtaining a system always presenting an attractive sliding region.

Second change of coordinates is given by $\mathbf{x}_1 = T_2T_3\mathbf{x} + N_2$. From it, cusp singularity of T_- and of T_+ are moved to the points $(-1, 0, 0)$ and $(1, 0, 0)$, respectively. Moreover, points $(-1, v, 0) \in T_-$ are fold singularities of the visible type for $v < 0$ and invisible for $v > 0$; while that $(1, v, 0) \in T_+$ are fold singularities of the visible type for $v > 0$ and invisible for $v < 0$.

The calculation of the important parameters a_{23} and a_{22} given in Lemma 7.1, as well as the other parameters of matrix A given in (7.5), are directly obtained by

$$A = \frac{2}{n_3^- - n_3^+} T^{-1}PT.$$

Chapter 8

Final Remarks

In Chapter 2, some aspects on the theory of DPWS systems were reviewed, giving tools for the analysis of dynamic behaviour of these systems and laying the groundwork for the course of the thesis. In this chapter we have stated a simple and accurate definition for TS-bifurcation. This is an important and original result of this thesis.

Our journey through the world of bifurcations in 3D-DPWS systems started in Chapter 3 where, from the dc-dc boost converter model with SMC-washout, we have studied the Hopf and Homoclinic bifurcations in the vector field sliding. The main contribution was the characterization of the mechanism for the annihilation of a limit cycle in the sliding vector field of 3D-DPWS systems with a two-fold point. Specifically, we have determined that the limit cycle which appears due to Hopf bifurcation at the pseudo-equilibrium disappears when touching an invisible-visible two-fold point, forming a homoclinic loop that closes at this point. This is a naturally expected result since the two-fold point is a saddle equilibrium of the sliding vector field in this situation. The case study made in this Chapter leave us motivated for new research addressing more general results and incorporating more elements such as another pseudo-equilibrium and/or two-fold.

In Chapter 4 we have thoroughly studied the TS-bifurcation, characterized by a pseudo-equilibrium transition from the attractive sliding region to the repulsive sliding region (or vice versa), where the transition point is a T-singularity. Such a bifurcation is associated with the birth of a crossing limit cycle (CLC). After carefully deriving a local canonical form, we have reviewed the previous works regarding this bifurcation and were provided, by means of a more direct approach, the critical coefficients that characterize the bifurcation, also giving computational procedures for them. The achieved results on TS-bifurcation were applied to some illustrative examples and also in a dc-dc boost converter under a sliding mode control strategy and washout filter. In this Chapter, we have contributed with a detailed computational procedure that allows to prove the occurrence of TS-bifurcation in 3D-DPWS systems, which were made easy to apply, since we have provided all the necessary tools. In particular, the possible existence of invariant tori (quasi-periodic behavior) and homoclinic tangles (chaotic regimes) for the crossing dynamics around the T-singularity deserve new research efforts. Also, for new research, it is in our interest to apply the proposed method of TS-bifurcation analysis in other systems known in the literature, especially those that are related to some sliding mode control application.

Chapter 5 was dedicated to the study of local and global bifurcations related to TS-bifurcation and crossing limit cycles (CLCs). For this we have considered the model of a dc-dc boost converter with sliding mode control and washout filter. As a consequence of our analysis, we have proved the occurrence of classical equilibria bifurcations (saddle-node, transcritical, Hopf), involving the pseudo-equilibrium of the system. Apart from the analytical verification of the TS-bifurcation in this power converter, we have numerically detected other non-local phenomena like a saddle-node bifurcation of CLCs. Experimental results to illustrate the effects of the TS-bifurcation in a real circuit prototype of a boost converter were also presented. Such a bifurcation can be induced varying the value of the resistive load, in such a way that

it changes the position of the operating point (a pseudo-equilibrium) and its stability from stable to unstable. This change is critical and creates a stable CLC, which can have a large amplitude with catastrophic effects for the converter. Thus, the analysis of the existence of TS-bifurcations becomes essential in the design and control of converters, since this is a dynamic phenomenon that is not desired and not easy to detect. Therefore, it is of great relevance to know the parametric conditions for the occurrence of this bifurcation and so to establish safeguards in order to avoid it. The identification of the Teixeira singularity in a real circuit of power electronic was the main contribution of this chapter, as well as the analytical, numerical and experimental results on bifurcations, which helped us to unravel the dynamical richness of this circuit. Among other contributions that can be highlighted in this chapter, we present (i) the numerical proof of the coexistence of two CLCs, one stable originated in the supercritical TS-bifurcation and another unstable arising from the subcritical TS-bifurcation; (ii) the numerical identification of global mechanisms for the vanishing (or birth) of CLC (saddle-node bifurcation and non-standard homoclinic bifurcation); (iii) the existence and stability analysis of a CLC from its birth to its annihilation; and (iv) the proposal of a numerical method to investigate the existence and the dynamics of CLCs, which can be applied to other physical systems modelled as 3D-DPWL systems and that exhibit the Teixeira singularity. As a goal for new research, we intend to repeat the numerical method of bifurcation analysis of CLCs in other systems related to real applications in the engineering or sciences.

Chapter 6 addressed a detailed analysis of bifurcations in 3D-DPWS systems that have two points of T-singularity. In addition, from the variation of a system parameter, these T-singularities collide and then they disappear along with the attractive sliding region. In this case a Fold bifurcation occurs and at the bifurcation point it appears a type of degenerate T-singularity. We have determined the conditions on the system parameters so that there is a real pseudo-equilibrium colliding with one of the T-singularities or the two T-singularities simultaneously

colliding with the pseudo-equilibrium. In the first case, a TS-bifurcation occurs and, in the second case, a non regular case of larger codimension of this bifurcation occurs, which we named double TS-bifurcation. Like the TS-bifurcation, the double TS-bifurcation is also associated with the birth of a CLC, but here, it arises from the 1-degenerate T-singularity. In general, we have made a detailed description of the sliding and crossing dynamics around the T-singularities, regular or degenerate, and also the sliding dynamics at the real pseudo-equilibrium. As a consequence of our study, we have identified the presence of two invariant (non-smooth) cones with its vertex in one of the regular T-singularities, which bifurcates from an invariant (non-smooth) ellipsoid with vertices at the two regular T-singularities. Moreover, some classical bifurcations (saddle-node, transcritical, pitchfork) were observed in the sliding vector field. From the unfolding dynamics of such phenomena we described the birth of CLCs, the stability and the bifurcations (saddle-node of limit cycles and a non-standard homoclinic), from the analysis of the first return map associated to the case study addressed. We have proved that the system considered in this case study can exhibit two coexisting CLCs at most. The fold bifurcation of T-singularities and the double TS-bifurcation are not yet known in the literature and we have contributed with this first contact with them, introducing important results and detailed characterizations of such bifurcations and their unfolding. For future works, we aim at determine more general results on the crossing dynamics prevailing in such bifurcations, and also to carry out other case studies.

In Chapter 7 we have studied a family of 3D-DPWS systems in which the vector fields are linear (in this case, are DPWL systems) on both sides of the switching boundary and with two parallel tangency lines containing a singularity cusp each. We showed that such an adopted model often appears in problems of engineering and it is used to describe the dynamics of discontinuous control systems such as sliding mode control. We provide a canonical form for such systems and, with that, we simplified the calculations and the geometry re-

lated to the topological configuration on the switching boundary. This canonical form is an important result obtained, since from this model we can study all types of boundary equilibrium bifurcations (BEBs) that can occur in the system family considered. The results obtained on the stability and the bifurcations were applied to two examples in power electronics systems involving the sliding mode control of dc-dc buck converters. The main results and contributions achieved in this chapter were: (i) The classification of BEBs in an important family of 3D-DPWL systems giving explicit conditions for the occurrence of each of the two scenarios, persistence and nonsmooth fold. In addition, we have presented in Section 7.5 some of the possible unfolding of BEBs in $\mathbb{R}^3$, from some examples taken with the canonical form. (ii) The complete characterization of the sliding dynamics in systems belonging to the family studied. In addition, we presented the classification of the possible types (saddle, node, focus, center) of pseudo-equilibrium and boundary equilibria. (iii) The proof of the existence of BEBs in power converters under a SMC strategy, the identification (from the simulated results, guided by the local analysis of bifurcations) of a stable limit cycle in $\mathbb{R}^3$ with sliding part (from a boundary focus collision) and also the identification of a *Grazing* bifurcation of limit cycle are unprecedented results in DIBs applications for 3D-DPWS systems. In this chapter we have explored a classification of some topologically distinct cases of BEBs in $\mathbb{R}^3$, a problem still open in the literature, which we take as objective for future works.

We close this thesis with the list of the articles published in journals and main works presented at scientific events, whose productions originate from this Thesis.

- Published:

  [1] L. Benadero, R. Cristiano, D. J. Pagano and E. Ponce. *Nonlinear Analysis of Interconnected Power Converters: A Case Study.* Emerging and Selected Topics in Circuits and Systems, IEEE Journal on, 5(3):326-335,2015.

[2] R. Cristiano, D. J. Pagano, L. Benadero and E. Ponce. *Bifurcation Analysis of a DC-DC Bidirectional Power Converter Operating with Constant Power Load.* International Journal of Bifurcation and Chaos, 26(4):1630010, 2016.

[3] R. Cristiano, T. Carvalho, D. J. Tonon and D. J. Pagano. *Hopf and Homoclinic bifurcations on the sliding vector field of switching systems in $\mathbb{R}^3$: A case study in power electronics.* Physica D: Nonlinear Phenomena, 347:12-20, 2017.

[4] R. Cristiano, D. J. Pagano, E. Freire and E. Ponce. *Revisiting the Teixeira Singularity Bifurcation Analysis. Application to the Control of Power Converters.* International Journal of Bifurcation and Chaos, 28(9)1850106 (31 pages), 2018.

- Works of scientific events:

[5] 13th DANCE Winter School RTNS2016. *Degenerate T-singularity Bifurcation in 3D Filippov Systems: A case study approach.* Rony Cristiano and Daniel J. Pagano. Institute of Mathematics of the University of Seville (IMUS), 25 - 29 January 2016.

[6] NoLineal 2016 - International conference on nonlinear mathematics and physics. *On the TS-Bifurcation in $\mathbb{R}^3$.* Rony Cristiano, Enrique Ponce, Emilio Freire and Daniel J. Pagano. Sevilla, June 7-10, 2016.

Bibliography

[1] A. Algaba, E. Freire, E. Gamero, and C. García. A bifurcation analysis of planar nilpotent reversible systems. *Nonlinear Dynamics*, 87(2):835–849, Jan 2017.

[2] A. A. Andronov, E. A. Leontovich, I. I. Gordon, and A. G. Maier. *Theory of Bifurcations of Dynamical Systems on a Plane*. Israel Program for Scientific Translations, Jerusalem, 1971.

[3] A. A. Andronov, A. A. Vitt, and S. E. Khaikin. *Theory of oscillators*. Pergamon Press Oxford, 1966.

[4] A. E. Aroudi. A new approach for accurate prediction of subharmonic oscillation in switching regulators - part I: Mathematical derivations. *IEEE Trans. on Power Electronics*, 32(7):5651–5665, July 2017.

[5] A. E. Aroudi. A new approach for accurate prediction of subharmonic oscillation in switching regulators - part II: Case studies. *IEEE Trans. on Power Electronics*, 32(7):5835–5849, July 2017.

[6] A. E. Aroudi, D. Giaouris, H. H.-C. Lu, and I. A. Hiskens. A review on stability analysis methods for switching mode power converters. *IEEE Journal on Emerging and Selected Topics in Circuit and Systems*, 5(3):302–315, 2015.

[7] J. P. Aubin and A. Cellina. *Differential Inclusions*. Springer-Verlag, Berlin, 1984.

[8] V. I. Babitskii. *Theory of Vibroimpact Systems. Approximate methods*. Nauka, Moscow, 1978.

[9] P. Baghernia, R. K. Moghaddam, and H. Kobravi. Cancer sliding mode control considering to chaotic manners of system. *Journal of Medical Imaging and Health Informatics*, 5, 06 2015.

[10] A. Barreiro, J. Aracil, and D. J. Pagano. Detection of attraction domains of non-linear systems using bifurcation analysis and Lyapunov functions. *Int. J. Control*, 75(5):314–327, 2002.

[11] F. Battelli and M. Feckan. Bifurcation and chaos near sliding homoclinics. *Journal of Differential Equations*, 248(9):2227 – 2262, 2010.

[12] L. Benadero, R. Cristiano, D. J. Pagano, and E. Ponce. Nonlinear analysis of interconnected power converters: A case study. *Emerging and Selected Topics in Circuits and Systems, IEEE Journal on*, 5(3):326–335, 2015.

[13] L. Benadero, E. Ponce, A. E. Aroudi, and F. Torres. Limit cycle bifurcations in resonant LC power inverters under zero current switching strategy. *Nonlinear Dynamics*, 91(2):1145–1161, Jan 2018.

[14] B. Biemond. *Nonsmooth dynamical systems: on stability of hybrid trajectories and bifurcations of discontinuous systems*. PhD thesis, TUE : Department of Mechanical Engineering, 2013.

[15] C. Bonet, T. M. Seara, E. Fossas, and M. R. Jeffrey. A unified approach to explain contrary effects of hysteresis and smoothing in nonsmooth systems. *Communications in Nonlinear Science and Numerical Simulation*, 50:142 – 168, 2017.

[16] H. Broer, R. Roussarie, and C. Simó. Invariant circles in the Bogdanov-Takens bifurcation for diffeomorphisms. *Ergodic Theory Dynamical Sustems*, 16:1147–1172, 1996.

[17] B. Brogliato. *Nonsmooth Mechanics*. Springer-Verlag, 1999.

[18] C. A. Buzzi, T. de Carvalho, and M. A. Teixeira. On three-parameter families of Filippov systems - the fold-saddle singularity. *International Journal of Bifurcation and Chaos*, 22(12):1250291, 18, 2012.

[19] V. Carmona, S. Fernández-García, and E. Freire. Saddle-node bifurcation of invariant cones in 3D piecewise linear systems. *Physica D: Nonlinear Phenomena*, 241(5):623 – 635, 2012.

[20] V. Carmona, E. Freire, E. Ponce, J. Ros, and F. Torres. Limit cycle bifurcation in 3D continuous piecewise linear systems with two zones: Application to Chua's circuit. *International Journal of Bifurcation and Chaos*, 15(10):3153–3164, 2005.

[21] T. Carvalho, L. F. O. Mello, and D. C. Braga. Limit cycles bifurcating from discontinuous centers. *IMA Journal of Applied Mathematics*, 82:849–863, 2017.

[22] T. Carvalho and D. J. Tonon. Normal forms for codimension one planar piecewise smooth vector fields. *International Journal of Bifurcation and Chaos*, 24(07):1450090, 2014.

[23] M. Castilla, L. C. de Vicuña, M. Lopez, O. Lopez, and J. Matas. On the design of sliding mode control schemes for quantum resonant converters. *IEEE Transactions on Power Electronics*, 15(6):960–973, 2000.

[24] A. Colombo. *A bifurcation analysis of discontinuous systems: theory and applications*. PhD thesis, Politecnico di Milano, Italy, 2009.

[25] A. Colombo, M. di Bernardo, E. Fossas, and M. R. Jeffrey. Teixeira singularities in 3D switched feedback control systems. *Systems & Control Letters*, 59:615–622, 2010.

[26] A. Colombo and M. R. Jeffrey. Nondeterministic chaos, and the two-fold singularity in piecewise smooth flows. *SIAM J. Applied Dynamical Systems*, 10(2):423–451, 2011.

[27] S. Coombes. Neuronal networks with gap junctions: A study of piecewise linear planar neuron models. *SIAM Journal on Applied Dynamical Systems*, 7(3):1101–1129, 2008.

[28] R. Cristiano, T. Carvalho, D. J. Tonon, and D. J. Pagano. Hopf and homoclinic bifurcations on the sliding vector field of switching systems in $\mathbb{R}^3$: A case study in power electronics. *Physica D: Nonlinear Phenomena*, 347:12 – 20, 2017.

[29] R. Cristiano, D. J. Pagano, L. Benadero, and E. Ponce. Bifurcation analysis of a DC-DC bidirectional power converter operating with constant power load. *International Journal of Bifurcation and Chaos*, 26(4):1630010 (18 pages), 2016.

[30] R. Cristiano, D. J. Pagano, E. Freire, and E. Ponce. Revisiting the Teixeira singularity bifurcation analysis. Application to the control of power converters. *International Journal of Bifurcation and Chaos*, 28(9):1850106 (31 pages), 2018.

[31] F. Cunha and J. Pagano. Bifurcation analysis of the Lotka-Volterra model subject to variable structure control. *IFAC Proceedings Volumes*, 35(1):101 – 106, 2002. 15th IFAC World Congress.

[32] B. R. de Freitas, J. Llibre, and J. C. Medrado. Limit cycles of continuous and discontinuous piecewise-linear differential systems in $\mathbb{R}^3$. *Journal of Computational and Applied Mathematics*, 338:311 – 323, 2018.

[33] H. de Jong, J.-L. Gouzé, C. Hernandez, M. Page, T. Sari, and J. Geiselmann. Qualitative simulation of genetic regulatory networks using piecewise-linear models. *Bulletin of Mathematical Biology*, 66(2):301 – 340, 2004.

[34] B. L. V. de Vrande, D. H. V. Campen, and A. de Kraker. An approximate analysis of dry-friction-induced stick-slip vibrations by a smoothing procedure. *Nonlinear Dynamics*, 19(2):159–171, 1999.

[35] F. Dercole, F. D. Rossa, A. Colombo, and Y. A. Kuznetsov. Two degenerate boundary equilibrium bifurcations in planar Filippov systems. *SIAM Journal on Applied Dynamical Systems*, 10(4):1525 – 1553, 2011.

[36] M. di Bernardo, C. Budd, and A. Champneys. Grazing, skipping and sliding: Analysis of the non-smooth dynamics of the DC/DC buck converter. *Nonlinearity*, 11(4):858–890, 1998.

[37] M. di Bernardo, C. J. Budd, A. R. Champneys, and P. Kowalczyk. *Piecewise-Smooth Dynamical Systems: Theory and Applications*. Springer, 2008.

[38] M. di Bernardo, C. J. Budd, A. R. Champneys, and P. Kowalczyk. *Bifurcation and chaos in piecewise smooth dynamical systems-theory and applications*. Springer-Verlag, London, UK, 2008a.

[39] M. di Bernardo, A. Colombo, and E. Fossas. Two-fold singularity in nonsmooth electrical systems. In *Circuits and Systems (ISCAS), IEEE International Symposium on*, pages 2713–2716, 2011.

[40] M. di Bernardo, M. Feigin, S. J. Hogan, and M. E. Homer. Local analysis of C-bifurcations in n-dimensional piecewise smooth dynamical systems. *Chaos Soliton Fract*, 10:1981–1908, 1999.

[41] M. di Bernardo, F. Garefalo, L. Glielmo, and F. Vasca. Switchings, bifurcations, and chaos in DC/DC converters. *Circuits and Systems I: Fundamental Theory and Applications, IEEE Transactions on*, 45(2):133–141, 1998.

[42] M. di Bernardo and S. J. Hogan. Discontinuity-induced bifurcations of piecewise smooth dynamical systems. *Philosophical*

Transactions of the Royal Society of London A: Mathematical, Physical and Engineering Sciences, 368(1930):4915–4935, 2010.

[43] M. di Bernardo, K. H. Johansson, and F. Vasca. Self-oscillations and sliding in relay feedback systems: Symmetry and bifurcations. *International Journal of Bifurcation and Chaos*, 11(04):1121–1140, 2001.

[44] M. di Bernardo, A. Nordmark, and G. Olivar. Discontinuity-induced bifurcations of equilibria in piecewise-smooth and impacting dynamical systems. *Physica D: Nonlinear Phenomena*, 237(1):119 – 136, 2008.

[45] M. di Bernardo, D. J. Pagano, and E. Ponce. Nonhyperbolic boundary equilibrium bifurcations in planar Filippov systems: A case study approach. *International Journal of Bifurcation and Chaos*, 18(5):1377–1392, 2008.

[46] R. W. Erickson and D. Maksimovic. *Fundamentals of power electronics*. Kluwer Academic Press, 2nd edition, 2004.

[47] M. Esteban, E. Ponce, and F. Torres. Bifurcation analysis of hysteretic systems with saddle dynamics. *Applied Mathematics and Nonlinear Sciences*, 2:449–464, 11 2017.

[48] M. I. Feigin. On the structure of C-bifurcation boundaries of piecewise-continuous systems. *Journal of Applied Mathematics and Mechanics*, 42(5):885 – 895, 1978.

[49] S. Fernandez-Garcia, D. A. Garcia, G. O. Tost, M. di Bernardo, and M. R. Jeffrey. Structural stability of the two-fold singularity. *SIAM Journal on Applied Dynamical Systems*, 11(4):1215–1230, 2012.

[50] A. F. Filippov. Differential equations with discontinuous right-hand side. *American Mathematical Society Translations*, 2(42):199 – 231, 1964.

[51] A. F. Filippov. *Differential Equations with Discontinuous Right-hand Sides.* Kluwer Academic Publishers, Dordrecht, 1988.

[52] E. Freire, E. Ponce, F. Rodrigo, and F. Torres. Bifurcation sets of continuous piecewise linear systems with two zones. *International Journal of Bifurcation and Chaos*, 08(11):2073–2097, 1998.

[53] E. Freire, E. Ponce, and J. Ros. Limit cycle bifurcation from center in symmetric piecewise-linear systems. *International Journal of Bifurcation and Chaos*, 9(5):895–907, 1999.

[54] E. Freire, E. Ponce, and F. Torres. Canonical discontinuous planar piecewise linear systems. *SIAM Journal on Applied Dynamical Systems*, 11(1):181–211, 2012.

[55] E. Freire, E. Ponce, and F. Torres. A general mechanism to generate three limit cycles in planar Filippov systems with two zones. *Nonlinear Dynamics*, 78(1):251–263, Oct 2014.

[56] U. Galvanetto. Some discontinuous bifurcations in a two-block stick-slip system. *Journal of Sound and Vibration*, 248(4):653 – 669, 2001.

[57] U. Galvanetto, S. R. Bishop, and L. Briseghella. Mechanical stick-slip vibrations. *International Journal of Bifurcation and Chaos*, 05(03):637–651, 1995.

[58] M. Gatto, D. Mandrioli, and S. Rinaldi. Pseudoequilibrium in dynamical systems. *Int. J. Syst. Sci.*, 4:809–824, 1973.

[59] P. A. Glendinning. *Stability, Instability and Chaos: an introduction to the teory of nonlinear differential equations.* Cambridge University Press, 1994.

[60] P. A. Glendinning. Classification of boundary equilibrium bifurcations in planar Filippov systems. *Chaos: An Interdisciplinary Journal of Nonlinear Science*, 26(1):013108, 2016.

[61] P. A. Glendinning. Shilnikov chaos, Filippov sliding and boundary equilibrium bifurcations. *European Journal of Applied Mathematics*, pages 1–21, 2018.

[62] P. A. Glendinning and M. R. Jeffrey. Grazing-sliding bifurcations, border collision maps and the curse of dimensionality for piecewise smooth bifurcation theory. *Nonlinearity*, 28(1):263, 2015.

[63] O. Gomide and M. A. Teixeira. Generic singularities of 3D piecewise smooth dynamical systems. *arXiv:1702.00613*, 2017.

[64] M. Guardia, T. Seara, and M. Teixeira. Generic bifurcations of low codimension of planar Filippov systems. *Journal of Differential Equations*, 250(4):1967 – 2023, 2011.

[65] J. Guckenheimer and P. Holmes. *Nonlinear Oscillations, Dynamical Systems and Bifurcations of Vector Fields*, volume 42. Springer-Verlag, New York, 1983.

[66] M. Haragus and G. Iooss. *Local bifurcations, center manifolds, and normal forms in infinite dimensional Dynamical Systems*. Springer-Verlag, London, 2011.

[67] S. J. Hogan, M. E. Homer, M. R. Jeffrey, and R. Szalai. Piecewise smooth dynamical systems theory: The case of the missing boundary equilibrium bifurcations. *Journal of Nonlinear Science*, 26(5):1161–1173, 2016.

[68] A. Jacquemard, M. A. Teixeira, and D. J. Tonon. Piecewise smooth reversible dynamical systems at a two-fold singularity. *International Journal of Bifurcation and Chaos*, 22(8):1250192, 13 pages, 2012.

[69] A. Jacquemard, M. A. Teixeira, and D. J. Tonon. Stability conditions in piecewise smooth dynamical systems at a two-fold singularity. *Journal of Dynamical and Control Systems*, 19(1):47–67, 2013.

[70] M. Jeffrey and S. Hogan. The geometry of generic sliding bifurcations. *SIAM Review*, 53(3):505–525, 2011.

[71] M. R. Jeffrey and A. Colombo. The two-fold singularity of discontinuous vector fields. *SIAM J. Applied Dynamical Systems*, 8(2):624–640, 2009.

[72] K. H. Johansson, A. Rantzer, and K. J. Astrom. Fast switches in relay feedback systems. *Automatica*, 35(4):539 – 552, 1999.

[73] J. G. Kassakian, M. F. Schlecht, and G. C. Verghese. *Principles of power electronics*. Addison-Wesley Publishing, 1st edition, 1991.

[74] K. U. Kristiansen and S. J. Hogan. On the use of blowup to study regularizations of singularities of piecewise smooth dynamical systems in $\mathbb{R}^3$. *SIAM J. Applied Dynamical Systems*, 14(1):382–422, 2015.

[75] V. Krivan. On the gause predator-prey model with a refuge: A fresh look at the history. *Journal of theoretical biology*, 274:67–73, 04 2011.

[76] M. Kunze. *Non-Smooth Dynamical Systems*, volume 1744 of *Lecture Notes in Mathematics*. Springer-Verlag, Berlin, 2000.

[77] Y. A. Kuznetsov. *Elements of Applied Bifurcation Theory*, volume 112. Springer-Verlag, New York, 2004.

[78] Y. A. Kuznetsov, S. Rinaldi, and A. Gragnani. One-parameter bifurcations in planar Filippov systems. *International Journal of Bifurcation and Chaos*, 13(8):2157–2188, 2003.

[79] H. C. Lee and E. H. Abed. Washout filter in the bifurcation control of high alpha flight dynamics. In *Proc. of the American Control Conference, Boston*, volume 1, pages 206–211, 1991.

[80] J. Leifeld. Non-smooth homoclinic bifurcation in a conceptual climate model. *European Journal of Applied Mathematics*, pages 1–14, 2018.

[81] R. I. Leine, D. H. V. Campen, and B. L. V. de Vrande. Bifurcations in nonlinear discontinuous systems. *Nonlinear Dynamics*, 23(2):105–164, Oct 2000.

[82] R. I. Leine and H. Nijmeijer. *Dynamics and Bifurcations of Non-Smooth Mechanical Systems*. Springer-Verlag, New York, 2004.

[83] L. Li and L. Huang. Concurrent homoclinic bifurcation and Hopf bifurcation for a class of planar Filippov systems. *Journal of Mathematical Analysis and Applications*, 411(1):83 – 94, 2014.

[84] J. Llibre and E. Ponce. Global first harmonic bifurcation diagram for odd piecewise linear control systems. *Dynamics and Stability of Systems*, 11(1):49–88, 1996.

[85] J. Llibre, E. Ponce, J. Ros, and F. Torres. On the Fold-Hopf bifurcation for continuous piecewise linear differential systems with symmetry. *Chaos*, 20(3), 2010.

[86] A. Lyapunov. *General Problem of Stability of Motion*. Mathematics Society of Kharkov, Kharkov, 1892.

[87] T. McGeer. Passive dynamic walking. *Int. J. Robot. Res.*, (9):62–82, 1990.

[88] J. Meiss. *Differential Dynamical Systems*. Society for Industrial and Applied Mathematics, 2007.

[89] L. H. A. Monteiro. *Sistemas Dinâmicos*. Livraria da Física, 3nd edition, 2011.

[90] D. J. Pagano and R. Cristiano. Bifurcações de equilíbrio de fronteira no controle de um conversor bidirecional conectado a uma microrede cc. In *Proceeding Series of the Brazilian Society of Computational and Applied Mathematics: CMAC-Sul, Curitiba-PR, 2014*, volume 2, pages 010024/1–010024/6, Feb 2014.

[91] D. J. Pagano and E. Ponce. On the robustness of the DC-DC Boost converter under Washout SMC. In *Power Electronics Conference, Brazil, 2009*, pages 110–115, 2009.

[92] D. J. Pagano and E. Ponce. Sliding mode controllers design through bifurcation analysis. In *Preprints of the 8th IFAC on Nonlinear Control Systems, Bologna, Italy*, pages 1284–1289, 2010.

[93] D. J. Pagano, E. Ponce, and F. Torres. On double boundary equilibrium bifurcations in piecewise smooth planar systems. *Qualitative Theory of Dynamical Systems*, 10(2):277–301, 2011.

[94] L. M. Perko. Global families of limit cycles of planar analytic systems. *Transactions of the American Mathematical Society*, 322:627 – 656, 1990.

[95] L. M. Perko. *Differential Equations and Dynamical Systems*, volume 7. Texts in Applied Mathematics, Springer-Verlag, New York, 1991.

[96] L. M. Perko. Multiple limit cycle bifurcation surfaces and global families of multiple limit cycles. *Journal of Differential Equations*, 122(1):89 – 113, 1995.

[97] F. Peterka. Part 1: Theoretical analysis of n-multiple (1/n)-impact solutions. *CSAV Acta Technica*, 26(2):462–473, 1974.

[98] E. Ponce and D. J. Pagano. Sliding dynamics bifurcations in the control of boost converters. In *Preprints of the 18th IFAC World Congress, Milano, Italy*, pages 13293–13298, 2011.

[99] E. Ponce, J. Ros, E. Freire, and A. Amador. Unravelling the dynamical richness of 3d canonical memristor oscillators. *Microelectronic Engineering*, 182:15 – 24, 2017.

[100] E. Ponce, J. Ros, and E. Vela. The boundary focus-saddle bifurcation in planar piecewise linear systems. application to the

analysis of memristor oscillators. *Nonlinear Analysis: Real World Applications*, 43:495 – 514, 2018.

[101] J. A. G. Roberts and G. R. W. Quispel. Chaos and time-reversal symmetry. order and chaos in reversible dynamical systems. *Physics Reports*, 216(2-3):63–177, 1992.

[102] F. D. Rossa and F. Dercole. Generic and generalized boundary operating points in piecewise-linear (discontinuous) control systems. In *Decision and Control (CDC), 2012 IEEE 51st Annual Conference on*, pages 7714–7719, Dec 2012.

[103] A. Sabanovic, K. Jezernik, and N. Sabanovic. *Sliding Modes Applications in Power Electronics and Electrical Drives*, pages 223–251. Springer Berlin Heidelberg, Berlin, Heidelberg, 2002.

[104] D. J. W. Simpson. The instantaneous local transition of a stable equilibrium to a chaotic attractor in piecewise-smooth systems of differential equations. *Physics Letters A*, 380(38):3067 – 3072, 2016.

[105] D. J. W. Simpson. A general framework for boundary equilibrium bifurcations of Filippov systems. *Chaos: An Interdisciplinary Journal of Nonlinear Science*, 28(10):103114, 2018.

[106] D. J. W. Simpson and R. Kuske. Stochastic perturbations of periodic orbits with sliding. *Journal of Nonlinear Science*, 25(4):967–1014, Aug 2015.

[107] D. J. W. Simpson and J. D. Meiss. Andronov-Hopf bifurcations in planar, piecewise-smooth, continuous flows. *Physics Letters A*, 371(3):213 – 220, 2007.

[108] H. Sira-Ramirez and R. Silva-Ortigoza. *Control Design Techniques in Power Electronics Devices (Power Systems)*. Springer, Berlin, 2010.

[109] J. Sotomayor and M. A. Teixeira. Vector fields near the boundary of a 3-manifold. In *Lecture Notes in Mathematics*, volume 1331, pages 169–195. Springer-Verlag, Berlin/New Yor, 1988.

[110] R. Szalai and M. R. Jeffrey. Nondeterministic dynamics of a mechanical system. *Phys. Rev. E*, 90:022914, Aug 2014.

[111] A. P. N. Tahim, D. J. Pagano, M. L. Heldwein, and E. Ponce. Control of interconnected power electronic converters in dc distribution systems. In *XI Brazilian Power Electronics Conference*, pages 269–274, Sept 2011.

[112] A. P. N. Tahim, D. J. Pagano, and E. Ponce. Nonlinear control of boost bidirectional converters in stand-alone dc microgrids. In *51st IEEE Conference on Decision and Control - CDC, Maui, Hawaii, USA*, 2012.

[113] S. C. Tan, Y. M. Lai, C. K. Tse, and M. K. H. Cheung. Adaptive feedforward and feedback control schemes for sliding mode controlled power converters. *IEEE Transactions on Power Electronics*, 21(1), 2006.

[114] S. Tang, J. Liang, Y. Xiao, and R. A. Cheke. Sliding bifurcations of Filippov two stage pest control models with economic theshholds. *SIAM Journal on Applied Mathematics*, 72(4):1061–1080, 2012.

[115] M. A. Teixeira. Generic bifurcation of certain singularities. *Bolletino dell Unione Matematice Italiana*, 9(2):238–254, 1979.

[116] M. A. Teixeira. On topological stability of divergent diagrams of folds. *Math. Z.*, 180:361–371, 1982.

[117] M. A. Teixeira. Stability conditions for discontinuos vector fields. *Journal of Differential Equations*, 88:15–29, 1990.

[118] M. A. Teixeira. Generic bifurcation of sliding vector fields. *J. Math. Anal. Appl.*, 176:436–457, 1993.

[119] J. M. T. Thompson and H. B. Stewart. *Nonlinear Dynamics and Chaos*. John Wiley and Sons Ltd, England, 2002.

[120] R. Thul and S. Coombes. Understanding cardiac alternans: A piecewise linear modeling framework. *Chaos*, 20(4):045102/1–13, 2010.

[121] C. K. Tse and M. di Bernardo. Complex behavior in switching power converters. *Proceedings of the IEEE*, 90(5):768–781, May 2002.

[122] V. I. Utkin. *Sliding Modes in Control Optimization*. Springer, 1992.

[123] V. I. Utkin, J. Guldner, and J. Shi. *Sliding Mode Control in Electro-Mechanical Systems*. Automation and Control Engineering. CRC Press, 2009.

[124] J. A. C. Valenzuela. *Formas Normales y Bifurcaciones de Ciclos Limite en Sistemas Lineales por Pedazos Discontinuos*. PhD thesis, Universidad de Sonora, Programa de Posgrado en Matematicas, 2017.

[125] V. Vaziri, M. Kapitaniak, and M. Wiercigroch. Suppression of drill-string stick-slip vibration by sliding mode control: Numerical and experimental studies. *European Journal of Applied Mathematics*, pages 1–21, 2018.

[126] J. Walsh, E. Widiasih, J. Hahn, and R. McGehee. Periodic orbits for a discontinuous vector field arising from a conceptual model of glacial cycles. *Nonlinearity*, 29(6):18–43, 2016.

[127] H. Wang and E. H. Abed. Bifurcation control of a chaotic system. *Automatica*, 31:1213–1226, 1995.

[128] B. Xu, F. Yang, Y. Tang, and M. Lin. Homoclinic bifurcations in planar piecewise-linear systems. *Discrete Dynamics in Nature and Society*, 2013:732321, 9 pages, 2013.